Establishment and validation of an immortalized *in vitro* human blood-brain barrier (BBB) model for drug permeability studies, and application to natural product derived leads

Inauguraldissertation

zur

Erlangung der Würde eines Doktors der Philosophie

vorgelegt der

Philosophisch-Naturwissenschaftlichen Fakultät

der Universität Basel

von

Daniela Elisabeth Eigenmann

aus Waldkirch, St. Gallen

Basel, 2016

Genehmigt von der Philosophisch-Naturwissenschaftlichen Fakultät
auf Antrag von

Prof. Dr. Matthias Hamburger
Prof. Dr. Laurent A. Decosterd

Basel, den 08.12.2015

Prof. Dr. Jörg Schibler
Dekan

Namensnennung-Keine kommerzielle Nutzung-Keine Bearbeitung 3.0 Schweiz
(CC BY-NC-ND 3.0 CH)

Sie dürfen: **Teilen** — den Inhalt kopieren, verbreiten und zugänglich machen

Unter den folgenden Bedingungen:

Namensnennung — Sie müssen den Namen des Autors/Rechteinhabers in der von ihm festgelegten Weise nennen.

Keine kommerzielle Nutzung — Sie dürfen diesen Inhalt nicht für kommerzielle Zwecke nutzen.

Keine Bearbeitung erlaubt — Sie dürfen diesen Inhalt nicht bearbeiten, abwandeln oder in anderer Weise verändern.

Wobei gilt:

- **Verzichtserklärung —** Jede der vorgenannten Bedingungen kann **aufgehoben** werden, sofern Sie die ausdrückliche Einwilligung des Rechteinhabers dazu erhalten.
- **Public Domain (gemeinfreie oder nicht-schützbare Inhalte) —** Soweit das Werk, der Inhalt oder irgendein Teil davon zur Public Domain der jeweiligen Rechtsordnung gehört, wird dieser Status von der Lizenz in keiner Weise berührt.
- **Sonstige Rechte —** Die Lizenz hat keinerlei Einfluss auf die folgenden Rechte:
    - Die Rechte, die jedermann wegen der Schranken des Urheberrechts oder aufgrund gesetzlicher Erlaubnisse zustehen (in einigen Ländern als grundsätzliche Doktrin des **fair use** bekannt);
    - Die **Persönlichkeitsrechte** des Urhebers;
    - Rechte anderer Personen, entweder am Lizenzgegenstand selber oder bezüglich seiner Verwendung, zum Beispiel für **Werbung** oder Privatsphärenschutz.
- **Hinweis —** Bei jeder Nutzung oder Verbreitung müssen Sie anderen alle Lizenzbedingungen mitteilen, die für diesen Inhalt gelten. Am einfachsten ist es, an entsprechender Stelle einen Link auf diese Seite einzubinden.

Quelle: http://creativecommons.org/licenses/by-nc-nd/3.0/ch/ Datum: 12.11.2013

To my dear friends and family

Simplicity is the ultimate sophistication.

Leonardo da Vinci (1452–1519)

Table of contents

List of abbreviations

ABC	ATP-binding cassette
AJ	Adherens junction
APCI	Atmospheric pressure chemical ionization
AUC	Area under the curve
BB19	Immortalized human brain capillary endothelial cells
BBB	Blood-brain barrier
BCRP	Breast cancer resistance protein
BCSFB	Blood-cerebrospinal fluid barrier
BSCB	Blood-spinal cord barrier
Cal	Calibrator
C_{CL}	Cell layer capacitance
CNS	Central nervous system
CSF	Cerebrospinal fluid
CV	Coefficient of variation
EMA	European Medicines Agency
ER	Efflux ratio
ESI	Electrospray ionization
EVOM	Epithelial voltohmmeter
FBS	Fetal bovine serum
FDA	Food and Drug Administration
F/T	Freeze and thaw
$GABA_A$ receptor	γ-Aminobutyric acid type A receptor
hBMEC	Immortalized human brain microvascular endothelial cell line
HBPCT	Immortalized human brain pericyte cell line
HC	Hydrocortisone
hCMEC/D3	Immortalized human cerebral microvascular endothelial cell line D3
HPLC	High performance liquid chromatography
I.S.	Internal standard
ISF	Interstitial fluid
JAM	Junction-associated molecules
LC-MS	Liquid chromatography coupled to mass spectrometry
LC-MS/MS	Liquid chromatography coupled to triple (tandem) quadrupole mass spectrometry
LC-UV/Vis	Liquid chromatography coupled to ultraviolet/visible absorbance detection
LLE	Liquid-liquid extraction
LLOQ	Lower limit of quantification

LY	Lucifer yellow
MRM	Multiple reaction monitoring
MRP	Multidrug resistance-associated protein
MS	Mass spectrometry
MW	Molecular weight
Na-F	Sodium fluorescein
NP	Natural product
PAMPA-BBB	Parallel artificial membrane permeation assay for blood-brain barrier
P_{app}	Apparent permeability coefficient
P_e	Endothelial permeability coefficient
P-gp	P-glycoprotein
PP	Protein precipitation
PSA	Polar surface area
QC	Quality control
RE	Relative error
RHB	Ringer HEPES buffer
S.D.	Standard deviation
S.E.M.	Standard error of the mean
SLC	Solute carrier
SLE	Supported-liquid extraction
SOP	Standard operating procedure
SPE	Solid-phase extraction
SRM	Selected reaction monitoring
SVG-A	Immortalized human astrocyte cell line
TEER	Transendothelial electrical resistance
TJ	Tight junction
TRPV-1	Transient receptor potential vanilloid 1
TY10	Conditionally immortalized human brain microvascular endothelial cell line
UHPLC	Ultra-high performance liquid chromatography
ULOQ	Upper limit of quantification
VE-cadherin	Vascular endothelial-cadherin
WS	Working solution
ZO-1	Zonula occludens protein-1

Summary

In the human brain, the endothelial cells lining the cerebral microvessels form a uniquely tight cellular layer separating the brain tissue from the bloodstream. This cellular barrier, designated as "blood-brain barrier" (BBB), prevents the entry of xenobiotics and neurotoxic metabolites into the central nervous system (CNS) and thus protects the nerve tissue from chemical damage. More than 98% of small molecule drugs have been estimated to not cross the BBB. For drugs targeting the CNS, however, low BBB permeability may lead to limited brain penetration, culminating in insufficient drug concentrations at the target sites and thus therapeutic failure. On the other hand, low BBB permeation is desirable for non-CNS drugs, as this reduces the risk of CNS-related side effects. Regardless of the therapeutic area, drug lead candidates should therefore be screened for their ability to permeate the BBB already at an early stage of the drug development process, in order to reduce their attrition rate at a later stage.

In the past years, a broad spectrum of cell-based *in vitro* BBB models has been developed and implemented in academia and industry to bring forward molecules with high potential for CNS exposure. Despite considerable efforts, there is still an urgent need for reliably predictive BBB models, in particular human ones. Primary human cells are difficult to obtain on ethical grounds, are laborious to cultivate, suffer from batch-to-batch variation, and are thus suitable only for low throughput screenings. To overcome these limitations, immortalized human brain microvascular endothelial cell lines have been generated by transfection with tumor genes. Unlike primary cultures, immortalized cells are easy to cultivate, proliferate indefinitely, and maintain their differentiating properties even after repeated passaging. These properties render them highly suitable for standardized screenings amenable to higher throughput. Regrettably, currently available immortalized human brain capillary endothelial cell lines often show deficiencies such as low barrier tightness, relatively high leakage of barrier integrity markers, and insufficient expression of key transporter systems. Consequently, careful optimization and validation of human cell line-based *in vitro* BBB models have to be carried out prior to their application to permeability screening of drug candidates.

The aim of this thesis was to establish a human *in vitro* BBB model based on an immortalized human brain capillary endothelial cell line, to validate it with a representative series of drug substances known to cross the BBB to a varying extent, and to apply it to BBB permeability studies of promising lead compounds of natural origin.

To establish an improved *in vitro* human BBB model, we evaluated in a first step four currently available immortalized human brain capillary endothelial cell lines (hCMEC/D3, hBEMC, TY10, and BB19) regarding their ability to produce endothelial cell monolayers with sufficient barrier tightness in a 24-well Transwell system. Transendothelial electrical resistance (TEER) values were recorded in

real-time using an automated CellZscope system to obtain highly standardized data. Culture conditions (growth medium composition, tissue culture insert material, coating material and procedure, cell seeding density) were systematically optimized, the impact of co-cultured immortalized human astrocytes (SVG-A cell line) and pericytes (HBPCT cell line) on barrier integrity of endothelial cell monolayers was investigated, and biochemical and immunocytochemical characterization of cell-type specific cellular junction proteins was performed. Under the conditions examined in our experiments, mono-cultures of hBMEC cell line exhibited highest TEER values (around 40 Ωcm^2) and lowest leakage of two fluorescent barrier integrity markers (sodium fluorescein, Na-F; and lucifer yellow, LY) (apparent permeability coefficients (P_{app}) in the range of 3–5 x 10^{-6} cm/s). Furthermore, hBMEC cells were shown to express the tight junction proteins ZO-1 and claudin-5, and the endothelial marker protein VE-cadherin, confirming their endothelial lineage. Thus, we concluded that hBMEC cell line was the most suitable cell line in terms of barrier tightness for the establishment of an immortalized *in vitro* human BBB model.

The hBMEC cell line-based *in vitro* human BBB model was validated in a next step with a representative series of structurally diverse compounds known to cross the BBB to a different extent. Antipyrine, caffeine, diazepam, and propranolol were selected as positive controls, while atenolol, cimetidine, quinidine, and vinblastine served as negative controls. For each compound, a quantitative ultra-high performance liquid chromatography tandem mass spectrometry (UHPLC-MS/MS) assay in Ringer HEPES buffer (RHB) was developed and validated in terms of selectivity, precision, and reliability according to current international guidelines. During method validation, numerous biological and analytical challenges were encountered, demonstrating that major precautions have to be taken prior to quantification, and underlining the importance of careful method development. All compounds were screened in the *in vitro* human BBB model with the barrier integrity marker Na-F in parallel, and endothelial permeability coefficients (P_e) across hBMEC monolayers were determined by means of the validated UHPLC-MS/MS methods. The *in vitro* human BBB model correctly predicted BBB permeability of the selected compounds, with the exception of one negative control (quinidine, a small basic lipophilic P-glycoprotein (P-gp) inhibitor and substrate). A limitation of the model may thus be the lack of discrimination between passively diffusing compounds and substrates of active efflux. Complementary assays to determine efflux pump interaction are therefore recommended. Nevertheless, we conclude that our model represents a promising tool for early BBB permeability assessment of lead candidates in drug discovery, as it is of human origin (thus reducing the risk for data confounded by species differences), easy and fast to set up, and thus amenable to moderate to higher throughput screening.

After validation, we screened the alkaloid piperine from black pepper (*Piper nigrum* L.) and five selected piperine analogs with positive allosteric γ-aminobutyric acid type A ($GABA_A$) receptor modulatory activity for their ability to permeate the BBB in the immortalized *in vitro* human BBB

model. Since $GABA_A$ receptors are expressed in the CNS, lead compounds modulating this target need to cross the BBB to reach their sites of action. For comparative purposes, the compounds were screened in parallel in a human stem cell-derived and in a well-established primary animal (bovine endothelial/rat astrocytes co-culture) *in vitro* BBB model. For each compound, a quantitative UHPLC-MS/MS assay in the corresponding matrix was developed, and permeability coefficients in each model were determined. *In vitro* predictions from both human models were in good agreement, while permeability data from the animal model differed to some extent. In all three BBB models, piperine and the semisynthetic analog SCT-64 displayed highest BBB permeability, which was corroborated by *in silico* prediction data. For the other piperine analogs, BBB permeability was low to moderate in the two human models, and moderate to high in the animal model. Efflux ratios (ER) calculated from bidirectional permeability experiments indicated that the compounds were not substrates of active efflux transporters.

In addition to $GABA_A$ receptor modulating compounds, the indolinone derivative (*E,Z*)-3-(4-hydroxy-3,5-dimethoxybenzylidene)indolin-2-one (indolinone) from woad (*Isatis tinctoria* L.) was screened in our immortalized *in vitro* human BBB model. The compound had previously been shown to possess potent histamine release inhibitory and anti-inflammatory properties, and thus represents a promising lead candidate for the development of new anti-allergic drugs. *In vitro* data from the immortalized *in vitro* BBB model indicated a high BBB permeation potential for indolinone, which was corroborated by *in vitro* permeability data obtained from two well-established primary animal models, and by *in silico* prediction data. Furthermore, P-gp interaction of the compound was assessed with the aid of two specific efflux pump interaction assays. Both assays suggested that no active mediated transport mechanism was involved for the compound.

In conclusion, we have successfully established and validated an easy and fast to set up human *in vitro* BBB model, and applied it to in-house BBB drug permeability assays of promising lead candidates of natural origin.

Zusammenfassung

Die Blut-Hirn-Schranke ist eine zelluläre Barriere im menschlichen Gehirn, welche die Hirnsubstanz vom Blutstrom trennt. Sie besteht aus den dicht verbundenen Endothelzellen der zerebralen Blutgefässe, und schützt das zentrale Nervensystem (ZNS) vor im Blut zirkulierenden Xenobiotika und neurotoxischen Metaboliten. Schätzungen zufolge sind mehr als 98% aller niedermolekularen Verbindungen nicht in der Lage, die Blut-Hirn-Schranke zu durchdringen. Um eine therapeutische Wirkung entfalten zu können, müssen ZNS-aktive Arzneistoffe jedoch zwingend durch diese Barriere permeieren, um so ihren Wirkort im Gehirn zu erreichen. Demgegenüber ist eine geringe Blut-Hirn-Schranken-Permeabilität erwünscht für Substanzen, deren Wirkort in der Peripherie ist, da dies das Risiko von unerwünschten ZNS-Nebenwirkungen minimiert. Leitstrukturen sollten dementsprechend bereits früh auf ihre Blut-Hirn-Schranken-Gängigkeit hin getestet werden, um ein späteres Scheitern der Substanzen in der präklinischen oder klinischen Phase zu verhindern.

In den letzten Jahren wurde von Forschenden in Akademie und Industrie eine Vielzahl von zellbasierten *in vitro* Modellen etabliert, um vielversprechende Moleküle auf ihre Blut-Hirn-Schranken-Permeabilität hin zu testen. Trotz erheblicher Bemühungen besteht jedoch weiterhin ein dringender Bedarf an verlässlichen *in vitro* Blut-Hirn-Schranken-Modellen, insbesondere an solchen menschlichen Ursprungs, welche die Permeabilität von Testsubstanzen korrekt voraussagen. Primäre menschliche Zellen sind aus ethischen Gründen nur schwer zugänglich, erfordern eine aufwändige Kultivierung, variieren beträchtlich von Charge zu Charge, und sind somit nur für Screenings mit geringem Durchsatz geeignet. Um diesen Nachteilen vorzubeugen, wurden in den letzten Jahren zahlreiche immortalisierte menschliche Endothelzelllinien durch die Transfektion mit Tumorgenen generiert. Diese sind im Gegensatz zu primären Zellen einfach zu kultivieren, proliferieren unbegrenzt, und erhalten ihre differenzierenden Eigenschaften selbst nach mehrfacher Passagierung. Dies ist für standardisierte Screenings mit höherem Durchsatz von grossem Vorteil. Die derzeit erhältlichen humanen Endothelzelllinien sind jedoch oftmals charakterisiert durch limitierte *in vitro* Schranken-Dichte, erhöhte Durchlässigkeit von Negativkontrollen, und unzureichende Expression von Transportproteinen. Blut-Hirn-Schranken-Modelle, die auf diesen Zelllinien basieren, sollten aus diesem Grund sorgfältig optimiert und validiert werden, bevor sie für Permeabilitätsstudien von Substanzen eingesetzt werden.

Das Ziel dieser Thesis war die Etablierung eines *in vitro* Blut-Hirn-Schranken-Modells basierend auf einer menschlichen zerebralen Endothelzelllinie, die Validierung des Modells mit strukturell verschiedenen Substanzen mit unterschiedlicher Blut-Hirn-Schranken-Gängigkeit, und das anschliessende Testen von Leitstrukturen pflanzlichen Ursprungs im Modell bezüglich ihrer Blut-Hirn-Schranken-Permeabilität.

In einem ersten Schritt wurden vier derzeit verfügbare humane zerebrale Endothelzelllinien (hCMEC/D3, hBMEC, TY10 und BB19) auf ihre Fähigkeit hin untersucht, einen ausreichend dichten Zellmonolayer in einem Transwell-System (24-Well-Format) auszubilden. Der transendotheliale elektrische Widerstand (TEER) wurde in Echtzeit mithilfe eines automatisierten CellZscope-Systems gemessen, um hoch standardisierte Daten zu erhalten. Die Kultivierungsbedingungen wurden systematisch optimiert, und der Einfluss von ko-kultivierten immortalisierten menschlichen Astrozyten und Perizyten auf die Schranken-Dichte der Endothelzellen wurde untersucht. Zudem wurden zelltypspezifische Markerproteine biochemisch und immunozytochemisch nachgewiesen. Unter den durchgeführten experimentellen Bedingungen konnte gezeigt werden, dass Zellmonolayer der hBMEC-Zelllinie die höchsten TEER-Werte (ca. 40 Ωcm^2) ausbildeten, sowie die geringste Durchlässigkeit von zwei fluoreszierenden Integritätsmarkern aufwiesen (Natrium-Fluorescein, Na-F; und Lucifer Yellow, LY) (Permeabilitätskoeffizienten ca. 3–5 x 10^{-6} cm/s). Des Weiteren konnte gezeigt werden, dass hBMEC-Zellen die Tight Junction Proteine ZO-1 und Claudin-5 sowie das endotheliale Markerprotein VE-Cadherin exprimieren. Die hBMEC-Zelllinie wurde somit als die am besten geeignete humane endotheliale Zelllinie in Bezug auf Schranken-Dichte für die Etablierung eines menschlichen *in vitro* Blut-Hirn-Schranken-Modells betrachtet.

Das auf der humanen hBMEC-Zelllinie basierende *in vitro* Blut-Hirn-Schranken-Modell wurde in einem nächsten Schritt mit acht strukturell verschiedenen Wirkstoffen mit unterschiedlicher Blut-Hirn-Schranken-Permeabilität validiert. Antipyrin, Coffein, Diazepam und Propranolol wurden als Positivkontrollen gewählt. Atenolol, Cimetidin, Chinidin und Vinblastin dienten als Negativ-kontrollen. Für jede Substanz wurde eine Quantifizierungsmethode in Ringer-HEPES-Puffer mittels Ultra-Hochleistungs-Flüssigkeits-Chromatographie gekoppelt an Tandem-Massenspektrometrie (UHPLC-MS/MS) entwickelt, welche gemäss aktuellen internationalen Richtlinien hinsichtlich Selektivität, Präzision und Verlässlichkeit validiert wurde. Im Verlauf der Methodenvalidierung traten zahlreiche biologische und analytische Probleme auf, welchen durch entsprechende Massnahmen in der Probenvorbereitung und UHPLC-MS/MS-Analyse vorgebeugt wurde. Die Substanzen wurden im humanen *in vitro* Modell auf ihre Blut-Hirn-Schranken-Gängigkeit hin getestet, und Permeabilitäts-koeffizienten wurden bestimmt. Das menschliche *in vitro* Blut-Hirn-Schranken-Modell war in der Lage, die Permeabilität der ausgewählten Testsubstanzen korrekt vorauszusagen, mit Ausnahme einer einzigen Negativkontrolle (Chinidin, ein Substrat und Inhibitor von P-Glykoprotein). Trotz dieser Limitation stellt das etablierte Modell ein vielversprechendes Hilfsmittel für Blut-Hirn-Schranken-Permeabilitätsstudien dar, da es menschlichen Ursprungs ist (was das Risiko minimiert, verzerrte Daten aufgrund von Spezies-Unterschieden zu erhalten), einfach und schnell aufzusetzen ist, und sich somit für Screenings mit höherem Durchsatz eignet.

Nach der Validierung des Modells wurden das in schwarzem Pfeffer (*Piper nigrum* L.) vorkommende Alkaloid Piperin sowie fünf Piperinanaloga mit positiver allosterischer $GABA_A$-Rezeptor-Aktivität auf

ihre Blut-Hirn-Schranken-Gängigkeit hin überprüft. Leitstrukturen, die dieses Target modulieren, müssen die Blut-Hirn-Schranke überqueren können. Zu Vergleichszwecken wurden die Substanzen zusätzlich in einem auf menschlichen Stammzellen basierenden Modell sowie in einem gut etablierten tierischen Blut-Hirn-Schranken-Modell getestet. Um Permeabilitätskoeffizienten bestimmen zu können, wurde für jede Substanze eine UHPLC-MS/MS Quantifizierungsmethode in der entsprechenden Matrix entwickelt. *In vitro* Daten der beiden menschlichen Modelle wiesen auf eine hohe Blut-Hirn-Schranken-Gängigkeit von Piperin und dem semisynthetischen Derivat SCT-64 hin, während die übrigen Piperinanaloga nur geringe bis moderate Permeabilität zeigten. Dementgegengesetzt zeigten alle Substanzen eine moderate bis hohe Blut-Hirn-Schranken-Gängigkeit im tierischen Modell. Bidirektionale Permeabilitätsexperimente wiesen darauf hin, dass die Substanzen keine Substrate von aktiven Efflux-Transportproteinen sind.

Zusätzlich zu den $GABA_A$-Rezeptor-Modulatoren wurde das Alkaloid (*E*,*Z*)-3-(4-Hydroxy-3,5-dimethoxybenzyliden)indolin-2-on (Indolinon) aus Färberwaid (*Isatis tinctoria* L.) im immortalisierten humanen *in vitro* Blut-Hirn-Schranken-Modell getestet. Die Substanz wurde in vorangehenden Studien als eine vielversprechende Leitstruktur für die Entwicklung von neuartigen anti-allergischen Medikamenten identifiziert. *In vitro* Permeabilitätsdaten wiesen auf eine hohe Blut-Hirn-Schranken-Gängigkeit von Indolinon hin, was durch *in vitro* Daten aus zwei gut etablierten *in vitro* Blut-Hirn-Schranken-Modellen tierischen Ursprungs sowie durch *in silico* Berechnungen bestätigt wurde. Des Weiteren wurde die Interaktion der Substanz mit P-Glykoprotein in zwei spezifischen Assays untersucht. Beide Assays wiesen darauf hin, dass kein aktiver Transportmechanismus für Indolinon in dessen Blut-Hirn-Schranken-Permeabilität involviert ist.

Abschliessend kann gesagt werden, dass im Zuge dieser Dissertation ein einfach und schnell aufzusetzendes humanes *in vitro* Blut-Hirn-Schranken-Modell etabliert und validiert wurde, und ausgewählte Naturstoffe und Naturstoff-Analoga auf ihre Blut-Hirn-Schranken-Permeabilität hin im Modell getestet wurden.

1 Aim of the work

Central nervous system (CNS) drugs need to penetrate the brain in order to reach their target sites of action. This process is controlled by the blood-brain barrier (BBB), a tight cellular layer of endothelial cells lining the cerebral microvessels that prevents the entry of most molecules into the nerve tissue. Low permeability across the BBB, however, may lead to low brain exposure, culminating in insufficient drug concentrations at the target. For CNS drugs, high permeability across this barrier is thus favorable. For non-CNS drugs, on the other hand, limited BBB permeation is desirable, as this reduces the risk of causing CNS-related side effects. Regardless of the therapeutic area, BBB permeability of lead compounds should therefore be assessed at an early stage of the drug development process.

Cell-based *in vitro* BBB models have been widely implemented in academia and industry for early prediction of brain penetration of lead candidates. However, there is still a considerable lack of reliably predictive BBB models, in particular of human ones. Primary cells of human origin are difficult to obtain due to ethical reasons. Moreover, isolation, purification, and cultivation of primary cultures are tedious and time-consuming, and yield and lifespan of endothelial cells are limited. To overcome these limitations, immortalized brain microvascular endothelial cell lines have been generated by transfection with various tumor genes. Unlike primary cultures, immortalized cells are easy to cultivate and maintain their phenotype after repeated passaging, which renders them suitable for standardized screenings. Regrettably, currently available immortalized human brain capillary endothelial cell lines show deficiencies such as low barrier tightness, relatively high leakage of barrier integrity markers, and insufficient expression of key transporter systems. Consequently, careful optimization and validation of human cell line-based *in vitro* BBB models have to be carried out prior to their application to permeability screening of drug candidates.

The aim of this thesis was to establish and validate an immortalized human *in vitro* BBB model for the assessment of BBB permeability of natural product derived lead compounds with promising *in vitro* activity.

In a first step, we aimed at establishing a human *in vitro* BBB model by comparing four available immortalized human brain capillary endothelial cell lines (hCMEC/D3, hBMEC, TY10, and BB19) regarding their ability to produce endothelial cell monolayers with sufficient barrier tightness. Our objective was to systematically optimize culture conditions, and to evaluate the influence of co-cultured immortalized human astrocytes and pericytes on barrier integrity of the endothelial cells.

The second part of the thesis aimed at validating the optimized human *in vitro* BBB model with a representative series of compounds known to cross or not to cross the BBB. Antipyrine, caffeine, diazepam, and propranolol were selected as positive controls. Atenolol, cimetidine, quinidine, and vinblastine served as negative controls. For each compound, the objective was to develop a quantitative ultra-high performance liquid chromatography tandem mass spectrometry (UHPLC-

MS/MS) assay in Ringer HEPES buffer (RHB) and validate it with respect to selectivity, precision, and reliability according to current international guidelines. By means of the validated UHPLC-MS/MS quantification methods, we aimed at determining permeability coefficients for each compound across the endothelial cell monolayers.

CNS disorders such as anxiety, sleep disturbances, and epilepsy are currently treated primarily with γ-aminobutyric acid type A ($GABA_A$) receptor modulators including the benzodiazepines and other CNS depressants. However, these drugs induce clinically relevant side effects such as amnesia, unwanted sedation, and drug dependence, complicating their long-term application [1]. Hence, there is a high medical need for novel lead compounds acting on the $GABA_A$ receptor disposing of lower adverse effect profiles.

In our research group, numerous studies have previously been carried out on the identification of $GABA_A$ receptor modulators from nature [2–4]. In order to reach their sites of action, lead candidates modulating this target need to enter the brain by crossing the BBB. The aim of the third part of the thesis was thus to screen the alkaloid piperine from *Piper nigrum* L. (Piperaceae) and five selected structurally modified piperine analogs with positive $GABA_A$ receptor modulatory activity for their ability to cross the BBB [4–7]. Also, we aimed at corroborating the *in vitro* data by calculation of *in silico* descriptors relevant for BBB permeation.

Beyond the screening of $GABA_A$ receptor modulators, we aimed at evaluating the BBB permeability of the indolinone derivative (*E*,*Z*)-3-(4-hydroxy-3,5-dimethoxybenzylidene)indolin-2-one from *Isatis tinctoria* L. (Brassicaceae) in the immortalized human *in vitro* BBB model. The compound had previously been identified to possess potent histamine release inhibitory and anti-inflammatory properties, and thus represents a promising lead for the development of new anti-allergic drugs [8]. To minimize CNS-related adverse effects, low permeability of the compound across the BBB would be of advantage.

References

[1] H. Möhler, GABAA receptors in central nervous system disease: anxiety, epilepsy, and insomnia, J. Recept. Signal Transduct. 26 (2006) 731–740.

[2] J. Zaugg, S. Khom, D. Eigenmann, I. Baburin, M. Hamburger, S. Hering, Identification and characterization of GABAA receptor modulatory diterpenes from *Biota orientalis* that decrease locomotor activity in mice, J. Nat. Prod. 74 (2011) 1764–1772.

[3] D.C. Rueda, M. De Mieri, S. Hering, M. Hamburger, HPLC-based activity profiling for GABAA receptor modulators in *Adenocarpus cincinnatus*, J. Nat. Prod. 77 (2014) 640–649.

[4] J. Zaugg, I. Baburin, B. Strommer, H.-J. Kim, S. Hering, M. Hamburger, HPLC-based activity profiling: discovery of piperine as a positive GABAA receptor modulator targeting a benzodiazepine-independent binding site, J. Nat. Prod. 73 (2010) 185–191.

[5] S. Khom, B. Strommer, A. Schöffmann, J. Hintersteiner, I. Baburin, T. Erker, et al., GABAA receptor modulation by piperine and a non-TRPV1 activating derivative, Biochem. Pharmacol. 85 (2013) 1827–1836.

[6] A. Schöffmann, L. Wimmer, D. Goldmann, S. Khom, J. Hintersteiner, I. Baburin, et al., Efficient modulation of γ-aminobutyric acid type A receptors by piperine derivatives, J. Med. Chem. 57 (2014) 5602–5619.

[7] L. Wimmer, D. Schönbauer, P. Pakfeifer, A. Schöffmann, S. Khom, S. Hering, et al., Developing piperine towards TRPV1 and GABAA receptor ligands – synthesis of piperine analogs via Heck-coupling of conjugated dienes, Org. Biomol. Chem. 13 (2015) 990–994.

[8] S. Kiefer, A.C. Mertz, A. Koryakina, M. Hamburger, P. Küenzi, (*E*,*Z*)-3-(3’,5’-Dimethoxy-4’-hydroxy-benzylidene)-2-indolinone blocks mast cell degranulation, Eur. J. Pharm. Sci. 40 (2010) 143–147.

2 Introduction

2.1 Blood-brain barrier (BBB)

2.1.1 Historic background

The discovery of the blood-brain barrier (BBB) dates back to more than one hundred years. In 1885, the German scientist Paul Ehrlich (1854–1915) observed that after injecting water soluble aniline dyes into the peritoneum of rats, all animal organs were colored with the exception of brain and spinal cord [1,2]. Ehrlich initially attributed this effect to a different binding affinity of the dyes to different body tissues [3]. However, the early theory was outdated somewhat later when Ehrlich's student Edwin Goldmann (1862–1913) reversed the dye experiment by injecting the acidic dye trypan blue directly into the cerebrospinal fluid (CSF) of dogs and rabbits [2,4]. He observed that brain and spinal cord were colored, but not the remaining body of the animals, providing hence first evidence for the existence of a physical barrier between brain and peripheral circulation [4]. Max Lewandowsky (1876–1918), a German neurologist, was the first to speak of the "*Bluthirnschranke"* ("blood-brain barrier", abbreviated BBB). He introduced this term after performing experiments with cholic acid and ferrocyanide, two plasma membrane impermeable compounds. After injecting the substances directly into brain ventricles of animals, Lewandowsky observed neurological symptoms of the animals, while this was not the case after an intravenous application of the compounds [5]. A more detailed understanding of the BBB at a fine structural level was obtained in the 1960s with the emergence of the electron microscope [2]. In 1967, Reese and Karnovsky reported the existence of a "barrier" at the endothelium of vessels in the cerebral cortex [6]. By means of electron microscopy, the two scientists discovered that cerebral endothelial cells form a continuous, impermeable cellular layer, sealed by extremely dense tight junction (TJ) proteins [6]. In the meantime, considerable progress in the understanding of structure and function of the BBB has been achieved and numerous scientific studies have confirmed the concept of the BBB [7–9].

2.1.2 Structure and function of the BBB

Anatomy and physiology

The BBB in humans and mammals is located at the brain capillary vessels, which are composed of tightly sealed endothelial cells (Figure 1) [10]. These cells are connected to each other at their margins through TJ and adherens junction (AJ) proteins, and form a one cell layer thick lining [11]. Brain microvascular endothelial cells are relatively thin cells, resulting in a distance between luminal side (blood side) and abluminal side (brain side) of the plasma membrane of merely 500 nm or less [10]. In the human brain, around 100 billion capillaries are present, with a total length of 600 km and a total surface area of 20 m^2 [12]. At the abluminal side of the BBB, the endothelial cells are discontinuously enclosed by pericytes (Figure 1) [10]. These cells are involved in various functional roles in the brain,

such as regulation of microvascular blood flow and vascular permeability of the BBB [13–15]. Both endothelial cells and pericytes are embedded in a local basement membrane, the so-called basal lamina [10], which is composed of collagen and further structural proteins, and which is believed to exert an external support function for the endothelium [16]. Likewise, astrocytes are in close contact to the endothelium (Figure 1). Through perivascular endfeet, they are connected to the outer surface of the lamina-covered capillaries and provide a cellular link of the endothelial cells to surrounding neurons [17]. By secreting various signaling molecules and growth factors, astrocytes contribute to the formation of an increased barrier function of the endothelial cells [18]. In the perivascular space, further cerebral cells such as microglial cells and (in arterioles) smooth muscle cells are present [17]. The term "blood-brain barrier" refers to both the brain capillary endothelium and to its function as a restrictive barrier [11], which is described in the section "Functions of the BBB".

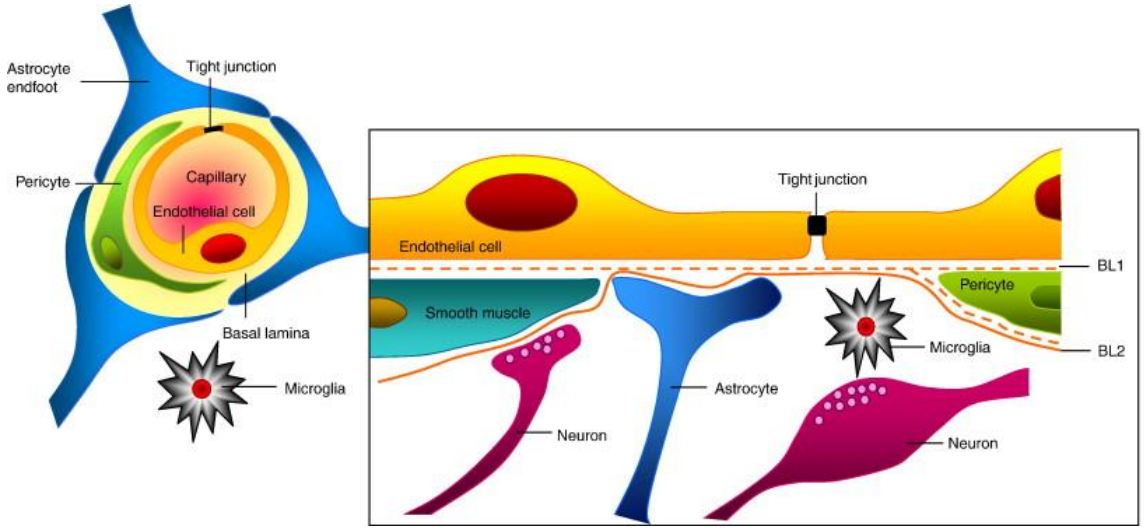

Figure 1: Schematic representation of the blood-brain barrier (BBB) in the human brain. Cerebral microvascular endothelial cells are connected to each other through tight junction (TJ) proteins and form a one cell layer thick lining that separates the bloodstream from brain tissue. Together with astrocytes, pericytes, neurons, and extracellular matrix (basal lamina), endothelial cells constitute a functional unit, which is often referred to as "neurovascular unit" [19]. Figure from Abbott et al. (2010) [10].

Tight junctions and adherens junctions

TJ proteins along with AJ proteins are responsible for the tight sealing of cerebral endothelial cells (Figure 2). AJ complexes are composed of the transmembrane proteins VE-cadherin and of the cytoplasmic scaffolding proteins α-, β-, and γ-catenin [6]. Cadherins are crucial for the mutual attachment of endothelial cells, and are required for the formation of TJs [17]. TJs, also called zonulae occludentes, are composed of the transmembrane proteins occludin, claudin-3, and claudin-5 [17]. In the intercellular cleft, they interact mutually with respective proteins from neighbouring cells, hence enabling a tight cellular attachment. Occludin and claudins are anchored in the endothelial cytosol with the scaffolding and regulatory zonula occludens proteins 1 to 3 (ZO-1, ZO-2, and ZO-3). ZO

proteins are in turn associated via cingulin, a 140 kDa protein localized in the cytoplasmic region of TJs [20], to the actin cytoskeleton of the cells. TJs in the human brain are denser than TJs in the peripheral vessels and rigorously restrict the paracellular diffusion of small polar molecules. Additionally, they act as a lateral fence and segregate transport proteins, efflux pumps, and lipid rafts, which enables a polarization of the endothelium [10]. Further proteins involved in cell-to-cell attachment are the junction-associated molecules (JAMs), and their expression affects TJ formation and function. JAMs belong to the immunoglobulin superfamily, and are believed to enable cell-adhesion of leukocytes to the endothelial cells [21].

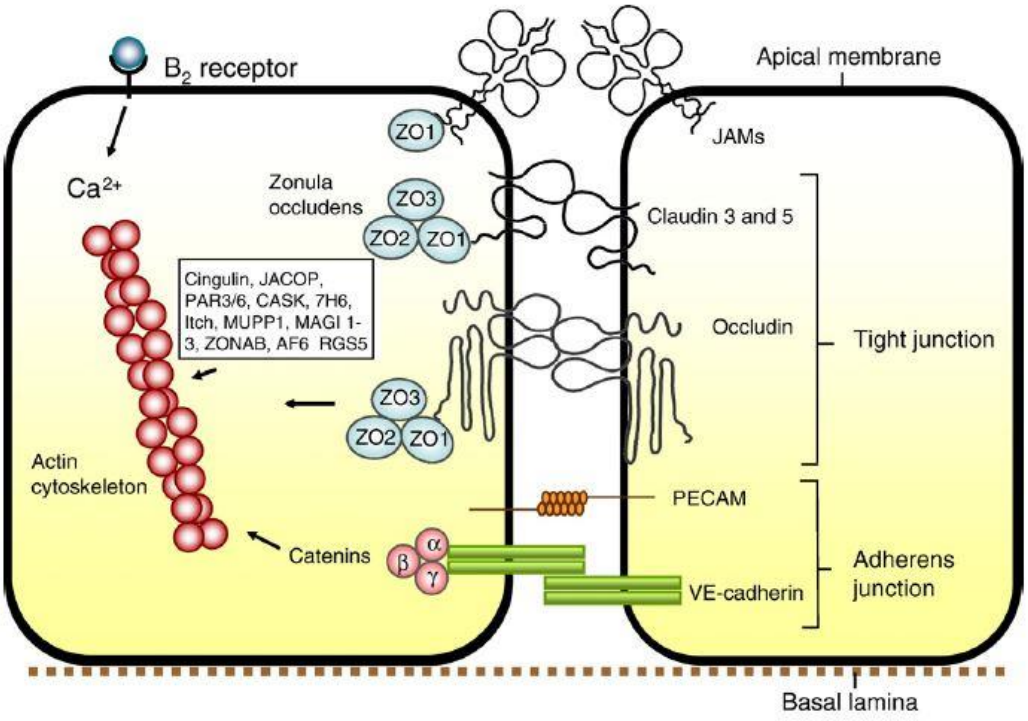

Figure 2: Brain microvascular endothelial cells are connected to each other through tight junctions (TJs), adherens junctions (AJs), and junction-associated molecules (JAMs). Figure from Abbott et al. (2010) [10].

Transport proteins at the BBB

At the luminal and abluminal sides of the plasma membranes of brain microvascular endothelial cells, various transmembrane proteins are expressed which mediate the transport of substances across the BBB [10,22,23]. These proteins may be expressed predominantly at only one side of the plasma membrane (either luminal or abluminal), resulting in polarized endothelial cells, and leading to preferential transport of compounds across the BBB in either a blood-to-brain or brain-to-blood direction [10,24]. Transporter proteins can be categorized into efflux pumps (belonging to the ATP-binding cassette (ABC) superfamily) and uptake transporters (belonging to the solute carrier (SLC) superfamily). Efflux pumps (ABC transporters) that are expressed in the luminal membrane of brain capillary endothelial cells, such as P-glycoprotein (P-gp), breast cancer resistance protein (BCRP),

multidrug resistance-associated proteins (MRP)-1, MRP-4, and MRP-5, transport substrate molecules from the endothelial cytosol back into the blood, and thus reduce brain exposure to drugs and toxicants [24]. Uptake transporters that are expressed in the luminal and abluminal membranes at the BBB, such as the organic anion transporter 3 (OAT3), mediate the uptake of various polar substances from the blood into the brain, thus providing the CNS with essential nutrients such as glucose, amino acids, nucleosides, and endogenous hormones [22–24]. In summary, all transport systems including ABC and SLC transport proteins work closely together to protect and support the brain [22].

Characteristics of the BBB

Brain capillaries show several unique features which distinguish them from blood vessels in the periphery. Cerebral capillary endothelial cells 1) form blood vessels which are tighter than anywhere else in the human body (due to the presence of denser TJs in the brain than in the periphery); 2) show a lower pinocytotic activity than other endothelial cells, resulting in reduced transcellular flux; 3) do not show wall fenestration, resulting in reduced paracellular flux [11]; 4) dispose of specialized transport systems across the endothelium [10,23]; and 5) have a higher mitochondrial content and high abundance of cytoplasmic enzymes such as cytochrome CYP3A4, indicating high metabolic activity [18,25]. All these characteristics lead to a unique physical barrier (tight vessels, low pinocytotic activity, no fenestration), transport barrier (efflux pumps and uptake proteins), and metabolic/enzymatic barrier (mitochondria and enzymes) [17].

Routes of transport across the BBB

There are various different transport routes of a substance across the BBB (Figure 3) [17]. Non-polar, lipid soluble substances may enter the brain by passive diffusion through the endothelial cell layer (Figure 3b). Some of the passively diffusing compounds, however, may be substrates of P-gp and/or BCRP or other efflux pumps, and may hence be pumped back into the bloodstream (Figure 3c). Polar and water soluble compounds are normally not able to cross the BBB (Figure 3a), unless these substances are substrates of uptake proteins (SLC transporters) that actively transport them from the bloodstream into the brain. Macromolecules may enter the central nervous system (CNS) via transcytosis, a process involving vesicles which transport their content across the endothelial cells. In receptor-mediated transcytosis, peptides and proteins bind to a specific receptor, whereupon internalization of ligand and receptor into the cell is initiated (Figure 3d). In adsorptive transcytosis, positively charged macromolecules adsorb to the cell surface in a non-specific manner, triggering endocytosis followed by transcytosis (Figure 3e). Cells such as leukocytes, monocytes, and macrophages may enter the CNS by diapedesis across the endothelial cell layer or, paracellularly, through altered TJs [10].

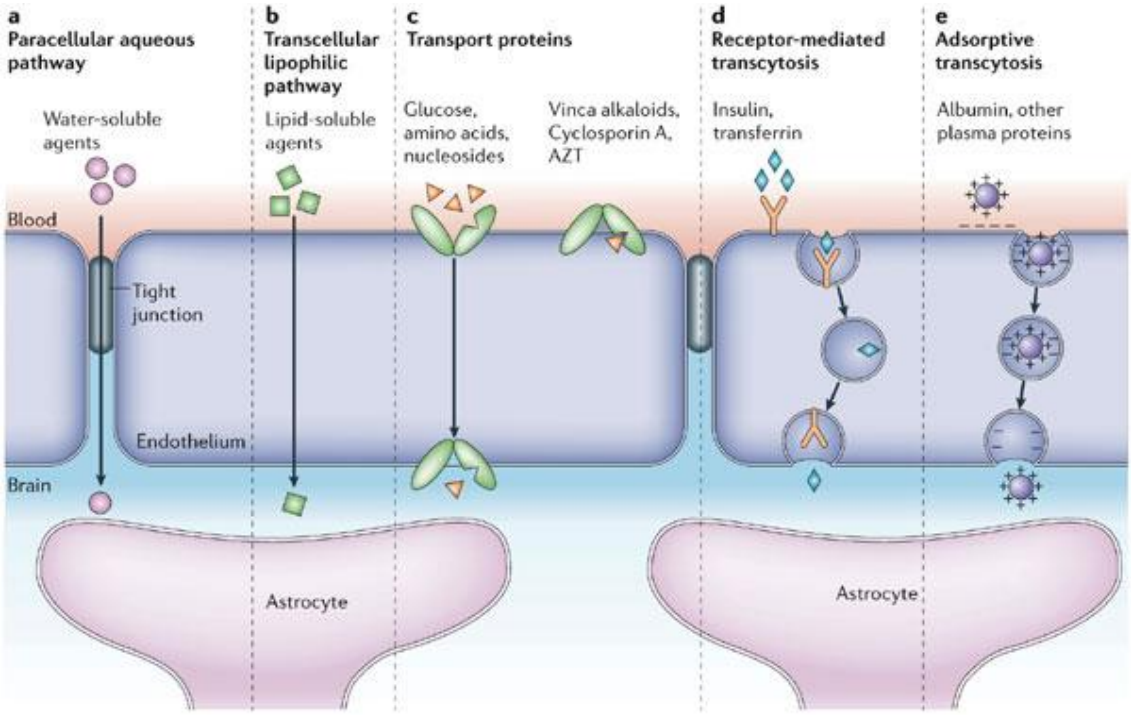

Figure 3: Routes of transport across the BBB. **(a)** Water soluble and polar substances may normally overcome a cellular barrier via the paracellular pathway. However, this route is greatly restricted at the BBB due to the presence of dense TJs. **(b)** Small lipophilic compounds may enter the brain by transcellular diffusion through the endothelial cells. **(c)** Lipophilic compounds that enter the endothelial cells by diffusion may be substrates of efflux pumps, and may hence be transported back into the bloodstream. On the other hand, small polar compounds (e.g. glucose, amino acids, and nucleosides) may be transported from the bloodstream into the endothelial cells via uptake transporters. Peptides and proteins may reach the brain via **(d)** receptor-mediated transcytosis or via **(e)** adsorptive transcytosis. Figure from Abbott et al. (2006) [17].

Functions of the BBB

The BBB serves several purposes: 1) it enables brain homeostasis for optimal neuronal signaling by protecting brain interstitial fluid (ISF) from ion fluctuations in the blood that may occur after meal or exercise (compared to blood plasma, brain ISF has a lower content of proteins, lower concentrations of K^+ and Ca^{2+}, but a higher concentration of Mg^+); 2) it prevents toxic endogenous metabolites, xenobiotics, and bacteria from entering the brain and, hence, causing damage to the nerve tissue; 3) it mediates efflux of waste products from the brain back into the bloodstream; 4) it supplies the brain with essential nutrients; 5) it separates the pools of neurotransmitters in the CNS and neuroactive agents in the periphery, enabling them to act in the two different compartments without interfering with each other. Taken together, the BBB enables, regulates, and maintains an appropriate microenvironment in the brain that is required for optimal CNS activity [17,24,26].

2.1.3 Other barriers in the central nervous system (CNS)

In addition to the BBB, further cellular barriers in the human brain exist, namely the blood-CSF barrier (BCSFB), the arachnoid barrier, the fetal CSF-brain barrier, and the blood-spinal cord barrier (BSCB) (Figure 4). The BCSFB is located at the choroid plexus in the four ventricles of the human brain and is formed by specialized epithelial cells (Figure 4b). These epithelial cells produce and secret CSF into the ventricles and build a physical barrier between intraventricular CSF and blood due to the presence of TJs between adjacent cells. Hence, paracellular diffusion of polar compounds from the blood directly into the CSF is reduced. In contrast to the BBB, the microvasculature underlying the epithelial choroid plexus cells shows fenestration, and is not the barrier itself. The BCSFB is thus a barrier built up by epithelial cells, and not by endothelial cells. At the brain-facing surface of the ventricles, neuroependymal cells form a functional barrier which separates CSF from brain parenchyma (Figure 4d). However, this barrier is only present in the embryo [3]. In the adult brain, the barrier function of the neuroependymal cells is lost, and free diffusion of molecules from one brain compartment to the other is possible (Figure 4e). A further barrier in the human brain is formed by the arachnoid membrane, which is a multi-layered epithelium completely enclosing the brain (Figure 4c) [10]. This barrier separates blood and subarachnoid CSF [17]. At last, a barrier between the blood and the spinal cord (BSCB) exists, which provides a specialized microenvironment for the cells constituting the spinal cord [27]. Similarly to the BBB, the BSCB is composed of nonfenestrated endothelial cells tightly sealed by TJ proteins [27,28].

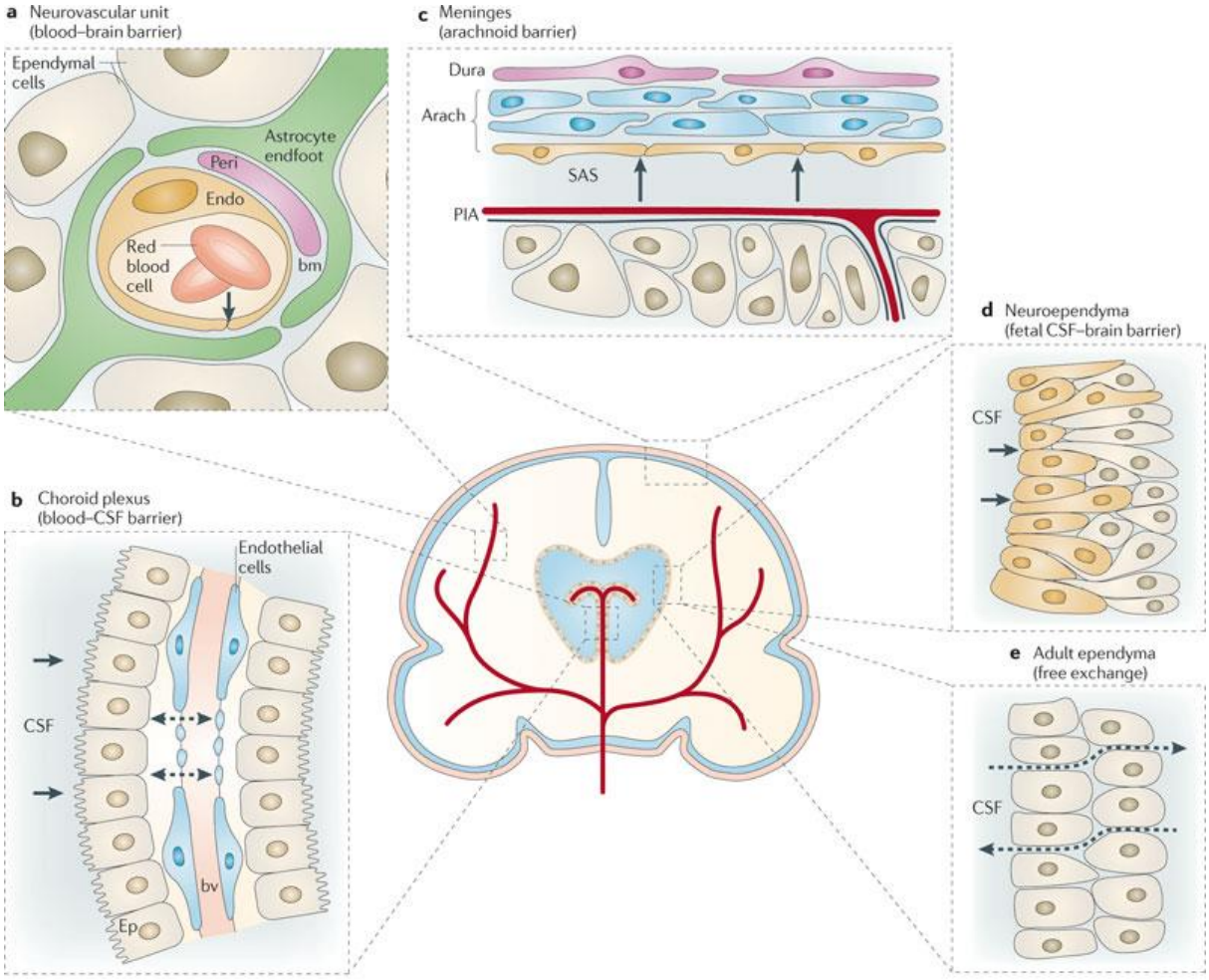

Figure 4: Cellular barriers in the human brain. **(a)** Blood-brain barrier (BBB). **(b)** Blood-CSF barrier (BCSFB). **(c)** Arachnoid barrier. PIA: pia mater, innermost layer of the meninges. SAS: CSF-filled subarachnoid space. **(d)** Fetal CSF-brain barrier, formed by neuroependymal cells separating CSF and brain parenchyma. This barrier is only present in the embryo. **(e)** In the adult brain, the barrier function of the neuroependymal cells on the brain-facing surface of the ventricles is lost, and free exchange of molecules from brain tissue into CSF is enabled. Figure from Neuwelt et al. (2011) [29].

2.1.4 Importance of the BBB for drug delivery to the brain

In order to elicit pharmacological effects at their target sites, CNS drugs need to penetrate the brain by permeating the barriers that separate the brain tissue from the bloodstream. Even though the BBB is not the only restrictive barrier in the human brain, it is by far the most important cerebral barrier from a pharmaceutical point of view. With a total surface area of 20 m^2 [12], the BBB disposes of the largest surface area for the exchange of substances from blood to brain [10]. Furthermore, each brain cell is very close to a brain vessel (separated by a distance of not more than approx. 25 µm), and practically every neuron is supplied by its own capillary [30]. Diffusion paths of drug molecules from endothelial cells to brain cells are thus short [10], which is particularly favorable for drug candidates targeting these cells. Intracerebroventricular (ICV) administration of drugs may be an alternative route

of drug delivery to the brain. ICV injected drugs, however, need to diffuse from the CSF compartments into brain tissue in order to reach their targets (e.g. neurons). In principle, this is possible, as the CSF-brain barrier in adults has lost its barrier function and free exchange of molecules from CSF into brain tissue is enabled (Figure 3e). However, this diffusion process is greatly counteracted by the CSF bulk flow from the ventricles through the subarachnoid space into the arachnoid villi [31]. Drugs administered ICV are, therefore, transported relatively rapidly out of the brain into the blood. Delivering drugs to the brain cells via the BBB remains thus the favored route of drug delivery to the brain [10].

References

[1] P. Ehrlich, Sauerstoff-Bedürfniss des Organismus. Eine farbenanalytische Studie, Berlin, 1885.
[2] D. Ribatti, B. Nico, E. Crivellato, M. Artico, Development of the blood-brain barrier: a historical point of view, Anat. Rec. 289B (2006) 3–8.
[3] S. Liddelow, Fluids and barriers of the CNS: a historical viewpoint, Fluids Barriers CNS. 8 (2011) 1–16.
[4] E.E. Goldmann, Die äussere und innere Sekretion des gesunden Organismus im Lichte der "Vitalen Färbung," H. Laupp'schen Buchhandlung, 1909.
[5] R. Leshan, T. Milner, D.W. Pfaff, Blood-brain barrier, in: D.W. Pfaff (Ed.), Neuroscience in the 21st century, Springer Verlag, New York Heidelberg Dordrecht London, 2013: pp. 1621–1629.
[6] T.S. Reese, M.J. Karnovsky, Fine structural localization of a blood-brain barrier to exogenous peroxidase, J. Cell. Biol. 34 (1967) 207–217.
[7] M.W. Brightman, T.S. Reese, Junctions between intimately apposed cell membranes in the vertebrate brain, J. Cell. Biol. 40 (1969) 648–677.
[8] R.D. Broadwell, B.J. Balin, M. Salcman, R.S. Kaplan, Brain-blood barrier? Yes and no, P. Natl. Acad. Sci. USA. 80 (1983) 7352–7356.
[9] D.M. Long, Capillary Ultrastructure and the blood-brain barrier in human malignant brain tumors, J. Neurosurg. 32 (1970) 127–144.
[10] N.J. Abbott, A.A.K. Patabendige, D.E.M. Dolman, S.R. Yusof, D.J. Begley, Structure and function of the blood-brain barrier, Neurobiol. Dis. 37 (2010) 13–25.
[11] J. Fenstermacher, P. Gross, N. Sposito, V. Acuff, S. Pettersen, K. Gruber, Structural and functional variations in capillary systems within the brain, Ann. NY Acad. Sci. 529 (1988) 21–30.
[12] W.M. Pardridge, Blood-brain barrier drug targeting: the future of brain drug development, Mol. Interventions. (2003) 90–105.
[13] K. Hayashi, S. Nakao, R. Nakaoke, S. Nakagawa, N. Kitagawa, M. Niwa, Effects of hypoxia on endothelial/pericytic co-culture model of the blood-brain barrier, Regul. Peptides. 123 (2004) 77–83.
[14] C. Kelley, P. D'Amore, H.B. Hechtman, D. Shepro, Microvascular pericyte contractility in vitro: comparison with other cells of the vascular wall, J. Cell. Biol. 104 (1987) 483–490.
[15] H.K. Rucker, H.J. Wynder, W.E. Thomas, Cellular mechanisms of CNS pericytes, Brain Res. Bull. 51 (2000) 363–369.
[16] G.W. Goldstein, A.L. Betz, Recent advances in understanding brain capillary function, Ann. Neurol. 14 (1983) 389–395.
[17] N.J. Abbott, L. Rönnbäck, E. Hansson, Astrocyte-endothelial interactions at the blood-brain barrier, Nat. Rev. Neurosci. 7 (2006) 41–53.
[18] M. Tajes, E. Ramos-Fernández, X. Weng-Jiang, M. Bosch-Morató, B. Guivernau, A. Eraso-Pichot, et al., The blood-brain barrier: Structure, function and therapeutic approaches to cross it, Mol. Membr. Biol. 31 (2014) 152–167.
[19] B.T. Hawkins, T.P. Davis, The blood-brain barrier/neurovascular unit in health and disease, Pharmacol. Rev. 57 (2005) 173–185.
[20] S. Citi, S. Paschoud, P. Pulimeno, F. Timolati, F. De Robertis, L. Jond, et al., The tight junction protein cingulin regulates gene expression and RhoA signaling, Ann. NY Acad. Sci. 1165 (2009) 88–98.
[21] B. Engelhardt, Development of the blood-brain interface, in: Blood-Brain Barriers, Wiley-VCH Verlag GmbH & Co. KGaA, 2006: pp. 9–39.
[22] S. Ohtsuki, M. Hirayama, S. Ito, Y. Uchida, M. Tachikawa, T. Terasaki, Quantitative targeted proteomics for understanding the blood–brain barrier: towards pharmacoproteomics, Expert Rev. Proteomics. 11 (2014) 303–313.
[23] B.L. Urquhart, R.B. Kim, Blood-brain barrier transporters and response to CNS-active drugs, Eur. J. Clin. Pharmacol. 65 (2009) 1063–1070.
[24] K.M. Giacomini, S.-M. Huang, D.J. Tweedie, L.Z. Benet, K.L.R. Brouwer, X. Chu, et al., Membrane transporters in drug development, Nat. Rev. Drug. Discov. 9 (2010) 215–236.
[25] E.H. Kerns, L. Di, Drug-like properties: concepts, structure design and methods: from ADME to toxicity optimization, Elsevier Inc., 2008.

[26] J. Bernacki, Physiology and pharmacological role of the blood-brain barrier, Pharmacol. Rep. 60 (2008) 600–622.
[27] V. Bartanusz, D. Jezova, B. Alajajian, M. Digicaylioglu, The blood-spinal cord barrier: morphology and clinical implications, Ann. Neurol. 70 (2011) 194–206.
[28] M.S. Alavijeh, M. Chishty, M.Z. Qaiser, A.M. Palmer, Drug metabolism and pharmacokinetics, the blood-brain barrier, and central nervous system drug discovery, NeuroRx. 2 (2005) 554–571.
[29] E.A. Neuwelt, B. Bauer, C. Fahlke, G. Fricker, C. Iadecola, D. Janigro, et al., Engaging neuroscience to advance translational research in brain barrier biology, Nat. Rev. Neurosci. 12 (2011) 169–182.
[30] A. Reichel, Addressing central nervous system (CNS) penetration in drug discovery: basics and implications of the evolving new concept, Chem. Biodiversity. 6 (2009) 2030–2049.
[31] W.M. Pardridge, Drug transport in brain via the cerebrospinal fluid, Fluids Barriers CNS. 8 (2011) 1–4.

2.2 CNS drug discovery

2.2.1 The burden of CNS disorders

Disorders of the CNS encompass an enormous diversity of psychiatric and neurological diseases. They are highly prevalent at all levels of society and represent an immense worldwide burden in many aspects [1]. Depression and schizophrenia, for instance, have been ranked by the World Health Organization (WHO) among the top ten leading causes for disability in males and females in the Global Burden of Disease report of 2008 [2]. Moreover, economical costs of brain diseases have been valued at nearly 800 billion US$ per year in the United States [1,3]. Due to the remarkable increase of the human life expectancy in the past century, CNS disorders that are associated with ageing (e.g. Alzheimer's and Parkinson's disease, brain cancer, stroke) are estimated to cause a financial burden of trillions of US dollars in the future [4,5]. Yet, the treatment of neuropsychiatric illnesses has so far remained relatively limited, and only a handful of new drugs with novel mechanisms of action has been approved in recent years [6]. New therapies that are more effective, act faster, and show fewer side effects for the treatment of CNS disorders are thus urgently needed [7].

2.2.2 Challenges in CNS drug discovery

Discovering and developing drugs is a long and expensive process. On average, it costs a pharmaceutical company 10–12 years and over 2 billion US$ to bring a single new drug to the market. For drugs targeting the CNS, this process has been estimated to be even more time-consuming (lasting up to 16 years) and costly, with the risk of failure being higher than in any other therapeutic area [5,8,9]. While on average 11% of drugs that enter clinical development reach the US market, only 3–5% of CNS drugs are eventually successful [6,10]. Reasons for this low success rate of neurotherapeutic drugs are manifold, but may be related, to a large extent, to the intricate anatomy and physiology of the human brain [11].

The human brain is one of the most complex organs of the human body. Despite tremendous advancements in diagnosing and treating CNS disorders in recent years, we still lack considerable knowledge about their etiology and underlying pathophysiology [3,11]. Identification of the right molecular targets in CNS drug discovery thus represents a major challenge [12]. With the successful sequencing of the human genome more than 10 years ago, a breakthrough was expected in this area [8,13]. It was anticipated that specific disease-associated genetic targets could be identified, facilitating the discovery of improved and more selective CNS drugs. However, neuropsychiatric diseases have shown to be linked to a large number of genes at the same time. For schizophrenia for instance, over 30 disease-associated genes have been identified, yet none of these has proven to be a

viable and specific drug target to date [13]. On the other hand, various genetic polymorphisms have been found to occur in several CNS disorders simultaneously, which drastically limits their attractiveness as selective biological targets [13].

Another persisting difficulty in CNS drug development is the lack of valid preclinical models. Experience has shown that animal models for neuropsychiatric disorders are mostly not able to correctly predict human efficacy [10]. While laboratory animals may certainly model various disease features and mechanisms, they are not able to model the disease itself [10].

Furthermore, clinical trials evaluating CNS drug efficacy are notoriously difficult to perform [14]. Obtaining sufficient numbers of study participants in the recruitment phase is challenging, and patient selection is problematic due the heterogeneity of brain illnesses coupled with relatively poor diagnosis techniques. Schizophrenia and depression, for example, are up to date still defined mainly by the patient's clinical symptoms rather than by pharmacological mechanisms. In clinical studies, where a mechanistic drug candidate is administered to patients that were diagnosed based only on symptoms, many non-responders may thus be found, concealing a possible positive outcome in a sub-population of patients [11]. Further difficulties are associated with the high liability of CNS drugs to cause potentially dangerous central side effects (e.g. dizziness and seizures), the frequently observed high placebo effect in control groups (particularly in studies of depression and anxiety), and the lack of valid biomarkers, resulting in ambiguous clinical endpoints [14].

Eventually, achieving adequate drug concentrations in the brain is difficult [15]. CNS drugs need to penetrate the brain, a process which is controlled by the BBB. This unique cellular barrier is highly restrictive to a wide spectrum of molecules and represents a major hurdle for neurotherapeutic drug candidates. In fact, only a minor percentage (2%) of small molecules has been estimated to successfully overcome the BBB [16]. Low permeation across the BBB, however, may lead to limited brain penetration of a compound and to inadequate concentrations at the target sites, culminating in insufficient efficacy [11,15].

Due to these difficulties, growing regulatory hurdles, and the increasing patient demand for safer, more efficacious, and innovative pharmaceuticals, bringing forward effective CNS drugs has proven to be one of the most difficult tasks for the pharmaceutical industry today [4,6,11]. This is reflected by the recent announcement of several Big Pharma companies such as GlaxoSmithKline (GSK), Astra Zeneca, and Pfizer to shut down their research activities within the neuroscience area [17,18]. Strategies that might increase the success rate of CNS pharmaceuticals are thus becoming more and more important for the future sustainability of neuroscience drug research [6].

2.2.3 How can the success rate of CNS drugs be improved?

Improving CNS drug discovery and development is a multi-facetted and difficult task [6]. For instance, endeavors should be made to identify novel CNS targets and disease pathways. Also, for each CNS disease, targeting multiple molecular targets and pathways may be of advantage due to the inherent complexity of neuropsychiatric illnesses [6]. Moreover, it is recommended to evaluate large numbers of structurally diverse compounds to have back-up lead candidates if compound-specific toxicity is encountered [6]. In order to avoid that a drug that has shown efficacy in animals fails later on in humans, efforts to develop better and more predictive preclinical models are urgently needed. Regarding clinical trials, pharmacogenetics might contribute to the identification and selection of study population groups that most likely respond to the administered drug. Furthermore, there is a need to develop valid biomarkers that indicate the presence, stage, and progression of the disease, which would enable more precise and concrete endpoints in clinical trials [14]. Finally, adequate exposure of the neurotherapeutic agent to the target within the CNS should be assessed, which includes the assessment of BBB permeability of drug candidates at an early stage of drug development [6]. Since there is no generally satisfying model for this purpose available today, there is an urgent need for better and valid *in vitro* BBB models which are amenable to the screening of compounds in a medium to high throughput manner.

2.2.4 CNS drug discovery and natural products

Natural products have played a significant role in the discovery process of new drugs since a long time. This is clearly reflected in the study by Newman and Cragg, in which 34% of all small molecule drugs that were approved by regulatory authorities from 1981 to 2010 were identified either as pure natural products (6%) or as natural product-derived substances (28%) [19]. Another 30% of the approved therapeutic agents were identified as "natural product mimics" (i.e. designed based on the information gained from a natural product) or as compounds that contain a pharmacophore from a natural product [19]. The main therapeutic areas where a large number of potent drugs have been developed from natural sources are infectious diseases and oncology [19]. However, also in the area of CNS diseases, several potent drugs have been discovered and developed from natural sources (Table 1) and various promising lead candidates are currently being tested in clinical trials [20].

Table 1: Selection of marketed CNS drugs originating from natural sources [20–24].

Drug (trade name)	Classification	Lead compound	Natural source	Year introduced	Mechanism	Indication
Morphine	NP	-	*Papaver somniferum*	Early 1800s	Opioid μ-receptor agonism	Pain
Acetylsalicylic acid (Aspirin)	NP derivative	Salicylic acid	*Salix species*	1899	COX inhibition	Pain
Dihydro-ergotamine (Dihydergot)	NP derivative	Ergotamine	*Claviceps species*	1946	Serotonin receptor agonism	Migraine and cluster headache
Bromocriptin (Parlodel)	NP derivative	Ergot alkaloids	*Claviceps species*	1975	Dopamine receptor agonism	Hyperprolactinemia, Parkinson's disease
Rivastigmine (Exelon)	NP analog	Physostigmine	*Physostigma venenosum*	1997	AChE inhibition	Alzheimer's disease
Galanthamine (Reminyl)	NP	-	*Galanthus nivalis*	2001	AChE inhibition	Alzheimer's disease
Ziconotid (Prialt)	Synthetic form of NP	ω-Conotoxin (peptide)	*Conus magnus*	2005	N-type voltage-sensitive calcium channel blocking	Severe chronic pain
Fingolimod (Gilenya)	NP analog	Myriocin	*Isaria singclairii*	2010	Sphingosine 1-phosphate receptor modulation	Multiple sclerosis

NP: natural product; AChE: acetylcholinesterase; COX: cyclooxygenase

Despite the undisputed success of pharmaceuticals originating from natural sources, pharmaceutical companies have largely reduced or even stopped their research activities in the natural products sector in the past decades and have shifted to more synthetic approaches [25]. Novel techniques such as combinatorial chemistry and high-throughput screening in the early 1990s have enabled the establishment of large synthetic compound libraries and the fast identification of synthetic lead molecules against biological targets. With the rapid turnaround of high-throughput-based discovery programs however, the classical and rather slow approach of natural product-based drug discovery could initially not keep up and received less and less attention [26,27].

Finding lead candidates from nature is linked to a variety of challenges. Secured access and supply of the natural source may, for example, be problematic and can be severely hampered by intellectual property issues [25]. Even if supply of the source is warranted, crude extracts are in the majority of the cases highly complex mixtures and may contain the biologically active compound only in extremely small amounts, which may complicate the supply of the drug candidate for preclinical and clinical studies if total synthesis is not feasible [25,28]. When plant extracts or fractions are subjected to high-throughput screening, several constituents may exert synergistic or antagonistic effects at the biological target (which may be lost upon separation of the compounds), and stability and solubility issues of the bioactive compound in the extract or solvent may be encountered [25]. Additionally,

bioactive natural products are likely to be highly complex in their structure, which may decelerate the identification and structure elucidation process [25].

Interestingly, despite considerable efforts and investments, the economic output of the synthetic approach to find new lead candidates has remained relatively modest to date [29]. This may be attributable to the fact that natural products are much more complex and diverse in their molecular structure compared to synthetic compounds, and often exhibit highly selective biological activities [30]. Furthermore, since natural products are natural metabolites, they are more likely to be the substrates of carrier proteins that can transport the compounds to an intracellular therapeutic target [26]. These assets of natural compounds, together with remarkable technological improvements, have contributed to the recent revived interest in drug discovery from natural sources [26]. Notably, only few higher plants (6% of the approximately 300'000 known species) and microorganisms, and hardly any marine sources, have been investigated pharmacologically [30]. Nature is therefore expected to retain a vast unexplored potential of compound diversity, and natural products are believed to continue being a valuable direct and indirect source in the discovery of pharmaceuticals for the treatment of human illnesses.

2.2.5 $GABA_A$ receptors – example of an important pharmacological target in the CNS

The γ-aminobutyric acid type A ($GABA_A$) receptors are ligand-gated ion channels in the membrane of neurons that mediate most fast synaptic inhibition in the CNS [31,32]. They are composed of five protein subunits of different classes forming a central pore selective for chloride ions [33,34]. Upon activation by the endogenous neurotransmitter GABA, the ion channels open, leading to an increased anion influx into the neuronal cell. This causes a hyperpolarization of the cell membrane and inhibition of neuronal activity [31]. Depending on their subunit composition, $GABA_A$ receptors exhibit distinct physiological and pharmacological properties [32].

Compounds that positively modulate $GABA_A$ receptors, such as the benzodiazepines, are currently used to treat a large variety of CNS diseases including anxiety, panic disorders, sleep disturbances, depression, and epilepsy [35]. However, these drugs lack $GABA_A$ receptor subtype selectivity, and induce thus clinically relevant side effects such as amnesia, unwanted sedation, and drug dependence, complicating their long-term application [35]. Hence, there is a high medical need for novel compounds that selectively interact with $GABA_A$ receptor subtypes and thus exhibit a lower adverse effect profile. Interestingly, various promising natural product derived lead candidates with selective $GABA_A$ receptor modulatory activity have been identified in recent years [36–39]. These compounds will need to be further evaluated in terms of their pharmacokinetic and toxicokinetic profile and, importantly, regarding their ability to permeate the BBB.

References

[1] J. Kelly, Principles of CNS drug development: from test tube to patient, 1st ed., John Wiley and Sons (Wiley-Blackwell), Chichester, West Sussex, UK, 2009.

[2] World Health Organization, The global burden of disease: 2004 update (2008) 1–160.

[3] D.J. Nutt, J. Attridge, CNS drug development in Europe – past progress and future challenges, Neurobiol. Dis. 61 (2014) 6–20.

[4] A.K. Ghose, T. Herbertz, R.L. Hudkins, B.D. Dorsey, J.P. Mallamo, Knowledge-based, central nervous system (CNS) lead selection and lead optimization for CNS drug discovery, ACS Chem. Neurosci. 3 (2012) 50–68.

[5] I. Kola, J. Landis, Can the pharmaceutical industry reduce attrition rates?, Nat. Rev. Drug Discov. 3 (2004) 711–716.

[6] M.N. Pangalos, L.E. Schechter, O. Hurko, Drug development for CNS disorders: strategies for balancing risk and reducing attrition, Nat. Rev. Drug Discov. 6 (2007) 521–532.

[7] H.K. Manji, E.B. DeSouza, CNS drug discovery and development: when will we rescue Tantalus?, Neuropsychopharmacol. 2 (2008) 1–4.

[8] M.S. Alavijeh, M. Chishty, M.Z. Qaiser, A.M. Palmer, Drug metabolism and pharmacokinetics, the blood-brain barrier, and central nervous system drug discovery, NeuroRx. 2 (2005) 554–571.

[9] A.M. Palmer, F.A. Stephenson, CNS drug discovery: challenges and solutions, Drug News Perspect. 18 (2005) 51–57.

[10] O. Hurko, J.L. Ryan, Translational research in central nervous system drug discovery, NeuroRx. 2 (2005) 671–682.

[11] A. Reichel, Addressing central nervous system (CNS) penetration in drug discovery: basics and implications of the evolving new concept, Chem. Biodiversity. 6 (2009) 2030–2049.

[12] J.C. Barnes, A.G. Hayes, CNS drug discovery realising the dream, Drug Discovery World Fall 2002 (2002) 54–57.

[13] S.J. Enna, M. Williams, Challenges in the search for drugs to treat central nervous system disorders, J. Pharmacol. Exp. Ther. 329 (2009) 404–411.

[14] J. Skripka-Serry, The great neuro-pipeline brain drain (and why Big Pharma hasn't given up on CNS disorders) Drug Discovery World Fall 13 (2013) 9–16.

[15] A.K. Deo, F.-P. Theil, J.-M. Nicolas, Confounding parameters in preclinical assessment of blood-brain barrier permeation: an overview with emphasis on species differences and effect of disease states, Mol. Pharmaceutics. 10 (2013) 1581–1595.

[16] W.M. Pardridge, The blood-brain barrier: bottleneck in brain drug development, Neurotherapeutics. 2 (2005) 3–14.

[17] A.A. Nierenberg, The perfect storm: CNS drug development in trouble, CNS Spectr. 15 (2010) 282–283.

[18] G. Wegener, D. Rujescu, The current development of CNS drug research, Int. J. Neuropsychoph. 16 (2013) 1687–1693.

[19] D.J. Newman, G.M. Cragg, Natural products as sources of new drugs over the 30 years from 1981 to 2010, J. Nat. Prod. 75 (2012) 311–335.

[20] B.B. Mishra, V.K. Tiwari, Natural products: an evolving role in future drug discovery, Eur. J. Med. Chem. 46 (2011) 4769–4807.

[21] G. Orhan, I. Orhan, N. Subutay-Oztekin, F. Ak, B. Sener, Contemporary anticholinesterase pharmaceuticals of natural origin and their synthetic analogues for the treatment of alzheimers disease, Recent Pat. CNS Drug Discov. 4 (2009) 43–51.

[22] A. Bauer, M. Brönstrup, Industrial natural product chemistry for drug discovery and development, Nat. Prod. Rep. 31 (2013) 35–60.

[23] P.L. Schiff, Ergot and its alkaloids, Am. J. Pharm. Educ. 70 (2006) 1–10.

[24] O. Potterat, M. Hamburger, Drug discovery and development with plant-derived compounds, in: F. Petersen, R. Amstutz (Eds.), Natural Compounds as Drugs Volume I, Birkhäuser Basel, 2008: pp. 45–118.

[25] J.W.-H. Li, J.C. Vederas, Drug discovery and natural products: end of an era or an endless frontier?, Science. 325 (2009) 161–165.

[26] A.L. Harvey, R. Edrada-Ebel, R.J. Quinn, The re-emergence of natural products for drug discovery in the genomics era, Nat. Rev. Drug Discov. 14 (2015) 111–129.
[27] O. Potterat, M. Hamburger, Concepts and technologies for tracking bioactive compounds in natural product extracts: generation of libraries, and hyphenation of analytical processes with bioassays, Nat. Prod. Rep. 30 (2013) 546–564.
[28] I. Paterson, E.A. Anderson, The renaissance of natural products as drug candidates, Science. 310 (2005) 451–453.
[29] X. Chen, M. Decker, Multi-target compounds acting in the central nervous system designed from natural products, Curr. Med. Chem. 20 (2013) 1673–1685.
[30] G.M. Cragg, D.J. Newman, Natural products: a continuing source of novel drug leads, Biochim. Biophys. Acta. 1830 (2013) 3670–3695.
[31] F.A. Stephenson, The GABAA receptors, Biochem. J. 310 (1995) 1–9.
[32] T.C. Jacob, S.J. Moss, R. Jurd, GABAA receptor trafficking and its role in the dynamic modulation of neuronal inhibition, Nat. Rev. Neurosci. 9 (2008) 331–343.
[33] E. Sigel, M.E. Steinmann, Structure, function, and modulation of GABAA receptors, J. Biol. Chem. 287 (2012) 40224–40231.
[34] M. Uusi-Oukari, E.R. Korpi, Regulation of GABAA receptor subunit expression by pharmacological agents, Pharmacol. Rev. 62 (2010) 97–135.
[35] H. Möhler, GABAA receptors in central nervous system disease: anxiety, epilepsy, and insomnia, J. Recept. Signal. Tr. 26 (2006) 731–740.
[36] J. Zaugg, I. Baburin, B. Strommer, H.-J. Kim, S. Hering, M. Hamburger, HPLC-based activity profiling: discovery of piperine as a positive GABAA receptor modulator targeting a benzodiazepinei binding site, J. Nat. Prod. 73 (2010) 185–191.
[37] J. Zaugg, S. Khom, D. Eigenmann, I. Baburin, M. Hamburger, S. Hering, Identification and characterization of GABAA receptor modulatory diterpenes from *Biota orientalis* that decrease locomotor activity in mice, J. Nat. Prod. 74 (2011) 1764–1772.
[38] J. Zaugg, E. Eickmeier, S.N. Ebrahimi, I. Baburin, S. Hering, M. Hamburger, Positive GABAA receptor modulators from *Acorus calamus* and structural analysis of (+)-dioxosarcoguaiacol by 1D and 2D NMR and molecular modeling, J. Nat. Prod. 74 (2011) 1437–1443.
[39] D.C. Rueda, M. De Mieri, S. Hering, M. Hamburger, HPLC-based activity profiling for GABAA receptor modulators in *Adenocarpus cincinnatus*, J. Nat. Prod. 77 (2014) 640–649.

2.3 Models to predict brain penetration

2.3.1 Brain penetration of drugs

Brain penetration of drugs has two fundamental components: 1) *rate* (at the initial state), and 2) *extent* (at steady state) (Figure 5) [1]. The *rate* of brain penetration depends on the permeability of the compounds across the BBB (by passive diffusion, active uptake and/or efflux). The *extent* of brain penetration is determined by the distribution of the drug between brain and plasma, and is affected by multiple factors including metabolic clearance, plasma protein binding, non-specific binding to brain tissue, and drug clearance from brain ISF into CSF [2]. Models to assess CNS penetration have typically been designed to measure either one of these two components (rate or extent).

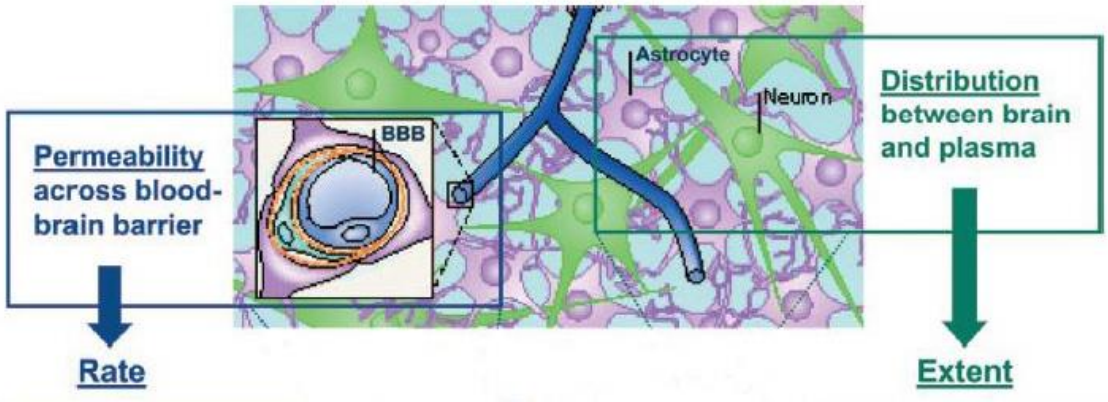

Figure 5: CNS penetration of a drug is impacted by the permeation across the BBB (determining the *rate* of penetration), and by the distribution to (and within) the brain (determining the *extent* of penetration). Figure modified from Reichel A. (2009) [3].

In the past decades, a broad spectrum of *in silico*, *in vitro*, and *in vivo* models providing parameters on different aspects of brain penetration has been developed and implemented in academia and industry to bring forward molecules with high potential for CNS exposure. In the following sections, several important models are discussed in more detail (for extensive reviews, please refer to references [4–7]).

2.3.2 Rule-based approaches and *in silico* models

Brain penetration of a molecule is greatly affected by its physicochemical properties such as lipophilicity, polar surface area (PSA), molecular weight (MW), hydrogen bonding, and ionization state. Researchers have therefore analyzed many data sets of CNS drugs and proposed various recommendations in terms of physicochemical properties required for optimal brain penetration. One

of the first set of rules was introduced in 1995 by Pardridge [8]. He stated that BBB permeability of a drug is likely if the number of total H-bonds is < 8–10, the MW < 400–600 Da, and if the compound is not an acid [8]. Subsequent studies have suggested that BBB permeation is favored if the sum of oxygen and nitrogen is ≤ 5, the PSA < 60–70 $Å^2$, the MW < 450 Da, and the LogD (at pH 7.4) between 1–3 [9–11].

Due to the increased need for high throughput methods in drug discovery in the past years, computational models to predict rate and extent of brain penetration of drug molecules have become increasingly popular. Various software programs have been developed, which are commercially or freely available (e.g. B_3PP by Martins et al. 2012 [12]). These models are considerably cheaper and faster compared to *in vitro* and *in vivo* methods, thus offering the great advantage of high screening capability at early stages of the drug discovery process. Nevertheless, data obtained by *in silico* experiments must be interpreted with caution, as many factors that affect CNS drug exposure (efflux, uptake, plasma protein and brain tissue binding, metabolic clearance etc.) complicate the correct modeling of drug brain penetration.

2.3.3 *In vitro* models

In vitro models can be subdivided into physicochemical methods and cell-based methods. The latter are performed using living cells, and are considered to be closer to the physiological BBB than physicochemical methods [13]. Generally, *in vitro* assays are applicable to medium to high throughput screening (depending on the assay set-up), and provide important information on BBB permeability (passive diffusion, efflux and/or uptake) and brain distribution at a relatively early stage of drug discovery and development.

Physicochemical methods

PAMPA-BBB (rate): The parallel artificial membrane permeation assay for BBB (PAMPA-BBB) is a simple and rapid method to predict passive transcellular diffusion of a compound through the BBB (which is mimicked by a porcine brain lipid extract on a solid support). The assay is a modification of the original PAMPA method, which was developed by Kansy et al. for intestinal permeability studies [14]. Advantages of the assay are its high throughput capability, its reproducibility, and the low associated costs. The main drawback of the method, however, is that it only provides information on passive BBB permeation of a drug [13].

IAM-HPLC (rate): Immobilized artificial membrane high performance liquid chromatography (IAM-HPLC) is a further method to predict BBB permeability of a compound [13]. For this technique, a HPLC system and a commercially available IAM column (packed with a stationary phase consisting of phospholipids bonded to the solid support) are required. By comparing retention times of test

compounds with those of standard drugs, BBB permeation of the former can be estimated. Limitations of the method are that prediction of BBB permeability may be poor if brain uptake is affected by active transport, plasma protein binding and/or metabolism, and that the approach has proved to be unsuitable for medium to high throughput operation [2,6].

Equilibrium dialysis (extent): Equilibrium dialysis is a high throughput *in vitro* method to obtain information on protein binding in brain homogenate and plasma and, hence, on the free (unbound) drug fractions in both matrices. On the one hand, information on free drug fractions in plasma is important as only unbound molecules are available to cross the BBB. Thus, if plasma protein binding is too high, the extent of brain penetration may be insufficient [15]. However, attention must be paid when using *in vitro* data on plasma protein binding of compounds. It has been shown that bound molecules within brain capillaries are able to dissociate more readily than in *in vitro* models, and thus the bioavailable fraction *in vivo* may be higher than expected [15]. Unbound drug fractions in the brain, on the other hand, can be used for the calculation of unbound drug concentrations in the brain, if *in vivo* data on total brain levels are available [16]. Finally, the ratio of free plasma to free brain fraction has been suggested as a parameter to predict the *in vivo* extent of brain distribution [17].

Cell-based methods

Isolated brain capillaries (rate): Brain microvessels from human or animal sources have been used in BBB research since their successful isolation more than three decades ago [18]. However, they are not suitable for *in vitro* BBB permeability screenings since the luminal side (blood side) of the capillaries is hardly accessible [5].

Cell culture models (rate): Cell-based *in vitro* BBB methods are used for the determination of the permeability of a compound across the BBB. Major advantages of these models are that, depending on the selection of cells, information on possible transporter interaction (e.g. P-gp and BCRP) can be obtained in addition to data on passive transcellular diffusion.

Cell culture-based models are primarily carried out in two-chamber vertical diffusion systems (branded as "Transwell" systems by Corning Costar®), which consist of commercial well plates and corresponding tissue culture inserts (available in the 6, 12, 24, and 96-well format) (Figure 6). Animal or human cells are seeded onto the semi-permeable filter membrane at the bottom of the tissue culture inserts, where they form a confluent monolayer mimicking the BBB. Usually, the filter membranes are coated with collagen or other structural proteins (representing the basal lamina). The test compound is introduced into the apical (luminal) compartment (blood side) of the two-chamber system, and the velocity of the compound to appear in the basolateral (abluminal) compartment (brain side) by diffusion through the cell monolayer is quantified, providing apparent or endothelial permeability coefficients (abbreviated as P_{app} or P_e, respectively, usually in the unit cm/s). To obtain information on

possible transporter interaction of a compound, the permeability experiments can be carried out in the reverse direction (from basolateral to apical). The ratio of the basolateral-to-apical to the apical-to-basolateral permeability (= efflux ratio, ER) reflects the potential of a compound to be transported out of or into the brain by efflux or uptake proteins (efflux is assumed if the ER is > 2, uptake if the ER is < 0.5) [19,20].

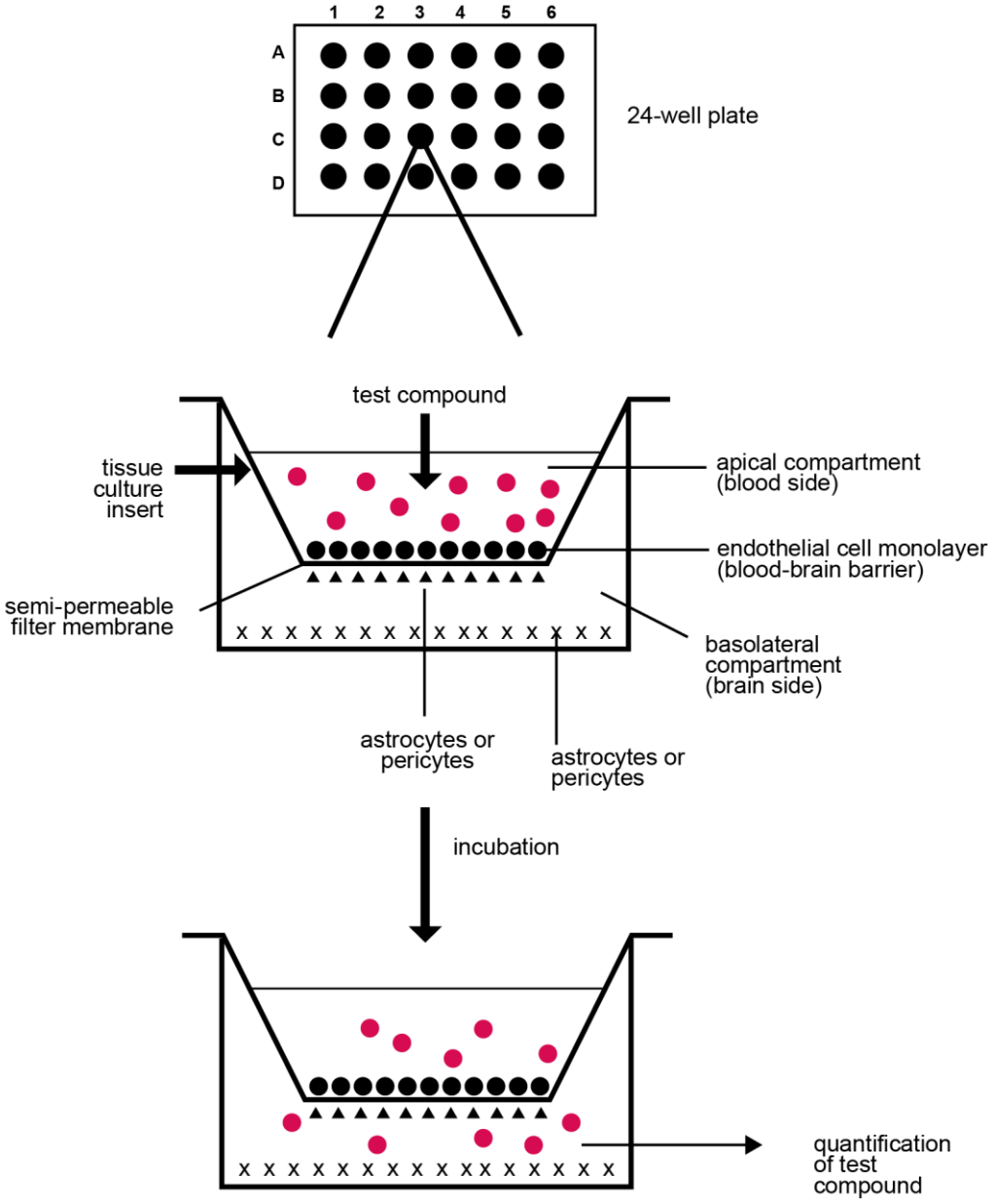

Figure 6: *In vitro* BBB model (24-well format) for the prediction of BBB permeability of a drug. Cells from animal or human origin are grown on collagen coated semi-permeable filter membranes of the tissue culture inserts, where they form a cell monolayer representing the BBB. Depending on the model, astrocytes and/or pericytes are cultured at the bottom of the wells or at the bottom side of the inserts. Test compounds are placed into the apical or basolateral chamber of the Transwell system, and their passage to the other compartment is measured over time. Figure by Tabea Gollin (2015).

The first *in vitro* BBB model using the two-chamber vertical diffusion system was established by Bowman et al. in 1983 by using freshly isolated bovine brain endothelial cells [21]. Since then, primary cells (i.e. cells directly obtained from living tissue) from porcine, murine, rat, monkey, and human origin have been used for the implementation of *in vitro* BBB models [22]. As mono-culture systems (with only endothelial cells) represent extremely simplified models, other brain-derived cells being part of the neurovascular unit, such as astrocytes, pericytes, and/or neurons have been incorporated into double and triple co-culture *in vitro* BBB models (Figure 6). Several of these cells (in particular astrocytes) have repeatedly been shown to favorably induce barrier tightness of endothelial cells [23,24].

The use of primary cells, however, suffers from various restraints. Isolation and purification procedures of the cells are cumbersome and time-consuming, the yield of cells is relatively low, the lifespan of cells is limited (rapid de-differentiation and loss of phenotype occur), and animal endothelial cells show differences in the expression of uptake proteins and efflux pumps when compared to human endothelial cells [25,26]. The use of primary cultures from human origin would avoid interspecies pharmacogenetic variation, but the availability of these cells is greatly limited due to ethical reasons.

Therefore, various immortalized cell lines from human and animal origin (Tables 2 and 3) have been used to model the BBB *in vitro*. These cell lines originate either from spontaneous transformation of the cells into tumor cells (e.g. ECV304), or were generated by transfection with a tumor gene (e.g. SV40 large-T antigen) after their isolation. Unlike primary cells, immortalized cells are easy to culture, proliferate indefinitely, and preserve their differentiating properties even after repetitive passaging. These properties render them highly suitable for high throughput and standardized screenings. Among immortalized cell lines, those originating from human brains are of greatest interest. Regrettably, currently available human brain capillary endothelial cell lines (Table 2) often show deficiencies (e.g. low transendothelial electrical resistance (TEER) values, relatively high paracellular permeation of negative control compounds, insufficient expression of key transporter systems). Hence, systematic optimization of culture conditions and careful validation of human cell line-based *in vitro* BBB models are needed. Significant advances in modeling the human BBB *in vitro* have been achieved recently by using endothelial cells derived from human pluripotent and hematopoietic stem cells [27,28]. As stem cells offer a high capacity of expansion by self-renewal while maintaining a homogenous genetic profile, stem cell-based models are promising, but require systematic benchmarking against established *in vitro* and *in vivo* models [29].

Table 2: Immortalized human brain capillary endothelial cell lines for the establishment of *in vitro* human BBB models.

Brain capillary endothelial cell line	Transfection method	Year (first publication)	Reference
BB19	E6E7 genes of HPV	1996	Prudhomme et al. [30]
HBEC-5I	SV40T	1996	Xiao et al. [31]
SV-HCEC	SV40T	1997	Muruganandam et al. [32]
hBMEC	SV40T	2001	Stins et al. [33]
hTERT-HBEC	hTERT	2003	Gu et al. [34]
hCMEC/D3	hTERT and SV40T	2005	Weksler et al. [35]
NKIM-6	E6E7 genes of HPV type 16	2007	Ketabi-Kiyanvash et al. [36]
TY08	hTERT and temperature-sensitive SV40T	2010	Sano et al. [37]
TY09	hTERT and temperature-sensitive SV40T	2010	Sano et al. [37]
HBMEC/ciβ	hTERT and temperature-sensitive SV40T	2012	Kamiichi et al. [38]
TY10	hTERT and temperature-sensitive SV40T	2012	Maeda et al. [39]

HPV: human papilloma virus; SV40T: simian virus 40 large-T antigen; hTERT: human telomerase reverse transcriptase

Table 3: Immortalized animal and non-brain human cell lines used to model the BBB *in vitro*.

Cell line	Description	Origin	Remarks
Caco-2	Human epithelial colon adenocarcinoma cell line	Human (colon)	Limited prediction of BBB permeability (poor correlation of *in vitro* Caco-2 and *in vivo* BBB permeability data) [40]
ECV304	Human endothelial umbilical vein (HUVEC) cell line [41]	Human (umbilical cord)	Non-brain origin, but cells show endothelial features, barrier tightness can be increased (up to TEER of 200 Ωcm^2) by co-cultivation with immortalized rat glioma cells (C6 cell line) or C6 conditioned medium [6,22]
LLC-PK1	Porcine kidney epithelial cell line [42]	Pig (kidney)	Relatively tight monolayers, cell line can be transfected with transporter genes (e.g. MDR1) for efflux studies
MDCK	Madin Darby Canine Kidney epithelial cell line [43]	Dog (kidney)	Tight monolayers (high TEER values), assay straight forward (3–4 days of culture), but only useful for determination of passive permeation (due to low expression of transporter proteins) [44,45]
MDR1-MDCK (type I or II) and BCRP-MDCK	MDCK transfected with human MDR1 gene (P-gp) or BCRP	Dog (kidney)	Tight monolayers (high TEER values), polarized expression of P-gp/BCRP, useful for P-gp/BCRP efflux studies (bidirectional transport assays) [46]
RBE4	Rat brain capillary endothelial cell line [47]	Rat (brain)	Leaky monolayers (relatively high permeability to small molecules) [47]
cEND	Murine immortalized brain (cerebral) capillary endothelial cell line [48]	Mouse (brain)	Relatively tight monolayers depending on cultivation protocol (TEER values up to 1000 Ωcm^2) [48]
bEnd3 and bEnd5	Mouse brain micro-vascular endothelial cell lines [49,50]	Mouse (brain)	Leaky monolayers (relatively low TEER values: bEnd3 40–130 Ωcm^2, bEnd5 around 120 Ωcm^2) [22,51]

TEER: transendothelial electrical resistance (reflects barrier tightness); TEER *in vivo* has been estimated to exceed 1000 Ωcm^2 [52,53]

2.3.4 *In vivo* models

In vivo models to assess CNS exposure of drug candidates provide some of the most reliable data concerning BBB permeability (rate) and brain distribution (extent) [2]. However, the methods are labor-intensive and low throughput, and are therefore mainly applied at later stages of the drug development process. Furthermore, *in vivo* methods are mostly not applicable to humans (with a few exceptions such as CSF sampling and receptor occupancy studies). This represents a major challenge, as *in vivo* data on brain penetration from animal models can be confounded due to species differences (e.g. in the expression and functional activity of efflux and uptake transporters, in brain lipid composition, and rate of CSF production) [54].

***In situ* brain perfusion (rate):** *In situ* brain perfusion is a generally accepted and reliable method to determine BBB permeability of a drug [46]. A catheter is inserted into the common carotid artery of an anesthetized animal (rat, mouse, guinea pig, rabbit) and a solution containing the test compound is slowly perfused through the brain capillaries [55]. Drug concentrations are quantified in the perfused brain hemisphere of the sacrificed animals, and permeability surface area (PS) values, reflecting BBB permeability, are calculated [56]. Limitations of the method are that it is costly, labor-intensive, and requires surgical skills and expertise [2].

Total brain-to-plasma ratio (extent): Determination of the total brain-to-plasma ratio (K_p) is the most widely implemented *in vivo* method to obtain data on brain distribution [13]. After animals are dosed with a test drug, they are sacrificed at designated time-point(s), and drug concentrations in brain homogenate and blood plasma are quantified. K_p values (or logBB = logarithm of K_p) are subsequently calculated based on the respective drug concentrations or areas under the curve (AUC) from both matrices ($K_p = C_{brain}/C_{plasma}$ or AUC_{brain}/AUC_{plasma}). Single time-point K_p values are of limited reliability, especially if the selected time-point was before the system could reach steady state [2,16]. K_p values based on AUC may be more useful, but require more resources in terms of costs, labor, and animals [54]. A disadvantage of this method is that K_p values are primarily determined by non-specific binding of a substance to brain tissue [57]. Optimizing drug candidates in terms of this parameter may thus bring forward only very lipophilic compounds with high non-specific binding to brain tissue, resulting in lower free drug concentrations at the target site.

Brain microdialysis (extent): Brain microdialysis is the method of choice to determine the free concentration of a compound in brain ISF [16]. A microdialysis probe with a semi-permeable membrane at the tip is implanted into a specific brain region of an animal (rat or mouse). Unbound molecules in brain ISF below a certain molecular weight freely diffuse through the membrane, and are captured in the fluid perfused through the microdialysis probe [58]. The unbound brain concentration can then be related to the unbound drug concentration in plasma, providing the parameter $K_{p,uu}$

(unbound brain-to-plasma ratio), which has proved to be more predictive than K_p values (total brain-to-plasma ratios) [3]. Regrettably, brain microdialysis is a technique with several limitations. Local brain tissue and the BBB may be damaged during implantation of the microdialysis probe, depending on the shape of the probe, surgical procedure, and technical skills. Additionally, problems with lipophilic compounds adsorbing to the membrane of the probe may be encountered. Also, due to its invasiveness, the method cannot readily be applied to humans [59].

CSF sampling (extent): CSF sampling is one of the few *in vivo* methods applicable to humans. Various studies have suggested using CSF concentrations to predict free drug concentration in brain ISF (as CSF protein levels are very low, and because CSF and brain ISF compartments are separated from each other by only a single layer of ependymal cells). However, data interpretation of CSF levels is complicated by the fact that molecules may enter the CSF compartment via the BCSFB, a barrier that differs in its transport activity from the BBB [60]. Hence, if a drug is subject to active uptake or efflux at only one of the two barriers, CSF concentrations will not correctly predict free drug concentrations in brain ISF. Further limitations of the method are the high turnover rate of CSF (around 6 hours in humans), which requires that CSF sampling is done at very specific time-points, and that the CSF compartment is not well-mixed, resulting in varying concentrations depending on the site of sample collection [19,54].

2.3.5 Favorable brain penetration characteristics of CNS drug candidates

For CNS drugs, a high *rate* of brain penetration (high BBB permeability) is favorable, in particular for diseases requiring rapid onset (e.g. epilepsy, stroke), and for compounds that are rapidly cleared from brain ISF into CSF [1]. If permeation of a compound across the BBB is too low, brain penetration may be limited [19]. Regarding interactions with transport proteins, CNS drugs should not be substrates of P-gp, BCRP, and/or other efflux pumps [19]. Active uptake of a drug, however, may be beneficial, as the case of gabapentin has shown (a hydrophilic antiepileptic drug which is actively carried across the BBB into the brain by an amino acid transporter) [44,61]. Additionally, high *extent* of brain penetration is advantageous for CNS drugs in order to obtain sufficiently high concentrations in the brain. One has to be aware, however, that only unbound molecules are able to interact with the target according to the free drug hypothesis. Hence, the free drug concentration at the site of action in the brain (and not the total brain concentration) is the critical factor for pharmacological activity [1]. Notably, compounds may have a high *rate* of brain penetration, but a low *extent*, or vice versa [1]. Evaluating both aspects of brain penetration of lead candidates is therefore of great importance, especially for molecules targeting the brain, but also for non-CNS drugs. For the latter, low *rate* and *extent* of brain penetration are beneficial, as this reduces the risk of causing CNS-related side effects.

2.3.6 Strategies for assessing brain penetration of lead candidates

Given the large variety of established models to predict brain penetration of lead compounds, the question arises as to which models should be utilized at which time point in the CNS drug discovery and development process. Generally, costs increase and throughput decreases with more complex models [13]. It is therefore recommended to initially utilize high to medium throughput models (*in silico* and *in vitro* methods) to screen larger numbers of compounds. A selected series of compounds showing favorable *in vitro* data may then be advanced to more sophisticated studies for assessment of *in vivo* brain exposure.

Since brain penetration can be differentiated into *rate* and *extent*, several complementary *in vitro* and *in vivo* parameters should be combined, taking into account that CNS exposure is affected by multiple factors [1]. Additionally, efforts should be made to measure pharmacologically relevant free drug concentrations at the target site and not total brain concentrations, given that the use of K_p values (total brain-to-plasma ratios) to evaluate brain distribution of a compound can be misleading [54]. Also, one has to recognize that the brain can be divided into several compartments (brain ISF, intracellular fluid, and CSF compartment), and that concentrations in one compartment (e.g. CSF) may not necessarily be predictive for drug concentrations in another compartment (e.g. brain ISF). Eventually, one has to be aware that species differences may confound *in vivo* data of brain exposure, and that various disease conditions (e.g. epilepsy and multiple sclerosis) can modify BBB permeability [54].

In an industrial setting, the following *in vitro* assays are currently being used: PAMPA-BBB (rate, passive diffusion), Transwell assays with MDR1-MDCK cells or Caco-2 cells (rate, passive diffusion, and P-gp efflux), and equilibrium dialysis (extent) [1]. At an early stage of the drug development process, it would be of great advantage to increasingly utilize humanized models (e.g. Transwell assays with immortalized brain capillary endothelial cells of human origin) to minimize brain penetration data confounded by species differences. Regrettably, no generally satisfying human model is yet available. Regarding *in vivo* methods, brain perfusion (rate) and determination of brain-to-plasma ratio (extent) are frequently applied. Importantly, data from the latter experiment should be combined with data from *in vitro* equilibrium dialysis, in order to obtain unbound drug concentrations in the brain.

Despite the rather large diversity of different models, assessment of brain penetration has remained a challenge due to the many limitations of *in vitro* and *in vivo* approaches. Nevertheless, past failures of CNS drug candidates in clinical trials strongly suggest that an early application of *in vitro* and *in vivo* models will improve the translation from animals into humans, and the clinical success of a compound [29].

References

[1] L. Di, E.H. Kerns, G.T. Carter, Strategies to assess blood-brain barrier penetration, Expert Opin. Drug Discov. 3 (2008) 677–687.

[2] N.J. Abbott, Prediction of blood-brain barrier permeation in drug discovery from in vivo, in vitro and in silico models, Drug Discov. Today Technol. 1 (2004) 407–416.

[3] A. Reichel, Addressing central nervous system (CNS) penetration in drug discovery: basics and implications of the evolving new concept, Chem. Biodiversity. 6 (2009) 2030–2049.

[4] O.O. Ogunshola, In vitro modeling of the blood-brain barrier: simplicity versus complexity, Curr. Pharm. Design. 17 (2011) 2755–2761.

[5] J.A. Nicolazzo, S.A. Charman, W.N. Charman, Methods to assess drug permeability across the blood-brain barrier, J. Pharm. Pharmacol. 58 (2006) 281–293.

[6] J. Mensch, J. Oyarzabal, C. Mackie, P. Augustijns, In vivo, in vitro and in silico methods for small molecule transfer across the BBB, J. Pharm. Sci. 98 (2009) 4429–4468.

[7] W.J. Geldenhuys, D.D. Allen, J.R. Bloomquist, Novel models for assessing blood-brain barrier drug permeation, Expert Opin. Drug Metab. Toxicol. 8 (2012) 647–653.

[8] W. Pardridge, Transport of small molecules through the blood-brain barrier: biology and methodology, Adv. Drug Deliver. Rev. 15 (1995) 5–36.

[9] D.E. Clark, In silico prediction of blood-brain barrier permeation, Drug Discov. Today. 8 (2003) 927–933.

[10] S.D. Krämer, Absorption prediction from physicochemical parameters, Pharm. Sci. Tech. Today. 2 (1999) 373–380.

[11] A.M. ter Laak, R.S. Tsai, G.M. Donné-Op den Kelder, P.-A. Carrupt, B. Testa, H. Timmerman, Lipophilicity and hydrogen-bonding capacity of H1-antihistaminic agents in relation to their central sedative side-effects, Eur. J. Pharm. Sci. 2 (1994) 373–384.

[12] I.F. Martins, A.L. Teixeira, L. Pinheiro, A.O. Falcao, A bayesian approach to in silico blood-brain barrier penetration modeling, J. Chem. Inf. Model. 52 (2012) 1686–1697.

[13] E.H. Kerns, L. Di, Drug-like Properties: Concepts, structure design and methods: from ADME to toxicity optimization, Elsevier Inc., 2008.

[14] M. Kansy, F. Senner, K. Gubernator, Physicochemical high throughput screening: parallel artificial membrane permeation assay in the description of passive absorption processes, J. Med. Chem. 41 (1998) 1007–1010.

[15] W.M. Pardridge, Log(BB), PS products and in silico models of drug brain penetration, Drug Discov. Today. 9 (2004) 392–393.

[16] Z. Rankovic, CNS drug design: balancing physicochemical properties for optimal brain exposure, J. Med. Chem. 58 (2015) 2584–2608.

[17] J.C. Kalvass, T.S. Maurer, G.M. Pollack, Use of plasma and brain unbound fractions to assess the extent of brain distribution of 34 drugs: comparison of unbound concentration ratios to in vivo P-glycoprotein efflux ratios, Drug Metab. Dispos. 35 (2007) 660–666.

[18] F. Joó, The blood-brain barrier in vitro: Ten years of research on microvessels isolated from the brain, Neurochem. Int. 7 (1985) 1–25.

[19] L. Di, H. Rong, B. Feng, Demystifying brain penetration in central nervous system drug discovery, J. Med. Chem. 56 (2013) A–K.

[20] I. Wilhelm, I.A. Krizbai, In vitro models of the blood-brain barrier for the study of drug delivery to the brain, Mol. Pharm. 11 (2014) 1949–1963.

[21] P.D. Bowman, S.R. Ennis, K.E. Rarey, A.L. Betz, G.W. Goldstein, Brain microvessel endothelial cells in tissue culture: a model for study of blood-brain barrier permeability, Ann. Neurol. 14 (1983) 396–402.

[22] M.A. Deli, Blood-Brain Barrier Models, in: A. Lajtha, M.E.A. Reith (Eds.), Handbook of Neurochemistry and Molecular Neurobiology, 3rd ed., Springer Verlag, Berlin Heidelberg, 2007: pp. 29–55.

[23] M.-P. Dehouck, S. Meresse, P. Delorme, J.-C. Fruchart, R. Cecchelli, An easier, reproducible, and mass-production method to study the blood-brain barrier in vitro, J. Neurochem. 54 (1990) 1798–1801.

[24] N.J. Abbott, L. Rönnbäck, E. Hansson, Astrocyte-endothelial interactions at the blood-brain barrier, Nat. Rev. Neurosci. 7 (2006) 41–53.
[25] S. Syvänen, Ö. Lindhe, M. Palner, B.R. Kornum, O. Rahman, B. Långström, et al., Species differences in blood-brain barrier transport of three positron emission tomography radioligands with emphasis on P-glycoprotein transport, Drug Metab. Dispos. 37 (2009) 635–643.
[26] M.S. Warren, N. Zerangue, K. Woodford, L.M. Roberts, E.H. Tate, B. Feng, et al., Comparative gene expression profiles of ABC transporters in brain microvessel endothelial cells and brain in five species including human, Pharmacol. Res. 59 (2009) 404–413.
[27] R. Cecchelli, S. Aday, E. Sevin, C. Almeida, M. Culot, L. Dehouck, et al., A stable and reproducible human blood-brain barrier model derived from hematopoietic stem cells, PLoS ONE. 9 (2014) 1–11.
[28] E.S. Lippmann, S.M. Azarin, J.E. Kay, R.A. Nessler, H.K. Wilson, A. Al-Ahmad, et al., Derivation of blood-brain barrier endothelial cells from human pluripotent stem cells, Nat. Biotech. 30 (2012) 783–791.
[29] D.B. Stanimirovic, M. Bani-Yaghoub, M. Perkins, A.S. Haqqani, Blood-brain barrier models: in vitro to in vivo translation in preclinical development of CNS-targeting biotherapeutics, Expert Opin. Drug Discov. 10 (2015) 141–155.
[30] J.G. Prudhomme, I.W. Sherman, K.M. Land, A.V. Moses, S. Stenglein, J.A. Nelson, Studies of Plasmodium falciparum cytoadherence using immortalized human brain capillary endothelial cells, Int. J. Parasitol. 26 (1996) 647–655.
[31] L. Xiao, C. Yang, K. Dorovini-Zis, N.N. Tandon, E.W. Ades, A.A. Lal, et al., Plasmodium falciparum: involvement of additional receptors in the cytoadherence of infected erythrocytes to microvascular endothelial cells, Exp. Parasitol. 84 (1996) 42–55.
[32] A. Muruganandam, L. Moorhouse Herx, R. Monette, J.P. Durkin, D.B. Stanimirovic, Development of immortalized human cerebromicrovascular endothelial cell line as an in vitro model of the human blood-brain barrier, FASEB J. 11 (1997) 1187–1197.
[33] M.F. Stins, J. Badger, K.S. Kim, Bacterial invasion and transcytosis in transfected human brain microvascular endothelial cells, Microb. Pathogenesis. 30 (2001) 19–28.
[34] X. Gu, J. Zhang, D.W. Brann, F.-S.X. Yu, Brain and retinal vascular endothelial cells with extended life span established by ectopic expression of telomerase, Invest. Ophth. Vis. Sci. 44 (2003) 3219–3225.
[35] B.B. Weksler, E.A. Subileau, N. Perriere, P. Charneau, K. Holloway, M. Leveque, et al., Blood-brain barrier-specific properties of a human adult brain endothelial cell line, FASEB J. 19 (2005) 1872–1874.
[36] N. Ketabi-Kiyanvash, C. Herold-Mende, F. Kashfi, S. Caldeira, M. Tommasino, W.E. Haefeli, et al., NKIM-6, a new immortalized human brain capillary endothelial cell line with conserved endothelial characteristics, Cell Tissue Res. 328 (2007) 19–29.
[37] Y. Sano, F. Shimizu, M. Abe, T. Maeda, Y. Kashiwamura, S. Ohtsuki, et al., Establishment of a new conditionally immortalized human brain microvascular endothelial cell line retaining an in vivo blood-brain barrier function, J. Cell. Physiol. 225 (2010) 519–528.
[38] A. Kamiichi, T. Furihata, S. Kishida, Y. Ohta, K. Saito, S. Kawamatsu, et al., Establishment of a new conditionally immortalized cell line from human brain microvascular endothelial cells: A promising tool for human blood-brain barrier studies, Brain Res. 1488 (2012) 113–122.
[39] T. Maeda, Y. Sano, M. Abe, F. Shimizu, Y. Kashiwamura, S. Ohtsuki, et al., Establishment and characterization of spinal cord microvascular endothelial cell lines, Clin. Exp. Neuroimmunol. 4 (2013) 326–338.
[40] S. Lundquist, M. Renftel, J. Brillault, L. Fenart, R. Cecchelli, M.-P. Dehouck, Prediction of drug transport through the blood-brain barrier in vivo: a comparison between two in vitro cell models, Pharm. Res. 19 (2002) 976–981.
[41] K. Takahashi, Y. Sawasaki, J.-I. Hata, K. Mukai, T. Goto, Spontaneous transformation and immortalization of human endothelial cells, In Vitro Cell Dev. Biol. 26 (1990) 265–274.
[42] R.N. Hull, W.R. Cherry, G.W. Weaver, The origin and characteristics of a pig kidney cell strain, LLC-PK1, In Vitro Cell Dev. Pl. 12 (1976) 670–677.
[43] B. Veronesi, Characterization of the MDCK cell line for screening neurotoxicants, Neurotoxicology. 17 (1996) 433–444.

[44] S.G. Summerfield, K. Read, D.J. Begley, T. Obradovic, I.J. Hidalgo, S. Coggon, et al., Central nervous system drug disposition: the relationship between in situ brain permeability and brain free fraction, J. Pharmacol. Exp. Ther. 322 (2007) 205–213.
[45] A. Braun, S. Hämmerle, K. Suda, B. Rothen-Rutishauser, M. Günthert, S.D. Krämer, et al., Cell cultures as tools in biopharmacy, Eur. J. Pharm. Sci. 11, Supplement 2 (2000) S51–S60.
[46] L. Di, E.H. Kerns, I.F. Bezar, S.L. Petusky, Y. Huang, Comparison of blood-brain barrier permeability assays: in situ brain perfusion, MDR1-MDCKII and PAMPA-BBB, J. Pharm. Sci. 98 (2009) 1980–1991.
[47] F. Roux, P.-O. Couraud, Rat brain endothelial cell lines for the study of blood-brain barrier permeability and transport functions, Cell Mol. Neurobiol. 25 (2005) 41–57.
[48] C. Förster, C. Silwedel, N. Golenhofen, M. Burek, S. Kietz, J. Mankertz, et al., Occludin as direct target for glucocorticoid-induced improvement of blood-brain barrier properties in a murine in vitro system, J. Physiol. 565 (2005) 475–486.
[49] Y. Omidi, L. Campbell, J. Barar, D. Connell, S. Akhtar, M. Gumbleton, Evaluation of the immortalised mouse brain capillary endothelial cell line, b.End3, as an in vitro blood-brain barrier model for drug uptake and transport studies, Brain Res. 990 (2003) 95–112.
[50] E.F. Wagner, W. Risau, Oncogenes in the study of endothelial cell growth and differentiation, Semin. Cancer Biol. 5 (1994) 137–145.
[51] T. Yang, K.E. Roder, T.J. Abbruscato, Evaluation of bEnd5 cell line as an in vitro model for the blood-brain barrier under normal and hypoxic/aglycemic conditions, J. Pharm. Sci. 96 (2007) 3196–3213.
[52] C. Crone, P. Olesen, Electrical resistance of brain microvascular endothelium, Brain Res. 241 (1982) 49–55.
[53] A.M. Butt, H.C. Jones, N.J. Abbott, Electrical resistance across the blood-brain barrier in anaesthetized rats: a developmental study, J. Physiol. 429 (1990) 47–62.
[54] A.K. Deo, F.-P. Theil, J.-M. Nicolas, Confounding parameters in preclinical assessment of blood-brain barrier permeation: an overview with emphasis on species differences and effect of disease states, Mol. Pharmaceutics. 10 (2013) 1581–1595.
[55] Q.R. Smith, Brain perfusion systems for studies of drug uptake and metabolism in the central nervous system, in: R.T. Borchardt, P.L. Smith, G. Wilson (Eds.), Models for assessing drug absorption and metabolism, Springer US, 1996: pp. 285–307.
[56] Y. Takasato, S.I. Rapoport, Q.R. Smith, An in situ brain perfusion technique to study cerebrovascular transport in the rat, Am. J. Physiol.-Heart C. 247 (1984) H484–H493.
[57] T.S. Maurer, D.B. DeBartolo, D.A. Tess, D.O. Scott, Relationship between exposure and nonspecific binding of thirty-three central nervous system drugs in mice, Drug Metab. Dispos. 33 (2005) 175–181.
[58] N. Plock, C. Kloft, Microdialysis–theoretical background and recent implementation in applied life-sciences, Eur. J. Pharm. Sci. 25 (2005) 1–24.
[59] Y. Deguchi, Application of in vivo brain microdialysis to the study of blood-brain barrier transport of drugs, Drug Metab. Pharmacokin. 17 (2002) 395–407.
[60] Z. Redzic, Molecular biology of the blood-brain and the blood-cerebrospinal fluid barriers: similarities and differences, Fluids Barriers CNS. 8 (2011) 1–25.
[61] H. Uchino, Y. Kanai, D.K. Kim, M.F. Wempe, A. Chairoungdua, E. Morimoto, et al., Transport of amino acid-related compounds mediated by L-type amino acid transporter 1 (LAT1): insights into the mechanisms of substrate recognition, Mol. Pharmacol. 61 (2002) 729–737.

2.4 Bioanalysis

2.4.1 Definition

Bioanalysis is a section of analytical chemistry focusing on the qualitative and quantitative determination of drugs, metabolites, and biomarkers in biological matrices such as blood, plasma, serum, CSF, urine, saliva, and tissue [1,2]. Detection and quantification of analytes in these matrices find application in the entire drug discovery and development process, ranging from *in vitro* testing to preclinical and clinical studies (e.g. bioavailability, bioequivalence, pharmacokinetic, and toxicokinetic studies), and in daily clinical routine [1,3–5].

2.4.2 Bioanalytical techniques

For qualitative and quantitative analysis of compounds in biological matrices, various techniques are employed. These include chromatography-based methods such as liquid chromatography (LC) and gas chromatography (GC) coupled to specific detectors (spectrophotometric, fluorescence, mass spectrometry (MS) detectors), and ligand-binding assays such as enzyme-linked immunosorbent assays (ELISA) and radio-immunoassays (RIA).

ELISA and RIA have been widely used in bioanalysis since their invention more than 40 years ago [6,7]. They both offer high sensitivity (analyte concentrations in the picogram range can be determined), are relatively easy to perform, and can be automated [8]. However, major drawbacks are the requirement of expensive analyte-specific antibodies and the occurrence of cross-reactions, which may lead to false positive outcomes. Moreover, RIA are hazardous to human health and produce radioactive waste. An alternative to ligand-binding assays are chromatography-based methods. For a long time, quantification was carried out using LC hyphenated to spectrophotometric detection such as ultraviolet/visible (UV/Vis) absorbance or, occasionally, fluorescence [9]. Both techniques are relatively robust, but require analytes that contain a chromophore or fluorophore, respectively. While fluorescence offers high sensitivity and specificity, UV/Vis absorbance generally does not [9]. Therefore, careful sample clean-up procedures and relatively long run times for reduction of interferences from co-eluting compounds may be necessary [9]. A considerably more sensitive technique than LC-UV/Vis is GC-MS. For this method, spectral libraries of compounds are available which facilitate the detection of known drugs, for example, in toxicological laboratories [8]. However, analytes for GC-MS analysis need to be sufficiently volatile and thermally stable, which is not the case for many drugs, endogenous metabolites, and biomolecules [10].

In the 1980s, the hyphenation of LC with MS became feasible with the introduction of atmospheric pressure ionization (API) interfaces [11,12]. Since then, LC-MS has gradually superseded any other

bioanalytical technique and has become the method-of-choice in bioanalysis of small drugs [13,14]. For most applications, a specific type of mass spectrometer is selected, namely the triple quadrupole mass analyzer (MS/MS) [15,16]. LC coupled to this detector (LC-MS/MS) is a highly sensitive, selective, and robust technique, and thus ideally suited for the determination of an analyte in a complex biological matrix. By using ultra-high performance liquid chromatography (UHPLC), run times of less than one minute can be achieved, resulting in increased speed required for higher throughput. A limitation of triple quadrupole mass spectrometers is that no full scan data can be collected when the instrument is operated in selected reaction monitoring (SRM) mode (the preferred mode in quantitative drug bioanalyis). Therefore, high-resolution mass analyzers (using either time-of-flight (TOF) or Orbitrap technology) that are able to simultaneously provide qualitative and quantitative analyses in the same LC run have increasingly been used in recent years [17]. However, LC coupled to high-resolution MS has not yet been widely accepted in bioanalytical laboratories, and international guidelines for method validation still remain to be elaborated by regulatory agencies [18].

Currently, LC-MS is the method-of-choice in particular for the analysis of small molecules (MW below 800 Da) [13]. For the quantification of therapeutic peptides, proteins, oligonucleotides, and biomarkers, on the other hand, ligand-binding assays are still mostly employed [13]. Yet, there seems to be a trend in recent years towards the use of LC-MS also in the analysis of larger molecules due to higher selectivity, wider linearity range, and faster method development for this technique compared to conventional ligand-binding assays [13,19].

2.4.3 Liquid chromatography coupled to triple quadrupole mass spectrometry (LC-MS/MS)

LC-MS/MS is the joining of two techniques: LC (for the separation of a complex mixture between two immiscible phases based on the physicochemical properties of the constituents) and triple (or tandem) quadrupole MS (for selective and sensitive detection of analytes). As LC system, HPLC or UHPLC can be selected (the acronym UPLC may also be used, but is strictly speaking a trademark of the manufacturer Waters Corp.). UHPLC instruments are able to operate at higher back-pressure than conventional HPLC systems, allowing the use of shorter columns with smaller particles as stationary phase [20,21]. This results in an enhancement of chromatographic performance (efficiency) and speed, which are major advantages for routine bioanalysis where high throughput of samples is required [21].

LC systems are predominantly coupled to triple quadrupole detectors via electrospray ionization (ESI) or atmospheric pressure chemical ionization (APCI) interfaces [16]. ESI and APCI are both soft ionization techniques, by which the analytes eluting from the LC column are ionized to positively ($M+H^+$) or negatively ($M-H^-$) charged ions which are transferred into gas phase, and finally introduced

into the MS detector [22]. While ESI sources are capable of ionizing almost any polar molecule, APCI sources are more suited for ionization of less polar and non-polar compounds [22].

Triple quadrupole mass spectrometers consist of three quadrupoles connected in series (Figure 7) [15,23]. A quadrupole typically consists of four molybdenum rods on which alternating DC (direct current) and RF (radio frequency) voltages are applied [23]. At a particular DC/RF ratio, only ions with a certain *m/z* value have a stable trajectory and are able to pass through the quadrupole [23]. In quantitative bioanalysis, triple quadrupole detectors are primarily operated in SRM mode. In this mode, the first (Q1) and third (Q3) quadrupole act as selective mass filters, while the second quadrupole (Q2), located between Q1 and Q3, serves as collision cell (RF voltage applied only) (Figure 7) [24]. Thus, only selected precursor ions with specific *m/z* values are allowed to pass through Q1. They subsequently collide in the collision cell (Q2) with inert gas (argon or nitrogen) and are fragmented into numerous product ions, a process called collision induced fragmentation (CID) [15]. Only selected product ions with certain *m/z* values are allowed to pass through Q3 and are finally detected typically by some type of electron multiplier (Figure 7) [25]. SRM mode offers highest selectivity and sensitivity, and ensures that only analytes of interest are being quantified, while interfering compounds such as matrix constituents are not detected.

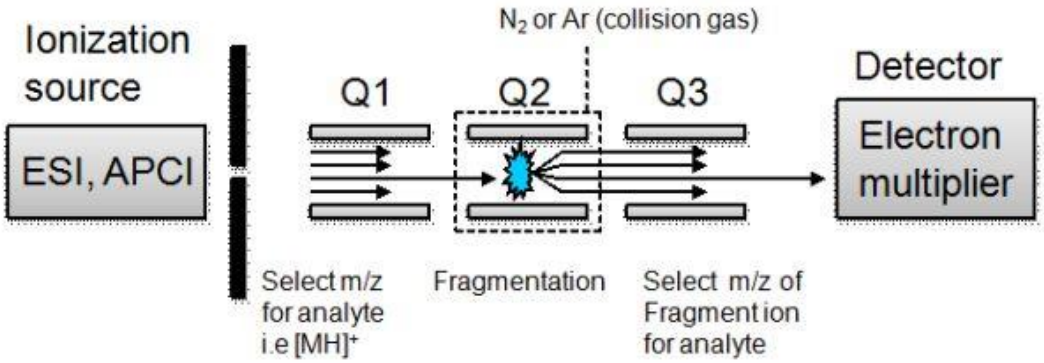

Figure 7: Schematic representation of a triple quadrupole mass detector. Figure from Ni et al. (2012) [26].

2.4.4 Sample preparation for LC-MS/MS

Biological matrices are extremely complex and contain a wide spectrum of cell components such as proteins, lipids, salts, and other endogenous substances. These components may interfere with the bioanalytical assay, and may thus lead to erroneous results and higher variation from sample to sample [27,28]. Therefore, a clean-up procedure (i.e. sample preparation) is necessary to obtain samples free from matrix components before sample analysis [27]. If done efficiently, sample preparation enhances selectivity and sensitivity of the LC-MS/MS methods, leads to higher reproducibility of data, and increases lifetime of LC column and instrumentation. In addition to purification from interfering

substances, main objectives of the clean-up procedure are the concentration of the analyte to improve detection limits, and dissolution of the analyte in a suitable solvent for instrumental analysis [27,29]. The most commonly used sample preparation procedures are dilution, protein precipitation (PP), liquid-liquid extraction (LLE), and solid-phase extraction (SPE) [1]. Besides these methods, newer techniques such as supported-liquid extraction (SLE) have emerged recently [30].

Dilution: Dilution of samples is a rapid clean-up procedure, during which biological samples (such as urine) are simply diluted with water or mobile phase solution prior to injection into the LC-MS (hence often referred to as "dilute-and-shoot" method) [8]. While this type of sample preparation is simple and time-efficient, its disadvantages are the missing step of removing interfering compounds and the lack of an analyte pre-concentration step, which may lead to insufficient selectivity and/or sensitivity [8].

Protein precipitation (PP): Protein precipitation (PP) is an efficient sample preparation technique by which proteins in the biological matrix are denatured by the use of a strong acid/base (resulting in a change of pH), by the application of heat, or by the addition of organic solvents such as methanol or acetonitrile [1,30]. During the denaturation process, proteins undergo a change in their tertiary and secondary structure, and analytes become thus freely soluble in the denaturing solvent. After centrifugation of samples, the denatured proteins form a pellet at the bottom of the tube, while the analytes are dissolved in the supernatant. After evaporation of the supernatant to dryness, and subsequent reconstitution in mobile phase or injection solvent, the sample is ready for LC-MS/MS analysis [27]. PP is simple, fast, and inexpensive, but results in samples which are less clean compared to samples obtained by LLE, SLE, or SPE [25].

Liquid-liquid extraction (LLE): The principle of liquid-liquid extraction (LLE) is based on the different solubility and partitioning equilibrium of a compound between an aqueous and an organic phase. Analytes are extracted from the original sample (aqueous phase) into an organic phase (e.g. ethyl acetate, methyl *tert*-butyl ether (MTBE), methylene chloride, hexane) which is immiscible with the water phase [20]. Small lipophilic drugs are easily extracted from the aqueous biological sample, while larger polar molecules (e.g. matrix components) remain in the water phase and are thus separated from the analyte. The LLE technique results in cleaner samples than PP, but it has a number of disadvantages: the extraction of hydrophilic analytes is limited, recoveries may be variable, and relatively large biological sample volumes are needed [1].

Solid-phase extraction (SPE): In solid-phase extraction (SPE), analytes are separated from the biological matrix by means of a solid (stationary) phase. The principle of this technique is based on the same separation principle as LC, where different affinities of substances towards a stationary phase are

exploited [27]. Biological samples are loaded onto a SPE cartridge filled with a stationary phase, where analytes are retained, but matrix constituents not. After a washing process, analytes are eluted using an appropriate elution solvent. As stationary phases, similar materials as in LC are being used, and both reverse and normal phase cartridges are commercially available. SPE is an efficient method which leads to relatively clean samples, but costs of this technique are considerably higher compared to PP and LLE.

Supported-liquid extraction (SLE): Supported-liquid extraction (SLE) has been developed in recent years by various manufacturers and is performed by using commercial 96-well plates (e.g. Isolute® SLE+ from Biotage) [31]. Each well is packed with a modified form of diatomaceous earth with a high capacity for retaining aqueous samples [30]. When a biological sample is loaded onto a well, the aqueous portion of the sample adsorbs as a thin film to the hydrophilic surface of the packing material (also called "support"), and analytes can subsequently be eluted by applying an appropriate eluent [31]. SLE results in clean extracts and offers high recovery and reproducibility, but is more expensive than PP and LLE [31].

2.4.5 Quantitative bioanalysis by LC-MS/MS

The ultimate goal of quantitative bioanalysis by LC-MS/MS is the determination of accurate drug concentrations in biological fluids or tissues. This process is difficult and challenging, as analyte concentrations are usually low and matrices are highly complex [32]. Erroneous results, however, may lead to wrong interpretation of findings, and may culminate, for example, in an inappropriate dosing of patients in the clinics with possibly fatal outcomes. Every effort should, therefore, be made to ensure that a quantification method is able to provide reliable and consistent results, and that it is suitable for the intended purpose [3]. The process of demonstrating the suitability of a method for biomedical application is called bioanalytical method validation. It can be divided into three phases: method development, method validation, and method application (study sample analysis) (Figure 8).

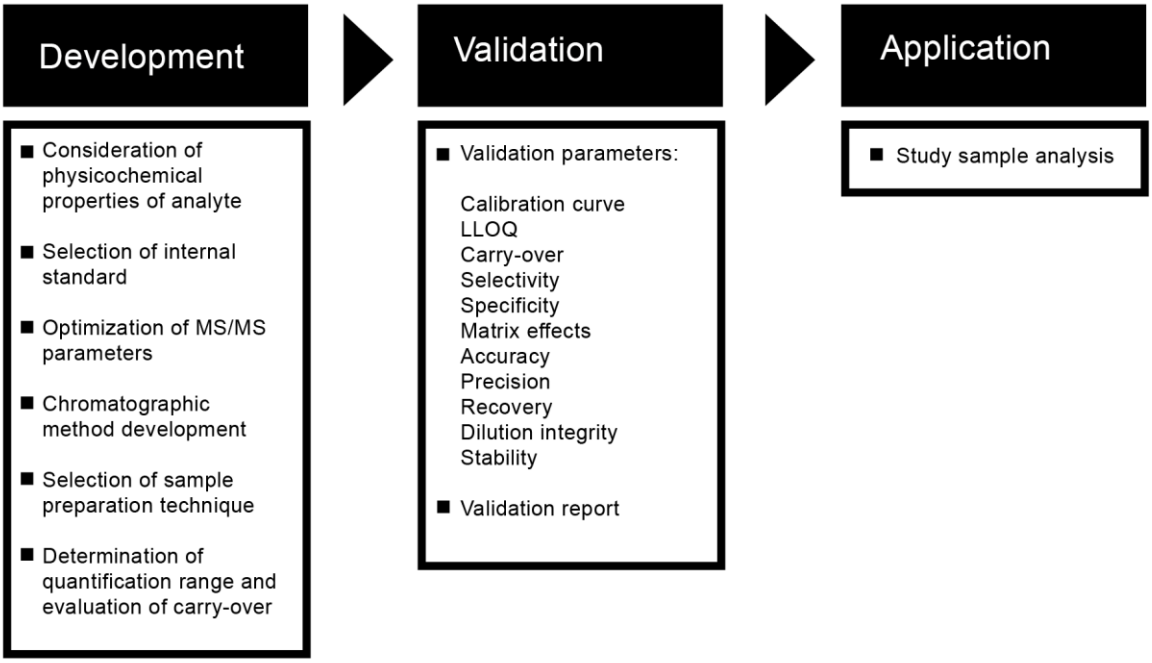

Figure 8: Quantitative bioanalysis of small molecules by LC-MS/MS consists of method development, method validation, and method application (study sample analysis). Figure by Tabea Gollin (2015).

2.4.6 Method development

Method development for LC-MS/MS encompasses several distinct steps which are carried out consecutively: 1) consideration of physicochemical properties of the analyte; 2) selection of a suitable internal standard (I.S.); 3) optimization of MS/MS parameters; 4) chromatographic method development; 5) selection of a sample preparation technique; and 6) determination of quantification range and evaluation of carry-over. Each step requires time and resources, but contributes significantly to a successful method validation and application later on.

(1) Physicochemical properties: As a first step (prior to starting with the development on the benchtop), physicochemical properties of the analyte(s) should be taken into consideration, such as solubility of the analyte in various solvents, lipophilicity (LogP/LogD), acidity (pKa), thermal and light stability, and molecular structure. Thus, suitable solvents can be selected and appropriate measures taken for successful sample processing (e.g. working in the dark with light sensitive compounds).

(2) Selection of a suitable internal standard (I.S.): An internal standard (I.S.) is a compound that is added at a known concentration to every quantification sample, correcting for variation in sample extraction, transfer/injection volumes, ionization efficiency, and detector response [33]. As first choice, stable isotopic-labeled analytes should be selected as I.S. due to equal physicochemical

characteristics and, thus, identical behavior as the unlabeled analyte during all steps of the analytical procedure. Regrettably, D (^{2}H), ^{13}C, ^{15}N, and ^{17}O-labeled compounds are expensive and may in certain cases not be available (e.g. for most natural products). As an alternative, structurally similar compounds may be employed, which closely mimic the analyte's properties [34]. These compounds should exhibit only small differences in functional groups when compared to the analyte, and should have similar chromatographic properties [34].

(3) Optimization of MS/MS parameters: After selection of an I.S., MS/MS parameters (SRM transitions, cone voltage, collision energy etc.) for both analyte and I.S. need to be generated and optimized for highest sensitivity and selectivity of the quantification method. This is usually done using a designated software program provided by the instrument manufacturer. If the sensitivity for the analyte is insufficient and/or no SRM transitions could be generated, a different ionization polarity (positive or negative) and/or ionization source may be tested (e.g. APCI instead of ESI).

(4) Chromatographic method development: After generation of MS/MS parameters, a chromatographic method needs to be developed in order to separate the analyte(s) of interest from interfering compounds in the sample. Different (U)HPLC columns (reverse phase, normal phase, hydrophilic interaction (HILIC) etc.) and mobile phases (eluents) are hereby tested. An optimal gradient is determined, and mobile phase flow rate and column oven temperature are optimized. If structure analogs are used as I.S., care should be taken that the retention times of analyte and I.S. are relatively close, as emerging matrix effects may otherwise not be compensated sufficiently.

(5) Selection of sample preparation technique: Since biological matrices are highly complex, an appropriate sample preparation technique (clean-up procedure) needs to be selected to extract the compound(s) of interest. The traditional approach is to start with the simplest extraction method such as PP or dilution [35]. If not successful, more sophisticated extraction methods such as LLE, SPE, and SLE may be evaluated. Also, phospholipid-removal plates (e.g. Ostro^{TM} plates from Waters) may be tested to specifically remove phospholipids from plasma samples.

(6) Quantification range and carry-over: The last steps during bioanalytical method development are the determination of the quantification range, and the evaluation of the carry-over for both analyte and I.S.. The quantification range should be defined based on the sample concentrations expected in a particular study, and the linearity of the analyte in the biological matrix in the selected concentration range has to be proven. Nowadays, lower limits of quantification (LLOQ; calibration standard with the lowest concentration) in the pg/mL range can be achieved in LC-MS/MS, depending on the type of triple quadrupole detector, HPLC separation, and sample clean-up procedure.

The carry-over should be evaluated by injecting a blank sample (pure matrix) after the upper limit of quantification (ULOQ; calibration standard with the highest concentration). According to EMA guidelines, carry-over should not exceed 20% for the analyte and 5% for the I.S. [36]. If these criteria are not met, appropriate measures should be taken to minimize the carry-over (e.g. change of washing needle solution, adaption of the quantification range, injection of blank samples after each sample).

2.4.7 Method validation

As soon as the LC-MS/MS method has been developed, method validation can be initiated. To which degree the validation should be performed depends on various factors: type of study, research field, and regulatory requirements. Typically, the most reliable bioanalytical data are obtained by means of methods validated according to good laboratory practice (GLP) guidelines defined by regulatory agencies. Among these recommendations, the European Medicines Agency (EMA) "Guideline on Bioanalytical Method Validation" (2009) and the US Food and Drug Administration (FDA) "Guidance for Industry, Bioanalytical Method Validation" (2001; new draft in 2013) belong to the most widely accepted ones [36–39]. Substantial efforts have been made to align different guidelines in recent years. A harmonized global guideline, however, does not yet exist [40].

In the pharmaceutical industry, bioanalytical method validation plays a pivotal role particularly in preclinical and clinical drug development (e.g. in bioavailability, bioequivalence, pharmacokinetic, and toxicokinetic studies in animals and humans) [9]. At the drug discovery stage, on the other hand, where studies are employed to select drug candidates for further development, validation is often reduced for the benefit of high throughput [9]. In an academic setting, requirements for how and to what extent to perform method validation may not be as clear as for the pharmaceutical industry. However, peer reviewed scientific journals have increasingly higher requirements concerning method validation [4].

Full validation, partial validation, and cross-validation

The EMA and FDA have defined different degrees of bioanalytical method validation in their guidelines. These are: full validation, partial validation, and cross-validation [36,37]. A full validation is required if a method is implemented for the first time, or if metabolites (i.e. new analytes) are added to an already existing method. If a fully validated method is slightly modified, a new full validation may be avoided by partially validating the method. Such modifications can be e.g. the transfer of the method from one laboratory to another, the change of the biological matrix within a species (e.g. human urine to human plasma), or the alteration of the sample processing procedure. Partial validation of a method may include as little as one intra-assay accuracy and precision determination, but it may also require an almost full validation if major modifications were performed. Cross-validation of a method is required if samples from one single study are analyzed in two different laboratories, or if

two or more different bioanalytical techniques (e.g. ELISA and LC-MS/MS) are employed for sample analysis.

Validation parameters

EMA and FDA guidelines have defined various validation parameters according to which quantitative LC-MS/MS methods should be validated. These include: calibration curve, LLOQ, carry-over, selectivity, specificity, matrix effects, accuracy, precision, recovery, dilution integrity, and stability [36,37].

Calibration curve and LLOQ: A calibration curve should consist of calibration standards (calibrators) and quality controls (QCs) at a minimum of three concentrations levels (low = QCL, middle = QCM, high = QCH) [36,37]. QCL should be within 3 times the lowest calibrator (LLOQ), QCM should be in the middle of the quantification range, and QCH should be approaching the high end of the range [36,37]. Calibrators and QCs should be prepared in the same biological fluid as the study samples by spiking the matrix with known concentrations of the analyte [37]. The calibration curve should be recorded as follows: a blank sample, a zero sample (sample processed with I.S., but without analyte), and six to eight calibrators covering the selected concentration range [37]. After the highest calibrator (ULOQ), another blank sample should be injected for carry-over assessment. For the LLOQ, the following conditions need to be met: the analyte response should be at least 5 times higher than the analyte response in the blank sample, and the signal to noise (S/N) ratio should be > 10 [36,37,41]. Each analytical run should begin and end with a series of calibrators (bracketed between blank samples) injected in increasing concentration. Between the two calibrator sets, six QCs should be inserted randomly into the analytical run. The simplest model that is able to appropriately describe the concentration versus MS response curve should be applied [37]. For 75% of calibrators and 67% of QCs (four out of six), the back-calculated concentrations should be within ± 15% of the nominal values, with exception of the LLOQ, for which a deviation of ± 20% is allowed [37].

Carry-over: Carry-over of analyte and I.S. should already be evaluated during method development by injecting a blank sample after each ULOQ. If carry-over occurs, it should be minimized as best as possible [36,38]. According to EMA guidelines, carry-over is not allowed to exceed 20% for the analyte and 5% for the I.S. [36]. During method validation and application, carry-over needs to be further monitored [36,38].

Selectivity and specificity: Selectivity is defined as the ability of an analytical method to differentiate and quantify the analyte in the presence of endogenous matrix components or other compounds in the sample [37]. It should be ensured at the LLOQ by using different batches of the same biological matrix [36,37]. Specificity of the method should be proven by

using independent sources of the same matrix [37]. It should be noted that selectivity is not the same as specificity. While selectivity can be graded, specificity cannot. It is an absolute characteristic that may be regarded as ultimate selectivity [42].

Matrix effects: In LC-MS, a common problem is the occurrence of matrix effects. This phenomenon is caused by molecules originating from the biological matrix that co-elute with the analyte(s) and may interfere with the ionization process in the mass spectrometer (leading to ion suppression or enhancement) [43,44]. Matrix effects can occur in diverse and unexpected forms and may have a negative impact on precision and accuracy of a bioanalytical method. Therefore, they should be carefully investigated in the course of method validation to ensure that precision, selectivity, and sensitivity of the assay are not compromised [36,37].

Accuracy and precision: Accuracy of a bioanalytical method describes the closeness of mean test results obtained by the method to the nominal (true) value (concentration) of the compound. It is expressed as relative error (RE %). Precision describes the closeness of repeated individual measures, and is expressed as coefficient of variation (CV %).

$$RE\ (\%) = \frac{Mean\ experimental\ conc. - Nominal\ conc.}{Nominal\ conc.} \times 100$$

$$CV\ (\%) = \frac{Standard\ deviation\ (S.D.)}{Mean\ experimental\ conc.} \times 100$$

Accuracy and precision of a method can be subdivided into within-run and between-run accuracy and precision. The latter (between-run) reflects the reproducibility of a method [36,37]. During method validation, both within-run and between-run accuracy and precision should be assessed by replicate analysis of samples (at least five) at a minimum of three different concentration levels [37]. Means and S.D. should be calculated, from which RE % and CV % can be deduced. RE % should be within ± 15% (± 20% at the LLOQ), and CV % should not exceed 15% (20% at the LLOQ) of the nominal values.

Recovery (extraction yield): Recovery indicates the extraction efficiency (extraction yield) of a bioanalytical method, and should be assessed by comparison of extracted samples at three concentration levels (QCL, QCM, and QCH) with unextracted samples representing 100% recovery [37, 45]. According to FDA guidance, recovery does not need to be 100%, but it should be consistent, precise, and reproducible [37].

Dilution integrity: Study samples may need to be diluted if the analyte concentration is higher than the ULOQ. However, dilution of samples should not have an impact on accuracy

and precision of the bioanalytical method. Therefore, representative tests should be carried out during method validation in order to demonstrate that dilution of study samples later on does not interfere with the method [36,37].

Stability: During the entire bioanalysis chain (beginning with sample collection and ending with sample analysis after long-term and short-term storages), stability of the analyte in the biofluid should be guaranteed. Therefore, various stability tests should be carried out during method validation. According to FDA/EMA guidelines, these include: freeze and thaw (F/T) stability, benchtop stability (at room temperature), long-term stability at planned storage conditions, post-preparative stability (autosampler stability), and stock solution stability [37]. Importantly, conditions used in all these stability tests should reflect the conditions expected to be encountered during real sample handling and analysis.

Validation reports

After method validation, a report needs to be compiled which includes an operational description of the bioanalytical method, the performed validation tests, and obtained validation parameters [37]. Also, any deviation from standard operating procedures (SOP) or protocols needs to be noted and justified [37]. Finally, a SOP has to be written which can be used for the routine analysis of study samples. This protocol should describe the bioanalytical method in detail, i.e. should include information on storage conditions, preparation of calibrators and QCs, sample extraction, LC-MS/MS parameters, and calibration curve acceptance criteria [37].

2.4.8 Method application (analysis of study samples)

After successful method validation, the LC-MS/MS method can be applied to analyze study samples. Knowledge gained during method validation on the stability of analyte and I.S. and correct processing of samples needs to be taken into consideration, and SOPs need to be closely followed. Similarly as for method validation, an analytical run should consist of two series of calibrators (including two blank samples and one zero calibrator) injected at the beginning and at the end of the run. Study samples together with six QCs (duplicates of QCL, QCM, and QCH) are inserted randomly between the two calibrator series. An analytical run is only valid if the back-calculated concentrations of 75% of calibrators and 76% of QCs (four out of six) are within ± 15% (± 20% at the LLOQ) of the nominal values.

References

[1] P.L. Kole, G. Venkatesh, J. Kotecha, R. Sheshala, Recent advances in sample preparation techniques for effective bioanalytical methods, Biomed. Chromatogr. 25 (2011) 199–217.

[2] J. Smisterova, K. Ensing, De Zeeuw R. A., Methodological aspects of quantitative receptor assays, J. Pharmaceut. Biomed. 12 (1994) 723–745.

[3] O. González, M.E. Blanco, G. Iriarte, L. Bartolomé, M.I. Maguregui, R.M. Alonso, Bioanalytical chromatographic method validation according to current regulations, with a special focus on the non-well defined parameters limit of quantification, robustness and matrix effect, J. Chromatogr. A. 1353 (2014) 10–27.

[4] F.T. Peters, O.H. Drummer, F. Musshoff, Validation of new methods, Forensic Sci. Int. 165 (2007) 216–224.

[5] F. Bressolle, M. Bromet-Petit, M. Audran, Validation of liquid chromatographic and gas chromatographic methods Applications to pharmacokinetics, J. Chromatogr. B. 686 (1996) 3–10.

[6] E. Engvall, The ELISA, enzyme-linked immunosorbent assay, Clin. Chem. 56 (2010) 319–320.

[7] B.K. Van Weemen, A.H.W.M. Schuurs, Immunoassay using antigen-enzyme conjugates, FEBS Letters. 15 (1971) 232–236.

[8] V. Viette, M. Fathi, S. Rudaz, D. Hochstrasser, J.-L. Veuthey, Current role of liquid chromatography coupled to mass spectrometry in clinical toxicology screening methods, Clin. Chem. Lab. Med. 49 (2011) 1091–1103.

[9] R. Ramanathan, ed., Mass spectrometry in drug metabolism and pharmacokinetics, John Wiley & Sons, New Jersey, 2009.

[10] J.A. Masucci, G.W. Caldwell, General guidelines for setting up an in vitro LC/MS/MS assay, in: Optimization in drug discovery, 2nd ed., Springer Science+Business Media, New York Heidelberg Dordrecht London, 2014: pp. 431–443.

[11] C.M. Whitehouse, R.N. Dreyer, M. Yamashita, J.B. Fenn, Electrospray interface for liquid chromatographs and mass spectrometers, Anal. Chem. 57 (1985) 675–679.

[12] F. Pullen, The fascinating history of the development of LC-MS; a personal perspective, Chromatography Today. (2010) 4–6.

[13] W.D. van Dongen, W.M.A. Niessen, LC-MS systems for quantitative bioanalysis, Bioanalysis. 4 (2012) 2391–2399.

[14] W.A. Korfmacher, Foundation review: principles and applications of LC-MS in new drug discovery, Drug Discov. Today. 10 (2005) 1357–1367.

[15] R.A. Yost, C.G. Enke, Triple quadrupole mass spectrometry for direct mixture analysis and structure elucidation, Anal. Chem. 51 (1979) 1251–1264.

[16] W.M.A. Niessen, Progress in liquid chromatography-mass spectrometry instrumentation and its impact on high-throughput screening, J. Chromatogr. A. 1000 (2003) 413–436.

[17] M.-Q. Huang, Z.J. Lin, N. Weng, Applications of high-resolution MS in bioanalysis, Bioanalysis. 5 (2013) 1269–1276.

[18] E.N. Fung, M. Jemal, A.-F. Aubry, High-resolution MS in regulated bioanalysis: where are we now and where do we go from here?, Bioanalysis. 5 (2013) 1277–1284.

[19] K.J. Bronsema, R. Bischoff, N.C. van de Merbel, Internal standards in the quantitative determination of protein biopharmaceuticals using liquid chromatography coupled to mass spectrometry, J. Chromatogr. B. 893–894 (2012) 1–14.

[20] J.R. Mazzeo, U. D.Neue, M. Kele, R.S. Plumb, Advancing LC performance with smaller particles and higher pressure, Anal. Chem. 77 (2005) 460A–467A.

[21] R.N. Xu, L. Fan, M.J. Rieser, T.A. El-Shourbagy, Recent advances in high-throughput quantitative bioanalysis by LC-MS/MS, J. Pharmaceut. Biomed. 44 (2007) 342–355.

[22] J.H. Gross, Electrospray ionization, in: Mass spectrometry, 2nd ed., Springer Verlag, New York Heidelberg Dordrecht London, 2011: pp. 561–620.

[23] J.H. Gross, Instrumentation, in: Mass spectrometry, 2nd ed., Springer Verlag, New York Heidelberg Dordrecht London, 2011: pp. 117–221.

[24] E.B. Jones, Quadrupole, Triple-quadrupole, and hybrid linear ion trap mass spectrometers for metabolite analysis, in: R. Ramanathan (Ed.), Mass spectrometry in drug metabolism and pharmacokinetics, John Wiley & Sons, New Jersey, 2009: pp. 123–157.

[25] J.-S. Kang, Principles and applications of LC-MS/MS for the quantitative bioanalysis of analytes in various biological samples, in: J.K. Prasain (Ed.), Tandem mass spectrometry – applications and principles, InTech, Rijeka, Croatia, 2012: pp. 441–492.
[26] J. Ni, J. Rowe, Microdosing assessment to evaluate pharmacokinetics and drug metabolism using liquid chromatography-tandem mass spectrometry technology, in: J. Paxton (Ed.), Topics on drug metabolism, InTech, Rijeka, Croatia, 2012.
[27] S. Devanshu, M. Rahul, G. Annu, S. Kishan, N. Anroop, Quantitative bioanalysis by LC-MS/MS: a review, JPBMS. 7 (2010) 1–9.
[28] T.R. Krishnan, I. Ibraham, Solid-phase extraction technique for the analysis of biological samples, J. Pharmaceut. Biomed. 12 (1994) 287–294.
[29] L.A. Berrueta, B. Gallo, F. Vicente, A review of solid phase extraction: Basic principles and new developments, Chromatographia. 40 (1995) 474–483.
[30] M. Meng, P.K. Bennett, Method development, validation, and sample analysis for regulated quantitative bioanalysis using LC-MS/MS, in: Q.A. Xu, T.L. Madden (Eds.), LC-MS in drug bioanalysis, Springer Science+Business Media, New York Heidelberg Dordrecht London, 2012.
[31] J. Pan, X. Jiang, Y.-L. Chen, Automatic supported liquid extraction (SLE) coupled with HILIC-MS/MS: an application to method development and validation of erlotinib in human plasma, Pharmaceutics. 2 (2010) 105–118.
[32] C.A. James, M. Breda, E. Frigerio, Bioanalytical method validation: a risk-based approach?, J. Pharmaceut. Biomed. 35 (2004) 887–893.
[33] D.M. Ramanathan, R.M. LeLacheur, Evolving role of mass spectrometry in drug discovery and development, in: R. Ramanathan (Ed.), Mass spectrometry in drug metabolism and pharmacokinetics, John Wiley & Sons, New Jersey, 2009: pp. 1–85.
[34] J. Wieling, LC-MS-MS experiences with internal standards, Chromatographia. 55 (2002) S107–S113.
[35] Q.A. Xu, Madden, eds., LC-MS in drug bioanalysis, Springer Science+Business Media, New York Heidelberg Dordrecht London, 2012.
[36] Guideline on bioanalytical method validation, European Medicines Agency (EMEA/CHMP/EWP/192217/2009), London, 21 July 2011.
[37] Guidance for industry: bioanalytical method validation, US Food and Drug Administration (FDA), Center for Drug Evaluation and Research, May 2001.
[38] Guidance for industry: bioanalytical method validation, US Food and Drug Administration (FDA), Center for Drug Evaluation and Research, Draft Guidance September 2013.
[39] L.V. Sonawane, B.N. Poul, S.V. Usnale, P.V. Waghmare, L.H. Surwase, Bioanalytical method validation and its pharmaceutical application – a review, Pharm. Anal. Acta. 5 (2014) 1–7.
[40] B. DeSilva, F. Garofolo, M. Rocci, S. Martinez, I. Dumont, F. Landry, et al., 2012 White paper on recent issues in bioanalysis and alignment of multiple guidelines, Bioanalysis. 4 (2012) 2213–2226.
[41] Validation of analytical procedures: text and methodology Q2 (R1), International Conference of Harmonisation of Technical Requirements for Registration of Pharmaceuticals for Human Use (ICH) Harmonised Tripartite Guideline, November 1996.
[42] E. Rozet, R.D. Marini, E. Ziemons, B. Boulanger, P. Hubert, Advances in validation, risk and uncertainty assessment of bioanalytical methods, J. Pharmaceut. Biomed. 55 (2011) 848–858.
[43] P. Kebarle, L. Tang, From ions in solution to ions in the gas phase, Anal. Chem. 65 (1993) 972A–986A.
[44] A. Van Eeckhaut, K. Lanckmans, S. Sarre, I. Smolders, Y. Michotte, Validation of bioanalytical LC–MS/MS assays: Evaluation of matrix effects, J. Chromatogr. B. 877 (2009) 2198–2207.
[45] S. Bansal, A. DeStefano, Key elements of bioanalytical method validation for small molecules, AAPS J. 9 (2007) E109–E114.

3 Results and discussion

3.1 Comparative study of four immortalized human brain capillary endothelial cell lines, hCMEC/D3, hBMEC, TY10, and BB19, and optimization of culture conditions, for an *in vitro* blood-brain barrier model for drug permeability studies

Daniela E. Eigenmann, Gongda Xue, Kwang S. Kim, Ashlee V. Moses, Matthias Hamburger, Mouhssin Oufir

Fluids and Barriers of the CNS 10 (2013) 33–50
DOI: 10.1186/2045-8118-10-33

An immortalized human *in vitro* BBB model was established by evaluating four currently available human brain microvascular endothelial cell lines (hCMEC/D3, hBMEC, TY10, and BB19) regarding their ability to form endothelial cell monolayers with sufficient barrier tightness. Highest transendothelial electrical resistance (TEER) values and lowest leakage of two fluorescent barrier integrity markers (sodium fluorescein, Na-F; lucifer yellow, LY) were obtained with mono-cultures of hBMEC cell line. Culture conditions (growth medium composition, tissue culture insert material, coating material and procedure, cell seeding density) were systematically optimized, the influence of co-cultured immortalized human astrocytes and pericytes on endothelial barrier integrity was evaluated, and biochemical and immunocytochemical characterization of cell-type specific cellular junction proteins was performed.

My contributions to this publication: cultivation of cells, design of experiments, preparation of the human in vitro BBB models, performance of permeability experiments with Na-F and LY, recording and analysing data, writing the manuscript draft, and preparation of figures and tables.

Daniela Elisabeth Eigenmann

FLUIDS AND BARRIERS
OF THE CNS

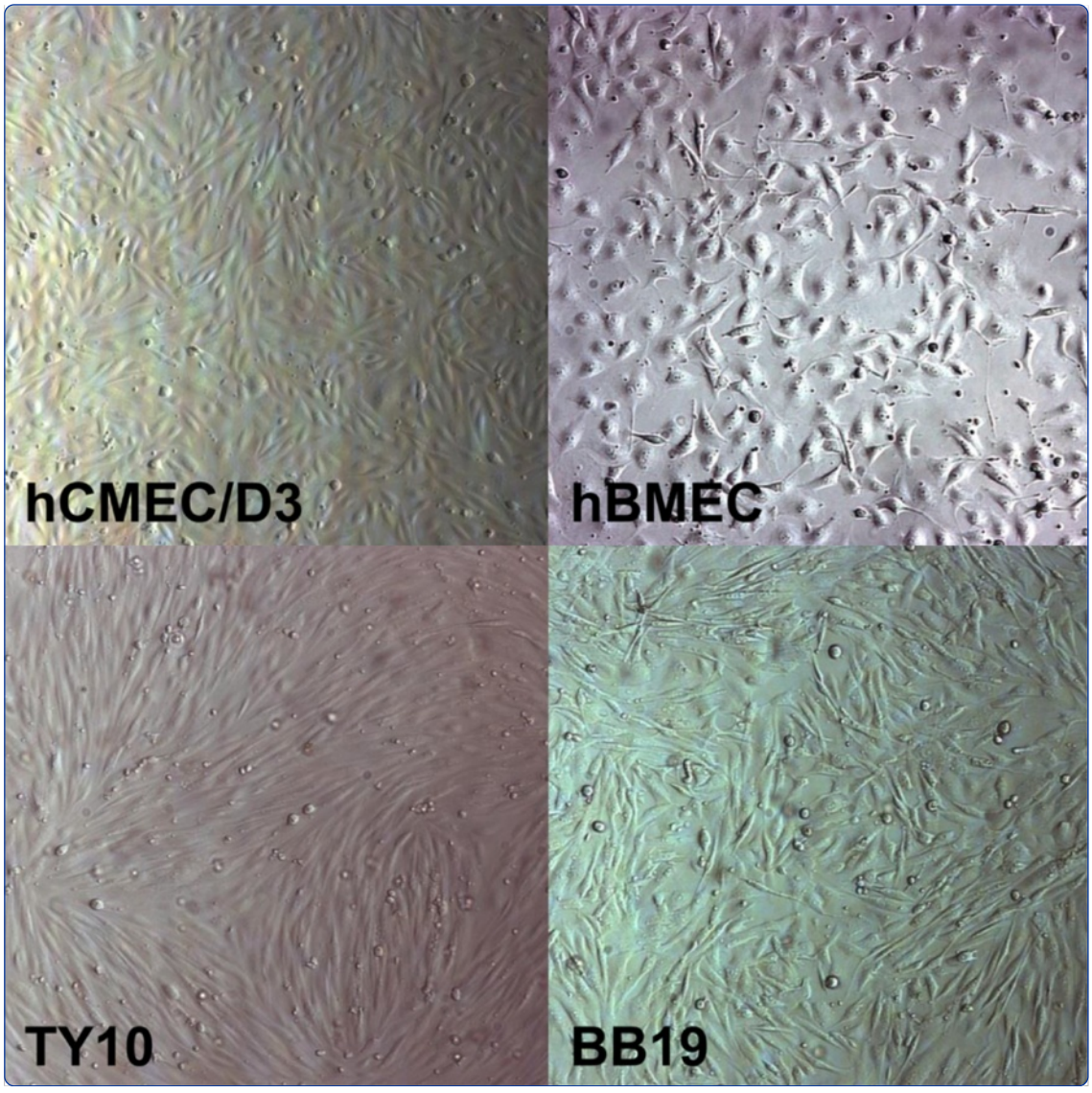

Comparative study of four immortalized human brain capillary endothelial cell lines, hCMEC/D3, hBMEC, TY10, and BB19, and optimization of culture conditions, for an *in vitro* blood–brain barrier model for drug permeability studies

Eigenmann *et al.*

BioMed Central

Eigenmann *et al. Fluids and Barriers of the CNS* 2013, **10**:33
http://www.fluidsbarrierscns.com/content/10/1/33

FLUIDS AND BARRIERS OF THE CNS

RESEARCH Open Access

Comparative study of four immortalized human brain capillary endothelial cell lines, hCMEC/D3, hBMEC, TY10, and BB19, and optimization of culture conditions, for an *in vitro* blood–brain barrier model for drug permeability studies

Daniela E Eigenmann[1], Gongda Xue[2], Kwang S Kim[3], Ashlee V Moses[4], Matthias Hamburger[1] and Mouhssin Oufir[1*]

Abstract

Background: Reliable human *in vitro* blood–brain barrier (BBB) models suitable for high-throughput screening are urgently needed in early drug discovery and development for assessing the ability of promising bioactive compounds to overcome the BBB. To establish an improved human *in vitro* BBB model, we compared four currently available and well characterized immortalized human brain capillary endothelial cell lines, hCMEC/D3, hBMEC, TY10, and BB19, with respect to barrier tightness and paracellular permeability. Co-culture systems using immortalized human astrocytes (SVG-A cell line) and immortalized human pericytes (HBPCT cell line) were designed with the aim of positively influencing barrier tightness.

Methods: Tight junction (TJ) formation was assessed by transendothelial electrical resistance (TEER) measurements using a conventional epithelial voltohmmeter (EVOM) and an automated CellZscope system which records TEER and cell layer capacitance (C_{CL}) in real-time.
Paracellular permeability was assessed using two fluorescent marker compounds with low BBB penetration (sodium fluorescein (Na-F) and lucifer yellow (LY)). Conditions were optimized for each endothelial cell line by screening a series of 24-well tissue culture inserts from different providers. For hBMEC cells, further optimization was carried out by varying coating material, coating procedure, cell seeding density, and growth media composition. Biochemical characterization of cell type-specific transmembrane adherens junction protein VE-cadherin and of TJ proteins ZO-1 and claudin-5 were carried out for each endothelial cell line. In addition, immunostaining for ZO-1 in hBMEC cell line was performed.

Results: The four cell lines all expressed the endothelial cell type-specific adherens junction protein VE-cadherin. The TJ protein ZO-1 was expressed in hCMEC/D3 and in hBMEC cells. ZO-1 expression could be confirmed in hBMEC cells by immunocytochemical staining. Claudin-5 expression was detected in hCMEC/D3, TY10, and at a very low level in hBMEC cells. Highest TEER values and lowest paracellular permeability for Na-F and LY were obtained with mono-cultures of hBMEC cell line when cultivated on 24-well tissue culture inserts from Greiner Bio-one® (transparent PET membrane, 3.0 μm pore size). In co-culture models with SVG-A and HBPCT cells, no increase of TEER could be observed, suggesting that none of the investigated endothelial cell lines responded positively to stimuli from immortalized astrocytic or pericytic cells.

(Continued on next page)

* Correspondence: mouhssin.oufir@unibas.ch
[1]Pharmaceutical Biology, Department of Pharmaceutical Sciences, University of Basel, Klingelbergstrasse 50, 4056 Basel, Switzerland
Full list of author information is available at the end of the article

(Continued from previous page)

Conclusions: Under the conditions examined in our experiments, hBMEC proved to be the most suitable human cell line for an *in vitro* BBB model concerning barrier tightness in a 24-well mono-culture system intended for higher throughput. This BBB model is being validated with several compounds (known to cross or not to cross the BBB), and will potentially be selected for the assessment of BBB permeation of bioactive natural products.

Keywords: Endothelial cell line, *In vitro* human blood–brain barrier (BBB) model, 24-well tissue culture insert, Transendothelial electrical resistance (TEER), Paracellular permeability, CellZscope

Background

Endothelial microvascular capillary cells in the human brain constitute a unique cellular barrier to sustain brain homeostasis and to protect the brain from xenobiotics and neurotoxic metabolites circulating in the bloodstream. It has been estimated that more than 98% of small-molecule drugs are not able to cross the blood–brain barrier (BBB) [1]. Hence, BBB penetration is a major challenge in the development of drugs acting on the central nervous system (CNS), where penetration into the brain is pivotal for achieving therapeutic effects [2]. On the other hand, low CNS penetration is desirable for drugs acting in the periphery. In early drug discovery and development, new chemical entities (NCEs) are now screened for their ability to cross the BBB.

For this purpose, a wide range of *in silico*, *in vitro*, and *in vivo* BBB models for early prediction of brain permeability of compounds have been developed and established [3]. Computational models and physicochemical methods such as the Parallel Artificial Membrane Permeability Assay (PAMPA-BBB) offer high-throughput screening capability at early stages of drug discovery, but are only able to predict passive permeation [4,5]. In contrast, *in vivo* models such as *in situ* brain perfusion provide high-quality data and some of the most reliable measurements of BBB drug penetration [6]. However, they are expensive in terms of time and resources and, therefore, only suitable for testing of compounds at more advanced stages of development [7]. Cell-based *in vitro* BBB models using primary or immortalized brain capillary endothelial cells from animal or human origin cultivated on microporous filter membranes of Transwell systems may bridge the gap between *in silico* and *in vivo* studies. They have been used for *in vitro* drug BBB permeability assessment for a long time, and their simple design allows for cost-efficient high-throughput screening [8-10].

Since mono-culture systems represent a highly simplified model and are far from mimicking *in vivo* conditions, further brain-derived cells being part of the neurovascular unit, such as astrocytes, pericytes, and/or neurons, have been incorporated into double and triple co-culture *in vitro* BBB models [10]. Whereas astrocytes have repeatedly been shown to favorably influence barrier tightness of endothelial cells [11-14], the impact of pericytes on BBB models is still a matter of controversy. It was shown that a syngeneic tri-culture model with primary rat brain capillary endothelial cells, astrocytes, and pericytes yielded highest transendothelial electrical resistance (TEER) values [15]. In contrast, another study showed that a barrier strengthening effect of pericytes critically depended on the differentiation state of cells [16].

In vitro animal BBB models using primary or low passage porcine, bovine, rat, or mouse cells, partly in double and triple co-culture systems, are generally characterized by relatively high TEER values and by low paracellular permeability of marker compounds [17]. Despite these favorable features, *in vitro* animal models show major drawbacks. Isolation and purification procedures of primary cells are tedious and time-consuming and require substantial experience [9]. Yields and lifespan of isolated cells are limited, and animal endothelial cells show differences in the expression of drug transporters and efflux pumps when compared to human brain capillary endothelial cells [18]. The use of primary cultures from human origin would avoid interspecies pharmacogenetic variation, yet the availability of these cells is greatly limited on ethical grounds [19]. Immortalized human brain capillary endothelial cells can be used as an alternative. These cells proliferate indefinitely and preserve their differentiating properties after repetitive passages, which is desirable for standardized screenings [9]. However, the establishment of a reliable human cell-line based BBB model has proven to be difficult [17]. These cells typically form only limited restrictive monolayers *in vitro,* with TEER values in the range 20 to 200 Ωcm^2 [17,20,21]. Compared to *in vivo* conditions where TEER values have been estimated to exceed 1000 Ωcm^2 [22,23], this is considerably lower. Despite this limitation, *in vitro* models with human immortalized cell lines possess several advantages and may be favorable tools for obtaining first mechanistic insights into BBB permeability of drugs. However, optimization of *in vitro* human BBB models for best barrier tightness is a prerequisite.

This study provides comparative data on four known immortalized human brain capillary endothelial cell lines, hCMEC/D3 [24], hBMEC [25], TY10 [26], and BB19 [27], regarding their ability to form a restrictive barrier in an *in vitro* 24-well format BBB model intended for higher

throughput drug permeability screening. For the first time, immortalized human astrocytes (SVG-A cell line [28]) and immortalized human pericytes (HBPCT cell line [29]) were included into co-culture models with these endothelial cell lines, with the objective to increase barrier tightness. We also present here a large set of *in vitro* TEER data recorded for each endothelial cell line cultivated on a range of tissue culture inserts from different manufacturers, with the aid of a CellZscope on-line TEER recording system [30]. This information was important prior to optimizing an *in vitro* BBB model with a particular cell line, since material and pore size of the filter membrane of the tissue culture inserts have been reported to strongly affect the adherence of cells and barrier tightness [31,32]. Subsequent optimization of a model with hBMEC cells was done by systematically screening various coating materials and coating procedures, by testing a variety of growth media containing barrier-strengthening compounds, by replacing the commonly used fetal bovine serum (FBS) with human serum (HS), and by using astrocyte-conditioned medium (ACM). In addition to TEER measurements, paracellular permeability of two fluorescent tracer molecules that do not cross the BBB in a significant amount (sodium fluorescein (Na-F) and lucifer yellow (LY)) was assessed. Biochemical characterization of VE-cadherin, ZO-1, and claudin-5, three major components of adherens and tight endothelial junctions, was carried out for each endothelial cell line. Furthermore, we performed immunostaining for ZO-1 in hBMEC cells.

Methods

Chemicals and materials

NaCl, $CaCl_2$, $MgCl_2$, KCl, glucose, 4-(2-hydroxyethyl) piperazine-1-ethanesulfonic acid (HEPES), $NaHCO_3$, Dulbecco's modified Eagle medium (DMEM), human collagen type IV, fibronectin, hydrocortisone (HC), dexamethasone, human epidermal growth factor (hEGF), 8-(4-chlorophenylthio) adenosine-3',5'-cyclic monophosphate sodium salt (8-(4-CPT)cAMP), 4-(3-butoxy-4-methoxybenzyl) imidazolidin-2-one (RO-20-1724), sodium fluorescein (Na-F), radio-immunoprecipitation assay (RIPA) lysis buffer, phosphate buffered saline (PBS), Triton X-100, bovine serum albumin (BSA), and 4',6-diamidino-2-phenylindole dihydrochloride (DAPI) were purchased from Sigma-Aldrich (Steinheim, Germany). Fetal bovine serum (FBS) "Gold" was from PAA Laboratories (Pasching, Austria). Human AB serum (HS) from a healthy female donor was obtained from the blood donor bank (Blutspendezentrum Universität Basel, Switzerland). Both sera were heat inactivated for 30 min at 56°C before use. EBM-2 and Single-Quots (human vascular endothelial growth factor, insulin-like growth factor-1, human fibroblast growth factor-B, hEGF, ascorbic acid, heparin, and HC) were from Lonza (Basel, Switzerland). Lucifer Yellow VS dilithium salt (LY) was purchased from Santa Cruz (Heidelberg, Germany). Antibiotic-antimycotic solution, secondary antibody (Alexa Fluor 488 conjugation), and phalloidin (Alexa Fluor 647) were received from Life Technologies (Paisley, UK). Rat-tail collagen type I and matrigel were purchased from BD Biosciences (Bedford, USA) and from Trevigen (Gaithersburg, MD, USA). The antibodies specific for zonula occludens (ZO)-1 protein, claudin-5, and vascular endothelial (VE)-cadherin were from Abcam (Cambridge, UK). Protease inhibitor cocktail was from Roche (Basel, Switzerland). Tissue culture flasks were from BD Biosciences (Bedford, USA) and from TPP (Trasadingen, Switzerland). 24-well tissue culture inserts and 24-well plates were from Corning Incorporated® (Corning, NY, USA), Greiner Bio-one® (Frickenhausen, Germany), BD Falcon® (Le Pont de Claix, France), Millipore® (Billerica, MA, USA), Nunc® (Roskilde, Denmark), and Brand® (Wertheim, Germany).

Cell cultures

In this study, four immortalized human brain capillary endothelial cell lines, hCMEC/D3 [24], hBMEC [25], TY10 [26], and BB19 [27], were used (Figure 1). Immortalized hCMEC/D3 cell line was kindly provided by Prof. Pierre-Olivier Couraud (Institut Cochin, Université René Descartes, Paris, France). hBMEC cell line was obtained from Prof. Kwang Sik Kim and Prof. Dennis Grab (John Hopkins University, Baltimore, MD, USA) through the Swiss Tropical and Public Health Institute (Prof. Reto Brun, STPH, Basel, Switzerland). TY10 cell line, a new generation of conditionally immortalized cells coming from TY08 [33], which was established by the same method as TY09 cell line [34], was obtained from Prof. Takashi Kanda (Yamaguchi University Graduate School of Medicine, Ube, Yamaguchi, Japan). BB19 cells were kindly provided by Prof. Ashlee V. Moses (Oregon Health and Science University, Portland, OR, USA). The immortalized SVG-A cell line, an astrocytic cell subclone of the astroglial SVG cell line [28,35], was a generous gift from Prof. Avindra Nath (National Institute of Neurological Disorders and Stroke, Bethesda, MD, USA) and the immortalized human pericyte cell line HBPCT [29] was provided by Prof. Takashi Kanda (Yamaguchi University Graduate School of Medicine, Ube, Yamaguchi, Japan).

All cell lines (except TY10) were cultured and grown to confluence in rat-tail collagen type I coated tissue culture flasks at 37°C and 5% CO_2 in humid atmosphere. TY10 cells were cultured under similar conditions but at 33°C, since this cell line was immortalized with a hTERT and a temperature-sensitive SV40 large-T antigen allowing the cells to grow at the permissive temperature of 33°C and to differentiate into physiological endothelial cells at the non-permissive temperature of 37°C [26,33,34].

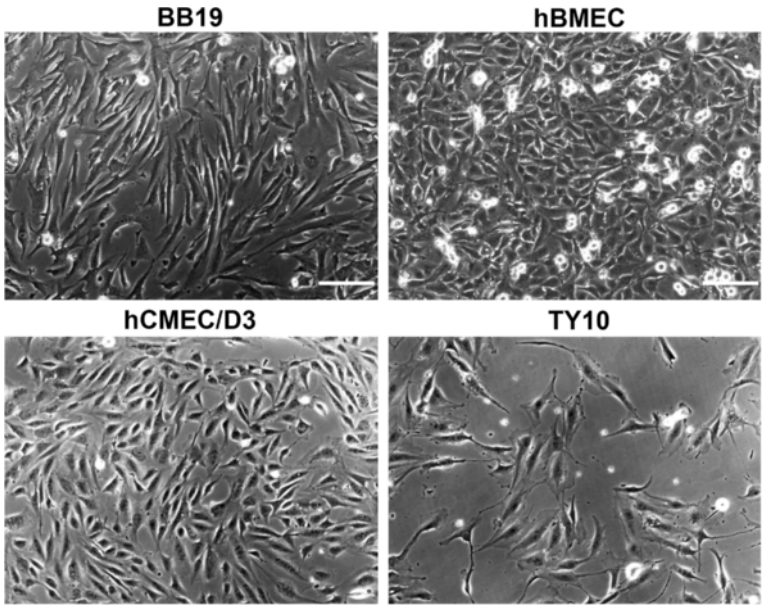

Figure 1 Phase contrast microscopy of four immortalized human brain capillary endothelial cell lines. Four endothelial cell lines were cultured in growth medium containing 20% FBS for 2 days and the representative cell morphology was imaged with a phase contrast microscope. Scale bar: 150 μm.

TY10, hBMEC, and BB19 cells were cultured in EBM-2 supplemented with Single-Quots, antibiotic-antimycotic solution, and 20% FBS (growth medium 20% FBS). hCMEC/D3 cells were cultured either in growth medium containing 20% FBS, or in the initial culture medium containing 5% FBS as described previously [24]. Culture medium for SVG-A and HBPCT cells was DMEM supplemented with antibiotic-antimycotic solution and 10% FBS. For experiments, hCMEC/D3 cells were between passage (P) 25 and 32, hBMEC cells were between P12 and P25, TY10 cells between P10 and P19, BB19 cells between P11 and P19, SVG-A cells between P7 and P10, and HBPCT cells between P13 and P19. All endothelial cell lines used in this study have been reported to preserve their phenotype for a limited range of passages (for hCMEC/D3: up to P33 [24], for hBMEC: up to P25, for TY10: at least up to P50 [34], and for BB19: up to P21 [27]).

Biochemical and immunocytochemical characterization of cellular junctions

Examined cells were lysed in standard RIPA lysis buffer supplied with protease inhibitor cocktail for 30 min on ice. Cleared supernatant corresponding to 50 μg of total protein per sample was subjected to SDS-PAGE and western blotting analysis. For immunochemistry studies, hBMEC cells grown on coverslips coated with rat-tail collagen type I were fixed with paraformaldehyde for 20 min at room temperature and subsequently permeabilized with PBS containing 0.2% Triton X-100 for 10 min. The cells were then blocked with 3% BSA for 30 min and incubated with ZO-1 antibody (1:100) at 4°C overnight. Secondary antibody (Alexa Fluor 488 conjugation) was incubated together with phalloidin (Alexa Fluor 647) for 1 h and the representative images were taken using a fluorescent microscope (Zeiss Z1). The nuclei were stained with DAPI.

In vitro co-culture BBB models and TEER measurements

Contact and non-contact co-culture BBB models using immortalized brain capillary endothelial cells and immortalized astrocytes or immortalized pericytes were established as follows. hCMEC/D3 (grown with initial medium), hBMEC, TY10, and BB19 cells were seeded separately on the apical side of the filter membranes of 24-well tissue culture inserts from Corning® (polycarbonate (PC) and polyester (PES) membranes, 0.4 μm and 3.0 μm pore size), coated with rat-tail collagen type I (10 μg/cm^2). The cell seeding density varied between 3.0×10^4 and 15×10^4 cells/cm^2 (hCMEC/D3: 6.0×10^4 cells/cm^2, hBMEC: between 3.0×10^4 and 4.5×10^4 cells/cm^2, TY10: 3.0×10^4 cells/cm^2, and BB19: between 7.5×10^4 and 15×10^4 cells/cm^2). Beforehand, SVG-A or HBPCT cells were seeded on the collagen type I coated (10 μg/cm^2) basal side of the porous filter membrane (SVG-A: between 3.0×10^4 and 9.0×10^4 cells/cm^2, HBPCT: 3.0×10^4 cells/cm^2) and allowed to attach for 1 h. For non-contact models, SVG-A cells were seeded at a cell density of 1.6×10^4 cells/cm^2 onto the culture plate and incubation thereafter was 2 h (37°C, 5% CO_2). After the start of the experiment, TEER values

were measured manually every 2–3 days using an epithelial voltohmmeter (EVOM) coupled to an Endohm-6 measurement chamber (World Precision Instruments, USA). Each TEER reading was followed by an exchange of medium. TEER values for cell layers, expressed in Ωcm^2, were calculated by subtracting the resistance of a coated control insert without cells from a coated insert with cells and by subsequent correction for surface area. For each experiment, at least 2 replicates were measured. Results are expressed as means ± S.E.M.

Screening of 24-well inserts from different providers for mono-culture BBB models

For the screening of 24-well tissue culture inserts from different providers (Corning®, Greiner Bio-One®, BD Falcon®, Millipore®, Nunc®, and Brand®), each endothelial cell line (hCMEC/D3 (cultured with growth medium 20% FBS), hBMEC, TY10, and BB19) was seeded separately on the apical side of the filter membrane at a density varying between 1.5×10^4 and 17×10^4 cells/cm^2. Prior to seeding, the membranes were coated with rat-tail collagen type I. The tissue culture inserts were placed into a 24-well cell module of a CellZscope system (NanoAnalytics, Münster, Germany) [30] which was placed inside an incubator (37°C and 5% CO_2). For *in vitro* models with TY10 cells, further experiments were performed for which the CellZscope system was first placed at 33°C (5% CO_2) for 2 days and subsequently transferred to 37°C (5% CO_2). The medium was refreshed every 2–4 days. TEER values were recorded in real-time every hour. TEER values for cell layers, expressed in Ωcm^2, were obtained by subtracting the TEER of a coated control insert without cells from a coated insert with cells. After placing the CellZscope system into the incubator, the cell module needs at least 6 h to reach 37°C. Since TEER values are highly temperature sensitive [36], recorded TEER values in this time period were not considered to be valid and are not reported. For each *in vitro* experiment, 2 or 3 replicates were measured. Results are expressed as means ± S.E.M. In addition to TEER values, the CellZscope system monitors the cell layer capacitance (C_{CL}) which reflects the membrane surface area. C_{CL} values in the range of 0.5-5.0 $\mu F/cm^2$ indicate cell confluency and validate TEER values [37,38]. All reported TEER values in the result section belong to a C_{CL} within this range, if not reported otherwise.

Optimization of mono-culture *in vitro* BBB models

For further optimization of mono-culture systems with hBMEC, various insert coating procedures using matrigel (80 $\mu g/cm^2$) and a mixture of collagen type IV/fibronectin (80/20 $\mu g/cm^2$) were assessed. Several growth media were tested containing compounds such as HC (500 nM; 1500 nM; in addition to HC already included in Single-Quots), dexamethasone (500 nM; 1000 nM), hEGF (50 ng/mL; 100 ng/mL; in addition to hEGF already included in Single-Quots), 8-(4-CPT)cAMP (250 μM), and RO-20-1724 (17.5 μM), which have been used in BBB studies to induce barrier tightness [17,21,39,40]. To avoid cytotoxic effects of DMSO or ethanol, their final concentration in the growth medium was below 0.25% [41]. Moreover, a culture medium (EBM-2, Single-Quots, and antibiotic-antimycotic solution) called "HS medium" supplemented with HS (10% and 20%, respectively) instead of FBS was evaluated. Astrocyte-conditioned media (ACM) were collected from SVG-A cells cultured with either growth medium for endothelial cell lines (ACM-1) or culture medium for SVG-A (ACM-2) and stored at −20°C until use.

BBB permeability studies with Na-F and LY

To further assess tight junction (TJ) integrity of endothelial cell layers, paracellular permeabilities of Na-F (MW 376.27) and LY (MW 550.39) were measured. These two fluorescent, non-P-glycoprotein (P-gp) substrate molecules have low BBB penetration and are widely used as barrier integrity markers for *in vitro* models. To obtain comparative data, hCMEC/D3 cells, hBMEC cells, and TY10 cells were seeded onto 24-well tissue culture inserts (Greiner Bio-one®, transparent polyethylene terephthalate (PET) membrane, 3.0 μm pore size, 0.6×10^6 pores/cm^2) and incubated at 37°C (5% CO_2) (except TY10 cells) inside the CellZscope cell module (Figure 2). For TY10, the CellZscope system was first put at 33°C (5% CO_2) for 2 days and was thereafter transferred to 37°C (5% CO_2) for 2 days prior to the permeability assay (Figure 3D). Cell seeding density for hCMEC/D3 and hBMEC was 6.0×10^4 cells/cm^2, and for TY10 it was 3.0×10^4 cells/cm^2. For hBMEC, contact co-culture models with SVG-A cells (9.0×10^4 cells/cm^2) or HBPCT cells (6.0×10^4 cells/cm^2) on the basal side of the coated filter membranes were tested.

TEER and C_{CL} values before and after the assays were monitored continuously for integrity control. All experiments for Na-F permeability were carried out at the time indicated with a black arrow in Figures 3A-D. For LY permeability assessment, TEER values were in the same range (graphs not shown). BB19 cells were not included in this permeability study since TEER values were extremely low.

For the permeability assay, tissue culture inserts were transferred into a 24-well plate containing 700 μL of pre-warmed (37°C) Ringer HEPES buffer (150 mM NaCl, 2.2 mM $CaCl_2$, 0.2 mM $MgCl_2$, 5.2 mM KCl, 2.8 mM glucose, 5 mM HEPES, and 6 mM $NaHCO_3$, pH 7.4) in each well (basolateral compartment). Medium in inserts (apical compartment) was then replaced with 300 μL of a pre-warmed (37°C) working solution containing Na-F

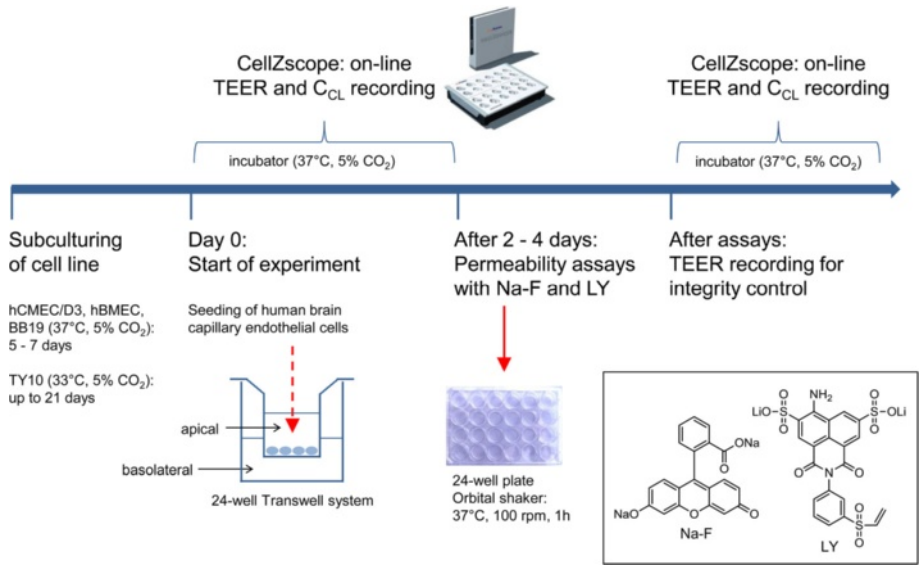

Figure 2 Scheme of preparation of the *in vitro* human BBB model. After subculturing the human cell lines for several days, the brain capillary endothelial cells were seeded on microporous filter membranes of 24-well tissue culture inserts (Greiner Bio-one®, transparent PET membrane, 3.0 μm pore size). The inserts were immediately transferred to a 24-well cell module of a CellZscope system which was placed inside an incubator (37°C and 5% CO_2). TEER and C_{CL} values were recorded on-line every hour. After 2–4 days (at the maximal TEER), paracellular permeability of Na-F and LY was assessed. To monitor barrier integrity after the assay, TEER and C_{CL} values were again recorded real-time using the CellZscope system.

or LY at 10 μg/mL in Ringer HEPES buffer. The 24-well plate was incubated at 37°C on an orbital shaker (ELMI DTS-2, Riga, Latvia) with moderate speed (100 rpm) and aliquots of 250 μL of both apical and basolateral compartments were collected after 1 h. All experiments were performed at least in triplicate. Quantification of fluorescence (Na-F: excitation 490 nm, emission 514 nm; LY: excitation 430 nm, emission 535 nm) was carried out using a Chameleon microplate reader (Hidex, Turku, Finland). The apparent permeability coefficient (P_{app}) for Na-F and LY was calculated in centimeters/second (cm/s) according to the equation:

$$P_{app}(cm/s) = V_B/(AC_{A0}) \times (\Delta C_B/\Delta t),$$

[42] where V_B is the volume in the basolateral compartment, A is the surface area of the filter membrane (0.336 cm^2 for Greiner Bio-one® inserts), C_{A0} is the initial concentration in the apical compartment, and $\Delta C_B/\Delta t$ is the change of concentration over time in the basolateral compartment.

Recovery (mass balance) of Na-F and LY was calculated with the following equation:

$$\text{Recovery } (\%) = (C_{Af}V_A + C_{Bf}V_B)/(C_{A0}V_A) \times 100\%,$$

[43] where C_{Af} and C_{Bf} are the final concentrations of the compound in the apical and basolateral compartment, respectively, C_{A0} is the initial concentration in the apical compartment, and V_A and V_B are the volumes in the apical and basolateral compartments, respectively. All results are expressed as means ± S.E.M.

Results

Biochemical and immunocytochemical characterization of cellular junctions

The four endothelial cell lines all expressed the endothelial marker protein VE-cadherin, albeit at different levels (Figure 4). The TJ protein ZO-1 was detected in hCMEC/D3 and in hBMEC at the same level, but it was expressed at much lower levels in BB19 and TY10 cell lines (Figure 4). ZO-1 expression in hBMEC cells was confirmed by immunocytochemical staining (Figure 5). Claudin-5 was not detected in BB19 cells, but was expressed at a high level in TY10 cells, at a low level in hCMEC/D3 cells, and at an even lower level in hBMEC cells (Figure 4).

Co-culture *in vitro* BBB models

In the beginning of this study, we aimed to establish an all-human *in vitro* BBB model by co-culturing separately several human brain capillary endothelial cell lines (hCMEC/D3, hBMEC, TY10, and BB19) with the human astrocyte cell line SVG-A and with the human pericyte cell line HBPCT. To find the most effective model regarding TJ resistance, each endothelial cell line was grown separately on the apical filter membrane with SVG-A cells or HBPCT cells grown on the basal filter membrane (contact models), or in the culture plate (non-contact models). Various 24-well tissue culture

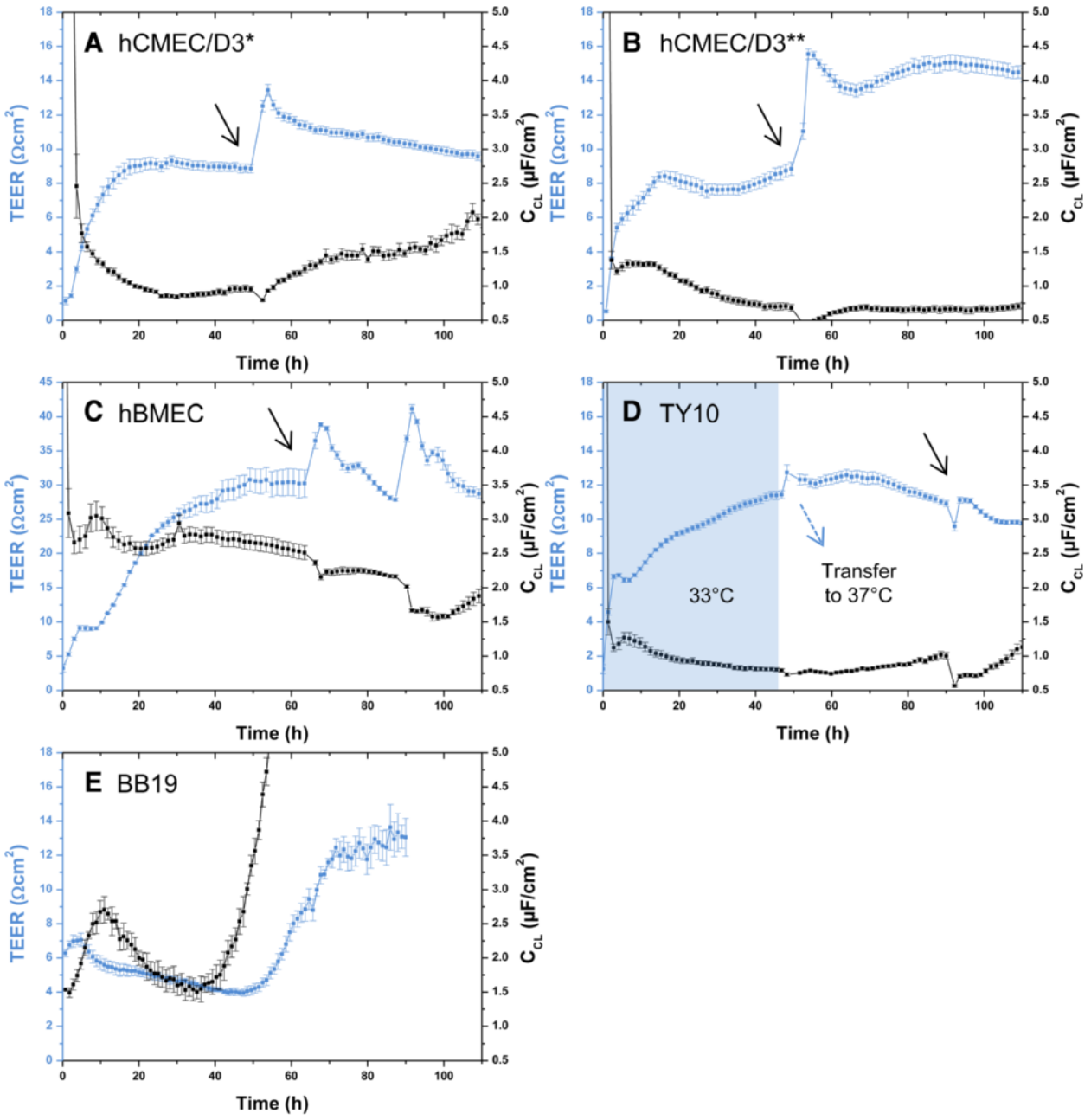

Figure 3 Mean TEER values (blue curve) and C_{CL} values (black curve) recorded real-time by the CellZscope system of four human brain capillary endothelial cell lines grown on 24-well tissue culture inserts. Black arrows indicate the time when the permeability assay with Na-F was performed (for resulting P_{app} values see Figures 7A and B). For hCMEC/D3 and TY10, the permeability assay was performed at TEER values in the range of 10 Ωcm^2 (hCMEC/D3: *cultured with initial medium **(A)**, **cultured with growth medium 20% FBS **(B)**. For hBMEC, the assay was carried out at TEER values in the range of 30 Ωcm^2. TEER values after the assay were in the same range or even higher as before, suggesting that cell layers were robust during the experiment and barrier integrity was maintained **(A-D)**. For each of the three cell lines, C_{CL} values were in the acceptable range of 0.5-5.0 $\mu F/cm^2$, indicating that cells were confluent. BB19 cell line **(E)** yielded very low TEER values in the range of 5 Ωcm^2. Since C_{CL} values were drastically increasing after 55 h, the experiment was stopped. BB19 cells were not included into permeability studies with Na-F and LY due to their low TEER. All experiments were performed with Greiner Bio-one® inserts (transparent PET membrane, 3.0 µm pore size, 0.6×10^6 pores/cm^2, n = 2–5).

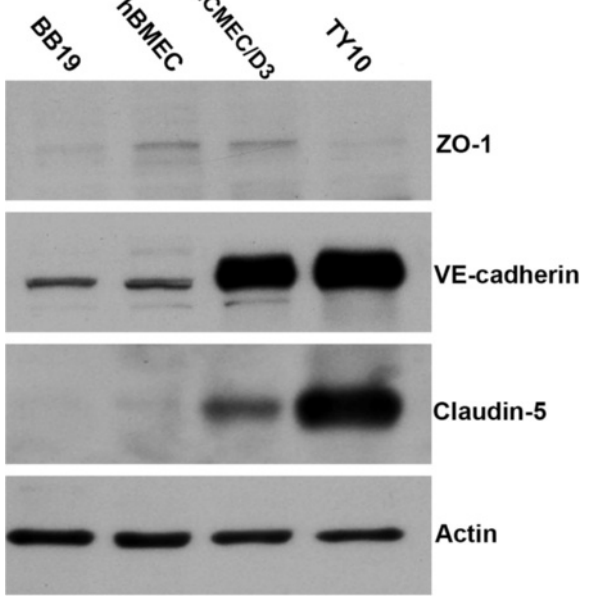

Figure 4 Western blot analysis of tight junction proteins ZO-1, claudin-5, and adherens junction protein VE-cadherin from cell lysates of four endothelial cell lines. The cells were lysed with RIPA buffer. 50 μg of total protein was subjected to SDS-PAGE and western blotting analysis for individual markers. Actin was used as loading control. The four cell lines all expressed the adherens junction protein VE-cadherin. The TJ protein ZO-1 was detected in hCMEC/D3, in hBMEC, and at much lower levels in BB19 and TY10 cell lines. Claudin-5 expression was detected in hCMEC/D3, TY10, and at a very low level in hBMEC cells.

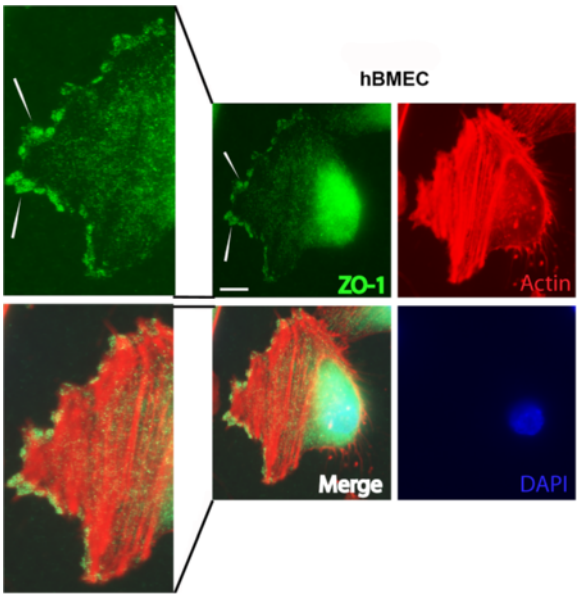

Figure 5 Immunofluorescence staining of tight junction protein ZO-1 in hBMEC cell line. hBMEC cells were grown on collagen-coated glass coverslips for 48 h followed by paraformaldehyde fixation. Even with a high background noise level especially on nuclei, ZO-1 was detected at the leading edge of migrating hBMEC cells (see white arrows). Scale bar: 30 μm.

inserts from Corning® with PC and PES membrane and pore sizes 0.4 μm and 3.0 μm were tested, since these insert types are mostly used for drug transport studies.

Maximal TEER values measured with the EVOM were obtained with mono-cultures of hBMEC cells (30.7 ± 0.660 Ωcm^2 on day 12) on tissue culture insert with PES membrane and 0.4 μm pore size (Figure 6, red curve). hBMEC cells grown in contact or non-contact co-culture models with SVG-A cells on the same kind of inserts resulted in lower maximal TEER values (24.3 ± 1.16 Ωcm^2 on day 7 and 22.3 ± 0.165 Ωcm^2 on day 9, respectively) (Figure 6, blue and black curves). In contact co-culture models with HBPCT cells, maximal TEER values were also lower than for hBMEC mono-cultures (26.2 ± 0.165 Ωcm^2 on day 12 compared to 30.7 ± 0.660 Ωcm^2 on day 12) (Figure 6, green curve). TEER values for hBMEC cells on additional tested 24-well tissue culture inserts, and TEER values for all other models using hCMEC/D3, TY10, and BB19 cells (in mono-cultures and in co-cultures), yielded maximal TEER values below 20 Ωcm^2 (data not shown). SVG-A cells and HBPCT cells did not significantly increase or decrease TEER values (data not shown).

Screening of 24-well tissue culture inserts for each endothelial cell line using the CellZscope

In the above described co-culture experiments, we observed i) that Transwell co-culture models with immortalized astrocytes and immortalized pericytes did not increase TJ resistance of the immortalized brain microvascular endothelial cells included in this study (for hBMEC, see Figure 6), and ii) that membrane material and pore size had a significant impact on barrier tightness. Therefore, we decided to optimize mono-culture models by systematically screening a range of 24-well tissue culture inserts from various providers (Corning®, Greiner Bio-one®, Millipore®, BD Falcon®, Nunc®, and Brand®) for each endothelial cell line, with the aim to increase TEER. For this screening, an automated CellZscope device [30] was used, which records the TEER in real-time every hour inside the incubator at 37°C and 5% CO_2. TEER values could not be recorded with 24-well tissue culture inserts from Nunc® (PC, 0.4 μm and 3.0 μm pore size) or Brand® (translucent PC, 0.4 μm and 3.0 μm pore size), because their particular design rendered them incompatible with the CellZscope cell module.

hCMEC/D3 mono-cultures

For hCMEC/D3 monolayers, low TEER values between 5.09 and 11.9 Ωcm^2 were obtained on all tested inserts (Table 1). It was not possible to identify conclusively the

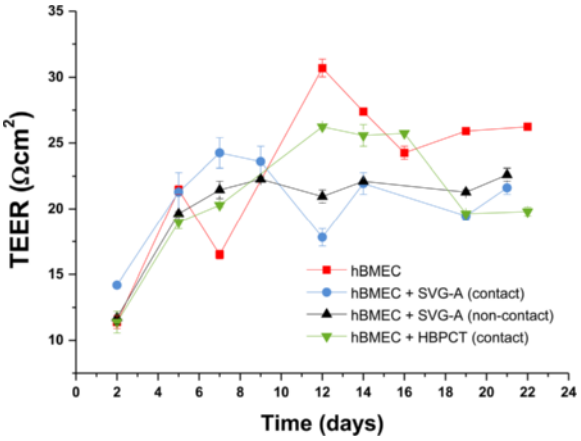

Figure 6 Mean TEER values for hBMEC cell line in mono-cultures and co-cultures with immortalized astrocytes (SVG-A) and immortalized pericytes (HBPCT). Experiments using 24-well tissue culture inserts from Corning® (transparent PES membrane, 0.4 μm pore size, 4.0×10^6 pores/cm^2, n = 2). Maximal TEER values (30.7 ± 0.660 Ωcm^2 on day 12) were obtained with hBMEC mono-cultures. Co-culture models with SVG-A and HBPCT cells did not result in increased TEER values. Data were recorded with an EVOM coupled to an Endohm-6 measurement chamber.

Table 1 Summary of maximal TEER values recorded real-time by the CellZscope system for hCMEC/D3, hBMEC, and TY10 mono-cultures

24-well tissue culture insert coated with collagen type I	hCMEC/D3		hBMEC		TY10	
	Time (d)	Mean max. TEER ± S.E.M. (Ωcm^2)	Time (d)	Mean max. TEER ± S.E.M. (Ωcm^2)	Time (d)	Mean max. TEER ± S.E.M. (Ωcm^2)
Corning® (translucent PC, 0.4 μm, 1.0×10^8 pores/cm^2, 0.33 cm^2)	4.75	6.72 (± 0.113)	2.46	2.79 (± 0.410)	2.37	4.56 (± 1.06)
Corning® (translucent PC, 3.0 μm, 2.0×10^6 pores/cm^2, 0.33 cm^2)	5.07	8.56 (± 0.217)	5.19	#9.09 (± 0.103)	7.73**	#11.2 (± 0.904)
Corning® (transparent PES, 0.4 μm, 4.0×10^6 pores/cm^2, 0.33 cm^2)	1.97*	7.04 (± 0.231)	2.79*	17.7 (± 0.152)	1.96	6.96 (± 0.199)
Corning® (transparent PES, 3.0 μm, 2.0×10^6 pores/cm^2, 0.33 cm^2)	3.38	9.44 (± 0.0877)	2.81	6.24 (± 0.0805)	2.37	7.94 (± 0.110)
Greiner Bio-one® (transparent PET, 0.4 μm, 2.0×10^6 pores/cm^2, 0.336 cm^2)	2.47	6.48 (± 0.125)	1.85	#7.27 (± 2.36)	1.45*	9.37 (± 0.690)
Greiner Bio-one® (translucent PET, 0.4 μm, 1.0×10^8 pores/cm^2, 0.336 cm^2)	2.34	5.18 (± 0.222)	5.13	7.42 (± 0.288)	1.66*	12.4 (± 2.11)
Greiner Bio-one® (transparent PET, 3.0 μm, 0.6×10^6 pores/cm^2, 0.336 cm^2)	2.34	11.9 (± 0.118)	2.75	28.4 (± 2.47)	1.15*	13.0 (± 0.0151)
Greiner Bio-one® (translucent PET, 3.0 μm, 2.0×10^6 pores/cm^2, 0.336 cm^2)	2.34	9.39 (± 0.166)	2.49	5.85 (± 0.357)	1.32*	7.26 (± 0.0949)
Millipore® (translucent PET, 0.4 μm, 1.0×10^8 pores/cm^2, 0.33 cm^2)	2.34	5.35 (± 0.312)	2.49	2.92 (± 0.164)	1.37*	5.98 (± 0.200)
Millipore® (translucent PET, 3.0 μm, 2.0×10^6 pores/cm^2, 0.33 cm^2)	2.34	10.2 (± 0.0304)	2.53	15.0 (± 0.348)	2.37	11.2 (± 0.806)
BD Falcon® (transparent PET, 0.4 μm, 2.0×10^6 pores/cm^2, 0.3 cm^2)	2.34	5.09 (± 0.133)	3.34	8.40 (± 0.524)	3.11	4.72 (± 0.00525)
BD Falcon® (transparent PET, 3.0 μm, 0.8×10^6 pores/cm^2, 0.3 cm^2)	2.34	8.75 (± 0.180)	3.21	24.1 (± 0.0595)	1.54*	6.19 (± 0.429)

All tested 24-well tissue culture inserts were coated with collagen type I. The cell seeding density varied between 3.0×10^4 and 15×10^4 cells/cm^2 for hCMEC/D3, between 4.5×10^4 and 17×10^4 cells/cm^2 for hBMEC, and between 1.5×10^4 and 15×10^4 cells/cm^2 for TY10 (n = 2–3).
#C_{CL} outside the acceptable range of 0.5-5.0 μF/cm^2 almost during the whole experiment, indicating that cells were not confluent; PC: polycarbonate; PES: polyester; PET: polyethylene terephthalate; *before first change of medium; **after third change of medium.

most suitable tissue culture insert for this cell line, since differences between TEER values were not significant. Highest TEER values were observed with 24-well tissue culture inserts from Corning® (transparent PES membrane, 3.0 μm pore size, 2.0 × 10^6 pores/cm^2), from Millipore® (translucent PET membrane, 3.0 μm pore size, 2.0 × 10^6 pores/cm^2), and from Greiner Bio-one® (transparent PET membrane, 3.0 μm pore size, 0.6 × 10^6 pores/cm^2), with a maximum TEER up to 12 Ωcm^2 (Table 1). For these experiments, hCMEC/D3 cells were cultured with growth medium containing 20% FBS to allow for direct comparisons between all cell lines. When hCMEC/D3 cells were cultured with initial medium containing 5% FBS, maximal TEER values were in the same range (around 10 Ωcm^2) as when cultured in growth medium containing 20% FBS (Figures 3A and B).

hBMEC mono-cultures

TEER values of hBMEC monolayers were between 2.79 and 28.4 Ωcm^2. The highest value was measured on 24-well tissue culture inserts (transparent PET membrane, 3.0 μm pore size, 0.6 × 10^6 pores/cm^2) from Greiner Bio-one® (Table 1 and Figure 3C).

TY10 mono-cultures

TEER values for TY10 monolayers were between 4.56 and 13.0 Ωcm^2. The highest value was recorded when cells were cultured at 37°C from the start of the experiment on inserts from Greiner Bio-one® (transparent PET membrane, 3.0 μm pore size, 0.6 × 10^6 pores/cm^2) (Table 1). TEER values were not increased when culturing TY10 monolayers at the permissive temperature of 33°C for 2 days before transferring them to 37°C (Figure 3D).

BB19 mono-cultures

With monolayers of BB19 cells on various 24-well tissue culture inserts, only extremely low TEER values in the range of 5 Ωcm^2 were obtained (Figure 3E). Despite repeated experiments, C_{CL} values remained outside of the acceptable range of 0.5-5.0 μF/cm^2, indicating that cell layers were not confluent. Since barrier restriction with such a low TJ resistance was not sufficient for reliable *in vitro* BBB models, BB19 cell line was not further included in our studies for paracellular tightness assessment using the integrity markers Na-F and LY.

Further optimization of hBMEC mono-cultures

Since TEER values were highest (28.4 ± 2.47 Ωcm^2) with monolayers of hBMEC cells cultivated on Greiner Bio-one® inserts (transparent PET membrane, 3.0 μm pore size, 0.6 × 10^6 pores/cm^2) coated with collagen type I (Table 1), we optimized this particular mono-culture system by varying parameters such as cell seeding density, coating material and procedure, and by testing different growth media compositions.

Optimization resulted in TEER values in the range of 40 Ωcm^2 (Table 2). A maximal TEER value of 43.6 ± 3.89 Ωcm^2 (after 3.19 days *in vitro*) was obtained when hBMEC cells were cultured under normal growth conditions (growth medium containing 20% FBS) at a seeding density of 4.5 × 10^4 cells/cm^2 (Table 2). Lower or higher cell seeding densities resulted in decreased maximal TEER values (25.9 ± 0.635 Ωcm^2 at 3.0 × 10^4 cells/cm^2 and 28.4 ± 2.47 Ωcm^2 at 15 × 10^4 cells/cm^2). The duration of coating the tissue culture inserts with collagen type I did not have an impact on TEER (data not shown). Coating the inserts with collagen type IV/fibronectin did not further improve barrier tightness. However, coating the tissue culture inserts with matrigel resulted in a decrease of maximal TEER values (16.6 ± 0.183 Ωcm^2 compared to 28.4 ± 2.47 Ωcm^2). Growth media containing barrier inducing compounds such as dexamethasone (500 nM and 1000 nM, respectively), 8-(4-CPT)-cAMP (250 μM), RO-20-1724 (17.5 μM), additional HC (500 nM and 1500 nM, respectively), or additional hEGF (50 ng/mL and 100 ng/mL, respectively) did not significantly increase the TEER of hBMEC monolayers. Growth medium supplemented with HS (10% and 20%, respectively) instead of 20% FBS resulted in a decreased maximal TEER (20.4 ± 0.867 Ωcm^2 and 26.2 ± 0.324 Ωcm^2, respectively, compared to 28.4 ± 2.47 Ωcm^2). The use of ACM-1 resulted in a decrease of the maximal TEER (13.5 ± 0.614 Ωcm^2, compared to 28.4 ± 2.47 Ωcm^2). A similar result, i.e. a decrease of maximal TEER, was obtained when using a mixture of ACM-2 and growth medium 20% FBS (1:1) (23.8 ± 0.572 Ωcm^2, compared to 28.4 ± 2.47 Ωcm^2).

Evaluation of paracellular permeability through mono-cultures

Since highest TEER values were observed when hBMEC monolayers were cultured on rat-tail collagen type I coated Greiner Bio-one® inserts (transparent PET membrane, pore size 3.0 μm, 0.6 × 10^6 pores/cm^2) at a cell seeding density of 4.5 × 10^4 cells/cm^2 (Table 1), this insert was selected for permeability studies using Na-F (MW 376.27) and LY (MW 550.39). For hBMEC cell line, the mean P_{app} for Na-F was 5.08 ± 0.220 × 10^{-6} cm/s (Figure 7A). For LY, the mean P_{app} was 5.39 ± 0.364 × 10^{-6} cm/s (Figure 7B). For hCMEC/D3, mean P_{app} values for Na-F and LY were 12.5 ± 0.326 × 10^{-6} cm/s and 10.0 ± 0.498 × 10^{-6} cm/s, respectively, when cells were grown with initial medium containing 5% FBS (Figures 7A and B). When hCMEC/D3 cells were cultivated with growth medium containing 20% FBS, mean P_{app} values for Na-F and LY were 13.4 ± 0.484 × 10^{-6} cm/s and 11.7 ± 0.957 × 10^{-6} cm/s, respectively (Figures 7A

Table 2 Summary of maximal TEER values recorded real-time by the CellZscope system for hBMEC mono-cultures using a range of different culture conditions

Culture conditions	Cell seeding density (cells/cm^2)	Time (d)	Mean max. TEER ± S.E.M. (Ωcm^2)
Cell seeding density: 3.0 × 10^4 cells/cm^2, coating: collagen type I (10 μg/cm^2)	3.0 × 10^4	1.72*	25.9 (± 0.635)
Cell seeding density: 4.5 × 10^4 cells/cm^2, coating: collagen type I (10 μg/cm^2)	4.5 × 10^4	3.19	43.6 (± 3.89)
Growth medium with additional HC (500 nM) for 3 days (only apical), coating: collagen type I (10 μg/cm^2)	4.5 × 10^4	3.19	43.2 (± 4.27)
Growth medium with additional HC (1500 nM) for 3 days (only apical), coating: collagen type I (10 μg/cm^2)	4.5 × 10^4	3.19	40.4 (± 0.646)
Cell seeding density: 6.0 × 10^4 cells/cm^2, coating: collagen type I (10 μg/cm^2)	6.0 × 10^4	1.72*	36.3 (± 2.06)
Cell seeding density: 9.0 × 10^4 cells/cm^2, coating: collagen type I (10 μg/cm^2)	9.0 × 10^4	4.15	38.9 (± 0.928)
Growth medium with dexamethasone (500 nM) for 3 days (only apical), coating: collagen type I (10 μg/cm^2)	9.0 × 10^4	4.15	35.9 (± 0.338)
Growth medium with dexamethasone (1000 nM) for 3 days (only apical), coating: collagen type I (10 μg/cm^2)	9.0 × 10^4	4.15	38.0 (± 1.26)
Growth medium with additional hEGF (50 ng/mL) for 3 days (only apical), coating: collagen type I (10 μg/cm^2)	9.0 × 10^4	4.15	36.4 (± 0.902)
Growth medium with additional hEGF (100 ng/mL) for 3 days (only apical), coating: collagen type I (10 μg/cm^2)	9.0 × 10^4	4.15	40.0 (± 1.94)
Growth medium with 8-(4-CPT)cAMP (250 μM) and RO-20-1724 (17.5 μM) (apical and basolateral), coating: collagen type I (10 μg/cm^2)	9.0 × 10^4	2.84	20.0 (± 0.509)
Growth medium with 8-(4-CPT)cAMP (250 μM) and RO-20-1724 (17.5 μM), added after 2 days *in vitro* (apical and basolateral), coating: collagen type I (10 μg/cm^2)	9.0 × 10^4	2.84	20.9 (± 1.36)
Cell seeding density: 15 × 10^4 cells/cm^2, coating: collagen type I (10 μg/cm^2)	15 × 10^4	2.75	28.4 (± 2.47)
Coating: collagen type IV/fibronectin (80/20 μg/cm^2)	15 × 10^4	2.75	29.3 (± 1.10)
Coating: matrigel (80 μg/cm^2)	15 × 10^4	2.75	16.6 (± 0.183)
Growth medium with 10% HS (apical and basolateral), coating: collagen type I (10 μg/cm^2)	15 × 10^4	1.26*	20.4 (± 0.867)
Growth medium with 20% HS (apical and basolateral), coating: collagen type I (10 μg/cm^2)	15 × 10^4	1.21*	26.2 (± 0.324)
ACM-1 (apical and basolateral), coating: collagen type I (10 μg/cm^2)	15 × 10^4	1.64*	13.5 (± 0.614)
Mixture of ACM-2 and growth medium 20% FBS (1:1) (apical and basolateral), coating: collagen type I (10 μg/cm^2)	15 × 10^4	3.35	23.8 (± 0.572)

24-Well tissue culture inserts were from Greiner Bio-one® (transparent PET membrane, pore size 3.0 μm, 0.6 × 10^6 pores/cm^2, n = 2–3). *Before first change of medium.

and B). For TY10, mean P_{app} values for Na-F and LY were 12.4 ± 0.155 × 10^{-6} cm/s and 9.68 ± 0.413 × 10^{-6} cm/s, respectively (Figures 7A and B). Mean recoveries for Na-F in all experiments were between 75% and 87% (Figure 7C). For LY, mean recoveries were between 66% and 79% (Figure 7D). According to Hubatsch et al. (2007), a mass balance of at least 80% would be optimal to give an acceptable approximation of the P_{app} value [44]. After each experiment, TEER values were in the same range as before the assay (or even higher) (Figures 3A-D), suggesting that cell monolayers were robust during the experiment and barrier integrity was maintained.

Evaluation of paracellular permeability through contact co-cultures

Since lowest P_{app} values were obtained with hBMEC monolayers (Figures 7A and B), we established co-culture models with SVG-A and HBPCT cells to further assess paracellular permeability. Mean P_{app} values for Na-F through hBMEC co-cultured with SVG-A and HBPCT cells were 7.43 ± 0.200 × 10^{-6} cm/s and 8.26 ± 0.893 × 10^{-6} cm/s, respectively (compared to 5.08 ± 0.220 × 10^{-6} cm/s through hBMEC mono-cultures). Since a culture medium supplemented with growth factors may mask the potential BBB inducing effect of astrocytes and pericytes, further experiments were performed using culture medium without growth factors. Mean P_{app} values for Na-F through hBMEC monolayers cultured without growth factors was 5.11 ± 0.0487 × 10^{-6} cm/s (Figure 8). Through hBMEC cells co-cultured with SVG-A or HBPCT cells using medium deprived of growth factors, mean P_{app} values were slightly higher (6.88 ± 0.516 × 10^{-6} cm/s and 7.22 ± 0.455 × 10^{-6} cm/s, respectively) (Figure 8). In all experiments, mean recoveries were between 98% and 102%.

Discussion

There is a need for predictive assays amenable to medium to high-throughput screening for the assessment of brain

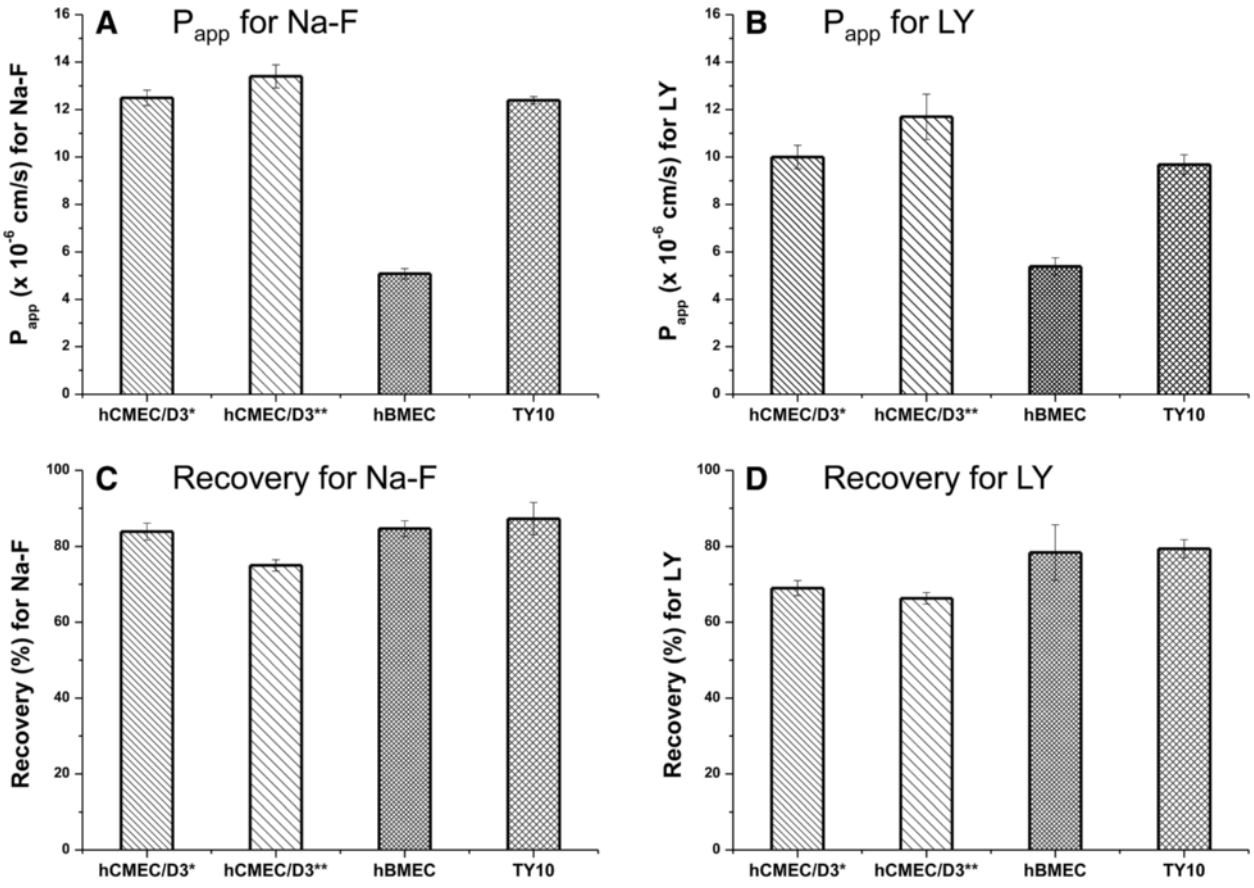

Figure 7 Mean P_{app} values (A, B) and mean recoveries (C, D) for Na-F and LY through hCMEC/D3, hBMEC, and TY10 monolayers. 24-Well tissue culture inserts from Greiner Bio-one® (transparent PET membrane, 3.0 μm pore size, 0.6×10^6 pores/cm^2) were used (n = 3–5). **A**, **B**: Lowest paracellular permeability of Na-F and LY was obtained through hBMEC monolayers ($5.08 \pm 0.220 \times 10^{-6}$ cm/s and $5.39 \pm 0.364 \times 10^{-6}$ cm/s, respectively). All experiments for Na-F permeability were carried out at the time indicated with a black arrow in Figures 3A-D. For LY, permeability measurements were carried out at TEER values in the same range (graphs not shown). **C**, **D**: Mean recoveries of Na-F in all experiments were in the range of 75% and 87%. For LY, mean recoveries varied between 66% and 79%. *cultured with initial medium; **cultured with growth medium 20% FBS.

penetration of drug leads. To this date, only a few immortalized human brain capillary endothelial cell lines have been developed and used for the establishment of human *in vitro* BBB models [9]. The most extensively characterized human cell line is the hCMEC/D3 cell line, which has been reported to represent a promising *in vitro* human BBB model for drug transport studies [45,46]. TY10 cell line, transduced with a temperature-sensitive SV40 large-T antigen, has furthermore been reported to be a promising and advantageous cell line with excellent expression of TJ proteins such as claudin-5, occludin, and ZO-1 [26]. Whereas at 33°C, TY10 cells can be cultivated for more than 50 passages without undergoing morphological changes, a temperature shift from 33°C to 37°C results in the exclusion of the SV40 large-T antigen as a cancer gene [33,34].

However, monolayers of immortalized human brain capillary endothelial cell lines are known to form only moderately restrictive barriers, with TEER values in the range of 20–200 Ωcm^2 [17,20,21]. To increase barrier tightness of four currently available human brain capillary endothelial cell lines, hCMEC/D3, hBMEC, TY10, and BB19 (Figure 1), we tested co-culture models with immortalized human astrocytes (SVG-A cell line) and pericytes (HBPCT cell line). Interestingly, we did not observe an increase of TJ resistance in immortalized human brain capillary endothelial cells under co-culture conditions. All co-culture models produced TEER values that were comparable or lower than those recorded with mono-cultures (for hBMEC cell line, see Figures 6 and 8A). This suggested that the investigated endothelial cell lines were unable to respond positively to stimuli from immortalized astrocytic or pericytic cells.

These findings are in accord with previous reports in which no additional benefit in terms of TEER was observed when culturing hCMEC/D3 cells with ACM or

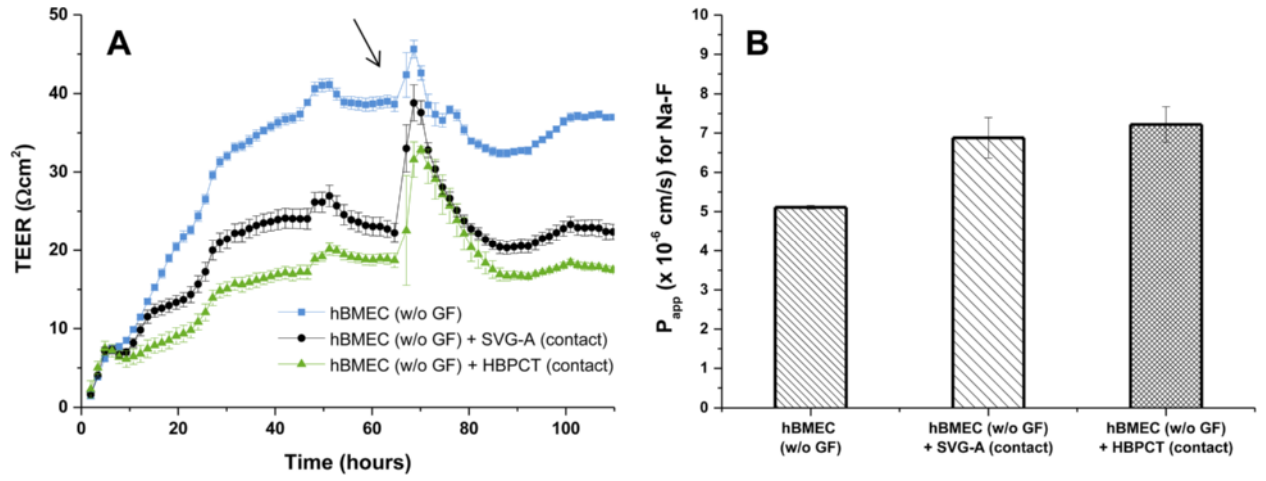

Figure 8 Mean TEER (A) and P_{app} (B) values for hBMEC cultured without growth factors in mono-cultures and contact co-cultures with SVG-A and HBPCT cells. A: Mean TEER values recorded real-time by the CellZscope system for hBMEC cells cultured without growth factors (w/o GF) in mono-cultures and co-cultures with SVG-A (black curve) or HBPCT cells (green curve). 24-Well tissue culture inserts from Greiner Bio-one® (transparent PET membrane, 3.0 μm pore size, 0.6×10^6 pores/cm^2) were used (n = 3). Compared to co-cultures with SVG-A and HBPCT cells, hBMEC mono-cultures produced higher TEER values in the range of 40 Ωcm^2 (blue curve). C_{CL} values were in the acceptable range of 0.5-5.0 μF/cm^2 (data not shown), indicating that hBMEC cells were confluent. The black arrow indicates the time when the permeability assay with Na-F was performed. **B**: Mean P_{app} values for Na-F through hBMEC cultured without growth factors through mono-cultures and co-cultures with SVG-A or HBPCT cells. Lowest P_{app} values for Na-F ($5.11 \pm 0.0487 \times 10^{-6}$ cm/s) were obtained through hBMEC mono-cultures. Mean recoveries in all experiments were between 98% and 102% (n = 3).

when co-culturing the endothelial cells with human astrocytes, respectively [24,47]. In contrast, our results do not support recent findings which showed that TJ resistance of hCMEC/D3 and TY08 cells was significantly increased in co-cultures with human brain astrocytes/pericytes and HBPCT cells, respectively [29,48]. This divergent effect might possibly be due to the difference of culture conditions and the nature of cell types.

We observed that membrane material of inserts and pore size had a significant impact on barrier tightness, and we optimized mono-culture systems by systematically screening a large set of 24-well tissue culture inserts from different providers for each cell line (Table 1). Highest TEER values (28.4 ± 2.47 Ωcm^2) were observed with hBMEC mono-cultures on 24-well tissue culture inserts from Greiner Bio-one® with transparent PET membrane and 3.0 μm pore size (Table 1). Our findings clearly show that the selection of an appropriate tissue culture insert is critical when establishing a BBB model using these immortalized human brain capillary endothelial cell lines, corroborating previous findings in which a substantial impact of material characteristics on the adherence of cells and barrier tightness was demonstrated [31,32]. hCMEC/D3 and TY10 cells produced TEER values in the range of 10 Ωcm^2 (Table 1). BB19 cells were not included into the screening of tissue culture inserts, since these cells yielded extremely low TEER values (around 5 Ωcm^2, Figure 3E). These findings are in agreement with previous studies suggesting that the use of BB19 cells as an *in vitro* model of the human BBB is limited due to a high sucrose permeability [49].

Surprisingly, we consistently observed lower TEER values as compared to literature (hCMEC/D3 and hBMEC: TEER ranging from 40–200 Ωcm^2 [21,24,25], TY10: TEER in the range of 40 Ωcm^2 [26]). A possible explanation may be that we used a different system (automated CellZscope) for assessment of TEER [30]. Low TEER values might also arise from a high concentration of serum and growth factors in the growth medium, which has been reported to prevent TJ formation between endothelial cells [50]. However, hCMEC/D3 cells cultured with growth medium containing 5% FBS instead of 20% FBS, and hBMEC cells cultured in growth medium without growth factor supplementation did not result in increased TEER values or reduced paracellular permeability (for hCMEC/D3, see Figures 3A, 3B, Figures 7A, and 7B, for hBMEC see Figure 8). Furthermore, the selection of the well format might affect TEER values. Because we aimed to establish an *in vitro* BBB model suitable for higher throughput, we miniaturized the assay to a 24-well format that was selected previously for a bovine *in vitro* BBB model [41].

Subsequent optimization of the hBMEC mono-culture system resulted in TEER values in the range of 30–40 Ωcm^2 (Table 2). We found that the cell seeding density is critical, since highest TEER values were obtained when hBMEC cells were seeded at a density ranging between 4.5×10^4 and 9.0×10^4 cells/cm^2 onto coated

inserts (Table 2). These conditions seem to be best for cell growth and TJ development between adjacent cells on the surface area of the Greiner Bio-one® inserts (0.336 cm^2). As hBMEC cells are of human origin, we moreover investigated the effect of HS on barrier tightness. However, no increase in TEER could be observed (Table 2). These results do not confirm previous findings that the permeability of sucrose through hCMEC/D3 monolayers could significantly be reduced by HS supplementation [45]. One may speculate that this could be due to a different type of HS used in these experiments. An individual HS batch as used for our experiments is prone to higher batch-to-batch variation in soluble factors and proteins than pooled HS from commercial sources.

In the evaluation of paracellular permeability, mean P_{app} values for Na-F and LY were significantly lower with hBMEC monolayers ($5.08 \pm 0.220 \times 10^{-6}$ cm/s and $5.39 \pm 0.364 \times 10^{-6}$ cm/s, respectively) than with hCMEC/D3 and TY10 monolayers (Figures 7A and B), corroborating our measurements of TEER values. Permeability values in the order of 10^{-6} cm/s were obtained previously in various *in vitro* BBB models [7,20,39,51].

In the biochemical and immunocytochemical characterization of cellular junctions, VE-cadherin was detected in all cell lines, albeit at varying levels (Figure 4). This confirmed their endothelial lineage. Interestingly, the TJ protein claudin-5 was expressed at similar levels as VE-cadherin, confirming that VE-cadherin controls claudin-5 expression [52]. The cellular junction marker protein ZO-1 showed the same level of expression in hCMEC/D3 and hBMEC cells, but was expressed only at very low levels in BB19 and TY10 cells (Figure 4). Furthermore, white arrows in Figure 5 point to ZO-1 signal at the leading edge of migrating hBMEC cells, confirming findings of previous studies [13].

We used an automated CellZscope system [30] in order to obtain highly standardized data on-line. This system has several advantages over other methods of TEER measurement: TEER values are recorded in real-time every hour in the incubator, thereby reducing workload and avoiding any damage of the cell layer during growth. Also, a disruption of the cell layer is immediately visible from the recording. In addition, information about confluency (C_{CL} values) is obtained simultaneously, reducing the risk of false interpretation of TEER values [53]. Experiments with Caco-2 cells on 24-well inserts demonstrated that the CellZscope is likewise an efficient tool for evaluating barrier tightness in other cell lines, i.e. those used for the study of intestinal drug absorption. Again, independent of the membrane surface area, TEER values of Caco-2 monolayers measured with the CellZscope (24-well format) correlated to off-line TEER values measured manually with an EVOM using a 6-well format (data not shown). One limitation of the CellZscope system may be its design which does not allow the seeding of cells on the bottom of the plate. Investigation of triple co-culture model systems is hence not possible.

Conclusions

In the screening of four available immortalized human brain capillary endothelial cell lines, hBMEC proved to be the most suitable and promising cell line for a human *in vitro* BBB model in terms of barrier tightness and paracellular permeability in a 24-well mono-culture system. hBMEC cells express P-gp [54], claudin-1 [55], claudin-3 [56], occludin [55-57], ZO-1 [54-56,58], ß-catenin [58], ICAM-1 [56], and VCAM-1 [56], some of which were also shown under our experimental conditions (VE-cadherin, ZO-1, and claudin-5, see Figures 4 and 5). Interestingly, although all three examined markers were detected in hBMEC, the expression level of VE-cadherin and claudin-5 was much lower than in hCMEC/D3 and TY10 cells. As a next step, we are currently validating the hBMEC model with the aid of a series of compounds known to cross or not to cross the BBB. After validation, the *in vitro* human BBB model will be used for the screening of natural product derived leads, such as $GABA_A$ receptor modulators [59], regarding their ability to pass across the BBB.

Abbreviations

ACM: Astrocyte-conditioned medium; BB19: Immortalized human brain capillary endothelial cells; BBB: Blood–brain barrier; C_{CL}: Cell layer capacitance; CNS: Central nervous system; EVOM: Epithelial voltohmmeter; FBS: Fetal bovine serum; hBMEC: Immortalized human brain microvascular endothelial cell line; HBPCT: Human brain pericyte cell line; HC: Hydrocortisone; hCMEC/D3: Immortalized human cerebral microvascular endothelial cell line D3; hEGF: Human epidermal growth factor; HS: Human serum; LY: Lucifer yellow VS dilithium salt; Na-F: Sodium fluorescein; NCEs: New chemical entities; P_{app}: Apparent permeability coefficient; PC: Polycarbonate; PES: Polyester; PET: Polyethylene terephthalate; P-gp: P-glycoprotein; RIPA: Standard radio-immunoprecipitation assay; S.E.M.: Standard error of the mean; SVG-A: Human astrocyte cell line; TEER: Transendothelial electrical resistance; TJ: Tight junction; TY10: Conditionally immortalized human brain microvascular endothelial cell line; VE-cadherin: Vascular endothelial-cadherin; ZO-1: Zonula occludens-1 protein.

Competing interests

The authors declare that they have no competing interests.

Authors' contributions

DEE, MO, and GX designed and performed the experiments, analyzed the data and drafted the manuscript. DEE, MO, GX, KSK, AVM, and MH edited and critically reviewed the manuscript. KSK and AVM kindly supplied cells. All authors read and approved the final manuscript.

Acknowledgments

The authors would like to give special thanks to Profs. Pierre-Olivier Couraud, Babette B. Weksler, and Ignacio A. Romero for kindly providing the hCMEC/D3 cell line, to Profs. Kwang Sik Kim, Dennis Grab, and Reto Brun for providing the hBMEC cell line, to Profs. Takashi Kanda, Yasuteru Sano, and Fumitaka Shimizu for providing TY10 and HBPCT cell lines, to Prof. Ashlee Moses for providing BB19 cell line, and to Prof. Avindra Nath for providing the SVG-A cell line. Further thanks go to Orlando Fertig for his excellent technical assistance,

to Le-Ha Dieu for helpful discussions and support, and to Dr. Marcus Schaefer (NanoAnalytics, Münster, Germany) for technical advices. This research was supported by the Swiss National Science Foundation (SNSF) (grant 05320_126888/1 to MH).

Author details
[1]Pharmaceutical Biology, Department of Pharmaceutical Sciences, University of Basel, Klingelbergstrasse 50, 4056 Basel, Switzerland. [2]Mechanisms of Cancer, Friedrich Miescher Institute for Biomedical Research, Maulbeerstrasse 66, 4058 Basel, Switzerland. [3]Department of Pediatrics, John Hopkins University, 200 N. Wolfe Street, Baltimore, MD 21287, USA. [4]Vaccine and Gene Therapy Institute, Oregon Health and Science University (OHSU), 505 NW 185th Ave, Beaverton, OR 97006, USA.

Received: 22 July 2013 Accepted: 21 October 2013
Published: 22 November 2013

References

1. Pardridge WM: **The blood–brain barrier: bottleneck in brain drug development.** *Neurotherapeutics* 2005, **2:**3–14.
2. Di L, Rong H, Feng B: **Demystifying brain penetration in central nervous system drug discovery.** *J Med Chem* 2013, **56:**A–K.
3. Nicolazzo JA, Charman SA, Charman WN: **Methods to assess drug permeability across the blood–brain barrier.** *J Pharm Pharmacol* 2006, **58:**281–293.
4. Bickel U: **How to measure drug transport across the blood–brain barrier.** *NeuroRx* 2005, **2:**15–26.
5. Di L, Kerns EH, Bezar IF, Petusky SL, Huang Y: **Comparison of blood–brain barrier permeability assays: in situ brain perfusion, MDR1-MDCKII and PAMPA-BBB.** *J Pharm Sci* 2009, **98:**1980–1991.
6. Abbott NJ: **Prediction of blood–brain barrier permeation in drug discovery from in vivo, in vitro and in silico models.** *Drug Discov Today Technol* 2004, **1:**407–416.
7. Cecchelli R, Berezowski V, Lundquist S, Culot M, Renftel M, Dehouck M-P, Fenart L: **Modelling of the blood–brain barrier in drug discovery and development.** *Nat Rev Drug Discov* 2007, **6:**650–661.
8. Bowman PD, Ennis SR, Rarey KE, Betz AL, Goldstein GW: **Brain microvessel endothelial cells in tissue culture: a model for study of blood–brain barrier permeability.** *Ann Neurol* 1983, **14:**396–402.
9. Naik P, Cucullo L: **In vitro blood–brain barrier models: Current and perspective technologies.** *J Pharm Sci* 2012, **101:**1337–1354.
10. Ogunshola OO: **In vitro modeling of the blood–brain barrier: simplicity versus complexity.** *Curr Pharm Design* 2011, **17:**2755–2761.
11. Dehouck M-P, Meresse S, Delorme P, Fruchart J-C, Cecchelli R: **An easier, reproducible, and mass-production method to study the blood–brain barrier in vitro.** *J Neurochem* 1990, **54:**1798–1801.
12. Abbott NJ, Rönnbäck L, Hansson E: **Astrocyte-endothelial interactions at the blood–brain barrier.** *Nat Rev Neurosci* 2006, **7:**41–53.
13. Siddharthan V, Kim YV, Liu S, Kim KS: **Human astrocytes/astrocyte-conditioned medium and shear stress enhance the barrier properties of human barin microvascular endothelial cells.** *Brain Res* 2007, **1147:**39–50.
14. Rubin LL, Hall DE, Porter S, Barbu K, Cannon C, Horner HC, Janatpour M, Liaw CW, Manning K, Morales J, Tanner LI, Tomaselli KJ, Bard F: **A cell culture model of the blood–brain barrier.** *J Cell Biol* 1991, **115:**1725–1735.
15. Nakagawa S, Deli MA, Kawaguchi H, Shimizudani T, Shimono T, Kittel A, Tanaka K, Niwa M: **A new blood–brain barrier model using primary rat brain endothelial cells, pericytes and astrocytes.** *Neurochem Int* 2009, **54:**253–263.
16. Thanabalasundaram G, Schneidewind J, Pieper C, Galla H-J: **The impact of pericytes on the blood–brain barrier integrity depends critically on the pericyte differentiation stage.** *Int J Biochem Cell Biol* 2011, **43:**1284–1293.
17. Deli MA: **Blood–brain Barrier Models.** In *Handbook of Neurochemistry and Molecular Neurobiology.* 3rd edition. Edited by Lajtha A, Reith MEA. Berlin Heidelberg: Springer Verlag; 2007:29–55.
18. Uchida Y, Ohtsuki S, Katsukura Y, Ikeda C, Suzuki T, Kamiie J, Terasaki T: **Quantitative targeted absolute proteomics of human blood–brain barrier transporters and receptors.** *J Neurochem* 2011, **117:**333–345.
19. Lundquist S, Renftel M: **The use of in vitro cell culture models for mechanistic studies and as permeability screens for the blood–brain barrier in the pharmaceutical industry-Background and current status in the drug discovery process.** *Vascul Pharmacol* 2002, **38:**355–364.
20. Reichel A, Begley DJ, Abbott NJ: **An overview of in vitro techniques for blood–brain barrier studies.** *Methods Mol Med* 2003, **89:**307–324.
21. Förster C, Burek M, Romero IA, Weksler B, Couraud P-O, Drenckhahn D: **Differential effects of hydrocortisone and TNFalpha on tight junction proteins in an in vitro model of the human blood–brain barrier.** *J Physiol* 2008, **586:**1937–1949.
22. Butt AM, Jones HC, Abbott NJ: **Electrical resistance across the blood–brain barrier in anaesthetized rats: a developmental study.** *J Physiol* 1990, **429:**47–62.
23. Crone C, Olesen P: **Electrical resistance of brain microvascular endothelium.** *Brain Res* 1982, **241:**49–55.
24. Weksler BB, Subileau EA, Perriere N, Charneau P, Holloway K, Leveque M, Tricoire-Leignel H, Nicotra A, Bourdoulous S, Turowski P, Male DK, Roux F, Greenwood J, Romero IA, Couraud P-O: **Blood–brain barrier-specific properties of a human adult brain endothelial cell line.** *FASEB J* 2005, **19:**1872–1874.
25. Stins MF, Badger J, Kim KS: **Bacterial invasion and transcytosis in transfected human brain microvascular endothelial cells.** *Microb Pathogenesis* 2001, **30:**19–28.
26. Maeda T, Sano Y, Abe M, Shimizu F, Kashiwamura Y, Ohtsuki S, Terasaki T, Obinata M, Ueda M, Kanda T: **Establishment and characterization of spinal cord microvascular endothelial cell lines.** *Clin Exp Neuroimmunol*. in press.
27. Prudhomme JG, Sherman IW, Land KM, Moses AV, Stenglein S, Nelson JA: **Studies of Plasmodium falciparum cytoadherence using immortalized human brain capillary endothelial cells.** *Int J Parasitol* 1996, **26:**647–655.
28. Major EO, Miller AE, Mourrain P, Traub RG, De Widt E, Sever J: **Establishment of a line of human fetal glial cells that supports JC virus multiplication.** *Proc Natl Acad Sci U S A* 1985, **82:**1257–1261.
29. Shimizu F, Sano Y, Abe M-A, Maeda T, Ohtsuki S, Terasaki T, Kanda T: **Peripheral nerve pericytes modify the blood-nerve barrier function and tight junctional molecules through the secretion of various soluble factors.** *J Cell Physiol* 2010, **226:**255–266.
30. Wegener J, Abrams D, Willenbrink W, Galla H-J, Janshoff A: **Automated multi-well device to measure transepithelial electrical resistances under physiological conditions.** *Biotechniques* 2004, **37:**590–597.
31. Cecchelli R, Dehouck B, Descamps L, Fenart L, Buée-Scherrer V, Duhem C, Lundquist S, Renftel M, Torpier G, Dehouck M-P: **In vitro model for evaluating drug transport across the blood–brain barrier.** *Adv Drug Deliver Rev* 1999, **36:**165–178.
32. Wuest DM, Wing AM, Lee KH: **Membrane configuration optimization for a murine in vitro blood–brain barrier model.** *J Neurosci Meth* 2013, **212:**211–221.
33. Sano Y, Shimizu F, Abe M, Maeda T, Kashiwamura Y, Ohtsuki S, Terasaki T, Obinata M, Kajiwara K, Fujii M, Suzuki M, Kanda T: **Establishment of a new conditionally immortalized human brain microvascular endothelial cell line retaining an in vivo blood–brain barrier function.** *J Cell Physiol* 2010, **225:**519–528.
34. Sano Y, Kashiwamura Y, Abe M, Dieu L-H, Huwyler J, Shimizu F, Haruki H, Maeda T, Saito K, Tasaki A, Kanda T: **Stable human brain microvascular endothelial cell line retaining its barrier-specific nature independent of the passage number.** *Clin Exp Neuroimmunol* 2013, **4:**92–103.
35. Farrell BT, Lahue RS: **CAG · CTG repeat instability in cultured human astrocytes.** *Nucleic acids res* 2006, **34:**4495–4505.
36. Blume L-F, Denker M, Gieseler F, Kunze T: **Temperature corrected transepithelial electrical resistance (TEER) measurement to quantify rapid changes in paracellular permeability.** *Pharmazie* 2010, **65:**19–24.
37. Bertrand CA, Durand DM, Saidel GM, Laboisse C, Hopfer U: **System for dynamic measurements of membrane capacitance in intact epithelial monolayers.** *Biophys J* 1998, **75:**2743–2756.
38. Cole KS: *Membranes, Ions and Impulses*, Volume 1. Berkley: University of California Press; 1968.
39. Deli MA, Abraham CS, Kataoka Y, Niwa M: **Permeability studies on in vitro blood–brain barrier models: physiology, pathology, and pharmacology.** *Cell Mol Neurobiol* 2005, **25:**59–127.
40. Shi LZ, Zheng W: **Establishment of an in vitro brain barrier epithelial transport system for pharmacological and toxicological study.** *Brain Res* 2005, **1057:**37–48.
41. Culot M, Lundquist S, Vanuxeem D, Nion S, Landry C, Delplace Y, Dehouck M-P, Berezowski V, Fenart L, Cecchelli R: **An in vitro blood–brain barrier model for high throughput (HTS) toxicological screening.** *Toxicol in Vitro* 2008, **22:**799–811.
42. Youdim K, Avdeef A, Abbott NJ: **In vitro trans-monolayer permeability calculations: often forgotten assumptions.** *Drug Discov Today* 2003, **8:**997–1003.

43. Hellinger E, Veszelka S, Toth AE, Walter F, Kittel A, Bakk ML, Tihanyi K, Hada V, Nakagawa S, Duy TDH, Niwa M, Deli MA, Vastag M: **Comparison of brain capillary endothelial cell-based and epithelial (MDCK-MDR1, Caco-2, and VB-Caco-2) cell-based surrogate blood–brain barrier penetration models.** *Eur J Pharm Biopharm* 2012, **82:**340–351.
44. Hubatsch I, Ragnarsson EGE, Artursson P: **Determination of drug permeability and prediction of drug absorption in Caco-2 monolayers.** *Nat Protoc* 2007, **2:**2111–2119.
45. Poller B, Gutmann H, Krähenbühl S, Weksler B, Romero I, Couraud P-O, Tuffin G, Drewe J, Huwyler J: **The human brain endothelial cell line hCMEC/D3 as a human blood–brain barrier model for drug transport studies.** *J Neurochem* 2008, **107:**1358–1368.
46. Weksler B, Romero IA, Couraud P-O: **The hCMEC/D3 cell line as a model of the human blood brain barrier.** *Fluids Barriers CNS* 2013, **10:**16–25.
47. Cucullo L, Couraud P-O, Weksler B, Romero I-A, Hossain M, Rapp E, Janigro D: **Immortalized human brain endothelial cells and flow-based vascular modeling: a marriage of convenience for rational neurovascular studies.** *J Cerebr Blood F Met* 2008, **28:**312–328.
48. Hatherell K, Couraud P-O, Romero IA, Weksler B, Pilkington GJ: **Development of a three-dimensional, all-human in vitro model of the blood–brain barrier using mono-, co-, and tri-cultivation Transwell models.** *J Neurosci Meth* 2011, **199:**223–229.
49. Kusch-Poddar M, Drewe J, Fux I, Gutmann H: **Evaluation of the immortalized human brain capillary endothelial cell line BB19 as a human cell culture model for the blood–brain barrier.** *Brain Res* 2005, **1064:**21–31.
50. Nitz T, Eisenblätter T, Psathaki K, Galla H-J: **Serum-derived factors weaken the barrier properties of cultured porcine brain capillary endothelial cells in vitro.** *Brain Res* 2003, **981:**30–40.
51. Gaillard PJ, De Boer AG: **Relationship between permeability status of the blood–brain barrier and in vitro permeability coefficient of a drug.** *Eur J Pharm Sci* 2000, **12:**95–102.
52. Gavard J, Gutkind JS: **VE-cadherin and claudin-5: it takes two to tango.** *Nat Cell Biol* 2008, **10:**883–885.
53. Benson K, Cramer S, Galla H-J: **Impedance-based cell monitoring: barrier properties and beyond.** *Fluids Barriers CNS* 2013, **10:**5–15.
54. Grab DJ, Nikolskaia O, Kim YV, Londsdale-Eccles JD, Ito S, Hara T, Fukuma T, Nyarko E, Kim KJ, Stins MF, Delannoy MJ, Rodgers J, Kim KS: **African trypanosome interactions with an in vitro model of the human blood–brain barrier.** *J Parasitol* 2004, **90:**970–979.
55. Fletcher NF, Wilson GK, Murray J, Hu K, Lewis A, Reynolds GM, Stamataki Z, Meredith LW, Rowe IA, Luo G, Lopez-Ramirez MA, Baumert TF, Weksler B, Couraud P-O, Kim KS, Romero IA, Jopling C, Morgello S, Balfe P, McKeating JA: **Hepatitis C Virus Infects the Endothelial Cells of the Blood–brain Barrier.** *Gastroenterology* 2012, **142:**634–643.
56. Buttmann M, Lorenz A, Weishaupt A, Rieckmann P: **Atorvastatin partially prevents an inflammatory barrier breakdown of cultured human brain endothelial cells at a pharmacologically relevant concentration.** *J Neurochem* 2007, **102:**1001–1008.
57. Schubert-Unkmeir A, Konrad C, Slanina H, Czapek F, Hebling S, Frosch M: **Neisseria meningitidis induces brain microvascular endothelial cell detachment from the matrix and cleavage of occludin: a role for MMP-8.** *PLOS Pathog* 2010, **6:**1–15.
58. Palmela I, Sasaki H, Cardoso FL, Moutinho M, Kim KS, Brites D, Brito MA: **Time-dependent dual effects of high levels of unconjugated bilirubin on the human blood–brain barrier lining.** *Front Cell Neurosci* 2012, **6:**22–35.
59. Khom S, Strommer B, Schöffmann A, Hintersteiner J, Baburin I, Erker T, Schwarz T, Schwarzer C, Zaugg J, Hamburger M, Hering S: **GABAA receptor modulation by piperine and a non-TRPV1 activating derivative.** *Biochem Pharmacol* 2013, **85:**1827–1836.

doi:10.1186/2045-8118-10-33
Cite this article as: Eigenmann *et al.*: Comparative study of four immortalized human brain capillary endothelial cell lines, hCMEC/D3, hBMEC, TY10, and BB19, and optimization of culture conditions, for an *in vitro* blood–brain barrier model for drug permeability studies. *Fluids and Barriers of the CNS* 2013 **10**:33.

3.2 Validation of an immortalized human (hBMEC) *in vitro* blood-brain barrier model

Daniela E. Eigenmann, Evelyn A. Jähne, Martin Smieško, Matthias Hamburger, Mouhssin Oufir

Analytical and Bioanalytical Chemistry, in press
DOI: 10.1007/s00216-016-9313-6

We recently established and optimized an immortalized human *in vitro* blood-brain barrier (BBB) model based on the hBMEC cell line. In the present work, we validated this 24-well mono-culture model with a representative series of drug substances known to cross the BBB to a different extent (antipyrine, caffeine, diazepam, and propranolol as positive controls; atenolol, cimetidine, quinidine, and vinblastine as negative controls). For individual compounds, a quantitative ultra-high performance liquid chromatography tandem mass spectrometry (UHPLC-MS/MS) assay in Ringer HEPES buffer was developed and validated according to current regulatory guidelines, with respect to selectivity, precision, and reliability. Various biological and analytical challenges were met during method validation, highlighting the importance of careful method development. With the exception of one negative control (quinidine, a small basic lipophilic P-glycoprotein inhibitor and substrate), BBB permeability of control compounds was correctly predicted by this new, fast, and easy to set up human *in vitro* BBB model.

My contributions to this publication: development and validation of UHPLC-MS/MS quantification methods, cultivation of cells, preparation of the human in vitro BBB models, design and performance of permeability experiments, sample preparation and analysis, recording and analysing data, writing the manuscript draft, and preparation of figures and tables.

Daniela Elisabeth Eigenmann

Anal Bioanal Chem
DOI 10.1007/s00216-016-9313-6

RESEARCH PAPER

Validation of an immortalized human (hBMEC) in vitro blood-brain barrier model

Daniela Elisabeth Eigenmann[1] · **Evelyn Andrea Jähne**[1] · **Martin Smieško**[2] · **Matthias Hamburger**[1] · **Mouhssin Oufir**[1]

Received: 16 September 2015 / Revised: 12 November 2015 / Accepted: 5 January 2016

Abstract We recently established and optimized an immortalized human in vitro blood-brain barrier (BBB) model based on the hBMEC cell line. In the present work, we validated this mono-culture 24-well model with a representative series of drug substances which are known to cross or not to cross the BBB. For each individual compound, a quantitative UHPLC-MS/MS method in Ringer HEPES buffer was developed and validated according to current regulatory guidelines, with respect to selectivity, precision, and reliability. Various biological and analytical challenges were met during method validation, highlighting the importance of careful method development. The positive controls antipyrine, caffeine, diazepam, and propranolol showed mean endothelial permeability coefficients (P_e) in the range of 17–70 × 10^{-6} cm/s, indicating moderate to high BBB permeability when compared to the barrier integrity marker sodium fluorescein (mean P_e 3–5 × 10^{-6} cm/s). The negative controls atenolol, cimetidine, and vinblastine showed mean P_e values < 10 × 10^{-6} cm/s, suggesting low permeability. In silico calculations were in agreement with in vitro data. With the exception of quinidine (P-glycoprotein inhibitor and substrate), BBB permeability of all control compounds was correctly predicted by this new, easy, and fast to set up human in vitro BBB model. Addition of retinoic acid and puromycin did not increase transendothelial electrical resistance (TEER) values of the BBB model.

Keywords UHPLC-MS/MS · Method validation · FDA/EMA · In vitro human blood-brain barrier (BBB) model · Permeability coefficient · hBMEC cell line

Introduction

Central nervous system (CNS) drugs need to penetrate the brain in order to reach their targets. Brain penetration is controlled by the blood-brain barrier (BBB), a uniquely tight cellular layer of endothelial cells lining the cerebral capillaries which restricts the passage of molecules from the blood circulation into the brain [1, 2]. Only 2 % of small molecule drugs are able to reach the CNS [2]. Compounds targeted at the CNS should, therefore, be screened already at an early stage of drug development for BBB permeability, since low permeation across the BBB can limit CNS exposure [3].

Numerous cell-based in vitro BBB models have been implemented in academia and industry for early prediction of BBB permeability of lead compounds [4, 5]. However, despite considerable efforts in recent years, there is still a need for simple and reliably predictive BBB permeation assays based on human cells [6]. Primary endothelial cells of animal brain origin have repeatedly been shown to form relatively restrictive cellular barriers in vitro [7–10], but a limitation of such models is the species-dependent difference in expression of transporter proteins and efflux pumps [11, 12]. Models using primary cultures of human origin would avoid interspecies pharmacogenetic differences, but the availability of such cells is restricted due to ethical reasons. In addition, isolation, purification, and cultivation of primary cells are cumbersome and time-consuming;

Electronic supplementary material The online version of this article (doi:10.1007/s00216-016-9313-6) contains supplementary material, which is available to authorized users.

✉ Mouhssin Oufir
mouhssin.oufir@unibas.ch

[1] Pharmaceutical Biology, Department of Pharmaceutical Sciences, University of Basel, Klingelbergstrasse 50, 4056 Basel, Switzerland

[2] Molecular Modeling, Department of Pharmaceutical Sciences, University of Basel, Klingelbergstrasse 50, 4056 Basel, Switzerland

Published online: 21 January 2016

yields of cells are relatively low, and the lifespan of primary cells is limited due to rapid de-differentiation and loss of phenotype. Because of these limitations, immortalized cerebral capillary endothelial cells have been generated by transfection with tumor genes (e.g., SV40 large-T antigen) [13–17]. Unlike primary cells, immortalized cells are relatively easy to cultivate, and they maintain their phenotype even after repeated passaging. These properties render them highly suitable for standardized BBB permeability assays. Among immortalized cell lines, those derived from human brain tissues are of greatest interest. However, currently available human brain capillary endothelial cell lines often show deficiencies, such as low transendothelial electrical resistance (TEER) values, relatively high paracellular permeation of negative control compounds, and insufficient expression of key transporter systems [18]. Therefore, careful optimization of in vitro BBB models utilizing human cell lines and, even more importantly, validation of these models are needed prior to their application to permeability screenings of compounds.

We recently established and optimized a human in vitro BBB model, whereby four currently available immortalized human brain capillary endothelial cell lines (hCMEC/D3, hBMEC, BB19, and TY10) were compared regarding their ability to produce endothelial cell layers with sufficient barrier tightness [19]. The hBMEC cell line was found to be most suited for that purpose [13, 19]. The aim of the present study was to validate this 24-well model with a representative series of drug substances that are known to permeate the BBB to a different extent (antipyrine, caffeine, diazepam, and propranolol as positive controls; atenolol, cimetidine, quinidine, and vinblastine as negative controls) (Fig. 1). In order to ensure reliability of results, we developed for each compound a quantitative ultra-high-performance liquid chromatography coupled to tandem mass spectrometry (UHPLC-MS/MS) assay in Ringer HEPES buffer (RHB) and validated the assays in terms of selectivity, specificity, precision, accuracy, and reliability according to the bioanalytical method validation guidelines of the US Food and Drug Administration (FDA) and European Medicines Agency (EMA) [20, 21]. Finally, the compounds were screened in the human in vitro BBB model, and endothelial permeability coefficients (P_e) across hBMEC monolayers were determined by means of the validated UHPLC-MS/MS methods. Barrier tightness was assessed via continuous on-line measurement of TEER values and with the fluorescent barrier integrity marker sodium fluorescein (Na-F).

Materials and methods

Chemicals and reagents

Antipyrine, atenolol, caffeine, chloroquine, cimetidine, nizatidine, propranolol, quinidine, Na-F, Tween 20, and bovine serum albumin (BSA) were purchased from Sigma-Aldrich (Steinheim, Germany). Vinblastine and vincristine were obtained from Tocris (Bristol, UK). Diazepam and temazepam were supplied by Lipomed (Arlesheim, Switzerland). Acetonitrile, methanol, formic acid (FA), trifluoroacetic acid (TFA), and ammonium formate were all HPLC grade and were purchased from BioSolve (Valkenswaard, the Netherlands). Dimethyl sulfoxide (DMSO) was purchased from Scharlau (Scharlab AG, Sentmenat, Spain). HPLC grade water was obtained by a Milli-Q integral water purification system (Millipore Merck, Darmstadt, Germany). Ringer HEPES buffer (RHB) (150 mM NaCl, 2.2 mM $CaCl_2$, 0.2 mM $MgCl_2$, 5.2 mM KCl, 2.8 mM glucose, 5 mM HEPES, 6 mM $NaHCO_3$) was prepared in-house, adjusted to pH 7.4, filtered, and stored at 4 °C. 24-well plates and inserts (transparent PET membrane, 3.0-μm pore size, 0.6×10^6 pores/cm^2) were obtained from Greiner Bio-one (Frickenhausen, Germany). Immortalized human brain microvascular endothelial cell line (hBMEC) [13] was obtained from Profs. Kwang Sik Kim and Dennis Grab (Johns Hopkins University, Baltimore, MD, USA).

Stock solutions, calibration standards, and quality controls

Stock solutions of analytes and internal standards (IS) were prepared separately by dissolving at least 2 mg of compound in 10 mL of DMSO or high purity water (chloroquine). Weightings were done on a micro analytical balance (Sartorius, Switzerland). Working solutions (WS1) of analyte and IS at a concentration of 10, 20, or 100 μg/mL in methanol were prepared by further diluting the respective stock solutions. For analytes, calibration standards (calibrators) and quality controls (QCs) in RHB at low, medium, and high concentrations (QCL, QCM, and QCH) were prepared by serial dilution of the respective WS1 (range 2.00–200 ng/mL for atenolol, propranolol, and quinidine; 5.00–500 ng/mL for antipyrine, diazepam, and vinblastine; 10.0–1000 ng/mL for caffeine and cimetidine). For vinblastine, a modified RHB was used (RHB + 0.2 % Tween 20). The first concentration level of the calibrators was defined as lower limit of quantification (LLOQ) and the last level as upper limit of quantification (ULOQ). Calibrators and QCs were aliquoted into polypropylene tubes (or glass vials in the case of vinblastine) and stored below −65 °C until analysis. For the IS, a second working solution (WS2) in methanol was prepared daily by further diluting the respective WS1.

Sample extraction from Ringer HEPES buffer

RHB samples were extracted by means of protein precipitation. Sample aliquots (200 μL) were spiked with 100 μL of freshly prepared WS2 of the IS (chloroquine and propranolol

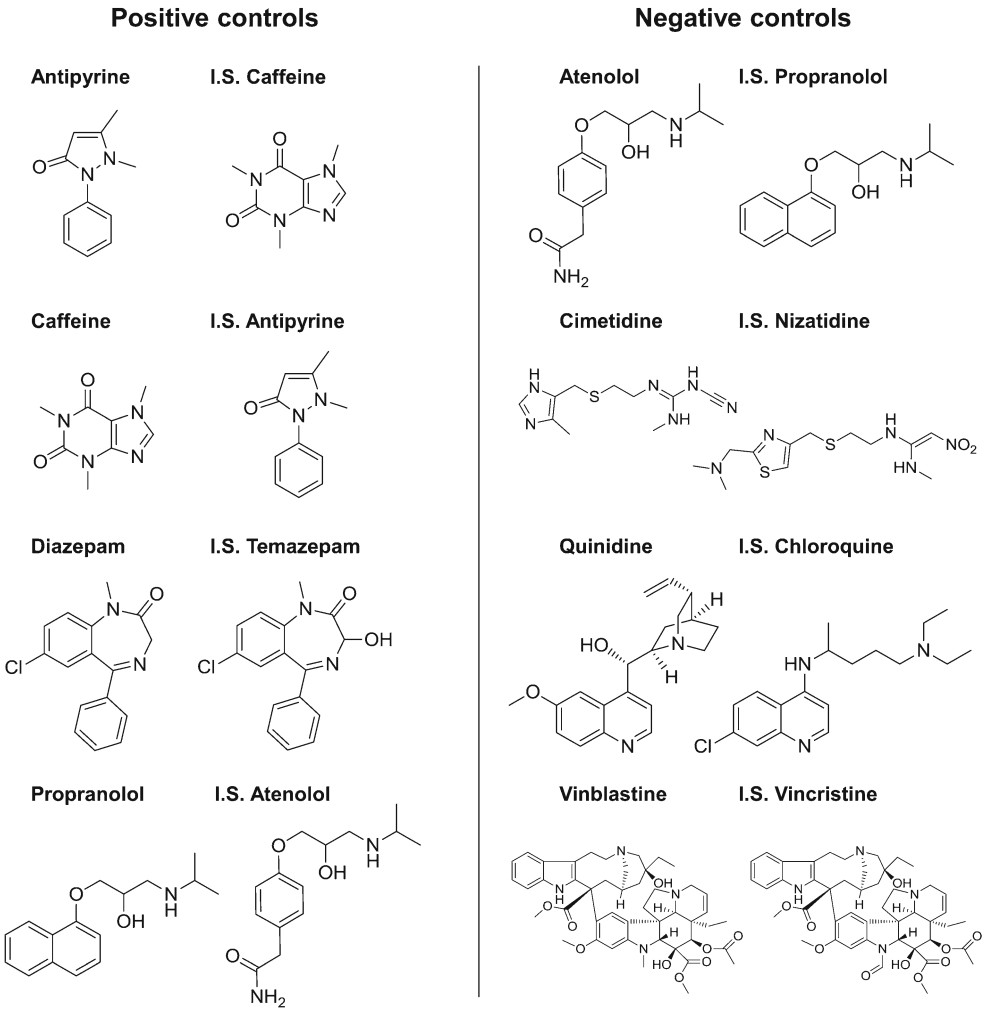

Fig. 1 Compounds used for the validation of the in vitro BBB model and corresponding IS for UHPLC-MS/MS quantitation

200 ng/mL; caffeine 250 ng/mL; antipyrine 500 ng/mL; atenolol, nizatidine, and temazepam 1000 ng/mL; vincristine 2000 ng/mL). Subsequently, samples were spiked with 200 μL BSA solution (60 g/L) and then subjected to protein precipitation with ice cold acetonitrile (1000 μL). After vortexing and stirring for 10 min on an Eppendorf Mixmate (Vaudaux-Eppendorf, Schönenbuch, Switzerland), the mixture was centrifuged for 20 min at 16,168*g* (13,200 rpm) (MiniSpin plus, Vaudaux-Eppendorf, Schönenbuch, Switzerland). The supernatant was transferred into a 96-deep well plate (96-DWP), dried under nitrogen (Evaporex EVX-96, Apricot Designs, Monovia, CA, USA), and thereafter reconstituted with corresponding injection solvent (200 μL) (see Electronic Supplementary Material (ESM) Table S1). For optimal reconstitution, the 96-DWP was stirred on an Eppendorf Mixmate for 30 min at 2000 rpm and subsequently centrifuged for 4 min at 2063*g* (3000 rpm) (Megafuge, Heraeus Instruments AG, Switzerland). Samples were injected into the UHPLC-MS/MS in full loop mode (injection volumes see ESM Table S1) directly out of the 96-DWP or transferred into glass vials in the case of vinblastine.

UHPLC-MS/MS settings

Method validation was performed on a Waters Acquity UPLC system coupled to a Waters Acquity TQD (Waters, Milford, MA, USA). The UPLC system consisted of a binary pump, a cooling autosampler (set at 10 °C, protected from light), and a column heater. Separation of analytes and IS was achieved with an Acquity UPLC HSS T3 column (C18; 2.1 × 100 mm; 1.8-μm particle size) heated to 45 °C, and for cimetidine, with an Acquity UPLC BEH column (C18; 2.1 × 50 mm; 1.7-μm particle size) heated to 70 °C (both columns from Waters, Milford, MA, USA). Columns were protected by an Acquity UPLC column in-line filter unit (0.2 μm in-line frit). For antipyrine, atenolol, caffeine, and diazepam, mobile phase A was 0.1 % FA in water, and mobile phase B was 0.1 % FA in acetonitrile (ESM Table S1). For cimetidine, propranolol, and quinidine, mobile phase A was 5 mM ammonium formate in water containing 0.05 % FA, and mobile phase B was 0.05 % FA in acetonitrile (ESM Table S1). For vinblastine, mobile phase A was 10 mM ammonium formate in water containing 0.1 % FA and mobile

phase B was 0.1 % FA in acetonitrile (ESM Table S1). Total run time was 4 min for vinblastine, 5 min for cimetidine, and 6 min for all other analytes (ESM Table S1). The flow rate of the mobile phase was set at 0.7 mL/min for cimetidine and at 0.4 mL/min for all other analytes (ESM Table S1). Gradients for all analytes are listed in ESM Table S1. Weak wash solution was a mixture of acetonitrile and water (50/50, *v*/*v*) containing 0.2 % TFA. Strong wash solution was a mixture of acetonitrile, isopropanol, and acetone (40/30/30, *v*/*v*/*v*) containing 0.2 % TFA. Seal wash solution was a mixture of acetonitrile and water (10/90, *v*/*v*).

The TQD system was equipped with an electrospray ionization (ESI) interface and operated in positive ion mode (ESI+) and in multiple reaction monitoring (MRM) mode. Nitrogen, provided by a nitrogen generator N2-Mistral (Schmidlin AG, Neuheim, Switzerland), was used both as desolvation gas and as cone gas. Argon was used as collision gas. Source temperature was set at 150 °C. MS/MS transitions and parameters were generated using Waters IntelliStart software and subsequently optimized manually. MRM transitions, cone voltage, and collision energy for analytes and IS are listed in Table 1. Data were acquired with MassLynx V4.1 software and quantification was done using QuanLynx software (Waters, Milford, MA, USA).

Method validation

Method validation for the quantification of analytes by UHPLC-MS/MS was performed according to the guidelines of the FDA [20] and EMA [21]. Imprecision in all validation tests was expressed by the coefficient of variation (CV %). According to the guidelines, the CV % had to be below 15 % (below 20 % at the LLOQ) of the nominal values at all concentration levels. Inaccuracy in all validation tests was expressed by the relative error (RE %) and had to be within ±15 % (within ±20 % at the LLOQ) of the nominal values at all concentration levels.

Table 1 Optimized MS/MS parameters in ESI positive mode for analytes and corresponding ISs

Analyte IS	MRM transitions	Cone voltage (V)	Collision energy (eV)
Antipyrine	189.00 → 56.00	28	22
IS caffeine	195.00 → 138.06	38	20
Atenolol	267.00 → 145.00	35	35
IS propranolol	260.00 → 116.10	35	18
Caffeine	195.00 → 138.06	38	20
IS antipyrine	189.00 → 56.00	28	22
Cimetidine	252.80 → 159.05	22	14
IS nizatidine	331.80 → 155.05	22	18
Diazepam	285.15 → 154.05	50	25
IS temazepam	300.80 → 255.00	30	24
Propranolol	260.10 → 116.05	34	19
IS atenolol	267.13 → 55.95	32	30
Quinidine	324.95 → 80.90	40	34
IS chloroquine	319.70 → 247.05	35	20
Vinblastine	811.00 → 355.10	60	38
IS vincristine	825.00 → 765.20	68	38

Calibration curve and regression parameters

Seven calibrators were injected with increasing concentration after a blank sample (blank RHB) and a calibrator zero (RHB only spiked with IS). Each validation run, performed on different days, consisted of a set of calibrators at the beginning and at the end of the run. The calibration curve was validated through six QCs (duplicates of QCL, QCM, and QCH), which were inserted randomly into the analytical run. The weighting factor was determined during the first run to obtain a consistent dispersion of measure errors across the range. According to the guidelines, a run was valid if at least 75 % of all calibrators were used to generate the calibration curve. For the LLOQ and the ULOQ, at least one replicate had to be accepted. For the six QCs, at least four replicates in total and at least one replicate at each level had to be accepted [20, 21].

Carryover

To assess the carryover of both analyte and IS in each analytical run, blank samples were injected after the ULOQ. Peak areas of analyte and IS in these blank samples were compared to the peak areas at the LLOQ. Mean carryover in each analytical run, expressed in %, had to be below 20 % for analytes and below 5 % for IS [21].

Specificity

A total of six blank samples (duplicates, three different batches of RHB) without analyte and IS were injected into the UHPLC-MS/MS within an analytical run. Peak areas were assessed using a valid calibration curve, and they had not to exceed 20 % of the mean peak areas of both replicates at the LLOQ.

Selectivity

Six samples at the LLOQ (duplicates, three different batches of RHB) were injected into the UHPLC-MS/MS within a validation run. Concentrations were calculated using a valid calibration curve. Selectivity imprecision (CV %) had to be below 20 % and inaccuracy (RE %) had to be within ± 20 % of the nominal values.

Within-run and between-run reproducibility

Six replicates at five concentration levels (LLOQ, QCL, QCM, QCH, and ULOQ) were injected into the UHPLC-MS/MS within three validation runs on three different days. In each validation run, within-run imprecision (CV %) of each level series had to be below 15 % (below 20 % at the LLOQ) and within-run inaccuracy (RE %) had to be within ± 15 % (within ± 20 % at the LLOQ) of the nominal values. Between-run imprecision (CV %) and inaccuracy (RE %) were assessed calculating the overall means and standard deviations (SD). The acceptance criteria for between-run imprecision (CV %) and inaccuracy (RE %) were the same as described above.

Dilution test

To assess the reliability of the method at concentration levels outside the calibration ranges, dilution tests were performed. From the WS1 of the analytes, a solution at a concentration fivefold higher than the ULOQ was prepared. This solution was first diluted to give a solution at a 10-fold lower concentration, then further diluted to give a second solution at a 20-fold (diazepam), 50-fold (cimetidine), or 100-fold (all other compounds) lower concentration. Six replicates of both levels were injected into the UHPLC-MS/MS system. For all replicates of both QC series, the concentration was assessed using a valid calibration curve and subsequently multiplied with the corresponding dilution factor. Resulting mean concentrations, imprecision, and inaccuracy were calculated. According to the FDA/EMA guidances, the imprecision (CV %) had to be below 15 % and the inaccuracy (RE %) had to be within ± 15 % of the nominal values [20].

Extraction yield (recovery)

The extraction yield of the analytes was determined using six replicates spiked with analyte at three different concentration levels (QCL, QCM, and QCH) before extraction and spiked with IS after extraction, compared to six replicates of blank RHB samples spiked after extraction with analyte at three different concentration levels (QCL, QCM, and QCH) and with IS. The extraction yield of IS was determined using six replicates spiked with IS before extraction and with analyte at medium concentration after extraction, compared to six replicates of blank RHB spiked after extraction with IS and analyte at medium concentration. According to the FDA guidance, the extent of recovery of the analyte and IS should be consistent, precise, and reproducible [20].

Short-term stability tests

Freeze and thaw (F/T) stability Six replicates of QCL and QCH were subjected to three freeze (below -65 °C) and thaw (F/T) cycles, processed, and subsequently analyzed using a valid calibration curve.

Benchtop stability at room temperature Six replicates of QCL and QCH were stored for 4 h at room temperature (RT), processed, and quantified using a valid calibration curve.

Processed sample stability at autosampler conditions Six replicates of QCL and QCH were injected into the UHPLC-MS/MS after processing and quantified using a valid calibration curve. These 12 QCs were stored in the autosampler (set at 10 °C, protected from light) for at least 24 h and reassessed using a new calibration curve.

In all short-term stability tests, the imprecision (CV %) had to be below 15 % and the inaccuracy (RE %) had to be within ±15 % of the nominal values at both concentration levels.

Long-term stability below −65 °C

Three replicates of QCL, QCM, and QCH were quantified using a valid calibration curve at time zero ($t = 0$), and three replicates at the same concentration levels (QCL, QCM, and QCH) were stored below −65 °C. After several days of storage, the samples were processed and quantified using a valid calibration curve generated by freshly prepared calibrators and QCs. Results from samples stored below −65 °C were plotted in function of results from time zero ($t = 0$), and a curve was fitted by linear regression (forced through zero). Samples were considered as stable when the slope was within 1 ± 0.15.

Stock solution stability

Fresh stock solutions for analytes and IS were prepared and kept at RT for 4–6 h. Old stock solutions which were stored below −65 °C for various time periods were thawed and similarly kept at RT for 4–6 h. Subsequently, working solutions for each compound at 5.00 μg/mL in respective injection solvent (ESM Table S1) were prepared, injected six times into the UHPLC-MS/MS system, and peak areas from old and fresh stock solutions were compared. The eventual degradation had to be below 5 %.

Human in vitro BBB model

The human mono-culture in vitro BBB model based on hBMEC cell line was prepared as reported previously, with minor modifications [19]. As culture medium, EBM-2 supplemented with Single-Quots (hydrocortisone, ascorbic acid, and heparin), antibiotic-antimycotic solution, and 20 % fetal bovine serum (heat inactivated at 56 °C for 30 min) was used [19]. TEER values and cell layer capacitance (C_{CL}) were

monitored every hour using a 24-well CellZscope system [22]. After 2.5–3 days of incubation of hBMEC monolayers in the CellZscope (at a maximal TEER in the range of 20–40 Ωcm^2), the permeability assays for the compounds were carried out. Briefly, the tissue culture inserts were transferred into a 24-well plate containing 1200 μL of pre-warmed (37 °C) RHB in each well (basolateral compartment). Medium in inserts (apical compartment) was subsequently replaced with 300 μL of a pre-warmed (37 °C) working solution containing the test compound (5 μM) and Na-F as barrier integrity marker (10 μg/mL) in RHB containing 0.2 % BSA. The 24-well plate was incubated at 37 °C on an orbital shaker (ELMI DTS-2, Riga, Latvia) with moderate speed (300 rpm), and aliquots of 250 μL of both apical and basolateral compartments were collected after several time points (15, 30, 60, and 120 min) (one insert per time point) and stored below −65 °C until analysis. Samples containing vinblastine were stored in tubes pre-coated with 0.2 % Tween 20. All experiments were performed at least in triplicate. Control experiments were performed for all compounds, with and without Na-F, to ensure that Na-F did not have an impact on the results. Na-F fluorescence was quantified with a Chameleon microplate reader (Hidex, Turku, Finland), and quantification of the test compounds was performed by means of the validated UHPLC-MS/MS methods.

Calculation of endothelial permeability coefficients (P_e)

Endothelial permeability coefficients (P_e) for each test substance and for Na-F were calculated as follows. For each replicate (controls and samples), the cleared volume was calculated according to the following equation [23, 24]:

$$\text{Clearance}(\mu\text{L}) = \frac{C_B V_B}{C_A}$$

where C_B and V_B are the concentration and volume in the basolateral compartments, respectively, and C_A is the initial concentration in the apical compartment. The cleared volume was plotted as a function of time, and the slope was estimated by linear regression analysis. Permeability-surface area products (PS) and P_e values were subsequently calculated according to the following equations [23, 24]:

$$\frac{1}{PS_{total}} - \frac{1}{PS_{filter}} = \frac{1}{PS_e}$$

$$\frac{PS_e}{A} = P_e$$

where PS_{total} is the slope of the clearance curve of cell monolayers with filter inserts, PS_{filter} is the slope of the clearance curve of control filter inserts without cells, PS_e is the slope of the clearance curve for the endothelial cell monolayers, and A is the surface area of the filter membrane (0.336 cm^2).

Recovery (mass balance) was calculated according to the following equation:

$$\text{Recovery}(\%) = \frac{C_{Af} V_A + C_{bf} V_B}{C_{A0} V_A} \times 100$$

where C_{Af} and C_{Bf} are the final concentrations of the compound in the apical and basolateral compartments, respectively, C_{A0} is the initial concentration in the apical compartment, and V_A and V_B are the volumes in the apical and basolateral compartments, respectively. All results are expressed as means ± SEM.

In silico prediction of BBB permeability

Three-dimensional computer models of studied compounds were built in Maestro modeling environment [25]. The global minimum geometry was used as an input for the QikProp application [26] to evaluate various descriptors relevant for drug permeability. The polar surface area (PSA) and the logarithm of partition and distribution coefficient (LogP and LogD7.4, respectively) descriptors were calculated using the Calculator plugin of Chemaxon Marvin application [27].

Results

Method validation

Chromatographic performance

Calibration curves in the range of 2.00–200 ng/mL (atenolol, propranolol, and quinidine), 5.00–500 ng/mL (antipyrine, diazepam, and vinblastine), and 10.0–1000 ng/mL (caffeine and cimetidine) were fitted by least-squares quadratic regression, and weighting factors of $1/X^2$ (caffeine and cimetidine) or $1/X$ (all other compounds) were applied (ESM Table S2). The mean coefficients of determination (R^2) ranged from 0.9941 to 0.9986 (Table S2), fulfilling FDA/EMA acceptance criteria ($R^2 > 0.96$) [20, 21].

Carryover

Mean carryover in blank RHB samples injected after the ULOQ was between 0.00 to 5.85 % for analytes and between 0.00 to 0.202 % for IS (Fig. 2, ESM Table S3). Acceptance criteria were hence fulfilled (below 20 % for analyte, below 5 % for IS), demonstrating that carryover did not affect precision and accuracy of the methods [21].

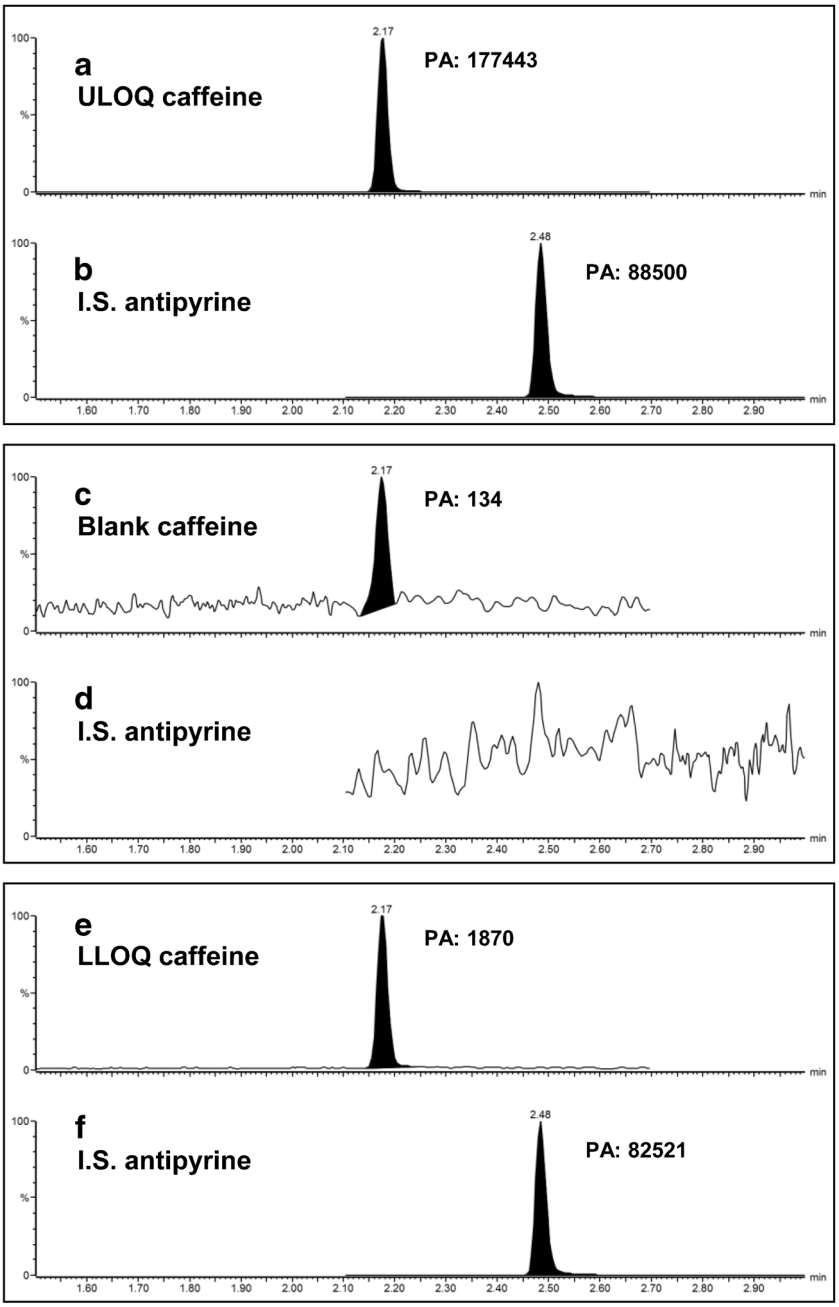

Fig. 2 Typical MRM chromatograms of RHB spiked at 1000 ng/mL (ULOQ) with caffeine (**a**) and at 500 ng/mL with IS antipyrine (**b**), of blank RHB injected directly after the ULOQ and monitored for caffeine (**c**) and for IS antipyrine (**d**), and of RHB spiked at 10.0 ng/mL (LLOQ) with caffeine (**e**) and at 500 ng/mL with IS antipyrine (**f**). *PA* peak area

Specificity

Peak areas of the six blank samples (duplicates, three different batches of RHB) were between 0.00 and 8.63 % of the mean peak areas of the LLOQ for all quantification methods (data not shown). Each UHPLC-MS/MS method was hence proved to be specific for the corresponding analyte.

Selectivity

Selectivity imprecision (CV %) for the six samples at the LLOQ (duplicates, three different RHB batches) was between 2.64 and 12.7 % (below 20 %), and inaccuracy (RE %) was between −10.5 and 14.2 % (within ±20 %) for all quantification methods (ESM Table S4). Hence, the quantification methods were shown to be selective for the respective analytes.

Within-run and between-run reproducibility

Within-run imprecision (CV %) was between 1.20 and 14.3 % (below 15 %) for all methods, and inaccuracy (RE %) was between −12.1 and 9.86 % (within ±15 %) at all QC levels (ESM Table S5). Between-run imprecision (CV %) ranged

from 1.98 to 8.79 % (below 15 %), and inaccuracy (RE %) ranged from −15.7 to 3.70 % at the LLOQ (within ±20 %) and between −9.40 and 11.2 % at all other QC levels (within ±15 %) (Table 2). FDA/EMA acceptance criteria were fulfilled, and the quantification methods proven to be precise, accurate, and reproducible.

Dilution test

For both QC series, imprecision (CV %) was between 0.959 and 7.63 % (below 15 %) for both dilution factors, and inaccuracy (RE %) was between −4.40 and 13.6 % (within ±15 %) for both dilution factors (ESM Table S6). It could hence be demonstrated that dilution of samples up to 20-fold (diazepam), 50-fold (cimetidine), or 100-fold (all other analytes) did not affect the precision and accuracy of the methods.

Table 2 Between-run imprecision (CV %) and inaccuracy (RE %) of QCs, based on three series of six replicates for each level

Compound		Nominal level (ng/mL)				
		2.00	6.00	100	160	200
Atenolol	Mean	1.91	5.76	93.2	157	207
	SD	0.106	0.217	5.28	5.86	13.9
	CV %	5.56	3.78	5.66	3.73	6.73
	RE %	−4.62	−4.08	−6.77	−1.75	3.41
Propranolol	Mean	1.69	5.44	102	166	210
	SD	0.0922	0.299	6.80	6.17	7.03
	CV %	5.47	5.51	6.65	3.73	3.35
	RE %	−15.7	−9.40	2.21	3.55	4.96
Quinidine	Mean	2.01	6.16	103	163	206
	SD	0.0749	0.188	2.85	4.85	6.10
	CV %	3.73	3.05	2.77	2.97	2.95
	RE %	0.536	2.68	3.18	2.05	3.17
		5.00	15.0	250	400	500
Antipyrine	Mean	4.99	14.3	249	404	532
	SD	0.278	0.907	21.7	29.8	46.7
	CV %	5.58	6.36	8.75	7.37	8.79
	RE %	−0.270	−4.96	−0.599	1.02	6.34
Diazepam	Mean	5.02	16.7	254	389	489
	SD	0.183	0.530	5.17	9.24	10.3
	CV %	3.65	3.18	2.04	2.37	2.11
	RE %	0.404	11.2	1.63	−2.65	−2.26
Vinblastine	Mean	5.19	14.7	254	405	498
	SD	0.407	0.843	8.93	12.6	15.3
	CV %	7.84	5.75	3.52	3.12	3.08
	RE %	3.70	−2.27	1.49	1.14	−0.464
		10.0	30.0	500	800	1000
Caffeine	Mean	9.69	27.8	498	783	1064
	SD	0.455	1.26	22.5	19.8	35.4
	CV %	4.69	4.51	4.53	2.53	3.32
	RE %	−3.10	−7.17	−0.477	−2.09	6.37
Cimetidine	Mean	9.68	28.0	488	775	950
	SD	0.287	0.554	25.6	48.6	43.9
	CV %	2.97	1.98	5.24	6.28	4.62
	RE %	−3.23	−6.56	−2.32	−3.11	−4.98

Extraction yield

Absolute recoveries were consistent at all levels (QCL, QCM, and QCH) for all analytes and IS (ESM Table S7).

Freeze and thaw (F/T) stability

Atenolol, antipyrine, caffeine, diazepam, quinidine, and vinblastine Imprecision (CV %) for the six replicates of QCL and of QCH subjected to three successive F/T cycles was between 0.660 and 10.5 % (below 15 %), and inaccuracy (RE %) was between −12.9 and 6.44 % (within ±15 %) (ESM Table S8). Hence, analytes were proven to be stable in RHB after three F/T cycles below −65 °C.

Cimetidine and propranolol Imprecision (CV %) for the six replicates of QCL and of QCH subjected to three F/T cycles exceeded 15 % and inaccuracy (RE %) was outside ±15 % of the nominal values (data not shown). This indicated that the analytes were not stable after three successive F/T cycles below −65 °C. Therefore, a new test with only two F/T cycles was carried out. Imprecision (CV %) for the six replicates of QCL and QCH was now between 0.990 and 4.10 % (below 15 %), and inaccuracy (RE %) for both QC series was between −4.43 and −0.622 % (within ±15 %) (ESM Table S8). The two analytes were thus proven to be stable in RHB after two successive F/T cycles below −65 °C.

Benchtop stability at room temperature

All analytes (except caffeine) Imprecision (CV %) for the six replicates of QCL and QCH in RHB stored for 4 h at RT was between 1.65 and 9.86 % (below 15 %), and inaccuracy (RE %) was between −9.57 and 3.33 % (within ±15 %) (ESM Table S8). The analytes proved hence to be stable in RHB when stored for 4 h at RT before sample extraction.

Benchtop stability at cold temperature

Caffeine Imprecision (CV %) for the six replicates of QCL and QCH in RHB stored for 4 h at RT exceeded 15 % and inaccuracy (RE %) was outside ±15 % of the nominal values (data not shown). Therefore, samples in RHB were stored for 3 h at 4 °C (on ice). Imprecision (CV %) for QCL and QCH was now 3.46 and 4.95 % (below 15 %), respectively, and inaccuracy (RE %) for QCL and QCH was now −8.74 and

−4.15 % (within ±15 %), respectively (ESM Table S8). Caffeine proved hence to be stable in RHB when stored for 3 h at 4 °C (on ice) prior to sample extraction.

Processed sample stability at autosampler conditions

Imprecision (CV %) for six replicates of QCL and QCH stored after extraction from RHB at autosampler conditions (10 °C, protected from light) was between 1.59 and 8.54 % (below 15 %), and inaccuracy (RE %) was between −12.9 and 11.3 % (within ±15 %) (ESM Table S8). Hence, processed samples protected from light and kept at 10 °C proved to be stable for 1–7 days (antipyrine and caffeine for 24 h; atenolol for 36 h; quinidine for 48 h; vinblastine for 3 days; cimetidine for 5 days; propranolol for 6 days; diazepam for 7 days) (ESM Table S8).

Long-term stability below −65 °C

Slopes of the calculated linear regressions were between 0.872 and 1.01 (within 1 ± 0.15) (ESM Table S9). Hence, stability of samples in RHB could be confirmed for various days of storage below −65 °C (atenolol and propranolol for 7 days; antipyrine for 9 days; caffeine for 14 days; quinidine for 15 days; vinblastine for 21 days; cimetidine for 39 days; diazepam for 55 days) (ESM Table S9).

Stock solution stability

For all compounds, the degradation expressed by the difference percentage was between −3.36 and 2.74 % (below 5 %), showing that stock solutions in DMSO (water for chloroquine) were stable for the corresponding time periods (ESM Table S10).

Validation of the immortalized human in vitro BBB model

Mean P_e values for the positive controls antipyrine, caffeine, diazepam, and propranolol were between 16.8 and 69.8×10^{-6} cm/s (Fig. 3, Table 3). Mean P_e values for the negative controls atenolol, cimetidine, and vinblastine were between 6.43 and 9.78×10^{-6} cm/s (Fig. 3, Table 3). For the negative control quinidine, the mean P_e value was $46.7 \pm 2.14 \times 10^{-6}$ cm/s, which is in a similar range as the positive controls (Fig. 3, Table 3). For the fluorescent barrier integrity marker Na-F, mean P_e values were between 2.78 and 5.35×10^{-6} cm/s (Fig. 3, Table 3). Mean TEER values at which permeability experiments were carried out were between 20.7 and 33.3 Ωcm^2 (Table 3). Mean TEER values after the assay were in the same range, or even higher as before (Table 3), suggesting that barrier integrity of hBMEC monolayers was maintained. Furthermore, C_{CL} values were in the range of 0.5–5.0 μF/cm^2 in all experiments (data not shown),

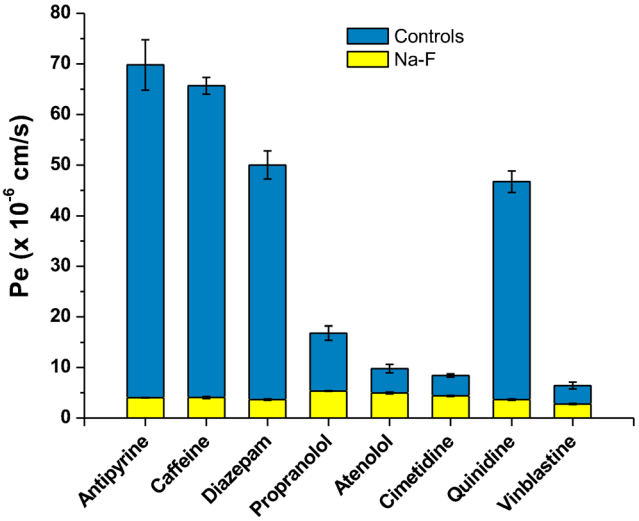

Fig. 3 Mean endothelial permeability coefficients (P_e) ± SEM values across hBMEC monolayers for control compounds (*blue bars*) and the fluorescent barrier integrity marker Na-F (*yellow bars*) screened in parallel with each analyte ($n = 3$–4). The positive controls antipyrine, caffeine, diazepam, and propranolol showed mean P_e values in the range of $17–70 \times 10^{-6}$ cm/s, suggesting moderate to high BBB permeability when compared to the mean P_e values of Na-F ($3–5 \times 10^{-6}$ cm/s). The negative controls atenolol, cimetidine, and vinblastine showed mean P_e values $< 10 \times 10^{-6}$ cm/s, indicating low permeability. Quinidine showed an unexpectedly high mean P_e value of $46.7 \pm 2.14 \times 10^{-6}$ cm/s. Mean recoveries were above 84 % for all compounds (except for propranolol: 62.6 ± 1.99 %) (Table 3)

confirming that hBMEC cell layers were confluent and that TEER values were reliable [28]. Concentrations of analytes in RHB were in a similar range for samples with and without Na-F (data not shown), indicating that Na-F did not have an impact on the results.

In silico prediction of BBB permeability

Calculated values of descriptors relevant for BBB permeation (Table 4) showed that antipyrine, caffeine, diazepam, propranolol, and quinidine had a PSA (ranging from 24 to 58 Å^2) below the recommended thresholds of 70 Å^2 [29] and 90 Å^2 [30], favoring their passive permeation across the BBB. Furthermore, the sum of their donor and acceptor hydrogen bonds (<7) as well as the number of rotatable bonds (≤6) were low. On the other hand, the negative controls atenolol, cimetidine, and vinblastine showed PSA values (85 to 154 Å^2) at or above the limit allowing for passive BBB permeation (70 Å^2 [29] or 90 Å^2 [30]). Moreover, calculated LogD7.4 values for atenolol (−1.8) and cimetidine (−0.22) did not fit into the range of recommended LogP values (i.e., between 1 to 4), while the molecular weight (MW) of vinblastine (811 g/Mol) was clearly above the upper limit (450 g/Mol) recommended for CNS drugs [30]. Compared to permeating compounds, the three non-permeating control compounds (atenolol, cimetidine, and vinblastine) had a larger sum of donor and

Table 3 Mean endothelial permeability coefficients (P_e) for analytes and Na-F ($n = 3–4$), mean recoveries for analytes ($n = 12–18$), and mean TEER values for hBMEC monolayers before and after the permeability assays ($n = 12–19$)

Compound	Transport[a]	Mean $P_e \pm$ SEM ($\times 10^{-6}$ cm/s) for analyte	Mean $P_e \pm$ SEM ($\times 10^{-6}$ cm/s) for Na-F	Mean recovery ± SEM (%) for analyte[b]	Mean TEER ± SEM (Ωcm^2) before assay	Mean TEER ± SEM (Ωcm^2) after assay
Positive controls						
Antipyrine	Passive lipophilic	69.8 ± 4.96	4.01 ± 0.0437	104 ± 0.570	31.8 ± 0.524	32.9 ± 0.380
Caffeine	Passive lipophilic, uptake: adenine transporter	65.7 ± 1.64	4.07 ± 0.213	104 ± 1.31	33.3 ± 0.343	36.8 ± 0.482
Diazepam	Passive lipophilic	50.0 ± 2.78	3.67 ± 0.142	95.5 ± 0.877	32.0 ± 0.328	36.9 ± 0.476
Propranolol	Passive lipophilic	16.8 ± 1.42	5.35 ± 0.0811	62.6 ± 1.99	25.7 ± 0.199	28.4 ± 0.273
Negative controls						
Atenolol	Passive hydrophilic	9.78 ± 0.834	4.96 ± 0.192	84.7 ± 1.43	20.7 ± 0.230	21.7 ± 0.262
Cimetidine	Efflux: P-gp, BCRP, OCT1-3	8.42 ± 0.314	4.38 ± 0.127	97.2 ± 0.747	32.2 ± 0.230	35.4 ± 0.543
Quinidine	Efflux: P-gp, OCT1	46.7 ± 2.14	3.65 ± 0.155	87.2 ± 1.37	33.1 ± 0.404	35.2 ± 0.369
Vinblastine	Efflux: P-gp, MRP1 and 2	6.43 ± 0.664	2.78 ± 0.114	102 ± 6.48	27.4 ± 0.590	33.4 ± 0.404

P-gp P-glycoprotein, *BCRP* breast cancer resistance protein, *OCT* organic cation transporter, *MRP* multidrug resistance-associated protein, *Na-F* sodium fluorescein (negative fluorescent barrier integrity marker; screened in parallel to each positive and negative control)

[a] Nakagawa et al. [7] and McCall et al. [48]

[b] Recoveries were assessed with the experimental concentrations of the working solutions

acceptor hydrogen bonds (>8) and a larger number of rotatable bonds (≥7). LogBB values for all compounds were between −1.15 and 0.19 (Table 4).

Discussion

There is a need for reliable human in vitro models for the prediction of BBB permeability of drug leads that are amenable to medium throughput screening. For that purpose, we previously established and optimized an immortalized mono-culture human in vitro BBB model based on the hBMEC cell line [13, 19]. We here validated this 24-well model with a representative series of structurally diverse drug substances (Fig. 1) known to permeate the BBB to a different extent. To ensure reliability of results, quantitative UHPLC-MS/MS assays in RHB were developed and validated according to FDA/EMA guidelines [20, 21].

During UHPLC-MS/MS method validation, biological and analytical challenges were encountered, such as inaccurate results due to the selection of unsuitable IS (data not shown), interferences of co-eluting compounds during UHPLC-MS/

Table 4 In silico calculation of BBB permeation for test compounds

Compound	QikProp descriptors (3D)							ChemAxon Marvin (2D)			Rotatable bonds
	MW	DonorHB[a]	AccptHB[b]	PSA (Å^2)	LogPo/w	Human oral absorption (%)	LogBB[c]	PSA (Å^2)	LogPo/w	LogD7.4	
Positive controls											
Antipyrine	188.2	0.0	4.0	35	0.38	91.8	0.12	24	1.22	1.22	1
Caffeine	194.2	0.0	5.0	74	−0.07	80.7	−0.27	58	−0.55	−0.55	0
Diazepam	284.7	0.0	4.0	47	2.99	100.0	0.19	33	3.08	3.08	1
Propranolol	259.3	2.0	3.9	38	3.09	100.0	0.06	41	2.58	0.36	6
Negative controls											
Atenolol	266.3	4.0	6.5	93	0.174	55.7	−1.15	85	0.43	−1.8	8
Cimetidine	252.3	3.0	5.5	91	0.45	77.0	−0.95	89	−0.11	−0.22	7
Quinidine	324.4	1.0	5.5	44	3.44	100.0	0.18	46	2.51	0.86	4
Vinblastine	811.0	2.0	12.3	141	5.814	39.1	−0.55	154	4.18	1.81	10

DonorHB donor hydrogen bonds, *AccptHB* acceptor hydrogen bonds, *LogBB* predicted brain/blood partition coefficient (for 95 % of known drugs values range between −3.0 and 1.2)

MS analysis (data not shown), non-specific adsorption of compounds to surfaces, and analyte instability in RHB after short-term and long-term storages. If not addressed properly, such issues lead to an incorrect determination of analyte concentrations in the matrix. Thus, appropriate measures were taken to overcome these problems.

Caffeine proved to be unstable in RHB when stored for 4 h at RT. In a subsequent validation test, samples were therefore stored for 3 h on ice. Under these conditions, benchtop stability of the compound in RHB could be confirmed (ESM Table S8), and study samples were treated accordingly. Furthermore, short-term stability issues were met during F/T stability assessment of cimetidine and propranolol. These analytes proved to be unstable in RHB when subjected to three successive F/T cycles below −65 °C. In a subsequent validation test, stability could be demonstrated when samples were subjected to only two cycles (ESM Table S8), and study samples were thus thawed only up to two times prior to UHPLC-MS/MS analysis. Processed sample stability at autosampler conditions was carried out to ensure that samples could be reinjected if technical incidents during UHPLC-MS/MS analysis occurred. At least 24 h of sample stability was thus needed. In the case of technical issues, samples were therefore reinjected only during the time period for which stability was proven (between 1 and 7 days) (ESM Table S8).

In general, all analytes showed relatively limited long-term stabilities (between 7–55 days) in RHB when stored below −65 °C (ESM Table S9). Hence, study samples were assessed within the time period for which stability of the compound was confirmed. An additional challenge was encountered for vinblastine. During UHPLC-MS/MS method development, non-specific adsorption of the compound to various surfaces was observed, resulting in unacceptable calibration curves (data not shown). We resolved this problem by using tubes (overnight) pre-coated with 0.2 % Tween 20 for study samples, and by spiking RHB with 0.2 % Tween 20 for the preparation of calibrators and QCs [31]. We observed no differences in calibration curves generated by calibrators in pre-coated tubes compared to curves generated by calibrators in spiked RHB (data not shown). As the latter procedure was more convenient and time-efficient, we decided to prepare calibrators and QCs in this way (calibration curves see ESM Table S2).

Extraction yields (recoveries) for diazepam were slightly lower (between 70.3 and 76.5 %) than recoveries for the other compounds (between 80.6 and 109 %) (ESM Table S7). This finding might possibly be due to compound loss during protein precipitation. According to the FDA guidance, the recovery of the analyte does not need to be 100 %, but the extent of recovery of an analyte and of IS should be consistent, precise, and reproducible [20]. Since recoveries for diazepam were similar at each concentration level (between 70.3 and 76.5 %), acceptance criteria were thus fulfilled.

Culture conditions for the in vitro BBB model using the hBMEC cell line were previously optimized in a comprehensive study [19]. As part of the present work, further optimizations were carried out by evaluating the effect of retinoic acid (RA) and puromycin on the barrier tightness of hBMEC monolayers. RA had been previously found to increase TEER values in a human stem cell-based BBB model [32], and puromycin was reported to decrease the permeability of the negative marker mannitol through Caco-2 cell monolayers [33]. In the hBMEC model, however, no increase of TEER values could be observed when cells were cultured with media containing RA or puromycin at different concentrations (ESM Fig. S1).

For the positive controls antipyrine, caffeine, and diazepam mean P_e values were in the range of 50–70 × 10^{-6} cm/s (Fig. 3, Table 3). Compared to the mean P_e values of the negative control Na-F (3–5 × 10^{-6} cm/s), these values were considerably higher and were thus indicating high BBB permeation. The positive control propranolol showed a lower mean P_e value (16.8 ± 1.42 × 0^{-6} cm/s) than the other positive controls. An explanation for this finding might be the low recovery of propranolol (62.6 ± 1.99 %) (Table 3), possibly due to compound accumulation and/or metabolization in the endothelial cells resulting in an underestimation of BBB permeability for this compound [34]. Nevertheless, propranolol could be classified as a permeable compound (mean P_e value of 16.8 ± 1.42 × 10^{-6} cm/s) when compared to the mean P_e values of Na-F (3–5 × 10^{-6} cm/s).

Mean P_e values for the negative controls atenolol, cimetidine, and vinblastine ranged from 6 to 10 × 10^{-6} cm/s (Fig. 3, Table 3). These values were in a similar range than the mean P_e values for Na-F and were thus indicative of limited BBB permeability. The negative control quinidine, however, showed an unexpectedly high mean P_e value (46.7 ± 2.14 × 10^{-6} cm/s). Quinidine is an inhibitor and substrate of P-glycoprotein (P-gp), and the high BBB permeability might be due to low expression of P-gp by hBMEC cells and/or saturation of P-gp, enabling the compound to easily permeate the monolayer [33, 35]. According to calculated descriptor values (Table 4), quinidine should be able to permeate the BBB. A detailed study of expression and functional activity of P-gp in hBMEC cells would be necessary to clarify this apparently contradictory experimental finding.

In silico LogBB values (logarithm of total brain-to-plasma ratio) for the compounds were between −1.15 and 0.19 (Table 4). For the positive control caffeine, the negative LogBB value (−0.27) seemed not to correlate with the high P_e value (65.7 ± 1.64 × 10^{-6} cm/s) observed in the in vitro BBB model (Tables 3 and 4). Also, literature LogBB values for caffeine and antipyrine were negative (−0.055 and −0.097, respectively) [36–38] and appeared not to be in agreement with observed P_e values. However, LogBB values are a measure of the *extent* of brain penetration (i.e., of the distribution

of a drug between plasma and brain, which is influenced by multiple factors such as plasma protein and brain tissue binding), while P_e values predict the *rate* of brain penetration (i.e., BBB permeability by passive diffusion, active uptake, and/or efflux) [39, 40]. The two parameters thus describe different aspects of brain drug penetration and are not necessarily in agreement [40, 41].

The TEER values of hBMEC cell monolayers were rather low (20–40 Ωcm^2) (Table 3) [19], when compared to TEER values reported for in vitro BBB models using primary animal cells, where TEER values in the range of 400–1500 Ωcm^2 can be reached [7–10]. However, mean P_e values for Na-F were in a similar range as those measured in other primary animal in vitro BBB models (0.5–6×10^{-6} cm/s) [7, 8]. Also, mean P_e values for the negative controls atenolol, cimetidine, and vinblastine obtained in our model ($6–10 \times 10^{-6}$ cm/s) were similar to those from a primary triple-culture rat in vitro model (P_e values between 2 and 3×10^{-6} cm/s) [7]. Interestingly, observed P_e values for the positive controls selected for this study were considerably lower than those observed in several other in vitro models ($170–2000 \times 10^{-6}$ cm/s) [7, 42]. Nevertheless, our model was able to discriminate between permeable and non-permeable compounds (mean P_e values in the range of $17–70 \times 10^{-6}$ cm/s for permeable compounds; mean P_e values around $6–10 \times 10^{-6}$ cm/s for non-permeable compounds). Also, BBB permeability data from our immortalized human model were in agreement with data from two well-established animal primary models for the natural products (*E*,*Z*)-3-(4-hydroxy-3,5-dimethoxybenzylidene)indolin-2-one [43], tryptanthrin (unpublished data), and several phenolic compounds (unpublished data). A limitation of the model may be the fact that discrimination between passive diffusion and active efflux of compounds is not possible, as the case of quinidine showed. Specific assays to evaluate possible interaction with efflux pumps may thus be recommended. Despite this limitation, the hBMEC model is a promising tool for early BBB permeability assessment of lead candidates in drug discovery, as it is easy and fast to set up, and is amenable to moderate throughput screening.

Conclusions

We successfully validated an immortalized human monoculture in vitro BBB model (24-well format) based on the hBMEC cell line with a representative series of structurally diverse drugs that are known to cross the BBB to a different extent. For each compound, a quantitative UHPLC-MS/MS method in RHB was developed and validated according to current regulatory guidelines [20, 21]. During UHPLC-MS/MS method validation, various biological and analytical challenges were met, indicating that major precautions for sample analysis need to be taken before quantification. The human in vitro BBB model correctly predicted the BBB permeability of control compounds, with the exception of one negative control (quinidine, a small lipophilic P-gp inhibitor and substrate). We are currently screening selected natural product-derived leads, such as $GABA_A$ receptor modulators, for their ability to cross the BBB [44–47].

Acknowledgments The authors are grateful to Profs. Kwang Sik Kim, Dennis Grab, Reto Brun, and Tanja Wenzler for provision of the hBMEC cell line. Thanks go to Orlando Fertig for technical assistance and to the Swiss National Science Foundation (SNSF) for financial support (grant 05320_126888/1 to MH).

Compliance with ethical standards

Conflict of interest The authors declare that they have no competing interests.

References

1. Abbott NJ, Patabendige AAK, Dolman DEM, Yusof SR, Begley DJ. Structure and function of the blood-brain barrier. Neurobiol Dis. 2010;37:13–25.
2. Pardridge WM. The blood-brain barrier: bottleneck in brain drug development. NeuroRx. 2005;2:3–14.
3. Di L, Rong H, Feng B. Demystifying brain penetration in central nervous system drug discovery. J Med Chem. 2013;56:2–12.
4. Deli MA. In: Lajtha A, Reith MEA, editors. Handb. Neurochem. Mol. Neurobiol. 3rd ed. Berlin Heidelberg: Springer Verlag; 2007. p. 29–55.
5. Tóth A, Veszelka S, Nakagawa S, Niwa M, Deli MA. Patented *in vitro* blood-brain barrier models in CNS drug discovery. Recent Pat CNS Drug Discov. 2011;6:107–18.
6. Reichel A. Addressing central nervous system (CNS) penetration in drug discovery: basics and implications of the evolving new concept. Chem Biodivers. 2009;6:2030–49.
7. Nakagawa S, Deli MA, Kawaguchi H, Shimizudani T, Shimono T, Kittel A, et al. A new blood-brain barrier model using primary rat brain endothelial cells, pericytes and astrocytes. Neurochem Int. 2009;54:253–63.
8. Helms HC, Waagepetersen HS, Nielsen CU, Brodin B. Paracellular tightness and claudin-5 expression is increased in the BCEC/astrocyte blood-brain barrier model by increasing media buffer capacity during growth. AAPS J. 2010;12:759–70.
9. Patabendige A, Skinner RA, Abbott NJ. Establishment of a simplified *in vitro* porcine blood-brain barrier model with high transendothelial electrical resistance. Brain Res. 2012;1521:1–15.
10. Dehouck M-P, Meresse S, Delorme P, Fruchart J-C, Cecchelli R. An easier, reproducible, and mass-production method to study the blood-brain barrier *in vitro*. J Neurochem. 1990;54:1798–801.
11. Syvänen S, Lindhe Ö, Palner M, Kornum BR, Rahman O, Långström B, et al. Species differences in blood-brain barrier transport of three positron emission tomography radioligands with emphasis on P-glycoprotein transport. Drug Metab Dispos. 2009;37:635–43.
12. Warren MS, Zerangue N, Woodford K, Roberts LM, Tate EH, Feng B, et al. Comparative gene expression profiles of ABC transporters

in brain microvessel endothelial cells and brain in five species including human. Pharmacol Res. 2009;59:404–13.
13. Stins MF, Badger J, Kim KS. Bacterial invasion and transcytosis in transfected human brain microvascular endothelial cells. Microb Pathog. 2001;30:19–28.
14. Weksler BB, Subileau EA, Perriere N, Charneau P, Holloway K, Leveque M, et al. Blood-brain barrier-specific properties of a human adult brain endothelial cell line. FASEB J. 2005;19:1872–4.
15. Sano Y, Shimizu F, Abe M, Maeda T, Kashiwamura Y, Ohtsuki S, et al. Establishment of a new conditionally immortalized human brain microvascular endothelial cell line retaining an *in vivo* blood-brain barrier function. J Cell Physiol. 2010;225:519–28.
16. Maeda T, Sano Y, Abe M, Shimizu F, Kashiwamura Y, Ohtsuki S, et al. Establishment and characterization of spinal cord microvascular endothelial cell lines. Clin Exp Neurol. 2013;4:326–38.
17. Prudhomme JG, Sherman IW, Land KM, Moses AV, Stenglein S, Nelson JA. Studies of Plasmodium falciparum cytoadherence using immortalized human brain capillary endothelial cells. Int J Parasitol. 1996;26:647–55.
18. Deli MA, Abraham CS, Kataoka Y, Niwa M. Permeability studies on *in vitro* blood-brain barrier models: physiology, pathology, and pharmacology. Cell Mol Neurobiol. 2005;25:59–127.
19. Eigenmann DE, Xue G, Kim KS, Moses AV, Hamburger M, Oufir M. Comparative study of four immortalized human brain capillary endothelial cell lines, hCMEC/D3, hBMEC, TY10, and BB19, and optimization of culture conditions, for an *in vitro* blood-brain barrier model for drug permeability studies. Fluids Barriers CNS. 2013;10:33–50.
20. Guidance for Industry: Bioanalytical Method Validation, US Food and Drug Administration (FDA), Center for Drug Evaluation and Research (CDER), May 2001.
21. Guideline on bioanalytical method validation, European Medicines Agency (EMEA/CHMP/EWP/192217/2009), London, 21 July 2011.
22. Wegener J, Abrams D, Willenbrink W, Galla H-J, Janshoff A. Automated multi-well device to measure transepithelial electrical resistances under physiological conditions. BioTechniques. 2004;37:590–7.
23. Siflinger-Birnboim A, del Vecchio PJ, Cooper JA, Blumenstock FA, Shepard JM, Malik AB. Molecular sieving characteristics of the cultured endothelial monolayer. J Cell Physiol. 1987;132:111–7.
24. Dehouck M-P, Jolliet-Riant P, Brée F, Fruchart J-C, Cecchelli R, Tillement J-P. Drug transfer across the blood-brain barrier: correlation between *in vitro* and *in vivo* models. J Neurochem. 1992;58:1790–7.
25. Maestro, version 9.9, Schrödinger, LLC, New York, NY, 2014.
26. QikProp, version 4.1, Schrödinger, LLC, New York, NY, 2014.
27. Marvin 15.4.13.0, 2015, ChemAxon (http://www.chemaxon.com).
28. Bertrand CA, Durand DM, Saidel GM, Laboisse C, Hopfer U. System for dynamic measurements of membrane capacitance in intact epithelial monolayers. Biophys J. 1998;75:2743–56.
29. Kelder J, Grootenhuis PD, Bayada DM, Delbressine LP, Ploemen JP. Polar molecular surface as a dominating determinant for oral absorption and brain penetration of drugs. Pharm Res. 1999;16:1514–9.
30. van de Waterbeemd H, Camenisch G, Folkers G, Chretien JR, Raevsky OA. Estimation of blood-brain barrier crossing of drugs using molecular size and shape, and H-bonding descriptors. J Drug Target. 1998;6:151–65.
31. Ji AJ, Jiang Z, Livson Y, Davis JA, Chu JX, Weng N. Challenges in urine bioanalytical assays: overcoming nonspecific binding. Bioanalysis. 2010;2:1573–86.
32. Lippmann ES, Al-Ahmad A, Azarin SM, Palecek SP, Shusta EV. A retinoic acid-enhanced, multicellular human blood-brain barrier model derived from stem cell sources. Sci Rep. 2014;4:1–10.
33. Sevin E, Dehouck L, Fabulas-da Costa A, Cecchelli R, Dehouck MP, Lundquist S, et al. Accelerated Caco-2 cell permeability model for drug discovery. J Pharmacol Toxicol Methods. 2013;68:334–9.
34. Hubatsch I, Ragnarsson EGE, Artursson P. Determination of drug permeability and prediction of drug absorption in Caco-2 monolayers. Nat Protoc. 2007;2:2111–9.
35. Kusuhara H, Suzuki H, Terasaki T, Kakee A, Lemaire M, Sugiyama Y. P-Glycoprotein mediates the efflux of quinidine across the blood-brain barrier. J Pharmacol Exp Ther. 1997;283:574–80.
36. Salminen T, Pulli A, Taskinen J. Relationship between immobilised artificial membrane chromatographic retention and the brain penetration of structurally diverse drugs. J Pharm Biomed Anal. 1997;15:469–77.
37. Platts JA, Abraham MH, Zhao YH, Hersey A, Ijaz L, Butina D. Correlation and prediction of a large blood-brain distribution data set—an LFER study. Eur J Med Chem. 2001;36:719–30.
38. Usansky HH, Sinko PJ. Computation of LogBB values for compounds transported through carrier-mediated mechanisms using *in vitro* permeability data from brain microvessel endothelial cell (BMEC) monolayers. Pharm Res. 2003;20:390–6.
39. Rankovic Z. CNS drug design: balancing physicochemical properties for optimal brain exposure. J Med Chem. 2015;58:2584–608.
40. Hammarlund-Udenaes M, Fridén M, Syvänen S, Gupta A. On the rate and extent of drug delivery to the brain. Pharm Res. 2008;25:1737–50.
41. Hammarlund-Udenaes M. The use of microdialysis in CNS drug delivery studies: pharmacokinetic perspectives and results with analgesics and antiepileptics. Adv Drug Deliv Rev. 2000;45:283–94.
42. Lundquist S, Renftel M, Brillault J, Fenart L, Cecchelli R, Dehouck M-P. Prediction of drug transport through the blood-brain barrier *in vivo*: a comparison between two *in vitro* cell models. Pharm Res. 2002;19:976–81.
43. Jähne EA, Eigenmann DE, Culot M, Cecchelli R, Walter FR, Deli MA, et al. Development and validation of a LC-MS/MS method for assessment of an anti-inflammatory indolinone derivative by *in vitro* blood-brain barrier models. J Pharm Biomed Anal. 2014;98:235–46.
44. Zaugg J, Baburin I, Strommer B, Kim H-J, Hering S, Hamburger M. HPLC-based activity profiling: discovery of piperine as a positive GABAA receptor modulator targeting a benzodiazepine-independent binding site. J Nat Prod. 2010;73:185–91.
45. Khom S, Strommer B, Schöffmann A, Hintersteiner J, Baburin I, Erker T, et al. GABAA receptor modulation by piperine and a non-TRPV1 activating derivative. Biochem Pharmacol. 2013;85:1827–36.
46. Schöffmann A, Wimmer L, Goldmann D, Khom S, Hintersteiner J, Baburin I, et al. Efficient modulation of γ-aminobutyric acid type A receptors by piperine derivatives. J Med Chem. 2014;57:5602–19.
47. Wimmer L, Schönbauer D, Pakfeifer P, Schöffmann A, Khom S, Hering S, et al. Developing piperine towards TRPV1 and GABAA receptor ligands—synthesis of piperine analogs via Heck-coupling of conjugated dienes. Org Biomol Chem. 2015;13:990–4.
48. McCall AL, Millington WR, Wurtman RJ. Blood-brain barrier transport of caffeine: dose-related restriction of adenine transport. Life Sci. 1982;31:2709–15.

Analytical and Bioanalytical Chemistry

Electronic Supplementary Material

Validation of an immortalized human (hBMEC) *in vitro* blood-brain barrier model

Daniela Elisabeth Eigenmann, Evelyn Andrea Jähne, Martin Smiesko, Matthias Hamburger, Mouhssin Oufir

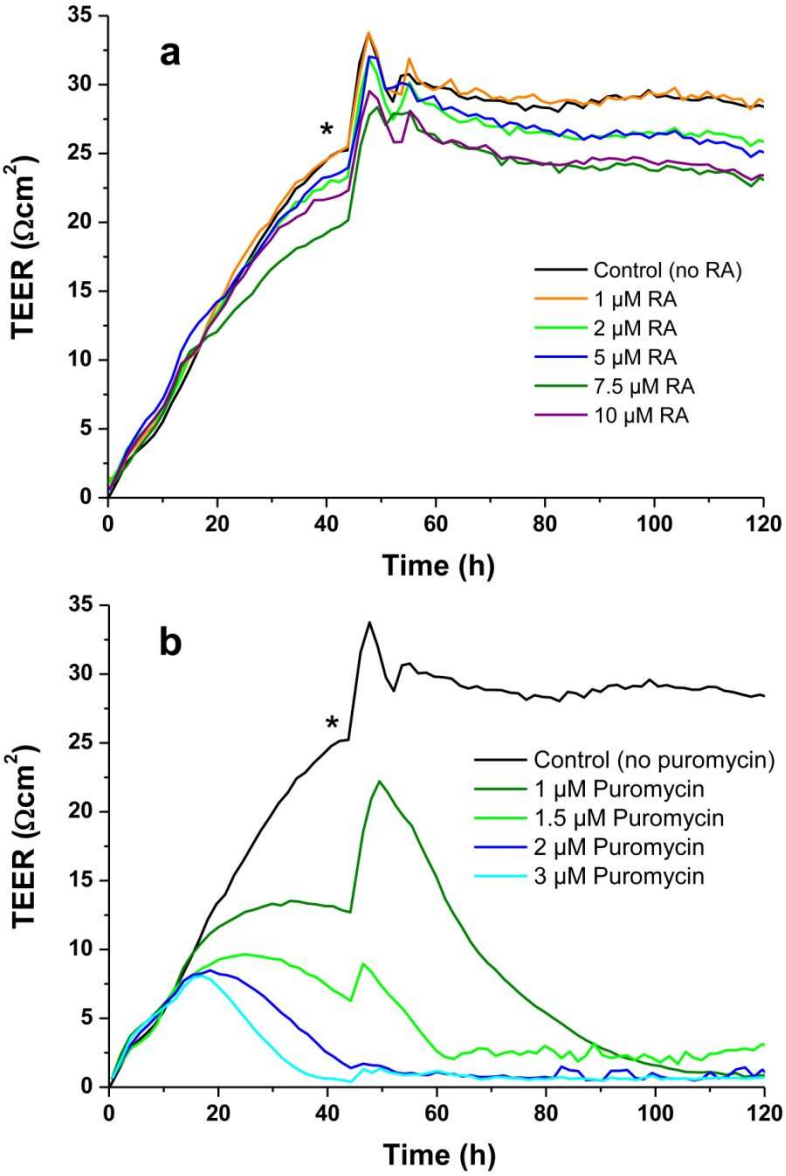

Fig. S1 TEER values recorded real-time by the CellZscope system for hBMEC monolayers cultured with media containing different concentrations of (a) retinoic acid (RA) and (b) puromycin (n = 1). Treatment with RA (at 1, 2, 5, 7.5, and 10 μM) and puromycin (1, 1.5, 2, and 3 μM) did not result in increased TEER values of hBMEC monolayers. *Change of medium

Table S1 Optimized UHPLC parameters for compounds

Compound	Total run time (min)	Eluents	Gradient	Injection solvent	Injection volume (µL)	Column	Column temperature (˚C)	Flow rate (mL/min)
Antipyrine	6.00	A1 + B1	2–90% B1 in 3.5 min	I	5	A	45	0.4
Atenolol	6.00	A1 + B1	2–90% B1 in 3.5 min	I	5	A	45	0.4
Caffeine	6.00	A1 + B1	2–90% B1 in 3.5 min	I	10	A	45	0.4
Cimetidine	5.00	A2 + B2	0–100% B2 in 2.5 min	I	10	B	70	0.7
Diazepam	6.00	A1 + B1	2–90% B1 in 3.5 min	I	10	A	45	0.4
Propranolol	6.00	A2 + B2	2–90% B2 in 3.5 min	I	10	A	45	0.4
Quinidine	6.00	A2 + B2	10–70% B2 in 3.5 min	II	10	A	45	0.4
Vinblastine	4.00	A3 + B1	20–80% B1 in 2.5 min	III	2	A	45	0.4

A1: high purity water + 0.1% FA acid; A2: 5 mM ammonium formate in high purity water + 0.05% FA; A3: 10 mM ammonium formate in high purity water + 0.1% FA; B1: acetonitrile + 0.1% FA; B2: acetonitrile + 0.05% FA

Injection solvent I: 65% A1 + 35% B1; Injection solvent II: 65% A2 + 35% B2; Injection solvent III: 65% A3 + 35% B1

Column A: Waters Acquity UPLC HSS T3 (C18; 2.1 x 100 mm; 1.8 µm particle size)

Column B: Waters Acquity UPLC BEH (C18; 2.1 x 50 mm; 1.7 µm particle size)

Table S2 Calibrators and calibration curve parameters for analytes. Response: A x Conc.^{2} + B x Conc. + C, quadratic regression, weighting factor 1/X (exception caffeine and cimetidine: 1/X^2), origins: included

Compound		Nominal level (ng/mL)							Regression parameters			
		2.00	**10.0**	**20.0**	**40.0**	**80.0**	**160**	**200**	**A**	**B**	**C**	**R^2**
Atenolol	**Mean**	1.99	10.5	21.0	40.1	77.7	158	203	-0.0108	8.05	2.10	0.9980
	S.D.	0.114	0.781	1.30	2.19	3.87	6.61	7.19	0.000968	0.775	-	-
	CV %	5.75	7.45	6.21	5.47	4.98	4.18	3.54	-	-	-	-
	RE %	-0.650	4.79	5.12	0.292	-2.88	-1.16	1.68	-	-	-	-
Propranolol	**Mean**	2.03	9.90	19.9	40.4	80.4	157	202	-0.00000342	0.00603	0.000297	0.9974
	S.D.	0.117	0.462	1.57	2.06	2.77	12.0	8.94	0.00000119	0.000455	-	-
	CV %	5.78	4.67	7.88	5.08	3.45	7.61	4.43	-	-	-	-
	RE %	1.60	-0.951	-0.615	1.07	0.496	-1.66	0.924	-	-	-	-
Quinidine	**Mean**	1.97	10.1	21.2	39.9	77.6	162	200	-0.00000938	0.00729	0.000712	0.9978
	S.D.	0.0773	0.343	1.15	1.52	3.12	9.17	14.1	0.000000570	0.000392	-	-
	CV %	3.93	3.41	5.43	3.81	4.02	5.64	7.03	-	-	-	-
	RE %	-1.59	0.615	5.80	-0.287	-2.95	1.55	0.0820	-	-	-	-
		5.00	**25.0**	**50.0**	**100**	**200**	**400**	**500**	**A**	**B**	**C**	**R^2**
Antipyrine	**Mean**	4.97	26.2	51.5	98.9	198	397	506	-0.00000418	0.00766	0.00369	0.9986
	S.D.	0.165	1.14	2.56	4.59	10.0	11.2	24.9	0.000000304	0.000365	-	-
	CV %	3.32	4.35	4.97	4.64	5.06	2.81	4.93	-	-	-	-
	RE %	-0.542	4.65	2.97	-1.13	-1.20	-0.699	1.19	-	-	-	-
Diazepam	**Mean**	5.21	24.4	48.7	98.9	205	396	501	0.0000000929	0.000262	0.0000594	0.9978
	S.D.	0.445	1.86	3.39	7.24	12.4	13.1	14.4	0.00000000963	0.0000154	-	-
	CV %	8.55	7.62	6.96	7.32	6.04	3.30	2.87	-	-	-	-
	RE %	4.22	-2.23	-2.52	-1.13	2.47	-0.929	0.270	-	-	-	-
Vinblastine	**Mean**	5.17	24.8	49.6	102	198	401	500	-0.000000587	0.00705	0.00168	0.9980
	S.D.	0.390	1.67	1.96	5.51	11.9	15.7	19.9	0.000000380	0.00102	-	-
	CV %	7.55	6.73	3.96	5.40	6.04	3.92	3.98	-	-	-	-
	RE %	3.38	-0.794	-0.754	2.08	-1.16	0.139	0.0389	-	-	-	-
		10.0	**50.0**	**100**	**200**	**400**	**800**	**1000**	**A**	**B**	**C**	**R^2**
Caffeine	**Mean**	10.3	50.9	97.1	195	394	799	1016	-0.000000204	0.00221	0.00149	0.9941
	S.D.	0.800	2.70	4.41	14.1	26.9	60.3	64.0	0.000000179	0.000333	-	-
	CV %	7.75	5.31	4.54	7.22	6.82	7.55	6.29	-	-	-	-
	RE %	3.28	1.71	-2.85	-2.60	-1.43	-0.170	1.64	-	-	-	-
Cimetidine	**Mean**	10.1	50.7	100	197	382	801	1042	-0.000000766	0.00331	0.000990	0.9964
	S.D.	0.531	3.47	4.95	12.3	15.4	42.0	54.1	0.000000180	0.000200	-	-
	CV %	5.23	6.84	4.92	6.26	4.05	5.25	5.19	-	-	-	-
	RE %	1.49	1.41	0.431	-1.33	-4.56	0.102	4.21	-	-	-	-

Table S3 Carry-over assessment for both analytes and I.S. (n = 7–10)

Compound	Mean carry-over (%)
Atenolol I.S. Propranolol	0.00 0.0137
Propranolol I.S. Atenolol	0.0730 0.00117
Quinidine I.S. Chloroquine	0.00 0.00
Antipyrine I.S. Caffeine	0.915 0.202
Diazepam I.S. Temazepam	0.00 0.00
Vinblastine I.S. Vincristine	0.00 0.00
Caffeine I.S. Antipyrine	5.85 0.0181
Cimetidine I.S. Nizatidine	0.164 0.0189

Table S4 Selectivity test at the LLOQ, based on 3 different RHB batches (n = 6)

Compound	**Nominal level (ng/mL)**	**2.00**
Atenolol	Mean	2.14
	S.D.	0.0830
	CV %	3.89
	RE %	6.86
Propranolol	Mean	2.12
	S.D.	0.158
	CV %	7.44
	RE %	6.20
Quinidine	Mean	1.96
	S.D.	0.0517
	CV %	2.64
	RE %	-2.17
	Nominal level (ng/mL)	**5.00**
Antipyrine	Mean	5.09
	S.D.	0.358
	CV %	7.04
	RE %	1.72
Diazepam	Mean	4.99
	S.D.	0.285
	CV %	5.71
	RE %	-0.227
Vinblastine	Mean	4.47
	S.D.	0.567
	CV %	12.7
	RE %	-10.5
	Nominal level (ng/mL)	**10.0**
Caffeine	Mean	11.4
	S.D.	0.383
	CV %	3.35
	RE %	14.2
Cimetidine	Mean	9.62
	S.D.	0.748
	CV %	7.78
	RE %	-3.83

Table S5 Within-run imprecision (CV %) and inaccuracy (RE %) of QCs (n = 6)

Compound		Nominal level (ng/mL)				
		2.00	**6.00**	**100**	**160**	**200**
Atenolol	Mean	1.87	5.75	92.2	156	203
	S.D.	0.0847	0.168	4.32	5.62	10.9
	CV %	4.53	2.91	4.68	3.61	5.37
	RE %	-6.57	-4.14	-7.80	-2.80	1.48
Propranolol	Mean	1.76	5.79	106	165	213
	S.D.	0.100	0.311	9.11	7.31	13.1
	CV %	5.69	5.37	8.55	4.42	6.16
	RE %	-12.1	-3.50	6.48	3.28	6.34
Quinidine	Mean	2.11	6.48	106	167	209
	S.D.	0.0732	0.197	2.67	5.68	9.54
	CV %	3.46	3.04	2.51	3.40	4.57
	RE %	5.68	8.06	6.18	4.20	4.39
		5.00	**15.0**	**250**	**400**	**500**
Antipyrine	Mean	5.07	14.0	245	408	539
	S.D.	0.189	1.13	16.4	22.1	76.9
	CV %	3.73	8.09	6.68	5.42	14.3
	RE %	1.38	-6.95	-1.90	1.95	7.86
Diazepam	Mean	4.98	16.5	257	391	490
	S.D.	0.197	0.425	3.08	11.7	11.9
	CV %	3.96	2.58	1.20	3.00	2.44
	RE %	-0.363	9.86	2.67	-2.30	-2.06
Vinblastine	Mean	5.23	14.5	246	397	486
	S.D.	0.425	1.06	7.94	10.4	7.15
	CV %	8.12	7.29	3.23	2.63	1.47
	RE %	4.55	-3.35	-1.77	-0.754	-2.84
		10.0	**30.0**	**500**	**800**	**1000**
Caffeine	Mean	9.96	28.3	489	784	1071
	S.D.	0.502	1.52	17.1	23.5	31.5
	CV %	5.04	5.37	3.49	3.00	2.94
	RE %	-0.443	-5.66	-2.17	-1.96	7.14
Cimetidine	Mean	9.58	27.5	470	794	1015
	S.D.	0.268	0.693	24.3	25.7	51.1
	CV %	2.80	2.52	5.17	3.23	5.04
	RE %	-4.21	-8.22	-5.98	-0.730	1.46

Table S6 Dilution test (n = 6)

Compound	Nominal level (ng/mL)	1000	
	Dilution factor	**10X**	**100X**
Atenolol	Mean	1035	1136
	S.D.	25.3	28.2
	CV %	2.44	2.49
	RE %	3.55	13.6
Propranolol	Mean	1117	1139
	S.D.	33.6	33.0
	CV %	3.01	2.89
	RE %	11.7	13.9
Quinidine	Mean	992	1033
	S.D.	27.7	9.91
	CV %	2.80	0.959
	RE %	-0.812	3.31
	Nominal level (ng/mL)	**2500**	
	Dilution factor	**10X**	**100X**
Antipyrine	Mean	2491	2631
	S.D.	108	137
	CV %	4.34	5.22
	RE %	-0.341	5.23
Vinblastine	Mean	2598	2744
	S.D.	78.4	209
	CV %	3.02	7.63
	RE %	3.91	9.76
	Dilution factor	**10X**	**20X**
Diazepam	Mean	2773	2765
	S.D.	69.0	102
	CV %	2.49	3.68
	RE %	10.9	10.6
	Nominal level (ng/mL)	**5000**	
	Dilution factor	**10X**	**100X**
Caffeine	Mean	5533	5613
	S.D.	180	280
	CV %	3.25	4.99
	RE %	10.7	12.3
	Dilution factor	**10X**	**50X**
Cimetidine	Mean	4780	5105
	S.D.	96.3	104
	CV %	2.02	2.04
	RE %	-4.40	2.10

Table S7 Absolute extraction yield of analytes and I.S. (n = 6)

Analyte	**Nominal level (ng/mL)**	**6.00**	**100**	**160**
Atenolol	Absolute recovery (%)	107	104	101
	CV %	7.40	1.62	3.07
	S.D.	7.91	1.68	3.10
I.S.	**Nominal level (ng/mL)**	**86.67**		
I.S. Propranolol	Absolute recovery (%)	86.5	-	-
	CV %	2.35	-	-
	S.D.	2.03	-	-
Analyte	**Nominal level (ng/mL)**	**6.00**	**100**	**160**
Propranolol	Absolute recovery (%)	89.1	92.2	98.1
	CV %	3.42	2.17	2.64
	S.D.	3.05	2.00	2.59
I.S.	**Nominal level (ng/mL)**	**433.33**		
I.S. Atenolol	Absolute recovery (%)	101	-	-
	CV %	1.88	-	-
	S.D.	1.90	-	-
Analyte	**Nominal level (ng/mL)**	**6.00**	**100**	**160**
Quinidine	Absolute recovery (%)	93.2	100	105
	CV %	2.28	1.45	1.86
	S.D.	2.13	1.46	1.95
I.S.	**Nominal level (ng/mL)**	**86.67**		
I.S. Chloroquine	Absolute recovery (%)	85.2	-	-
	CV %	2.80	-	-
	S.D.	2.39	-	-
Analyte	**Nominal level (ng/mL)**	**15.0**	**250**	**400**
Antipyrine	Absolute recovery (%)	91.7	85.9	86.3
	CV %	11.9	7.51	7.26
	S.D.	10.9	6.45	6.26
I.S.	**Nominal level (ng/mL)**	**108.33**		
I.S. Caffeine	Absolute recovery (%)	89.5	-	-
	CV %	6.25	-	-
	S.D.	5.60	-	-
Analyte	**Nominal level (ng/mL)**	**15.0**	**250**	**400**
Diazepam	Absolute recovery (%)	70.3	70.7	76.5
	CV %	15.8	6.54	9.11
	S.D.	11.1	4.62	6.97
I.S.	**Nominal level (ng/mL)**	**433.33**		
I.S. Temazepam	Absolute recovery (%)	87.2	-	-
	CV %	5.99	-	-
	S.D.	5.22	-	-
Analyte	**Nominal level (ng/mL)**	**15.0**	**250**	**400**
Vinblastine	Absolute recovery (%)	89.3	85.5	83.5
	CV %	8.85	3.24	3.12
	S.D.	7.90	2.77	2.61
I.S.	**Nominal level (ng/mL)**	**866.67**		
I.S. Vincristine	Absolute recovery (%)	80.6	-	-
	CV %	3.50	-	-
	S.D.	2.82	-	-
Analyte	**Nominal level (ng/mL)**	**30.0**	**500**	**800**
Caffeine	Absolute recovery (%)	93.1	98.7	98.4
	CV %	6.77	1.91	3.19
	S.D.	6.30	1.89	3.14
I.S.	**Nominal level (ng/mL)**	**216.67**		
I.S. Antipyrine	Absolute recovery (%)	105	-	-
	CV %	7.32	-	-
	S.D.	7.69	-	-
Analyte	**Nominal level (ng/mL)**	**30.0**	**500**	**800**
Cimetidine	Absolute recovery (%)	109	106	103
	CV %	3.29	1.04	1.15
	S.D.	3.58	1.11	1.18
I.S.	**Nominal level (ng/mL)**	**433.33**		
I.S. Nizatidine	Absolute recovery (%)	85.9	-	-
	CV %	6.03	-	-
	S.D.	5.18	-	-

Table S8 Short-term stabilities during storage at various conditions expressed as CV % and RE % (n = 6)

		CV %		RE %	
Compound	**Nominal level (ng/mL)**	**6.00**	**160**	**6.00**	**160**
Atenolol	3 successive F/T cycles below -65°C	3.43	4.90	2.38	-1.15
	Stored samples at RT for 4 hours	2.80	2.03	2.69	0.121
	Processed samples at 10°C for 36 hours	3.02	2.19	8.30	-4.62
Propranolol	2 successive F/T cycles below -65°C	4.10	1.86	-3.83	-0.622
	Stored samples at RT for 4 hours	4.11	2.25	-6.37	1.12
	Processed samples at 10°C for 6 days	2.36	2.74	0.142	3.13
Quinidine	3 successive F/T cycles below -65°C	2.76	0.660	6.44	-6.69
	Stored samples at RT for 4 hours	3.33	2.09	-7.34	-9.57
	Processed samples at 10°C for 48 hours	2.81	3.94	-2.95	-12.9
	Nominal level (ng/mL)	**15.0**	**400**	**15.0**	**400**
Antipyrine	3 successive F/T cycles below -65°C	5.28	7.93	-12.9	-4.93
	Stored samples at RT for 4 hours	9.86	5.27	-2.76	-5.88
	Processed samples at 10°C for 24 hours	5.24	8.54	-7.45	-11.5
Diazepam	3 successive F/T cycles below -65°C	7.46	1.50	4.93	-6.73
	Stored samples at RT for 4 hours	4.24	3.53	3.33	-3.57
	Processed samples at 10°C for 7 days	6.43	2.40	3.37	3.41
Vinblastine	3 successive F/T cycles below -65°C	10.5	1.95	-3.63	-2.55
	Stored samples at RT for 4 hours	6.91	2.40	-1.99	2.00
	Processed samples at 10°C for 3 days	5.39	3.06	11.3	12.2
	Nominal level (ng/mL)	**30.0**	**800**	**30.0**	**800**
Caffeine	3 successive F/T cycles below -65°C	3.30	5.92	-9.67	2.44
	Stored samples at 4°C (on ice) for 3 hours	3.46	4.95	-8.74	-4.15
	Processed samples at 10°C for 24 hours	3.87	1.59	-6.38	-8.51
Cimetidine	2 successive F/T cycles below -65°C	1.54	0.990	-4.43	-3.45
	Stored samples at RT for 4 hours	2.16	1.65	-5.76	-9.37
	Processed samples at 10°C for 5 days	2.51	2.49	1.41	-2.26

Table S9 Long-term stabilities expressed as difference (%) between t=0 and t=last and slopes (n = 3)

Compound	**Nominal level (ng/mL)**	**6.00**	**100**	**160**	**Slope**
Atenolol	Stored samples below -65°C for 7 days	-10.4	-10.9	-13.2	0.872
Propranolol	Stored samples below -65°C for 7 days	-0.843	-2.56	2.04	1.01
Quinidine	Stored samples below -65°C for 15 days	1.51	-2.68	-12.2	0.894
	Nominal level (ng/mL)	**15.0**	**250**	**400**	**Slope**
Antipyrine	Stored samples below -65°C for 9 days	1.04	1.69	-8.49	0.941
Diazepam	Stored samples below -65°C for 55 days	-12.3	0.249	-5.31	0.961
Vinblastine	Stored samples below -65°C for 21 days	-3.90	0.231	-0.411	0.997
	Nominal level (ng/mL)	**30.0**	**500**	**800**	**Slope**
Caffeine	Stored samples below -65°C for 14 days	-3.90	1.92	-9.06	0.935
Cimetidine	Stored samples below -65°C for 39 days	-7.24	-4.09	-8.77	0.925

Table S10 Stock solution stability of compounds

Compound	Solvent	Long-term stability below -65°C (days)	Hours kept at RT (h)	Difference (%)
Atenolol	DMSO	206	6	2.74
Propranolol	DMSO	206	6	-1.09
Antipyrine	DMSO	88	6	0.113
Caffeine	DMSO	88	6	-2.05
Cimetidine	DMSO	148	6	0.546
Nizatidine	DMSO	148	6	-2.40
Quinidine	DMSO	39	6	0.0984
Chloroquine	Water	39	6	0.393
Vinblastine	DMSO	74	6	-3.36
Vincristine	DMSO	74	6	-2.23
Diazepam	DMSO	182	4	1.95
Temazepam	DMSO	138	4	-3.25

3.3 *In vitro* blood-brain barrier permeability predictions for $GABA_A$ receptor modulating piperine analogs

Daniela E. Eigenmann, Carmen Dürig, Evelyn A. Jähne, Martin Smieško, Maxime Culot, Fabien Gosselet, Roméo Cecchelli, Hans Christian Cederberg Helms, Birger Brodin, Laurin Wimmer, Marko D. Mihovilovic, Matthias Hamburger, Mouhssin Oufir

Submitted to: *European Journal of Pharmaceutics and Biopharmaceutics*

The alkaloid piperine from black pepper (*Piper nigrum* L.), and several synthetic piperine analogs were previously identified as positive allosteric modulators of γ-aminobutyric acid type A ($GABA_A$) receptors. To evaluate their potential to penetrate the brain, we screened the compounds in our recently validated immortalized human *in vitro* BBB model, in a human stem cell *in vitro* BBB model, and in a primary bovine endothelial/rat astrocytes co-culture *in vitro* BBB model. In addition, *in silico* data for BBB permeability were calculated. For each compound, a quantitative UHPLC-MS/MS assay in the corresponding matrix was developed, and permeability coefficients in each model were determined. *In vitro* predictions from the two human models were in good agreement, while permeability data from the animal model differed to some extent. In all three models, piperine and the semisynthetic analog SCT-64 displayed highest BBB permeation, which was corroborated by *in silico* prediction data. For the other piperine analogs (SCT-66, SCT-29, LAU397, and LAU399), BBB permeability was low to moderate in the two human models, and moderate to high in the animal model. Efflux ratios (ER) calculated from bidirectional permeability experiments indicated that the compounds were not substrates of active efflux.

My contributions to this publication: development of UHPLC-MS/MS quantification methods, cultivation of cells, preparation of the immortalized human in vitro BBB models, design and performance of permeability experiments, sample preparation and analysis, recording and analysing data, writing the manuscript draft, and preparation of figures and tables.

Daniela Elisabeth Eigenmann

MANUSCRIPT

EUROPEAN JOURNAL OF PHARMACEUTICS AND BIOPHARMACEUTICS

In vitro blood-brain barrier permeability predictions for GABAA receptor modulating piperine analogs

Daniela Elisabeth Eigenmann[a], Carmen Dürig[a], Evelyn Andrea Jähne[a], Martin Smieško[b], Maxime Culot[c], Fabien Gosselet[c], Romeo Cecchelli[c], Hans Christian Cederberg Helms[d], Birger Brodin[d], Laurin Wimmer[e], Marko D. Mihovilovic[e], Matthias Hamburger[a], and Mouhssin Oufir[a,*]

[a]Pharmaceutical Biology, Department of Pharmaceutical Sciences, University of Basel, Klingelbergstrasse 50, CH-4056 Basel, Switzerland

[b]Molecular Modeling, Department of Pharmaceutical Sciences, University of Basel, Klingelbergstrasse 50, CH-4056 Basel, Switzerland

[c]Univ. Artois, EA 2465, Laboratoire de la Barrière Hémato-Encéphalique (LBHE), F-62300 Lens Cedex, France

[d]Drug Transporters in ADME, Department of Pharmacy, Faculty of Health and Medical Sciences, University of Copenhagen, Universitetsparken 2, DK-2100 Copenhagen, Denmark

[e]Institute of Applied Synthetic Chemistry, TU Wien, Getreidemarkt 9, A-1060 Vienna, Austria

*Corresponding author. Pharmaceutical Biology, Department of Pharmaceutical Sciences, University of Basel, Klingelbergstrasse 50, CH-4056 Basel, Switzerland. Tel: +41 61 2671425; fax: +41 61 2671474.
E-mail address: mouhssin.oufir@unibas.ch (M. Oufir).

Keywords: Piperine, $GABA_A$ receptor, *in vitro* blood-brain barrier (BBB) model, primary cells, immortalized cell line, human stem cells, UHPLC-MS/MS, permeability coefficient

Abbreviations: BBB, blood-brain barrier; BLEC, human brain-like endothelial cells; BSA, bovine serum albumin; C_{CL}, cell layer capacitance; CNS, central nervous system; CV, coefficient of variation; DMEM, Dulbecco's Modified Eagle Medium; ER, efflux ratio; FA, formic acid; FBS, fetal bovine serum; $GABA_A$ receptor, γ-aminobutyric acid type A receptor; hBMEC, human brain microvascular endothelial cell line; I.S., internal standard; LLOQ, lower limit of quantification; MRM, multiple reaction monitoring; Na-F, sodium fluorescein; P_{app}, apparent permeability coefficient; P_e, endothelial permeability coefficient; P-gp, P-glycoprotein; QC, quality control; RE, relative error; RHB, Ringer HEPES buffer; TEER, transendothelial electrical resistance; TFA, trifluoroacetic acid; TRPV1, transient receptor potential vanilloid 1; UHPLC-MS/MS, ultra-high performance liquid chromatography tandem mass spectrometry; ULOQ, upper limit of quantification; WS, working solution.

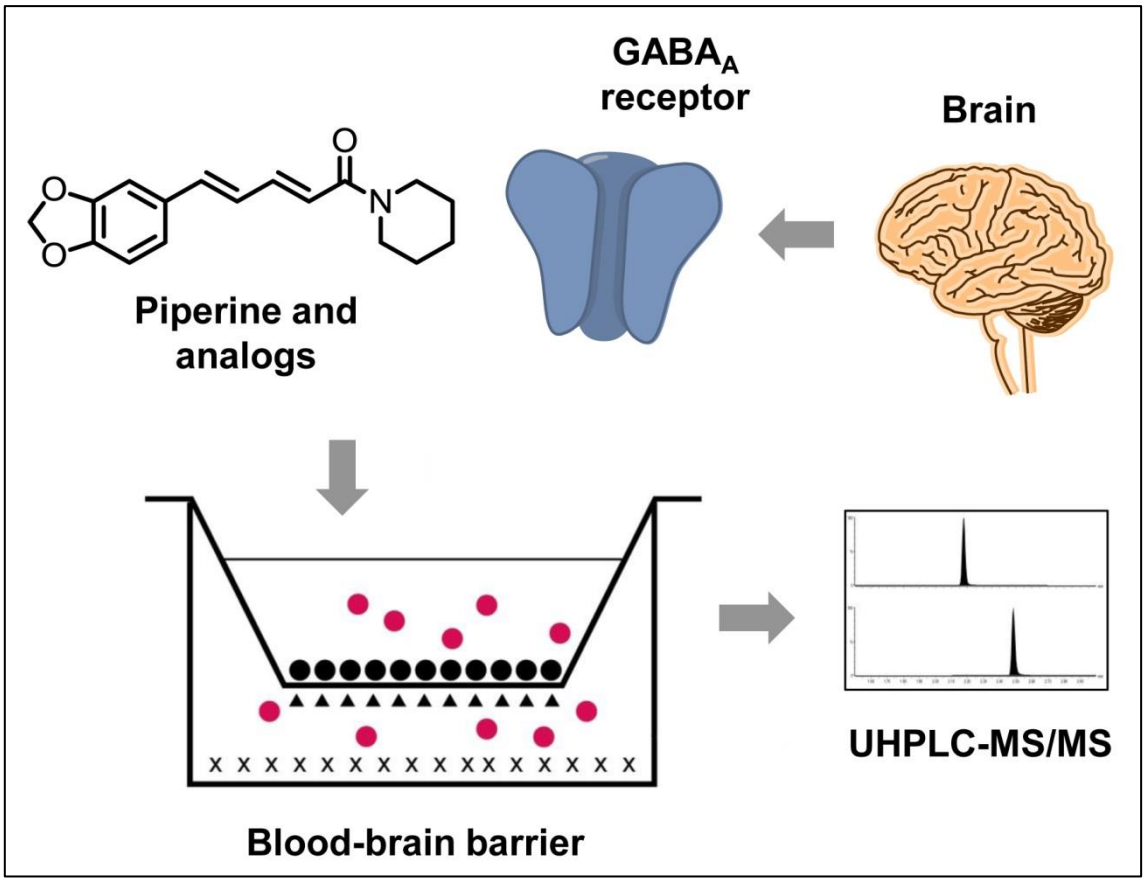

Abstract

The alkaloid piperine from black pepper (*Piper nigrum* L.) and several synthetic piperine analogs were recently identified as positive allosteric modulators of γ-aminobutyric acid type A ($GABA_A$) receptors. In order to reach their target sites of action, these compounds need to enter the brain by crossing the blood-brain barrier (BBB). We here evaluated piperine and five selected analogs (SCT-66, SCT-64, SCT-29, LAU397, and LAU399) regarding their BBB permeability. Data were obtained in three *in vitro* BBB models, namely a recently established human model with immortalized hBMEC cells, a human brain-like endothelial cells (BLEC) model, and a primary animal (bovine endothelial/rat astrocytes co-culture) model. For each compound, quantitative UHPLC-MS/MS methods in the range of 5.00–500 ng/mL in the corresponding matrix were developed, and permeability coefficients in the three BBB models were determined. *In vitro* predictions from the two human BBB models were in good agreement, while permeability data from the animal model differed to some extent, possibly due to high protein binding of the screened compounds. In all three BBB models, piperine and SCT-64 displayed the highest BBB permeation potential. This was corroborated by data from *in silico* prediction. For the other piperine analogs (SCT-66, SCT-29, LAU397, and LAU399), BBB permeability was low to moderate in the two human BBB models, and moderate to high in the animal BBB model. Efflux ratios (ER) calculated from bidirectional permeability experiments indicated that the compounds were not substrates of active efflux transporters.

1 Introduction

The alkaloid piperine, the major pungent component of black pepper (*Piper nigrum* L.), was recently identified as a positive allosteric γ-aminobutyric acid type A ($GABA_A$) receptor modulator. The compound showed anxiolytic-like activity in behavioral mouse models, and was found to interact with the $GABA_A$ receptors at a binding site that was independent of the benzodiazepine binding site [1,2]. Given that the compound complied with Lipinski's "rule of five" [1], it represented a new scaffold for the development of novel $GABA_A$ receptor modulators [1–3].

Given that piperine also activates the transient receptor potential vanilloid 1 (TRPV1) receptors [4] which are involved in pain signaling and regulation of the body temperature [5,6], structural modification of the parent compound was required to dissect $GABA_A$ and TRPV1 activating properties.

In a first step, the piperidine ring of piperine was replaced by a *N*,*N*-diisobutyl residue, resulting in a non-TRPV1 activating derivative (designated as SCT-66) (Fig. 1) [2]. Compared to piperine, SCT-66 increased chloride currents through $GABA_A$ receptors more potently and efficiently, and showed a stronger anxiolytic effect in mice [7]. Based on these findings, a library of 76 piperine analogs with modifications at the amide functionality and at the linker region was synthesized [7]. In this compound series, SCT-64 and SCT-29 (Fig. 1) showed the strongest modulation and highest potency, respectively, at $GABA_A$ receptors expressed in *Xenopus laevis* oocytes [7]. Both analogs were devoid of TRPV1 receptor activating properties *in vitro*, exerted pronounced anxiolytic effects in mice, and appeared in significant concentration in mouse plasma after intraperitoneal application [7]. However, all compounds synthesized up to that point contained the metabolically liable 1,3-benzodioxole group [8]. Hence, a set of 15 aryl-modified piperine analogs was synthesized bearing the non-natural dibutylamide function [9]. Of these, the analogs LAU397 and LAU399 (Fig. 1) were significantly more efficient at the $GABA_A$ receptor than piperine while being devoid of *in vitro* TRPV1 receptor interaction [9].

For drugs acting on the central nervous system (CNS), brain penetration is required. This process is controlled by the blood-brain barrier (BBB), a tight layer of endothelial cells lining the brain capillaries that limits the passage of molecules from the blood circulation into the brain [10]. Since low BBB permeability can reduce CNS exposure [11], lead compounds should be evaluated at an early stage of the drug development process for their ability to permeate the BBB [12].

In the present study, we assessed the BBB permeability of piperine and five selected piperine analogs (Fig. 1) in three *in vitro* cell-based human and animal BBB models [13–16]. Permeability coefficients across the monolayers were determined by means of UHPLC-MS/MS, whereby quantitative UHPLC-MS/MS assays in the corresponding matrices were developed for each compound. In addition, we calculated descriptors relevant for BBB permeation and compared them with the *in vitro* data from the BBB models.

2 Materials and methods

2.1 Chemicals and reagents

The piperine analogs (2*E*,4*E*)-5-(benzo[*d*][1,3]dioxol-5-yl)-*N*,*N*-diisobutylpenta-2,4-dienamide (SCT-66), (2*E*,4*E*)-5-(benzo[*d*][1,3]dioxol-5-yl)-*N*,*N*-dipropylpenta-2,4-dienamide (SCT-64), (2*E*,4*E*)-5-(benzo[*d*][1,3]-dioxol-5-yl)-*N*,*N*-dibutylpenta-2,4-dienamide (SCT-29), (2*E*,4*E*)-*N*,*N*-dibutyl-5-(4-methoxyphenyl)penta-2,4-dienamide (LAU397; compound 6 in reference [9]), and (2*E*,4*E*)-*N*,*N*-dibutyl-5-(thiophen-3-yl)penta-2,4-dienamide (LAU399; compound 16 in reference [9]) were synthesized at TU Wien as described elsewhere [2,7,9]. Piperine, Tween 20, bovine serum albumin (BSA), Dulbecco's Modified Eagle Medium (DMEM) high glucose, and sodium fluorescein (Na-F) were purchased from Sigma-Aldrich (Steinheim, Germany). Fetal bovine serum (FBS) was from Pan-Biotech (Aidenbach, Germany). Immortalized human brain microvascular cell line (hBMEC) [17] was received from Prof. Kwang Sik Kim and Prof. Dennis Grab (Johns Hopkins University, Baltimore, MD, USA). Acetonitrile, methanol, formic acid (FA), trifluoroacetic acid (TFA), and ammonium formate were all HPLC grade and were obtained from BioSolve (Valkenswaard, the Netherlands). Dimethyl sulfoxide (DMSO) was purchased from Scharlau (Scharlab AG, Sentmenat, Spain). HPLC grade water was obtained by a Milli-Q integral water purification system (Millipore Merck, Darmstadt, Germany). Ringer HEPES buffer (RHB) (150 mM NaCl, 2.2 mM $CaCl_2$, 0.2 mM $MgCl_2$, 5.2 mM KCl, 2.8 mM glucose, 5 mM HEPES, 6 mM $NaHCO_3$) was prepared in-house, adjusted to pH 7.4, filtered, and stored at 4°C.

2.2 Stock solutions, calibration standards, and quality controls

Stock solutions of each compound were prepared in DMSO. Weighings were done on a 1 µg precision microbalance (Sartorius, Switzerland). Working solutions (WS1) of analytes and corresponding I.S. (Table 1) at a concentration of 10 µg/mL in methanol were subsequently prepared by diluting the respective stock solutions. For all compounds, calibration standards (calibrators) in the range of 5.00–500 ng/mL (5.00, 25.0, 50.0, 100, 200, 400, and 500 ng/mL) and quality controls (QCs) at low, middle, and high concentration (QCL = 15.0 ng/mL, QCM = 250 ng/mL, and QCH = 400 ng/mL) were prepared in modified RHB (RHB + 0.2% Tween 20) and modified DMEM (DMEM + 10% FBS for piperine, LAU397, and LAU399; DMEM + 10% FBS + 0.2% Tween 20 for the other analogs) by serial dilution of the respective WS1. The first concentration level of the calibrators was defined as lower limit of quantification (LLOQ), and the last level as upper limit of quantification (ULOQ). Calibrators and QCs were aliquoted into polypropylene tubes and stored below -65°C until analysis. For the I.S., a second working solution (WS2) in methanol was freshly prepared on the day of each analytical run by further diluting the corresponding WS1.

2.3 Sample extraction

Prior to sample injection into the UHPLC-MS/MS system, analytes and I.S. were extracted from the matrices by means of protein precipitation.

Samples in modified RHB: Sample aliquots in modified RHB (100 µL; exception LAU399: 200 µL) were spiked with a freshly prepared WS2 (between 200–1000 ng/mL) of the corresponding I.S. (100 µL) (Table 1). Samples were subsequently spiked with 200 µL BSA solution (60 g/L) and subjected to protein precipitation with ice cold acetonitrile (1000 µL). After vortexing and stirring for 10 min on an Eppendorf Mixmate (Vaudaux-Eppendorf, Schönenbuch, Switzerland), the mixture was centrifuged for 20 min at 13200 rpm

(MiniSpin plus, Vaudaux-Eppendorf). The supernatant (1200 µL) was transferred into a 96-deep well plate (96-DWP), dried under nitrogen (Evaporex EVX-96, Apricot Designs, Monovia, CA, USA) and reconstituted with injection solvent (65% mobile phase A and 35% mobile phase B, v/v). Prior to injection (5 µL) into the UHPLC and for optimal reconstitution, the 96-DWP was stirred on an Eppendorf Mixmate for 30 min at 2000 rpm and then centrifuged for 4 min at 3000 rpm (Megafuge, Heraeus Instruments AG, Switzerland).

Samples in modified DMEM: Sample aliquots in modified DMEM (100 µL) were spiked with a freshly prepared WS2 (between 200–1000 ng/mL) of the corresponding I.S. (100 µL) (Table 1) and directly subjected to protein precipitation by the addition of ice cold acetonitrile (1000 µL). After vortexing and stirring for 10 min on an Eppendorf Mixmate, the mixture was centrifuged for 20 min at 13200 rpm. The supernatant (1000 µL) was thereafter transferred into a 96-DWP. The subsequent procedure was the same as described above.

2.4 UHPLC-MS/MS settings

Method development was performed on a 1290 Infinity UHPLC system coupled to a 6460 Triple Quadrupole (QQQ) mass spectrometer (all Agilent, Waldbronn, Germany). Data were acquired with MassHunter software version B.07.00 (Agilent). The UHPLC system included a binary pump, a degasser, a cooling multisampler (set at 10°C), and a column heater. Separation was performed on a Kinetex PFP column (particle size 1.7 µm, 2.1 x 50 mm) (Phenomenex, Torrance, CA, USA) heated to 55°C. The column was protected by an UHPLC column in-line filter unit (0.2 µm in-line frit). Mobile phase A was 10 mM ammonium formate containing 0.05% FA, and mobile phase B was acetonitrile containing 0.05% FA. The flow rate was set at 0.5 mL/min. The gradient started at 1 min with 40% of B and increased to 70% of B within 3.00 min, followed by a column washing step with 100% of B for 1 min. Needle wash solution was a mixture of acetonitrile and water (50/50, v/v) containing 0.2% TFA, and seal wash solution was a mixture of methanol, isopropanol, and water (60/20/20, v/v).

The QQQ was equipped with an Agilent Jet Stream source, and measurements were performed in electrospray ionization positive ion mode (ESI+) and multiple reaction monitoring (MRM) mode. MS/MS parameters were optimized using Agilent Optimizer software and were as follows: drying gas (nitrogen) temperature and flow rate were 320°C and 10 L/min, respectively, nebulizer pressure was 20 psi, sheath gas (nitrogen) temperature was 400°C, and flow rate was 11 L/min. Capillary voltage was 2500 V. For samples containing LAU399 in modified DMEM, sheath gas temperature and flow rate were 300°C and 6 L/min, respectively, and capillary voltage was 3500 V. MRM transitions, fragmentor voltage, and collision energy for each compound are listed in Table 1. Quantification was done using MassHunter Quantitative Analysis software version B.07.00 (Agilent).

2.5 Analytical runs

2.5.1 Calibration curve and regression analysis

Each analytical run consisted of a set of seven calibrators injected with increasing concentration after a blank sample (blank matrix) and a calibrator zero (blank matrix only spiked with I.S.) at the beginning and at the end of the run. A calibration curve was considered valid if the coefficient of determination (R^2) was higher than 0.96 and if at least 75% of all calibrators were used to generate the calibration curve. The back calculated concentrations of the calibrators had to be within ± 15% of the nominal values at all concentration levels (exception LLOQ: within ± 20%). For the LLOQ and the ULOQ, at least one replicate had to be accepted. The

calibration curve was validated through six QCs (duplicates of QCL, QCM, and QCH), which were inserted randomly into the analytical run. The back calculated concentrations had to be within ± 15% of the nominal values at all QC levels. For the six QCs, at least four replicates in total and at least one replicate at each concentration level had to be accepted. Imprecision in all analytical runs was expressed by the coefficient of variation (CV %), and had to be below 15% (below 20% at the LLOQ) of the nominal values at all concentration levels. Inaccuracy was expressed by the relative error (RE %), and had to be within ± 15% (within ± 20% at the LLOQ) of the nominal values at all concentration levels [18,19].

2.5.2 Carry-over

To assess the carry-over of both analyte and I.S. in each analytical run, blank samples were injected after both replicates of the ULOQ. Peak areas of analyte and I.S. in these blank samples were then compared to the peak areas at the LLOQ. Mean carry-over in each analytical run, expressed in %, had to be below 20% for analytes, and below 5% for I.S. [19].

2.5.3 Between-run reproducibility

Between-run reproducibility was assessed by calculating the imprecision (CV %) and inaccuracy (RE %) at five concentration levels (LLOQ, QCL, QCM, QCH, and ULOQ) of two replicates injected within three analytical runs on three different days (n = 6).

2.6 Immortalized *in vitro* human BBB model (based on hBMEC cell line)

The immortalized human mono-culture *in vitro* BBB model (24-well format) based on hBMEC cell line was prepared as reported previously [13,14], with minor modifications. As cell culture medium for hBMEC cells, EBM-2 supplemented with Single-Quots (hydrocortisone, ascorbic acid, and heparin), antibiotic-antimycotic solution, and 20% FBS (heat inactivated at 56°C for 30 min) was used. Cells were seeded at a density of 60000 cells/cm^2 onto rat tail collagen I-coated 24-well tissue culture inserts (0.336 cm^2, transparent PET membrane, 3.0 µm pore size, Greiner Bio-one, Frickenhausen, Germany), and transferred into a 24-well module of a CellZscope device [20]. Transendothelial electrical resistance (TEER) and cell layer capacitance (C_{CL}) values were recorded in real-time every hour by the CellZscope system (NanoAnalytics, Münster, Germany) inside the incubator (37°C and 5% CO_2). The permeability experiments were carried out after 2.5–3 days of incubation of hBMEC monolayers. Pre-warmed (37°C) RHB was added to the receiver compartments (1200 µL in empty wells of a 24-well plate for transport from apical-to-basolateral (A→B), and 300 µL in inserts for transport from basolateral-to-apical (B→A)). Working solution containing the test compound (2 µM) and Na-F (10 µg/mL) in RHB + 0.1% BSA was added to the donor compartments (300 µL in inserts for A→B, and 1200 µL in empty wells for B→A). The 24-well plates were incubated on an orbital shaker at 37°C and 300 rpm (ELMI DTS-2, Riga, Latvia), and aliquots of apical and basolateral compartments were collected after several time points (15, 30, 60, and 120 min) (one insert per time point) and stored below -65°C until analysis. The experiments were performed at least in triplicate, and control experiments without cells were performed. Na-F fluorescence was quantified with a Chameleon microplate reader (Hidex, Turku, Finland), and quantification of test compounds was carried out by UHPLC-MS/MS. Before UHPLC-MS/MS analysis, samples were diluted with an equal volume of 0.4% Tween 20 in order to avoid non-specific adsorption to surfaces.

2.7 *In vitro* human brain-like endothelial cells (BLEC) BBB model

The human *in vitro* BBB model derived from hematopoietic stem cells (12-well format) was prepared as described previously [15]. Tissue culture inserts were from Corning (1.12 cm^2, polycarbonate membrane, 0.4 µm pore size, Corning, New York, USA), and were coated with matrigel. Prior to the permeability experiments, buffered Ringer's solution was added to the receiver compartments (1500 µL in empty wells of a 12-well plate for A→B transport, and 500 µL in inserts for B→A transport). Working solution containing the test compound (2 µM) and Na-F (10 µg/mL) in RHB + 0.1% BSA was added to the donor compartments (500 µL in inserts for A→B, and 1500 µL in empty wells for B→A), and the 12-well plates were incubated on an orbital shaker at 37°C and 60 rpm (Polymix, Kinematica). After 15, 30, and 60 min for A→B transport, inserts were transferred into a new receiver plate filled with transport buffer. After 15, 30, 60, and 120 min for A→B transport, or after two hours incubation for B→A, an aliquot from each donor and receiver compartment and working solution was withdrawn and stored below -65°C until analysis. Control inserts without cells were assayed for each test compound. Experiments were performed in triplicate. The amount of fluorescent tracer (Na-F) was analyzed with a fluorescence counter (Synergy H1, Biotek). Quantification of test compounds was carried out as described above.

2.8 *In vitro* primary bovine endothelial/rat astrocytes co-culture BBB model

The bovine endothelial/rat astrocytes co-culture model was prepared as described previously [21]. Tissue culture inserts were from Corning (1.12 cm^2, polycarbonate membrane, 0.4 µm pore size, Corning, New York, USA), and were coated with collagen/fibronectin. Experiments were performed in triplicate. Transcellular transport studies were performed directly in the culture medium (DMEM + 10% FBS) after 6 days of co-culture. TEER was measured after equilibration to RT prior to all experiments, using an Endohm-12 cup electrode chamber (World Precision Instruments, Sarasota, Florida, USA) connected to a Millicell-ERS device (Millipore, Massachusetts, USA). Cells were equilibrated to 37°C, and transport was started by addition of a working solution containing the test compound (5 µM) and Na-F (10 µg/mL) in DMEM + 10% FBS to the donor compartments (500 µL for A→B and 1000 µL for B→A). The cells were placed on a temperature-controlled shaking table at 37°C and 90 rpm. Aliquots (100 µL from the apical and 200 µL from the basolateral compartments) were withdrawn from the receiver compartments after 15, 30, 60, and 120 min, and from the donor compartment after 120 min. Withdrawn samples were replaced with pre-warmed (37°C) medium. Na-F signal was immediately measured in a NOVOstar plate reader (BMG Labtech GmbH, Offenburg, Germany), and Na-F concentration in the samples was calculated by comparison to a standard curve. Samples were subsequently stored at -20°C until UHPLC-MS/MS-analysis.

2.9 Calculation of permeability coefficients

For the two human *in vitro* BBB models, endothelial permeability coefficients (P_e) for each test compound and for Na-F were calculated as follows. For each replicate (control inserts without cells and inserts with cells), the clearance was calculated according to the following equation [22,23]:

$$\text{Clearance } (\mu L) = C_R V_R / C_D \quad (1)$$

where C_R and V_R are the concentration and volume in the receiver compartments, respectively, and C_D is the initial concentration in the donor compartment. The mean cleared volume was plotted as a function of time (15,

30, 60, and 120 min), and the slope was estimated by linear regression analysis. Permeability-surface area products (PS) and P_e values were subsequently calculated according to the following equations [22,23]:

$$1/PS_{total} - 1/PS_{filter} = 1/PS_e \quad (2)$$

$$PS_e/A = P_e \text{ (cm/s)} \quad (3)$$

where PS_{total} is the slope of the clearance curve of cell monolayers with filter inserts, PS_{filter} is the slope of the clearance curve of control filter inserts without cells, PS_e is the slope of the clearance curve of the endothelial monolayers, and A is the surface area of the filter membrane.

For all three models, apparent permeability coefficients (P_{app}) were calculated according to the following equations [24,25]:

$$P_{app} \text{ (cm/s)} = J/(AC_D) \quad (4)$$

where J is the rate of appearance of the compounds in the receiver compartment, A is the surface area of the filter membrane, and C_D is the initial concentration in the donor compartment.

Furthermore, efflux ratios (ER) were calculated:

$$ER = P_{app\ (B\rightarrow A)}/P_{app\ (A\rightarrow B)} \quad (5)$$

where $P_{app\ (B\rightarrow A)}$ and $P_{app\ (A\rightarrow B)}$ are the P_{app} values in the direction basolateral-to-apical and apical-to-basolateral, respectively. A high ER indicates a potentially significant role for efflux transporters in the passage of a compound across cell monolayers. Compounds with a ER > 2 are thus usually categorized as efflux transporter substrates [26,27].

Recovery (mass balance) of each compound was calculated according to the following equation:

$$\text{Recovery (\%)} = (N_{Df} + N_{Rf})/N_{Di} \times 100 \quad (6)$$

where N_{Df} and N_{Rf} are the final amounts of the compounds in the donor and receiver compartments, respectively, and N_{Di} is the initial amount in the donor compartment. All results are expressed as means ± standard deviation (SD).

2.10 *In silico* prediction of BBB permeability

Three-dimensional computer models of studied compounds were built in Maestro modeling environment [28]. The global minimum geometry was used as an input for the QikProp application [29] to evaluate various descriptors relevant for compound permeability through the BBB. The polar surface area (PSA) and the logarithm of partition and distribution coefficient (LogP and LogD7.4, respectively) descriptors were calculated using the Calculator plugin of Chemaxon Marvin application [30].

3 Results

3.1 UHPLC-MS/MS

3.1.1 Chromatographic performance

Calibration curves in the range of 5.00–500 ng/mL for each analyte were fitted by least-squares quadratic regression, and a weighting factor of 1/X was applied. The mean coefficients of determination (R^2) ranged from 0.9945 to 0.9996 (Tables S1 and S2).

3.1.2 Carry-over

Mean carry-over in blank matrix samples (modified RHB and modified DMEM) injected after the ULOQ were between 0.00% to 4.27% for analytes (below 20%), and between 0.00% and 0.0597% for I.S. (below 5%) (Table S3), indicating that carry-over did not have an impact on the results.

3.1.3 Between-run reproducibility

Between-run imprecision (CV %) was between 1.17% and 14.9% (below 15%), and between-run inaccuracy (RE %) was between -8.15% and 10.0% (within ± 15%) at all calibration levels in both matrices (modified RHB and modified DMEM) (Tables 2 and 3), indicating that the methods were accurate, precise, and reproducible.

3.2 Immortalized *in vitro* human BBB model (based on hBMEC cell line)

In the immortalized *in vitro* human BBB model [13,14], piperine showed a mean $P_{e\ (A\rightarrow B)}$ value of 53.7 ± 4.47 x 10^{-6} cm/s, indicating significant BBB permeability when compared to the mean $P_{e\ (A\rightarrow B)}$ value of the negative control Na-F (6.51 ± 0.163 x 10^{-6} cm/s) (Fig. 2A, Table 4). SCT-64 and LAU399 showed lower mean $P_{e\ (A\rightarrow B)}$ values (26.4 ± 1.48 x 10^{-6} cm/s and 21.6 ± 9.52 x 10^{-6} cm/s, respectively) than piperine (Fig. 2A, Table 4), but were still significantly higher than those for Na-F (4.50 and 4.83 x 10^{-6} cm/s), respectively). Compounds SCT-66, SCT-29, and LAU397 showed mean $P_{e\ (A\rightarrow B)}$ values between 4.29 and 9.32 x 10^{-6} cm/s (Fig. 2A, Table 4), suggesting low BBB permeability when compared to Na-F. The compounds could be ranked based on their $P_{e\ (A\rightarrow B)}$ values in the following order: piperine > SCT-64/LAU399 > SCT-66 > LAU397/SCT-29. ER values for the compounds (except SCT-29) were between 0.750 and 1.92 (Table S4), suggesting that permeability of the compounds was not affected by active efflux transporters [26,27].

Mean TEER values were between 20–40 Ωcm^2 for the BBB drug permeability experiments, and were in the same range after the assays (Fig. S1). Mean C_{CL} values were in the range of 0.5–5.0 $\mu F/cm^2$ (Fig. S1), indicating cell confluency of hBMEC monolayers and validating TEER values [31]. During the permeability assays, P_{app} values for Na-F were constant, indicating that barrier integrity of hBMEC monolayers was maintained throughout the experiments.

3.3 *In vitro* human brain-like endothelial cells (BLEC) BBB model

In the *in vitro* human BLEC model [15], piperine, SCT-66, and SCT-64 showed mean $P_{e\ (A\rightarrow B)}$ values between 26.7 and 97.8 x 10^{-6} cm/s (Fig. 2B, Table 5) that were indicative of moderate to high BBB permeability when compared to the mean $P_{e\ (A\rightarrow B)}$ values for Na-F (9.99–12.0 x 10^{-6} cm/s). The analogs SCT-29, LAU397, and LAU399 showed mean $P_{e\ (A\rightarrow B)}$ values between 4.61 and 12.4 x 10^{-6} cm/s (Fig. 2B, Table 5), suggesting low permeability when compared to Na-F. The compounds could be ranked regarding their $P_{e\ (A\rightarrow B)}$ values as follows: piperine > SCT-66/SCT-64 > LAU397 > LAU399/SCT-29.

For all compounds (except piperine), mean recoveries were rather low (between 55.7% and 68.5%) (Table 5), also in the absence of cells (data not shown). This was indicative of a possible non-specific binding of analytes to plastic surfaces and/or coating material of the inserts and transwell plates. Thus, $P_{e\ (A\rightarrow B)}$ values might be underestimated.

ER values for all compounds were between 0.406 and 0.804 (Table S5), suggesting that the compounds were not substrates of active efflux. Mean TEER values, at which permeability experiments were carried out, were between 150–200 Ωcm^2 [15].

3.4 *In vitro* primary bovine endothelial/rat astrocytes co-culture BBB model

In the primary bovine endothelial/rat astrocytes co-culture *in vitro* BBB model, the compounds showed mean $P_{app\ (A\rightarrow B)}$ values between 20.9 and 81.3 x 10^{-6} cm/s (Fig. 2C, Table 6). Compared to the mean $P_{app\ (A\rightarrow B)}$ values of Na-F (2.15–5.07 x 10^{-6} cm/s) (Table 6), these values were considerably higher, indicating high BBB permeability for all compounds. The compounds could be ranked based on their $P_{app\ (A\rightarrow B)}$ values in the following order: piperine > SCT-64 > LAU399/LAU397 > SCT-66/SCT-29.

However, the mean $P_{app\ (A\rightarrow B)}$ values for Na-F in presence of the test compounds (2.15–5.07 x 10^{-6} cm/s, Table 6) were up to five times higher than those usually obtained in the model (below 1 x 10^{-6} cm/s). Mean P_{app} values in the direction B→A for Na-F in presence of the compounds, on the other hand, were in this expected range (below 1 x 10^{-6} cm/s, Table S6). Hence, a polarized opening of the paracellular space may have occurred when the compounds were applied on the apical side (but not on the basolateral side). For piperine, we further investigated this junctional effect by applying the compound to the apical and basolateral side of the inserts (at 5 µM), and measuring TEER as a function of incubation time. Throughout a two hour incubation period, the TEER was relatively stable for control cell monolayers and for cell monolayers to which piperine was applied on the basolateral side (Fig. 3). However, TEER values decreased from 1261 to 268 Ωcm^2 for cell monolayers to which piperine was added on the apical side (Fig. 3), supporting the hypothesis of a polarized paracellular opening.

ER values for all compounds were between 0.340 and 0.584 (Table S6), indicating no involvement of active efflux transporters. TEER values, at which experiments were performed, were in the range of 1900–2500 Ωcm^2.

3.5 *In silico* prediction of BBB permeability

The analysis of descriptors relevant for the BBB permeation showed that the compounds had a PSA (26.9–48.1 $Å^2$) (Table 7) below the recommended thresholds of 70 $Å^2$ [32] and 90 $Å^2$ [33], which favors their passive permeation across the BBB. Similarly, their molecular weight (MW) was below the recommended value of 450 g/mol for CNS drugs (between 285 and 329 g/mol) (Table 7) [33]. All compounds had a low effective number of H-bond acceptors (< 5) and no H-bond donors (Table 7), which facilitates their desolvation before entering into the lipophilic phase of the cell membranes. The QikProp model for brain/blood partitioning predicted favorable LogBB parameters (between -0.51 and -0.12) for all compounds (for 95% of known drugs, values range between -3.0 and 1.2), and the predicted permeability across Madin-Darby Canine Kidney (MDCK) and Caco-2 cells was very high (> 2000 nm/s) (Table 7). LogP values for the compounds ranged from 3.27 to 5.34 (recommended values for CNS drugs are between 1–4), and the total numbers of rotatable bonds were between 3 and 10 (Table 7) (less than 6 rotatable bonds recommended for CNS drugs [34]).

4 Discussion

The alkaloid piperine was recently identified as a promising lead compound for the development of positive allosteric $GABA_A$ receptor modulating drugs interacting at an up to now poorly characterized binding site [1]. However, the compound concomitantly activates TRPV1 receptors [4], which is undesirable for a lead structure as unwanted side effects might possibly occur. A large series of semisynthetic and fully synthetic piperine analogs was therefore synthesized, with the objective to obtain compounds with improved $GABA_A$ receptor activity and reduced TRPV1 receptor interaction [2,7,9]. Among these, the analogs SCT-66, SCT-64, SCT-29, LAU397, and LAU399 (Fig. 1) modulated $GABA_A$ receptors more potently and/or efficiently than piperine, while being devoid of TRPV1 interaction [1,2,7,9].

Drugs acting on the CNS such as $GABA_A$ receptor modulators need to penetrate the brain by crossing the BBB in order to reach their target sites. In this study, we aimed thus at early screening piperine and five promising analogs (SCT-66, SCT-64, SCT-29, LAU397, and LAU399) for their ability to cross the BBB, in order to evaluate their potential as lead structures for the development of new $GABA_A$ receptor modulating drugs, and to select the most promising candidate molecule for further *in vivo* testing or for the next cycle of medicinal chemistry optimization.

For comparative purposes, we initially decided to select three human BBB models including immortalized, primary, and stem cell-derived human cell phenotypes. However, getting access to post-mortem human brains was critical, and we therefore utilized a highly tight animal BBB model. The compounds were thus screened in our previously established and validated immortalized human mono-culture *in vitro* BBB model based on hBMEC cell line [13,14], in a recently developed *in vitro* human BLEC BBB model [15], and in a well-established tight primary animal (bovine endothelial/rat astrocytes co-culture) *in vitro* BBB model [21]. For each compound, a specific quantitative UHPLC-MS/MS assay in the corresponding matrix was developed, and permeability coefficients across the endothelial monolayers were determined. For each model, we reported the permeability coefficients that are usually calculated for screened compounds (i.e. P_e for the two human models [14,15], and P_{app} for the animal model [21]).

During UHPLC-MS/MS method development, non-specific adsorption of the compounds in RHB to various surfaces was observed, leading to unacceptable calibration curves (data not shown). This problem was resolved by spiking RHB with 0.2% Tween 20 for the preparation of calibrators and QCs [35], and valid calibration curves could be obtained (Table S1). For compounds in modified DMEM, the addition of Tween 20 was only necessary for SCT-66, SCT-64, and SCT-29. For the other analogs, the presence of FBS (10%) in the matrix (DMEM) seemed to be sufficient to avoid non-specific adsorption to surfaces. However, the permeability assays could not be carried out using RHB spiked with Tween 20 since the detergent could affect the integrity of the endothelial barrier. Thus, samples were diluted after the assays with an equal volume of RHB containing 0.4% Tween 20 directly in the tubes for optimal desorption.

In the two human *in vitro* BBB models, piperine and SCT-64 displayed moderate to high BBB permeability, while SCT-29 and LAU397 displayed low BBB permeability (Fig. 2A and 2B, Tables 4 and 5). The derivative

SCT-66 showed moderate BBB permeability in the human BLEC BBB model (but low permeability in the immortalized model), while LAU399 showed moderate BBB permeation in the immortalized model (but low permeability in the human BLEC model) (Fig. 2A and 2B, Tables 4 and 5). With the exception of this minor difference, both human models provided a similar ranking of the compounds based on their $P_{e\ (A\rightarrow B)}$ values.

Results from the primary animal *in vitro* BBB model were not in complete agreement with permeability data from the two human models. In the animal model, all compounds showed high BBB permeability, while in the human models, two analogs (SCT-29 and LAU397) showed low BBB permeation (Fig. 2, Tables 4–6). These data discrepancies were most likely due to the different matrices used for the permeability screenings. In the animal model, transport experiments were carried out directly in cell culture medium containing 10% FBS. The presence of proteins in the receiver compartment thus created an additional sink, increasing the permeability for the lipophilic piperine analogs across the BBB due to a high protein binding [36].

According calculated descriptor values relevant for BBB permeation (i.e. PSA, MW, H-bond acceptors and donors, LogBB) (Table 7), all compounds should be able to permeate the BBB by passive diffusion. However, a closer consideration of two further descriptor values, namely LogP and number of rotatable bonds, may provide a further explanation for the low permeability observed for SCT-29 and LAU397 in the human BBB models. According to Brito-Sánchez et al. (2015), the total number of rotatable bonds should not exceed 6 to facilitate the permeation of a compound across the BBB [34]. For SCT-29 and LAU397, the total number of rotatable bonds of the compounds was rather high (9 and 10, respectively; counting according to Veber rules) (Table 7). Furthermore, SCT-29 and LAU397 showed relatively high LogP values (4.70 and 5.34, respectively) (Table 7) which are above the recommended range of 1–4 for CNS drugs. Compounds SCT-66 and SCT-64 also showed relatively high LogP values (4.59 and 3.96, respectively). However, their total number of rotatable bonds was lower (7). In case of LAU399, the high number of rotatable bonds (9) and non-optimal lipophilicity (LogP of 5.21) were probably compensated by its extremely small PSA (26.9 $Å^2$). Piperine showed moderate lipophilicity (LogP of 3.27), a low number of rotatable bonds (3), and was thus best suited for BBB permeation. In conclusion, it seemed that for the human models, BBB permeation of this series of compounds depended mainly on their number of rotatable bonds.

In the animal *in vitro* BBB model, mean $P_{app\ (A\rightarrow B)}$ values for Na-F in presence of the compounds were up to five times higher than those normally observed in this model (below 1 x 10^{-6} cm/s). However, mean P_{app} values in the direction B→A for Na-F in presence of the compounds were in this expected range (below 1 x 10^{-6} cm/s, Table S6). Thus, a polarized opening of the paracellular space may have occurred when the compounds were applied on the apical side (but not on the basolateral side). Therefore, mean P_{app} values in the direction B→A for the compounds may give a better estimation of their BBB permeability in a situation where there is no barrier opening.

For piperine, the polarized junctional effect was further investigated by applying the compound on the apical and basolateral side of the inserts (5 µM), and measuring the TEER as a function of incubation time. Throughout an incubation period of two hours, the TEER was relatively stable for control cell monolayers and for cell

monolayers to which piperine was applied on the basolateral side (Fig. 3). However, TEER values decreased from 1261 to 268 Ωcm^2 for cell monolayers to which piperine was added on the apical side (Fig. 3), supporting the hypothesis of a polarized paracellular opening. The apparent junctional opening could be caused by TRPV1 activation in brain endothelial cells, as has previously been demonstrated in anesthetized rats [38]. TRPV1 activation has been shown to decrease TEER and to cause occludin redistribution in a rat submandibular gland cell line (SMG-C6) [39], and may have caused similar effects in the bovine endothelial cells, which would imply an apical localization of TRPV1 receptors in the endothelial cells. The five tested piperine analogs were reported not to act on rat TRPV1 receptors [2,9], but affinities for the bovine form of the receptor may differ. However, more detailed studies to clarify these issues would be necessary. An opening of the barrier could not be observed in the human models with compounds at 2 μM, as P_e values for Na-F in both directions ($P_{e\ (A\rightarrow B)}$ see Table 7; $P_{e\ (B\rightarrow A)}$ data not shown) were in a similar range as usually obtained in the two models, indicating that barrier integrity was maintained throughout the experiments.

In previous studies, piperine and the analogs SCT-66, SCT-64, and SCT-29 were reported to exhibit anxiolytic effects in mice [2,7]. However, SCT-66 and SCT-29 did not cross the BBB significantly in the *in vitro* human models, while crossing the BBB in the *in vitro* bovine/rat model. As discussed above, the high permeability of the compounds in the animal model was likely due to the presence of FBS in the transport matrix, which created sink conditions in the receiver compartment, and thus improved P_{app} values due to a high protein binding of the compounds. To evaluate whether the compounds are able to reach the brain *in vivo*, further studies to assess protein binding and the *in vivo* extent of brain penetration (e.g. total brain-to-plasma ratio) of the compounds are therefore necessary, and are currently in progress in our laboratory. Also, free brain drug concentration *in vivo* of the compounds should be determined.

Finally, by performing bidirectional permeability experiments we did not evidence any effect of active efflux transporters on compound permeation across the BBB (ER below 2, Tables S4–S6). However, piperine has been reported to inhibit P-glycoprotein (P-gp) and phase I and II metabolism enzymes [40–42]. Thus, possible inhibition of P-gp and CYPs by the compounds needs to be assessed. Also, an evaluation of the metabolic stability is needed, especially for compounds containing the metabolically critical 1,3-benzodioxole group (piperine, SCT-66, SCT-64, and SCT-29) (Fig. 1).

5 Conclusions

Piperine and five selected piperine analogs with positive $GABA_A$ receptor modulatory activity were screened in three *in vitro* cell-based human and animal BBB models for their ability to cross the BBB. Data from the three models differed to some extent, possibly due to high protein binding of the piperine analogs. In all three models, piperine and SCT-64 displayed the highest BBB permeation potential, which could be corroborated by *in silico* prediction data. For the other piperine analogs (SCT-66, SCT-29, LAU397, and LAU399), BBB permeability was low to moderate in the two human models, and moderate to high in the animal model. ER calculated from bidirectional permeability experiments indicated that the compounds were not substrates of active efflux. We conclude that further *in vivo* experiments are necessary to evaluate the extent of brain penetration of the compounds. In addition, pharmacokinetic properties and drug metabolism of the compounds should be assessed.

Several studies are currently in progress in our laboratory, and will serve to select the most promising candidate molecule for further development or for the next cycle of medicinal chemistry optimization.

Acknowledgments

The authors are grateful to Prof. Kwang Sik Kim, Prof. Dennis Grab, Prof. Reto Brun, and Dr. Tanja Wenzler for providing the hBMEC cell line. Further thanks go to Orlando Fertig for technical assistance, and to Tabea Gollin for contribution to the graphical abstract. Hans Christian Cederberg Helms and Birger Brodin acknowledge the support from the Lundbeck Foundation via the "Research Initiative on Brain Barriers and Drug Delivery" (RIBBDD) grant. Laurin Wimmer is a fellow of the doctoral program W-1232 of the Austrian Research Fund (FWF). This research was supported by the Swiss National Science Foundation (SNSF) (grant 05320_126888/1 to MH).

Conflict of interest

The authors declare no conflict of interest.

References

[1] J. Zaugg, I. Baburin, B. Strommer, H.-J. Kim, S. Hering, M. Hamburger, HPLC-based activity profiling: discovery of piperine as a positive GABAA receptor modulator targeting a benzodiazepine-independent binding site, J. Nat. Prod. 73 (2010) 185–191.

[2] S. Khom, B. Strommer, A. Schöffmann, J. Hintersteiner, I. Baburin, T. Erker, et al., GABAA receptor modulation by piperine and a non-TRPV1 activating derivative, Biochem. Pharmacol. 85 (2013) 1827–1836.

[3] H. Möhler, GABAA receptors in central nervous system disease: anxiety, epilepsy, and insomnia, J. Recept. Signal Transduct. 26 (2006) 731–740.

[4] F.N. McNamara, A. Randall, M.J. Gunthorpe, Effects of piperine, the pungent component of black pepper, at the human vanilloid receptor (TRPV1), Br. J. Pharmacol. 144 (2005) 781–790.

[5] V. Di Marzo, G. Gobbi, A. Szallasi, Brain TRPV1: a depressing TR(i)P down memory lane?, Trends Pharmacol. Sci. 29 (2008) 594–600.

[6] N.R. Gavva, A.W. Bannon, S. Surapaneni, D.N. Hovland, S.G. Lehto, A. Gore, et al., The vanilloid receptor TRPV1 is tonically activated in vivo and involved in body temperature regulation, J. Neurosci. 27 (2007) 3366–3374.

[7] A. Schöffmann, L. Wimmer, D. Goldmann, S. Khom, J. Hintersteiner, I. Baburin, et al., Efficient modulation of γ-aminobutyric acid type A receptors by piperine derivatives, J. Med. Chem. 57 (2014) 5602–5619.

[8] S.M. Attia, Deleterious effects of reactive metabolites, Oxid. Med. Cell. Longev. 3 (2010) 238–253.

[9] L. Wimmer, D. Schönbauer, P. Pakfeifer, A. Schöffmann, S. Khom, S. Hering, et al., Developing piperine towards TRPV1 and GABAA receptor ligands – synthesis of piperine analogs via Heck-coupling of conjugated dienes, Org. Biomol. Chem. 13 (2015) 990–994.

[10] N.J. Abbott, A.A.K. Patabendige, D.E.M. Dolman, S.R. Yusof, D.J. Begley, Structure and function of the blood-brain barrier, Neurobiol. Dis. 37 (2010) 13–25.

[11] L. Di, H. Rong, B. Feng, Demystifying brain penetration in central nervous system drug discovery, J. Med. Chem. 56 (2013) 2–12.

[12] A. Reichel, Addressing central nervous system (CNS) penetration in drug discovery: basics and implications of the evolving new concept, Chem. Biodivers. 6 (2009) 2030–2049.

[13] D.E. Eigenmann, G. Xue, K.S. Kim, A.V. Moses, M. Hamburger, M. Oufir, Comparative study of four immortalized human brain capillary endothelial cell lines, hCMEC/D3, hBMEC, TY10, and BB19, and optimization of culture conditions, for an in vitro blood-brain barrier model for drug permeability studies, Fluids Barriers CNS. 10 (2013) 33–50.

[14] D.E. Eigenmann, E.A. Jähne, M. Smiesko, M. Hamburger, M. Oufir, Validation of an immortalized human (hBMEC) in vitro blood-brain barrier model, Anal. Bioanal. Chem. (2015) manuscript in revision (ABC–01639–2015–R1).

[15] R. Cecchelli, S. Aday, E. Sevin, C. Almeida, M. Culot, L. Dehouck, et al., A stable and reproducible human blood-brain barrier model derived from hematopoietic stem cells, PLoS ONE. 9 (2014) 1–11.

[16] H.C. Helms, M. Hersom, L.B. Kuhlmann, L. Badolo, C.U. Nielsen, B. Brodin, An electrically tight in vitro blood-brain barrier model displays net brain-to-blood efflux of substrates for the ABC transporters, P-gp, BCRP and MRP-1, AAPS J. 16 (2014) 1046–1055.

[17] M.F. Stins, J. Badger, K.S. Kim, Bacterial invasion and transcytosis in transfected human brain microvascular endothelial cells, Microb. Pathog. 30 (2001) 19–28.

[18] Guidance for Industry: Bioanalytical Method Validation, US Food and Drug Administration (FDA), Center for Drug Evaluation and Research (CDER), May 2001, (n.d.).

[19] Guideline on bioanalytical method validation, European Medicines Agency (EMEA/CHMP/EWP/192217/2009), London, 21 July 2011, (n.d.).

[20] J. Wegener, D. Abrams, W. Willenbrink, H.-J. Galla, A. Janshoff, Automated multi-well device to measure transepithelial electrical resistances under physiological conditions, BioTechniques. 37 (2004) 590–597.

[21] H.C. Helms, B. Brodin, Generation of primary cultures of bovine brain endothelial cells and setup of cocultures with rat astrocytes, in: R. Milner (Ed.), Cereb. Angiogenesis, Springer New York, 2014: pp. 365–382.

[22] A. Siflinger-Birnboim, P.J. del Vecchio, J.A. Cooper, F.A. Blumenstock, J.M. Shepard, A.B. Malik, Molecular sieving characteristics of the cultured endothelial monolayer, J. Cell. Physiol. 132 (1987) 111–117.

[23] M.-P. Dehouck, P. Jolliet-Riant, F. Brée, J.-C. Fruchart, R. Cecchelli, J.-P. Tillement, Drug transfer across the blood-brain barrier: correlation between in vitro and in vivo models, J. Neurochem. 58 (1992) 1790–1797.

[24] S. Lundquist, M. Renftel, J. Brillault, L. Fenart, R. Cecchelli, M.-P. Dehouck, Prediction of drug transport through the blood-brain barrier in vivo: a comparison between two in vitro cell models, Pharm. Res. 19 (2002) 976–981.

[25] E. Hellinger, S. Veszelka, A.E. Toth, F. Walter, A. Kittel, M.L. Bakk, et al., Comparison of brain capillary endothelial cell-based and epithelial (MDCK-MDR1, Caco-2, and VB-Caco-2) cell-based surrogate blood-brain barrier penetration models, Eur. J. Pharm. Biopharm. 82 (2012) 340–351.

[26] J.W. Polli, S.A. Wring, J.E. Humphreys, L. Huang, J.B. Morgan, L.O. Webster, et al., Rational use of in vitro P-glycoprotein assays in drug discovery, J. Pharmacol. Exp. Ther. 299 (2001) 620–628.

[27] K.M. Giacomini, S.-M. Huang, D.J. Tweedie, L.Z. Benet, K.L.R. Brouwer, X. Chu, et al., Membrane transporters in drug development, Nat. Rev. Drug Discov. 9 (2010) 215–236.

[28] Maestro, version 9.9, Schrödinger, LLC, New York, NY, 2014, (n.d.).

[29] QikProp, version 4.1, Schrödinger, LLC, New York, NY, 2014, (n.d.).

[30] Marvin 15.4.13.0, 2015, ChemAxon (http://www.chemaxon.com), (n.d.).

[31] C.A. Bertrand, D.M. Durand, G.M. Saidel, C. Laboisse, U. Hopfer, System for dynamic measurements of membrane capacitance in intact epithelial monolayers, Biophys. J. 75 (1998) 2743–2756.

[32] J. Kelder, P.D. Grootenhuis, D.M. Bayada, L.P. Delbressine, J.P. Ploemen, Polar molecular surface as a dominating determinant for oral absorption and brain penetration of drugs, Pharm. Res. 16 (1999) 1514–1519.

[33] H. van de Waterbeemd, G. Camenisch, G. Folkers, J.R. Chretien, O.A. Raevsky, Estimation of blood-brain barrier crossing of drugs using molecular size and shape, and H-bonding descriptors, J. Drug Target. 6 (1998) 151–165.

[34] Y. Brito-Sánchez, Y. Marrero-Ponce, S.J. Barigye, I. Yaber-Goenaga, C. Morell Pérez, H. Le-Thi-Thu, et al., Towards better BBB passage prediction using an extensive and curated data set, Mol. Inform. 34 (2015) 308–330.

[35] A.J. Ji, Z. Jiang, Y. Livson, J.A. Davis, J.X. Chu, N. Weng, Challenges in urine bioanalytical assays: overcoming nonspecific binding, Bioanalysis. 2 (2010) 1573–1586.

[36] I. Hubatsch, E.G.E. Ragnarsson, P. Artursson, Determination of drug permeability and prediction of drug absorption in Caco-2 monolayers, Nat. Protoc. 2 (2007) 2111–2119.

[37] G. Krishna, K. Chen, C. Lin, A.A. Nomeir, Permeability of lipophilic compounds in drug discovery using in vitro human absorption model, Caco-2, Int. J. Pharm. 222 (2001) 77–89.

[38] D.-E. Hu, A.S. Easton, P.A. Fraser, TRPV1 activation results in disruption of the blood-brain barrier in the rat, Br. J. Pharmacol. 146 (2005) 576–584.

[39] X. Cong, Y. Zhang, N.-Y. Yang, J. Li, C. Ding, Q.-W. Ding, et al., Occludin is required for TRPV1-modulated paracellular permeability in the submandibular gland, J. Cell Sci. 126 (2013) 1109–1121.

[40] R.K. Bhardwaj, H. Glaeser, L. Becquemont, U. Klotz, S.K. Gupta, M.F. Fromm, Piperine, a major constituent of black pepper, inhibits human P-glycoprotein and CYP3A4, J. Pharmacol. Exp. Ther. 302 (2002) 645–650.

[41] Y. Han, T.M. Chin Tan, L.-Y. Lim, In vitro and in vivo evaluation of the effects of piperine on P-gp function and expression, Toxicol. Appl. Pharmacol. 230 (2008) 283–289.

[42] L.P. Volak, S. Ghirmai, J.R. Cashman, M.H. Court, Curcuminoids inhibit multiple human cytochromes P450, UDP-glucuronosyltransferase, and sulfotransferase enzymes, whereas piperine is a relatively selective CYP3A4 inhibitor, Drug Metab. Dispos. 36 (2008) 1594–1605.

FIGURES

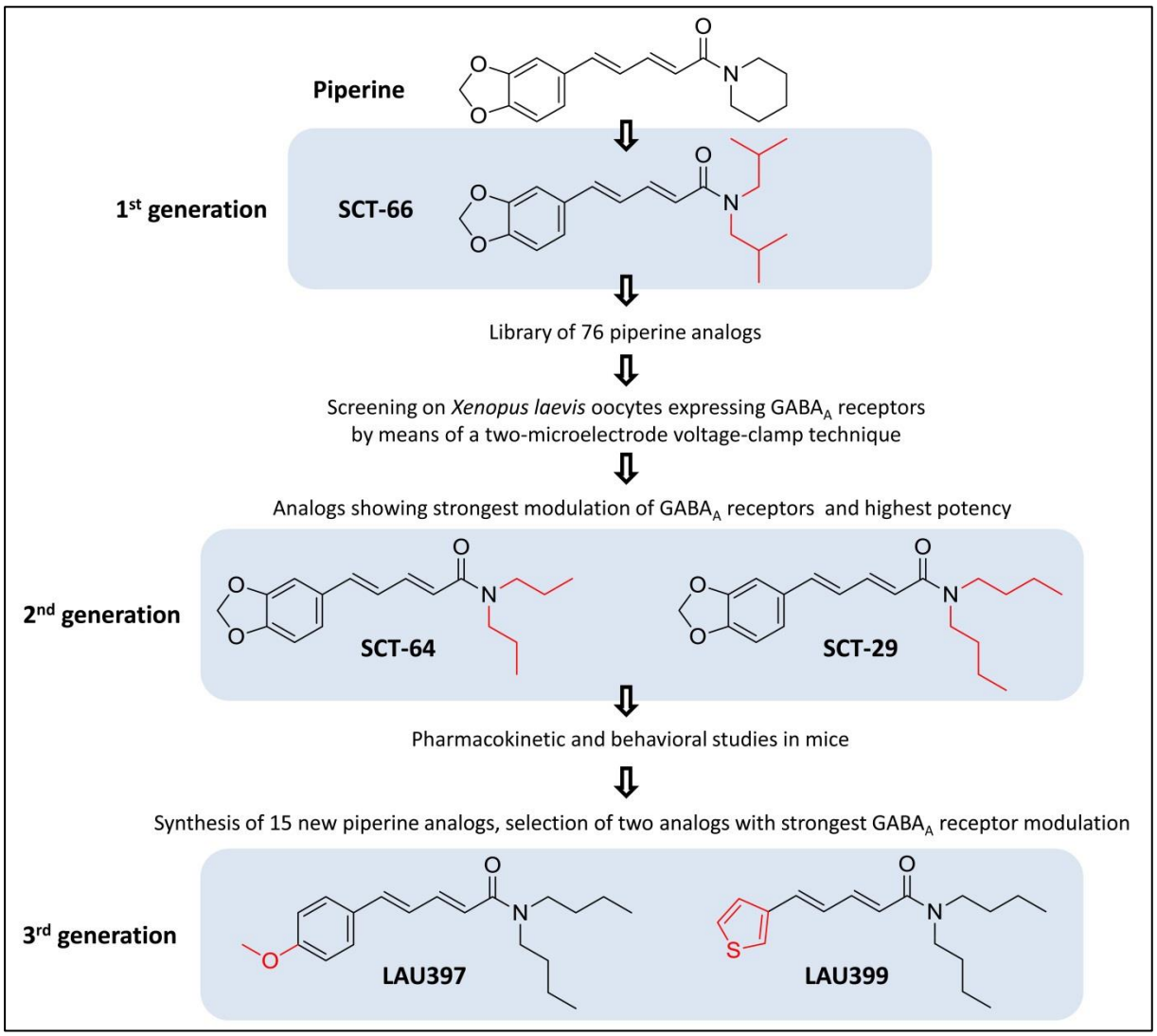

Fig. 1 Piperine and analogs analyzed in the *in vitro* BBB models. Selection and optimization process, and structures of compounds [1,2,7,9].

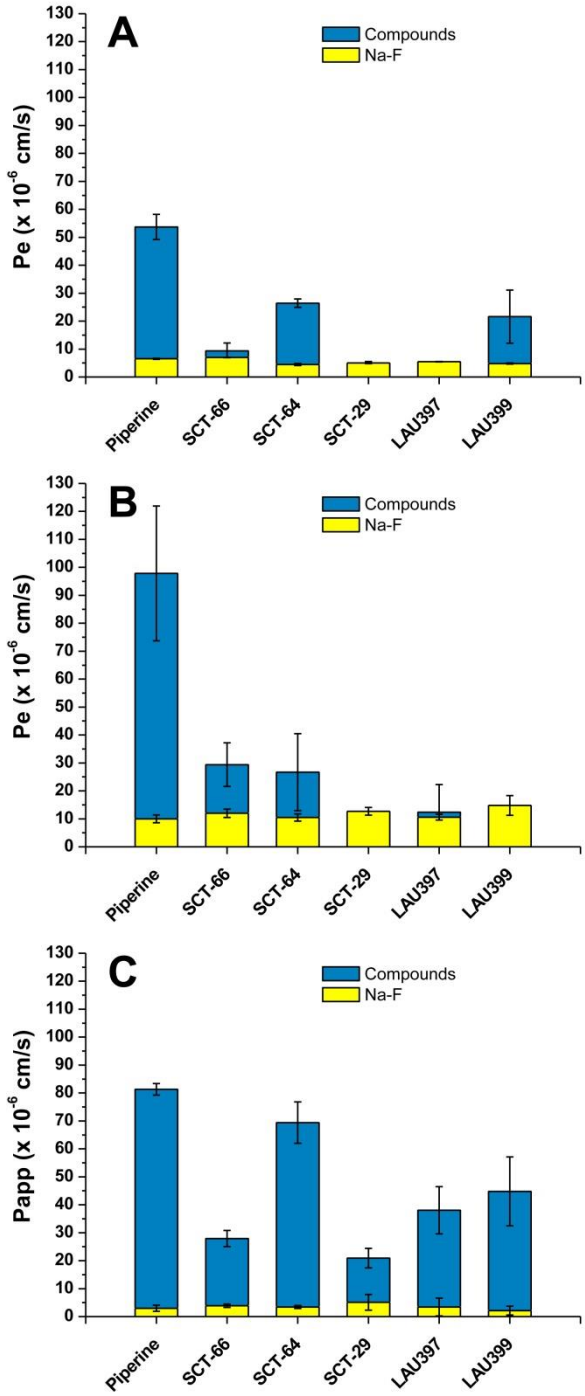

Fig. 2 Mean endothelial permeability coefficients ($P_{e\ (A\rightarrow B)}$) ± SD for piperine and five analogs in (**A**) the immortalized *in vitro* human BBB model (hBMEC cell line-based), (**B**) the *in vitro* human BLEC BBB model, and (**C**) mean apparent permeability coefficients ($P_{app\ (A\rightarrow B)}$) ± SD in the *in vitro* primary bovine endothelial/rat astrocytes co-culture BBB model.

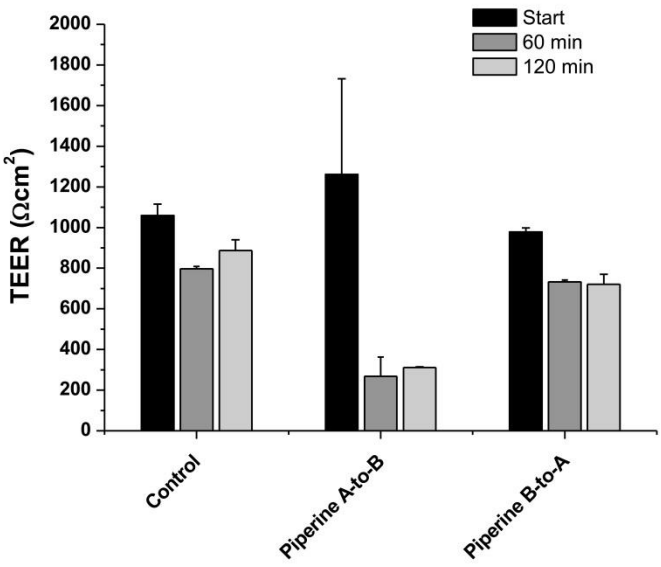

Fig. 3 Mean TEER ± SD values in the primary bovine endothelial/rat astrocytes co-culture *in vitro* BBB model for endothelial cell monolayers as a function of incubation time (n = 2). TEER values were relatively stable for a two hour incubation time for control cell monolayers, and for cell monolayers when piperine (5 µM) was applied on the basolateral side (Piperine B-to-A). However, TEER values of cell monolayers decreased from 1261 to 268 Ωcm^2 when piperine (5 µM) was applied on the apical side (Piperine A-to-B), suggesting a polarized opening of the paracellular space.

TABLES

Table 1 Optimized MS/MS parameters (MRM transitions, fragmentor voltage, and collision energy) in ESI positive mode for analytes and corresponding I.S.

Analyte I.S.	MRM transitions	Fragmentor voltage (V)	Collision energy (V)
Piperine (Quantifier)	286.15 → 115.00	117	54
Piperine (Qualifier)	286.15 → 143.00	117	34
I.S. SCT-64	302.18 → 115.00	117	58
SCT-66 (Quantifier)	330.21 → 201.10	127	22
SCT-66 (Qualifier)	330.21 → 115.10	127	62
I.S. SCT-64	302.18 → 115.00	117	58
SCT-64 (Quantifier)	302.18 → 115.00	117	58
SCT-64 (Qualifier)	302.18 → 143.00	117	34
I.S. SCT-66	330.21 → 201.10	127	22
SCT-29 (Quantifier)	330.21 → 201.00	177	22
SCT-29 (Qualifier)	330.21 → 115.00	177	62
I.S. SCT-64	302.18 → 115.00	117	58
LAU397 (Quantifier)	316.23 → 187.00	205	18
LAU397 (Qualifier)	316.23 → 144.00	205	38
I.S. LAU399	292.18 → 163.00	205	18
LAU399 (Quantifier)	292.18 → 163.00	205	18
LAU399 (Qualifier)	292.18 → 91.10	205	54
I.S. SCT-64	302.18 → 115.00	117	58

Table 2 Between-run imprecision (CV %) and inaccuracy (RE %) of QCs in modified RHB, based on 3 series of 2 replicates for each level (n = 18).

Compound		Nominal concentration (ng/mL)				
		5.00	**15.0**	**250**	**400**	**500**
Piperine	Mean	5.03	14.3	257	384	507
	S.D.	0.214	2.12	12.2	28.5	16.7
	CV %	4.25	14.9	4.76	7.43	3.29
	RE %	0.549	-4.97	2.81	-4.08	1.44
SCT-66	Mean	4.85	15.9	261	389	500
	S.D.	0.120	1.00	17.8	7.20	20.2
	CV %	2.47	6.27	6.80	1.85	4.04
	RE %	-2.94	5.76	4.52	-2.65	-0.0419
SCT-64	Mean	4.88	14.5	241	374	493
	S.D.	0.424	1.62	24.9	11.1	22.0
	CV %	8.69	11.2	10.3	2.98	4.46
	RE %	-2.47	-3.65	-3.59	-6.51	-1.48
SCT-29	Mean	5.20	16.5	244	397	494
	S.D.	0.296	1.37	22.0	36.3	12.6
	CV %	5.70	8.30	9.04	9.13	2.55
	RE %	4.06	9.98	-2.59	-0.735	-1.11
LAU397	Mean	5.05	15.2	256	398	501
	S.D.	0.446	0.918	11.0	7.98	26.3
	CV %	8.84	6.05	4.31	2.01	5.25
	RE %	0.961	1.25	2.54	-0.605	0.138
LAU399	Mean	4.83	16.0	264	403	499
	S.D.	0.0960	1.39	12.3	41.5	21.3
	CV %	1.99	8.68	4.65	10.3	4.27
	RE %	-3.50	6.81	5.63	0.851	-0.227

Table 3 Between-run imprecision (CV %) and inaccuracy (RE %) of QCs in modified DMEM, based on 3 series of 2 replicates for each level (n = 18).

Compound		**Nominal concentration (ng/mL)**				
		5.00	**15.0**	**250**	**400**	**500**
Piperine	Mean	4.81	15.9	247	393	503
	S.D.	0.250	1.09	22.1	8.64	7.42
	CV %	5.20	6.83	8.93	2.20	1.48
	RE %	-3.90	6.17	-1.17	-1.73	0.600
SCT-66	Mean	4.94	16.4	253	384	506
	S.D.	0.180	1.23	20.3	17.0	10.7
	CV %	3.65	7.54	8.05	4.42	2.12
	RE %	-1.21	9.13	1.03	-3.95	1.12
SCT-64	Mean	4.92	13.8	230	375	502
	S.D.	0.250	0.658	9.41	6.79	11.3
	CV %	5.08	4.75	4.10	1.81	2.24
	RE %	-1.53	-7.72	-8.15	-6.14	0.354
SCT-29	Mean	4.88	16.4	269	394	501
	S.D.	0.256	0.566	12.1	22.5	15.1
	CV %	5.24	3.46	4.50	5.71	3.02
	RE %	-2.34	9.11	7.77	-1.40	0.108
LAU397	Mean	4.72	16.5	242	379	507
	S.D.	0.144	1.22	14.8	9.78	5.93
	CV %	3.06	7.41	6.11	2.58	1.17
	RE %	-5.64	9.77	-3.35	-5.37	1.38
LAU399	Mean	5.24	16.5	254	408	506
	S.D.	0.234	0.431	10.1	13.7	7.69
	CV %	4.46	2.61	4.00	3.36	1.52
	RE %	4.89	10.0	1.42	1.97	1.25

Table 4 Mean endothelial permeability coefficients ($P_{e\ (A\rightarrow B)}$) for analytes and Na-F, and mean recoveries for analytes obtained in the immortalized *in vitro* human BBB model based on hBMEC cell line (n = 3–4).

Compound	**Mean P_e ± SD (x 10^{-6} cm/s)**	**Na-F: Mean P_e ± SD (x 10^{-6} cm/s)**	**Mean recovery ± SD for analyte (%)***
Direction	**A→B**	**A→B**	**A→B**
Piperine	53.7 ± 4.47	6.51 ± 0.163	107 ± 5.59
SCT-66	9.32 ± 2.82	7.01 ± 0.0817	86.7 ± 15.3
SCT-64	26.4 ± 1.48	4.50 ± 0.387	70.4 ± 4.55
SCT-29	4.29 ± 1.25	4.99 ± 0.205	88.2 ± 8.73
LAU397	4.49 ± 1.07	5.45 ± 0.0609	88.2 ± 3.41
LAU399	21.6 ± 9.52	4.83 ± 0.188	97.5 ± 13.3

*Recoveries were assessed with the experimental concentrations of the working solutions.

Table 5 Mean endothelial permeability coefficients ($P_{e\ (A\rightarrow B)}$) for analytes and Na-F, and mean recoveries for analytes obtained in the *in vitro* human BLEC BBB model (n = 3).

Compound	**Mean P_e ± SD (x 10^{-6} cm/s)**	**Na-F: Mean P_e ± SD (x 10^{-6} cm/s)**	**Mean recovery ± SD for analyte (%)***
Direction	**A→B**	**A→B**	**A→B**
Piperine	97.8 ± 24.1	9.99 ± 1.41	97.0 ± 8.02
SCT-66	29.4 ± 7.79	12.0 ± 1.47	68.5 ± 9.49
SCT-64	26.7 ± 13.8	10.5 ± 1.32	61.2 ± 5.83
SCT-29	4.61 ± 1.29	12.7 ± 1.38	56.1 ± 10.4
LAU397	12.4 ± 9.91	10.6 ± 1.05	55.7 ± 2.54
LAU399	7.79 ± 2.64	14.8 ± 3.57	60.1 ± 1.55

*Recoveries were assessed with the experimental concentrations of the working solutions.

Table 6 Mean apparent permeability coefficients ($P_{app\ (A\rightarrow B)}$) for analytes and Na-F, and mean recoveries for analytes obtained in the primary bovine endothelial/rat astrocytes co-culture *in vitro* BBB model (n = 3).

Compound	**Mean P_{app} ± SD (x 10^{-6} cm/s)**	**Na-F: Mean P_{app} ± SD (x 10^{-6} cm/s)**	**Mean recovery ± SD for analyte (%)***
Direction	**A→B**	**A→B**	**A→B**
Piperine	81.3 ± 2.04	3.00 ± 1.12	120 ± 5.70
SCT-66	27.9 ± 2.90	3.88 ± 0.573	78.4 ± 6.50
SCT-64	69.4 ± 7.40	3.39 ± 0.530	96.6 ± 3.20
SCT-29	20.9 ± 3.48	5.07 ± 2.81	68.4 ± 2.80
LAU397	38.0 ± 8.44	3.42 ± 3.19	125 ± 9.70
LAU399	44.8 ± 12.3	2.15 ± 1.58	118 ± 3.70

*Recoveries were assessed with the experimental concentrations of the working solutions.

Table 7 *In silico* calculation of BBB permeation for piperine and analogs.

	QikProp descriptors (3D based)									Marvin descriptors		
Compound	**MW**	**donorHB[a]**	**accptHB[b]**	**PSA (Å^2)**	**LogP (o/w)**	**Human Oral Absorption (%)**	**LogBB[c]**	**QPPCaco[d] (nm/s)**	**QPPMDCK[e] (nm/s)**	**PSA (Å^2)**	**LogP**	**Rotatable bonds[f]**
Piperine	285.3	0	4.5	48.1	3.27	100	-0.12	3996	2211	38.8	2.78	3
SCT-66	329.4	0	4.5	43.6	4.59	100	-0.25	5441	3087	38.8	4.42	7
SCT-64	301.4	0	4.5	45.5	3.96	100	-0.29	4893	2753	38.8	3.69	7
SCT-29	329.4	0	4.5	45.3	4.70	100	-0.42	4923	2772	38.8	4.57	9
LAU397	315.5	0	3.75	35.1	5.34	100	-0.51	4869	2739	29.5	4.79	10
LAU399	291.5	0	3	26.9	5.21	100	-0.30	4877	5545	20.3	4.72	9

[a]donorHB: donor hydrogen bonds; [b]accptHB: acceptor hydrogen bonds; [c]LogBB: Predicted brain/blood partition coefficient (for 95% of known drugs, values range between -3.0 and 1.2); [d]QPPCaco: predicted apparent Caco-2 cell permeability in nm/s (< 25 poor, > 500 great); [e]QPPMDCK: predicted apparent Madin-Darby Canine Kidney (MDCK) cell permeability in nm/s (< 25 poor, > 500 great); [f]Counting according to Veber rules.

ELECTRONIC SUPPLEMENTARY MATERIAL

SUPPLEMENTARY FIGURES

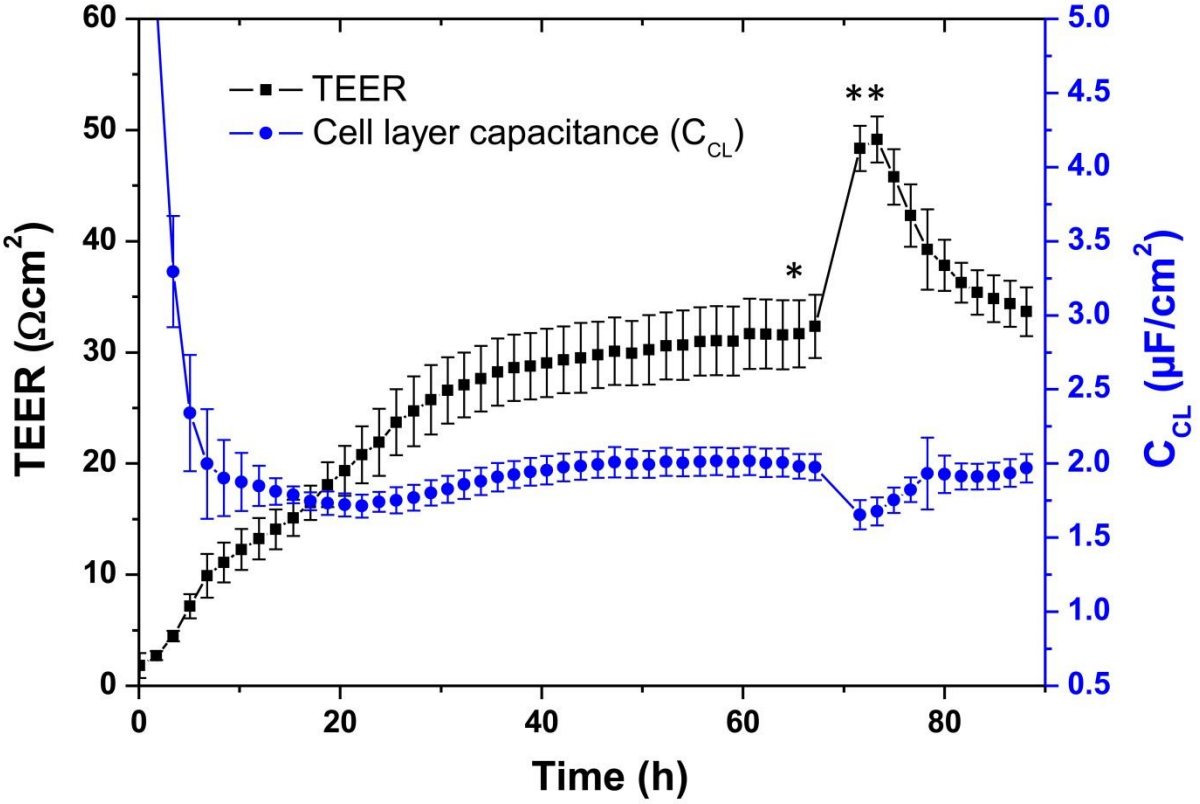

Fig. S1 Mean TEER ± SD values (black curve) and mean cell layer capacitance (C_{CL}) ± SD values (blue curve) recorded in real-time by the CellZscope system of hBMEC cell monolayers grown on 24-well tissue culture inserts (n = 14). C_{CL} values in the range of 0.5–5.0 µF/cm^2 indicate cell confluency and validate TEER values. *Permeability assay with SCT-64. **CellZscope transferred back into incubator (37°C, 5% CO_2) for barrier integrity control.

SUPPLEMENTARY TABLES

Table S1 Calibrators and calibration curve parameters for analytes in modified RHB. Response: A x Conc.^{2} + B x Conc. + C, quadratic regression, weighting factor 1/X, origin: included (n = 4–6).

Compound		Nominal concentration (ng/mL)							Regression parameters			
		5.00	**25.0**	**50.0**	**100**	**200**	**400**	**500**	**A**	**B**	**C**	**R^2**
Piperine	Mean	5.03	24.8	49.9	99.7	204	392	507	-0.0000429	0.141	-0.00451	0.9970
	S.D.	0.214	1.34	1.53	5.75	13.1	31.2	16.7	0.0000318	0.0228	-	-
	CV %	4.25	5.42	3.07	5.76	6.45	7.97	3.29	-	-	-	-
	RE %	0.549	-0.871	-0.140	-0.259	1.81	-2.11	1.44	-	-	-	-
SCT-66	Mean	4.85	25.8	48.7	99.6	199	401	500	0.000000456	0.00854	0.00587	0.9977
	S.D.	0.120	1.44	2.78	5.86	7.69	17.9	20.2	0.000000519	0.00468	-	-
	CV %	2.47	5.59	5.72	5.88	3.87	4.46	4.04	-	-	-	-
	RE %	-2.94	3.18	-2.67	-0.412	-0.457	0.162	-0.0419	-	-	-	-
SCT-64	Mean	4.88	25.6	51.0	97.5	197	413	493	0.000000141	0.00116	-0.000231	0.9945
	S.D.	0.424	1.84	3.60	6.88	10.4	34.7	22.0	0.000000375	0.000348	-	-
	CV %	8.69	7.17	7.05	7.06	5.29	8.40	4.46	-	-	-	-
	RE %	-2.47	2.55	2.07	-2.48	-1.60	3.17	-1.48	-	-	-	-
SCT-29	Mean	5.20	24.6	48.2	99.6	201	407	494	0.00000112	0.0242	-0.00513	0.9987
	S.D.	0.296	1.28	1.94	3.41	4.52	17.1	12.6	0.00000201	0.00461	-	-
	CV %	5.70	5.22	4.02	3.42	2.25	4.21	2.55	-	-	-	-
	RE %	4.06	-1.66	-3.51	-0.446	0.349	1.74	-1.11	-	-	-	-
LAU397	Mean	5.05	25.2	48.7	101	201	399	501	0.000000221	0.0102	0.0000172	0.9953
	S.D.	0.446	2.40	3.40	7.54	17.4	31.6	26.3	0.00000122	0.00246	-	-
	CV %	8.84	9.53	6.99	7.49	8.64	7.93	5.25	-	-	-	-
	RE %	0.961	0.617	-2.70	0.716	0.671	-0.372	0.138	-	-	-	-
LAU399	Mean	4.83	24.8	51.9	102	193	403	499	0.00000313	0.0127	0.000294	0.9972
	S.D.	0.0960	1.40	3.58	8.01	13.9	9.28	21.3	0.00000351	0.00166	-	-
	CV %	1.99	5.64	6.88	7.86	7.18	2.30	4.27	-	-	-	-
	RE %	-3.50	-0.701	3.89	1.96	-3.47	0.774	-0.227	-	-	-	-

765 **Table S2** Calibrators and calibration curve parameters for analytes in modified DMEM. Response: A x Conc.^{2} + B x Conc. + C, quadratic regression, weighting factor 1/X,
766 origin: included (n = 4–6).

Compound		Nominal concentration (ng/mL)							Regression parameters			
		5.00	**25.0**	**50.0**	**100**	**200**	**400**	**500**	**A**	**B**	**C**	**R^2**
Piperine	Mean	4.81	26.1	51.3	102	195	399	503	-0.00000140	0.00329	0.00150	0.9993
	S.D.	0.250	1.78	1.09	3.73	4.80	11.4	7.42	0.000000268	0.000188	-	-
	CV %	5.20	6.81	2.13	3.68	2.46	2.87	1.48	-	-	-	-
	RE %	-3.90	4.55	2.61	1.61	-2.37	-0.247	0.600	-	-	-	-
SCT-66	Mean	4.94	24.8	50.0	105	198	394	506	-0.00000231	0.0132	-0.0000265	0.9982
	S.D.	0.180	0.845	3.20	9.55	9.78	9.61	10.7	0.00000164	0.00178	-	-
	CV %	3.65	3.41	6.39	9.12	4.93	2.44	2.12	-	-	-	-
	RE %	-1.21	-0.966	-0.0246	4.81	-0.794	-1.58	1.12	-	-	-	-
SCT-64	Mean	4.92	25.3	50.0	100	200	398	502	0.000000117	0.000971	0.000155	0.9993
	S.D.	0.250	1.03	1.60	4.57	5.32	6.62	11.3	0.0000000466	0.000153	-	-
	CV %	5.08	4.08	3.20	4.54	2.66	1.66	2.24	-	-	-	-
	RE %	-1.53	1.10	-0.0164	0.481	-0.0658	-0.585	0.354	-	-	-	-
SCT-29	Mean	4.88	25.9	50.4	100	199	400	501	0.00000855	0.0815	0.0253	0.9990
	S.D.	0.256	0.701	1.22	3.05	3.48	14.5	15.1	0.00000607	0.0147	-	-
	CV %	5.24	2.71	2.42	3.07	1.75	3.63	3.02	-	-	-	-
	RE %	-2.34	3.41	0.778	-0.418	-0.323	-0.0902	0.108	-	-	-	-
LAU397	Mean	4.72	25.8	50.8	101	199	392	507	-0.000000531	0.00389	0.000852	0.9996
	S.D.	0.144	0.990	0.865	1.91	3.28	1.73	5.93	0.000000351	0.000345	-	-
	CV %	3.06	3.84	1.70	1.88	1.65	0.440	1.17	-	-	-	-
	RE %	-5.64	3.26	1.55	1.16	-0.608	-2.04	1.38	-	-	-	-
LAU399	Mean	5.24	24.6	48.4	103	204	390	506	0.000000955	0.00264	-0.00201	0.9988
	S.D.	0.234	3.01	2.22	3.08	4.58	8.13	7.69	0.000000116	0.000274	-	-
	CV %	4.46	12.3	4.59	2.98	2.25	2.09	1.52	-	-	-	-
	RE %	4.89	-1.70	-3.18	3.10	1.82	-2.58	1.25	-	-	-	-

767
768
769
770
771

772 **Table S3** Carry-over assessment for analytes and corresponding I.S. (n = 4–6).

Compound	Mean carry-over (%) in modified RHB	Mean carry-over (%) in modified DMEM
Piperine I.S. SCT-64	0.928 0.00	4.27 0.0501
SCT-66 I.S. SCT-64	0.266 0.00	1.61 0.0444
SCT-64 I.S. SCT-66	0.00 0.0130	0.355 0.0139
SCT-29 I.S. SCT-64	2.03 0.00	3.35 0.0140
LAU397 I.S. LAU399	0.747 0.00	3.74 0.0597
LAU399 I.S. SCT-64	0.00 0.00	3.70 0.0152

773
774
775
776
777
778
779
780
781
782
783
784
785
786
787
788
789
790
791
792
793
794
795
796
797
798
799
800
801

Table S4 Mean apparent permeability coefficients ($P_{app\ (A\rightarrow B)}$ and $P_{app\ (B\rightarrow A)}$) for analytes and Na-F, and efflux ratios (ER) for analytes obtained in the immortalized *in vitro* human BBB model based on hBMEC cell line (n = 3–4).

Compound	**Mean P_{app} ± SD (x 10^{-6} cm/s)**		**Na-F: Mean P_{app} ± SD (x 10^{-6} cm/s)**		**ER**
Direction	**A→B**	**B→A**	**A→B**	**B→A**	**-**
Piperine	26.1 ± 0.986	34.2 ± 2.20	5.74 ± 0.0406	6.53 ± 0.703	1.31
SCT-66	7.25 ± 1.70	13.9 ± 2.59	6.28 ± 0.0369	6.28 ± 0.197	1.92
SCT-64	15.6 ± 0.480	11.7 ± 1.59	4.20 ± 0.372	4.84 ± 0.0928	0.750
SCT-29	3.38 ± 0.856	7.30 ± 0.675	4.51 ± 0.217	4.51 ± 0.0859	2.16
LAU397	3.55 ± 0.769	4.14 ± 1.43	4.91 ± 0.0298	4.59 ± 0.0287	1.16
LAU399	14.0 ± 4.90	16.8 ± 2.16	4.42 ± 0.135	5.07 ± 0.312	1.20

Na-F: sodium fluorescein; A: apical; B: basolateral

Table S5 Mean apparent permeability coefficients ($P_{app\ (A\rightarrow B)}$ and $P_{app\ (B\rightarrow A)}$) for analytes and Na-F, and efflux ratios (ER) for analytes obtained in the *in vitro* human BLEC BBB model (n = 3).

Compound	**Mean P_{app} ± SD (x 10^{-6} cm/s)**		**Na-F: Mean P_{app} ± SD (x 10^{-6} cm/s)**		**ER**
Direction	**A→B**	**B→A**	**A→B**	**B→A**	**-**
Piperine	25.1 ± 0.931	19.5 ± 3.08	8.53 ± 0.615	9.01 ± 0.483	0.777
SCT-66	11.7 ± 0.806	5.59 ± 0.331	9.44 ± 0.644	8.53 ± 0.132	0.478
SCT-64	11.2 ± 1.87	9.03 ± 0.590	8.02 ± 0.465	7.79 ± 0.254	0.804
SCT-29	3.31 ± 0.891	1.37 ± 0.153	9.86 ± 0.478	8.36 ± 0.438	0.414
LAU397	3.44 ± 1.03	1.40 ± 0.174	8.33 ± 0.356	8.29 ± 0.177	0.406
LAU399	5.69 ± 0.822	2.81 ± 0.202	9.87 ± 1.02	7.87 ± 0.614	0.493

Na-F: sodium fluorescein; A: apical; B: basolateral

Table S6 Mean apparent permeability coefficients ($P_{app\ (A\rightarrow B)}$ and $P_{app\ (B\rightarrow A)}$) for analytes and Na-F, and efflux ratios (ER) for analytes obtained in the primary bovine endothelial/rat astrocytes co-culture *in vitro* BBB model (n = 3).

Compound	**Mean P_{app} ± SD (x 10^{-6} cm/s)**		**Na-F: Mean P_{app} ± SD (x 10^{-6} cm/s)**		**ER**
Direction	**A→B**	**B→A**	**A→B**	**B→A**	**-**
Piperine	81.3 ± 2.04	32.2 ± 1.64	3.00 ± 1.12	0.731 ± 0.00699	0.396
SCT-66	27.9 ± 2.90	13.7 ± 0.830	3.88 ± 0.573	0.501 ± 0.0235	0.490
SCT-64	69.4 ± 7.40	27.9 ± 1.53	3.39 ± 0.530	0.779 ± 0.0207	0.402
SCT-29	20.9 ± 3.48	12.2 ± 1.54	5.07 ± 2.81	0.864 ± 0.0399	0.584
LAU397	38.0 ± 8.44	17.3 ± 1.00	3.42 ± 3.19	0.610 ± 0.0517	0.460
LAU399	44.8 ± 12.3	15.2 ± 0.440	2.15 ± 1.58	0.738 ± 0.239	0.340

Na-F: sodium fluorescein; A: apical; B: basolateral

3.4 Development and validation of a LC-MS/MS method for assessment of an anti-inflammatory indolinone derivative by *in vitro* blood-brain barrier models

Evelyn A. Jähne, **Daniela E. Eigenmann**, Maxime Culot, Roméo Cecchelli, Fruzsina R. Walter, Mária A. Deli, Robin Tremmel, Gert Fricker, Martin Smieško, Matthias Hamburger, Mouhssin Oufir

Journal of Pharmaceutical and Biomedical Analysis 98 (2014) 235–246
DOI: 10.1016/j.jpba.2014.05.026

The anti-inflammatory and anti-allergic compound (*E,Z*)-3-(4-hydroxy-3,5-dimethoxybenzylidene)-indolin-2-one (indolinone) (Figure 1) from woad (*Isatis tinctoria* L., Brassicaceae) was screened in our previously established immortalized human *in vitro* BBB model and in two well-established animal *in vitro* BBB models. For this purpose, a quantitative LC-MS/MS method for the compound in modified Ringer HEPES buffer was developed and validated according to FDA and EMA guidelines. *In vitro* data from the three models showed good correlation and indicated a high BBB permeation potential of indolinone, corroborated by *in silico* prediction data. P-glycoprotein interaction of the compound was assessed with the aid of a calcein-AM uptake assay and bidirectional permeability experiments. Both assays suggested that no active mediated transport mechanism was involved for the compound.

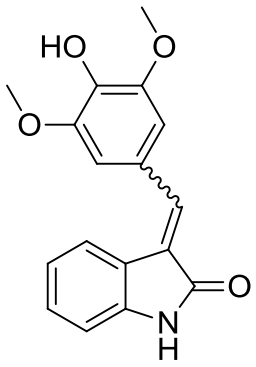

Figure 1 (*E,Z*)-3-(4-hydroxy-3,5-dimethoxybenzylidene)indolin-2-one (indolinone)

My contributions to this publication: cultivation of cells, preparation of the immortalized human in vitro BBB model, permeability experiments with indolinone, and contribution to writing of the manuscript.

Daniela Elisabeth Eigenmann

Journal of Pharmaceutical and Biomedical Analysis 98 (2014) 235–246

Contents lists available at ScienceDirect

Journal of Pharmaceutical and Biomedical Analysis

journal homepage: www.elsevier.com/locate/jpba

Development and validation of a LC–MS/MS method for assessment of an anti-inflammatory indolinone derivative by *in vitro* blood–brain barrier models

Evelyn A. Jähne[a], Daniela E. Eigenmann[a], Maxime Culot[b], Roméo Cecchelli[b], Fruzsina R. Walter[c], Mária A. Deli[c], Robin Tremmel[d], Gert Fricker[d], Martin Smiesko[e], Matthias Hamburger[a], Mouhssin Oufir[a,*]

[a] *Institute of Pharmaceutical Biology, Department of Pharmaceutical Sciences, University of Basel, Klingelbergstrasse 50, CH-4056 Basel, Switzerland*
[b] *Université Lille Nord de France, UArtois, BBB Laboratory EA 2465, IMPRT: IFR114, 62307 Lens Cedex, France*
[c] *Institute of Biophysics, Biological Research Centre, Hungarian Academy of Sciences, Temesvari krt. 62, H-6726 Szeged, Hungary*
[d] *Institute of Pharmacy and Molecular Biotechnology, Im Neuenheimer Feld 329, D-69120 Heidelberg, Germany*
[e] *Molecular Modeling, Department of Pharmaceutical Sciences, University of Basel, Klingelbergstrasse 50, CH-4056 Basel, Switzerland*

ARTICLE INFO

Article history:
Received 29 March 2014
Received in revised form 15 May 2014
Accepted 16 May 2014
Available online 27 May 2014

Keywords:
Isatis tinctoria
(*E,Z*)-3-(4-Hydroxy-3,5-dimethoxybenzylidene)indolin-2-one
Anti-inflammatory
LC–MS/MS
Blood–brain barrier (BBB)

ABSTRACT

The compound (*E,Z*)-3-(4-hydroxy-3,5-dimethoxybenzylidene)indolin-2-one (indolinone) was identified from lipophilic woad extracts (*Isatis tinctoria* L., Brassicaceae) as a compound possessing potent histamine release inhibitory and anti-inflammatory properties [1]. To further evaluate the potential of indolinone in terms of crossing the blood–brain barrier (BBB), we screened the compound in several *in vitro* cell-based human and animal BBB models. Therefore, we developed a quantitative LC–MS/MS method for the compound in modified Ringer HEPES buffer (RHB) and validated it according to FDA and EMA guidelines [2,3]. The calibration curve of indolinone in the range between 30.0 and 3000 ng/ml was quadratic, and the limit of quantification was 30.0 ng/ml. Dilution of samples up to 100-fold did not affect precision and accuracy. The carry-over was within acceptance criteria. Indolinone proved to be stable in RHB for 3 h at room temperature (RT), and for three successive freeze/thaw cycles. The processed samples could be stored in the autosampler at 10 °C for at least 28 h. Moreover, indolinone was stable for at least 16 days in RHB when stored below −65 °C. This validation study demonstrates that our method is specific, selective, precise, accurate, and capable to produce reliable results.

In the immortalized human BBB mono-culture model, the apparent permeability coefficient from apical to basolateral ($P_{app\ A\to B}$), and the P_{app} from basolateral to apical ($P_{app\ B\to A}$) were $19.2 \pm 0.485 \times 10^{-6}$ cm/s and $21.7 \pm 0.326 \times 10^{-6}$ cm/s, respectively. For the primary rat/bovine BBB co-culture model a $P_{app\ A\to B}$ of $27.1 \pm 1.67 \times 10^{-6}$ cm/s was determined. In the primary rat BBB triple co-culture model, the $P_{app\ A\to B}$ and the $P_{app\ B\to A}$ were $56.2 \pm 3.63 \times 10^{-6}$ cm/s and $34.6 \pm 1.41 \times 10^{-6}$ cm/s, respectively. The data obtained with the different models showed good correlation and were indicative of a high BBB permeation potential of indolinone confirmed by *in silico* prediction calculations. P-glycoprotein (P-gp) interaction for indolinone was studied with the aid of a calcein-AM uptake assay, and by calculation of the efflux ratio (ER) from the bidirectional permeability assays. For both bidirectional BBB models an ER below 2 was calculated, indicating that no active mediated transport mechanism is involved for indolinone. In porcine

Abbreviations: BBB, blood–brain barrier; BSA, bovine serum albumin; BBEC, primary bovine brain capillary endothelial cells; Cal, calibrator; cLogP, calculated logarithm of partitioning coefficient; Calcein-AM, calcein-acetoxymethylester; C_{CI}, cell layer capacitance; Conc., concentration; CNS, central nervous system; CV%, coefficient of variation; CPT-cAMP, 8-(4-chlorophenylthio)-adenosine-3′,5′-cyclic monophosphate, sodium salt; DMEM, Dulbecco's modified Eagle's medium; DMSO, dimethyl sulfoxide; DNase I, deoxyribonuclease type I; 96-DWP, 96-deep well plate; EMA, European Medicines Agency; ER, efflux ratio; ESI, electrospray ionization; FBS, fetal bovine serum; FDA, Food and Drug Administration; hBMEC, immortalized human brain microvascular endothelial cell line; HEPES, 4-(2-hydroxyethyl)-1-piperazineethanesulfonic acid; HPLC, high-performance liquid chromatography; I.S., internal standard; KRB, Krebs–Ringer buffer; LLOQ, lower limit of quantification; LTS, long-term stability; MRM, multiple reaction monitoring; MW, molecular weight; Na-F, sodium fluorescein; NMR, nuclear magnetic resonance; PBCEC, porcine brain capillary endothelial cells; PBS, phosphate buffered saline; P_{app}, apparent permeability coefficient; P-gp, P-glycoprotein; PSA, polar surface area; QC, quality control; QCH, quality control high; QCL, quality control low; QCM, quality control medium; RBEC, primary rat brain capillary endothelial cell; RE%, relative error; RHB, Ringer HEPES buffer; Rpm, revolutions per minute; RT, room temperature; SD, standard deviation; S.E.M., standard error of the mean; SS, stock solution; TEER, transendothelial electrical resistance; TFA, trifluoroacetic acid; TQD, tandem quadrupole detector; ULOQ, upper limit of quantification; UPLC–MS/MS, ultra performance liquid chromatography with tandem mass spectrometric detection; v/v, volume per volume; WS, working solution.

* Corresponding author. Tel.: +41 61 267 1425; fax: +41 61 267 1474.
E-mail address: mouhssin.oufir@unibas.ch (M. Oufir).

http://dx.doi.org/10.1016/j.jpba.2014.05.026
0731-7085/

brain capillary endothelial cells (PBCECs), the calcein-AM uptake assay demonstrated that indolinone is neither a P-gp substrate nor a P-gp inhibitor and is accumulated into cells at high extent.

1. Introduction

In the course of an investigation of anti-inflammatory and anti-allergic compounds in the ancient anti-inflammatory plant *Isatis tinctoria* [1,4–20] we identified (*E,Z*)-3-(4-hydroxy-3,5-dimethoxybenzylidene)indolin-2-one (indolinone) as the compound responsible for the inhibition of histamine release from activated mast cells [1]. The compound was a potent inhibitor of antigen-induced histamine release by stabilizing mast cells [1] by a molecular mode of action that is not yet fully understood but different from known compounds. The compound was shown not to act *via* targets upstream of the histamine containing granules and, hence, is thought to interact with the membrane of histamine-containing granules [1]. Given the new mechanism of action, low cytotoxicity, anti-allergic potency, and drug-like physicochemical properties [21], indolinone is a promising lead for the development of new anti-allergic drugs. For further assessment of the potential of indolinone we recently developed and validated an UPLC–MS/MS method for quantification of indolinone in lithium heparinized rat plasma for a preliminary pharmacokinetic study in Sprague-Dawley male rats [22]. To further evaluate the potential of indolinone in terms of blood–brain barrier (BBB) permeability, we screened the compound in several *in vitro* cell-based human and animal BBB models.

Blood–brain barrier (BBB) penetration is necessary for drugs acting on the central nervous system (CNS). High passive membrane permeability and low P-glycoprotein (P-gp) interaction favor CNS exposure [23]. On the other hand, low BBB penetration is desirable for drugs aimed at peripheral targets to minimize CNS-related side effects. Hence, regardless of the therapeutic area, assessment of BBB penetration is required at an early phase of the drug discovery process [24]. For this purpose, we developed a quantitative LC–MS/MS assay for indolinone in Ringer HEPES buffer (RHB) and validated it according to international guidelines [2,3]. Indolinone was screened in several cell-based *in vitro* human and animal BBB models [25–27], and the permeability of indolinone was assessed by LC–MS/MS. P-gp interaction was studied with the aid of a calcein-AM uptake assay in porcine brain capillary endothelial cells (PBCECs), and by calculation of the efflux ratio (ER) from the bidirectional permeability assays [25,27]. To further explore the transporter mechanism of indolinone, an uptake assay was performed in PBCECs.

2. Materials and methods

2.1. In silico prediction of blood–brain barrier permeability

Three-dimensional computer models of both (*E*)- and (*Z*)-3-(4-hydroxy-3,5-dimethoxybenzylidene)indolin-2-one (indolinone) were built in Maestro modeling environment (Maestro, version 9.3, Schrödinger, LLC, New York, NY, 2012), and the most favorable conformers were identified by the conformational search in MacroModel (MacroModel, version 9.9, Schrödinger, LLC, New York, NY, 2012) using the OPLS-2005 force-field, implicit solvent conditions (water), and 1000 iterations of the mixed serial/low mode sampling method. For each isomer, the conformers within 5 kcal/mol from the corresponding global minimum were used as input for the QikProp application (QikProp, version 3.5, Schrödinger, LLC, New York, NY, 2012), to evaluate various descriptors relevant for drug permeability. For comparison, the polar surface area (PSA) and the logarithm of partition coefficient (cLogP) descriptors were calculated also using the Calculator plugin of Chemaxon Marvin web-application (http://www.chemaxon.com/marvin/sketch/index.php, accessed on February 12, 2014) requiring only the 2D structural formula as input.

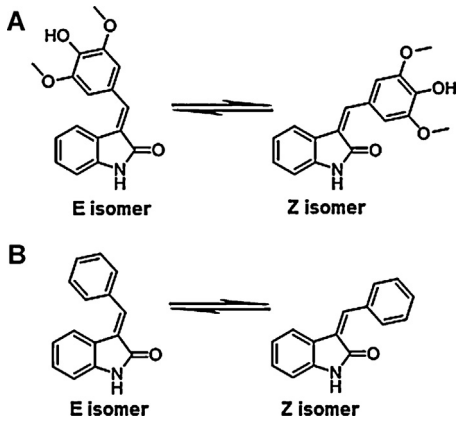

Fig. 1. Chemical structures of (*E,Z*)-3-(4-hydroxy-3,5-dimethoxybenzylidene)-indolin-2-one (indolinone) (A) and internal standard, (*E,Z*)-3-(benzylidenyl)-indolin-2-one (B) [22].

2.2. LC–MS/MS analysis

2.2.1. Chemicals and reagents

(*E,Z*)-3-(4-Hydroxy-3,5-dimethoxybenzylidene)indolin-2-one (indolinone) (Fig. 1A) and the internal standard (I.S.) (*E,Z*)-3-(benzylidenyl)-indolin-2-one (Fig. 1B) were synthesized according to a general protocol for indolinones [28]. Both compounds showed a purity of ≥99% as determined by HPLC–UV–ESI-MS and ^{1}H and ^{13}C NMR [29]. The ratio of *E* to *Z* isomers for indolinone and I.S. was assessed by ^{1}H NMR and HPLC as 71:29 and 75:25, respectively [22]. Preparative separation of isomers failed because of slow spontaneous isomerization at RT [9,28]. All used solvents were of HPLC grade. Acetonitrile and dimethyl sulfoxide (DMSO) were supplied by Scharlau (Barcelona, Spain). Methanol was from LabScan (Gliwice, Poland). Formic acid and trifluoroacetic acid (TFA) were purchased from BioSolve (Valkenswaard, Netherlands), and albumin from bovine serum (BSA) was supplied by Sigma–Aldrich (Steinheim, Germany). HPLC grade water was obtained by an EASYpure II (Barnstead, Dubuque, IA, USA) water purification system. Ringer HEPES buffer (RHB) (150 mM NaCl, 2.2 mM $CaCl_2$, 0.2 mM $MgCl_2$, 5.2 mM KCl, 2.8 mM glucose, 5 mM HEPES, 6 mM $NaHCO_3$, 0.2% BSA) was prepared in-house, adjusted to pH 7.4, and stored at 4 °C.

2.2.2. LC–MS/MS instrument and chromatographic conditions

Method validation was performed on an Acquity UPLC system consisting of a binary pump, an autosampler set at 10 °C, and a column heater set at 45 °C, which was coupled to an Acquity TQD (all Waters Corp., Milford, MA, USA). Separation of analyte (indolinone) and I.S. ((*E,Z*)-3-(benzylidenyl)-indolin-2-one) was achieved with a UPLC HSS T3 column (100 mm × 2.1 mm; 1.8 μm

particle size) (Waters Corp., Milford, MA, USA). The mobile phase consisted of water containing 0.1% formic acid (Eluent A) and acetonitrile containing 0.1% formic acid (Eluent B). Chromatographic separation was performed at a flow rate of 0.5 ml/min with the following gradient: 0–0.5 min, B 2%; 0.5–2 min, B 2–100%; 2–2.5 min, B 100%; 2.5–2.6 min, B 100–2%; 2.6–4 min, B 2%. The total run time was 4 min. As injection solvent a mixture of 35% water containing 0.1% formic acid and 65% methanol containing 0.1% formic acid was used (35:65, v/v). Weak and strong wash solvents were water–acetonitrile (50:50, v/v) containing 0.2% TFA, and acetonitrile–isopropanol–acetone (40:40:30, v/v/v) containing 0.2% TFA, respectively. The seal wash solvent consisted of a water–acetonitrile mixture (90:10, v/v).

MS detection was performed with electrospray ionization in positive ion mode (ESI+). Nitrogen, generated by a nitrogen generator N2-Mistral (Schmidlin AG, Neuheim, Switzerland), was used both as desolvation and nebulization gas. Argon was used as collision gas. MS/MS parameters were generated using Waters IntelliStart software followed by manual optimization.

MRM transitions were 297.7 > 265.0 for indolinone, and 221.8 > 194.0 for I.S. ((*E*,*Z*)-3-(benzylidenyl)-indolin-2-one). The capillary voltage was 3.5 kV. Cone voltage was 46 V, and collision energy was 21 eV for both indolinone and I.S. Source temperature was set at 150 °C, and the desolvation temperature was 400 °C. The flow rates for desolvation gas and cone gas were 900 l/h and 10 l/h, respectively. The dwell time was automatically set at 69 ms. Data were acquired with MassLynx V4.1 software and quantified by means of QuanLynx software (Waters Corp., Milford, MA, USA).

2.2.3. Standards and stock solutions

Stock solutions (SS) of analyte and I.S. were prepared by weighing pure compounds on an analytical balance (Mettler-Toledo, Switzerland) and dissolving them in DMSO. The working solutions (WS1) of analyte and I.S. were freshly prepared in methanol by further diluting the corresponding SS to obtain a concentration of 100 μg/ml for indolinone, and 10 μg/ml for the I.S. For the I.S., a daily second working solution (WS2) at a concentration of 1000 ng/ml was freshly prepared by diluting WS1 (10 μg/ml) with methanol. All SS and WS (except WS2, which was discarded after use) were stored below −65 °C until analysis.

2.2.4. Preparation of calibration and quality control samples

Seven calibration samples (calibrators) in the range of 30.0–3000 ng/ml and quality controls (QCs) at low, middle and high levels (QCL = 90.0 ng/ml, QCM = 1500 ng/ml, QCH = 2400 ng/ml) were prepared in RHB by serial dilution of the WS of indolinone (100 μg/ml). After dilution, all samples were vortexed, aliquoted into polypropylene tubes, and stored below −65 °C until analysis.

2.2.5. Sample extraction in Ringer HEPES buffer

To 200 μl of RHB containing indolinone, 100 μl of I.S. at 1000 ng/ml, 200 μl of BSA solution (60 g/l), and 1000 μl of ice cold acetonitrile were added. The mixture was briefly vortexed, mixed for 10 min at room temperature (RT) in an Eppendorf Thermomixer (1400 rpm), and centrifuged for 20 min at 13 200 rpm at 10 °C (Centrifuge 5415R, Eppendorf, Schoenenbuch, Switzerland). The supernatant (1300 μl) was transferred into a 96-deep well plate (DWP), dried under nitrogen gas flow (Evaporex EVX-96, Apricot Designs, Monovia, CA, USA), and reconstituted with 200 μl of injection solvent (35% solvent A + 65% solvent B, A: water + 0.1% formic acid, B: methanol + 0.1% formic acid). Afterwards, the 96-DWP was shaken for 45 min at RT in an Eppendorf Mixmate and centrifuged for 2 min at 3000 rpm (Megafuge, Heraeus Instruments AG, Switzerland). Due to nonspecific adsorption of I.S. onto the 96-DWP, each sample was transferred into a 300 μl glass insert of a HPLC vial before injection into the UPLC–MS/MS system in full loop mode (5 μl).

2.3. Method validation

The method was validated according to the guidelines of the US Food and Drug Administration (FDA) [2] and the European Medicines Agency (EMA) [3].

2.3.1. Chromatographic performance

The calibration curve was generated by seven calibrators ranging from 30.0 to 3000 ng/ml. To meet requirements of the FDA guidance, the coefficient of determination (R^2) has to be higher than 0.96 and at least 75% of all calibrators should be valid. Furthermore, for both levels: LLOQ and ULOQ, only one value could be omitted.

2.3.2. Regression parameters

Two sets of seven calibrators (ranging from 30.0 to 3000 ng/ml) were injected at the beginning and at the end of each analytical run, starting from the lower limit of quantification (LLOQ = 30.0 ng/ml) to the upper limit of quantification (ULOQ = 3000 ng/ml). The calibration curve was validated by six QCs (duplicates of QCL, QCM and QCH), which were inserted randomly into the analytical run.

2.3.3. Carry-over

To evaluate the carry-over of analyte and I.S. in each analytical run, an extracted RHB blank was injected immediately after the ULOQ (3000 ng/ml) of both sets of calibrators. Mean carry-over ($n = 2$) in the blank sample following the ULOQ should not exceed 20% of the signal of the LLOQ (30.0 ng/ml) for indolinone and 5% for I.S.

2.3.4. Selectivity

Six QC samples of indolinone at the LLOQ (duplicates, three different batches of RHB) were extracted and injected within a validation run into the UPLC–MS/MS system. Selectivity imprecision (CV%) had to be below 20% and inaccuracy (RE%) had to be within ±20% of the nominal values. Moreover, only one QC sample of each RHB batch was allowed to have an inaccuracy of more than ±20%.

2.3.5. Specificity

A total of six blank samples (duplicates, three different batches of RHB) without the addition of indolinone and I.S. were injected into the UPLC–MS/MS within an analytical run and quantified by means of a valid calibration curve. For all three batches of RHB, the peak areas evaluated in the blank samples were not allowed to exceed 20% of the mean LLOQ peak area.

2.3.6. Intra-run and inter-run repeatability

Six replicates of QCs at five concentration levels (30.0, 90.0, 1500, 2400, 3000 ng/ml) were processed and injected into the UPLC–MS/MS. To ensure the reproducibility, these sets of QCs were tested within three validation runs on three different days. In each run, intra-run imprecision (CV%) of each QC series had to be below 15% (20% at the LLOQ) and intra-run inaccuracy (RE%) had to be within ±15% of the nominal values (±20% at the LLOQ). At the end of the three series, inter-run imprecision and inaccuracy were assessed by calculating the overall mean and standard deviation (SD) for each QC level. The acceptance criteria for imprecision (CV%) and inaccuracy (RE%) were the same as described above.

2.3.7. Extraction yield

The absolute recovery of the analyte was calculated using six replicates of indolinone at low (90.0 ng/ml), medium (1500 ng/ml), and high concentration (2400 ng/ml) which were spiked with I.S. after extraction compared to six blank RHB samples which were

spiked with indolinone at three concentration levels (90.0, 1500, and 2400 ng/ml) and I.S. after extraction.

The extraction yield of I.S. was calculated by comparison of six processed samples containing I.S. which were spiked with indolinone at medium level (1500 ng/ml) after extraction *versus* six replicates of blank RHB samples which were spiked with I.S. and indolinone (1500 ng/ml) after extraction.

2.3.8. Dilution test

In order to demonstrate that the dilution of samples at higher concentration levels than the ULOQ (3000 ng/ml) did not affect the reliability of the method, a dilution test was performed. For this purpose, the matrix was spiked with the WS of indolinone (100 μg/ml) to obtain a final concentration of 15 000 ng/ml (*i.e.* 5× ULOQ). This solution was further serially diluted to give six replicates at a concentration of 1500 ng/ml (10-fold dilution) and six replicates at a concentration of 150 ng/ml (100-fold dilution). Concentrations of the replicates of each dilution level were calculated using a valid calibration curve. Furthermore, the resulting mean concentration, imprecision, and inaccuracy were calculated. According to guidelines [2,3], the imprecision (CV%) had to be below 15% and the inaccuracy had to be within ±15% of the nominal value.

2.3.9. Short-term stabilities of indolinone in Ringer HEPES buffer

2.3.9.1. Freeze and thaw cycles below −65 °C. Six replicates of QCL (90.0 ng/ml) and QCH (2400 ng/ml) were exposed to three freeze (below −65 °C, storage time > 24 h) and thaw (at RT) cycles before they were processed and quantified using a valid calibration curve. At both concentration levels, the imprecision (CV%) had to be below 15% and the inaccuracy (RE%) had to be within ±15% of the nominal value.

2.3.9.2. Biological sample stability on benchtop at RT. Six replicates of QCL (90.0 ng/ml) and QCH (2400 ng/ml) were stored at RT for 4 h and quantified using a valid calibration curve. At both concentration levels, the imprecision (CV%) had to be below 15% and the inaccuracy (RE%) had to be within ±15% of the nominal value.

2.3.9.3. Processed sample stability in the autosampler at 10 °C. Six replicates of QCL (90.0 ng/ml) and QCH (2400 ng/ml) were processed and quantified using a valid calibration curve. All QCs were stored for 28 h in the autosampler (set at 10 °C, protected from light) before they were re-injected and re-analyzed with freshly prepared calibrators and QCs. At both concentration levels, the imprecision (CV%) had to be below 15% and the inaccuracy (RE%) had to be within ±15% of the nominal value.

2.3.10. Long-term stability below −65 °C

Three replicates of RHB samples freshly prepared at low, medium and high concentration (90.0, 1500, 2400 ng/ml) were quantified at time zero ($t = 0$). Three other replicates at the same concentration levels (90.0, 1500, 2400 ng/ml) were stored below −65 °C. After 16 days of storage, the samples were processed and quantified by means of a valid calibration curve which consisted of two sets of freshly prepared calibrators and QCs. The mean values of each concentration level at 16 days were calculated and compared to the mean values of the appropriate concentration from the first day ($t = 0$) of the long-term stability test. The results of $t = 16$ days were plotted in function of $t = 0$ and a linear regression, forced through zero, was performed. To confirm the stability of the samples, the slope had to be within 1 ± 0.15.

2.3.11. Stock solutions stability test

According to the FDA guideline, the eventual degradation should not exceed the threshold of 5% for both compounds [2].

2.4. Blood–brain barrier permeability screening

2.4.1. Immortalized mono-culture human in vitro BBB model

Indolinone was screened in a human *in vitro* BBB model which we previously established using immortalized human brain microvascular endothelial cells (hBMEC cell line) [25,30]. Culture medium for hBMEC cells was EBM-2 supplemented with hydrocortisone, ascorbic acid, heparin, antibiotic-antimycotic solution, and 20% fetal bovine serum (FBS).

For the *in vitro* BBB model, hBMEC cells were seeded at a density of 6.0×10^4 cells/cm^2 on the apical side of collagen-coated filter membranes of 24-well tissue culture inserts from Greiner Bio-one® (transparent PET membrane, 3.0 μm pore size, 0.6×10^6 pores/cm^2). The tissue culture inserts were transferred into a 24-well cell module of a CellZscope system (NanoAnalytics, Münster, Germany) [31], incubated at 37 °C (5% CO_2), and transendothelial electrical resistance (TEER) values were recorded in real-time every hour. After 50 h, at a TEER value of $40.8 \pm 0.884\ \Omega\,cm^2$ (Fig. 4), the permeability assay for indolinone was carried out as follows. The tissue culture inserts were transferred into a 24-well plate containing 1200 μl of pre-warmed (37 °C) RHB in each well (basolateral compartment). Medium in inserts (apical compartment) was subsequently replaced with 300 μl of a pre-warmed (37 °C) WS containing indolinone (5 μM) and sodium fluorescein (Na-F) as integrity control marker (10 μg/ml) in RHB. The 24-well plate was incubated at 37 °C on an orbital shaker (ELMI DTS-2, Riga, Latvia) with moderate speed (100 rpm) and aliquots of 250 μl of both apical and basolateral compartments were collected after 1 hour. Quantification of Na-F fluorescence was carried out using a Chameleon microplate reader (Hidex, Turku, Finland). Quantification of indolinone was done by LC–MS/MS. All experiments were performed bidirectionally and in triplicate.

2.4.2. Animal in vitro BBB models

2.4.2.1. Primary co-culture rat/bovine in vitro BBB model. The method of Dehouck et al. [32] was used with minor modifications. Bovine brain capillary endothelial cells (BBECs) isolated from capillary fragments were co-cultured with primary mixed glial cells from newborn Sprague-Dawley rats. The glial cells were isolated according to the method of Booher and Sensenbrenner [33] and cultured for 3 weeks, plated on the bottom of cell culture clusters containing six wells each. The BBECs were seeded onto collagen-coated 6-well tissue culture inserts which were placed in the wells containing glial cells. The medium used for the co-culture was Dulbecco's modified Eagle's medium (DMEM, Life technologies, Saint Aubin, France) supplemented with 10% (v/v) newborn calf serum (Integro b.v., Zaandam, Netherlands), 10% (v/v) horse serum (Life technologies), 2 mM glutamine (Sigma Aldrich), 50 μg/ml gentamycin, and 1 ng/ml of basic fibroblast growth factor (bFGF, Sigma Aldrich). The medium was changed every second day. Under these conditions, BBECs formed a confluent monolayer after 5 days. The permeability assay for indolinone was carried out 7 days after confluency by transferring BBEC monolayers to six-well plates containing 2.5 ml of RHB per well. The solution containing 5 μM indolinone and 1 μM Na-F, used as integrity control marker, in RHB was added to the cell monolayer (1.5 ml for 6-well plate filters), and the plates were placed on an orbital shaker. After 1 hour, aliquots were taken from both compartments. Quantification of Na-F fluorescence was carried out using a Synergy H1 multiplates reader (BioTek Instruments, Vinooski, USA). Quantification of indolinone was done by LC–MS/MS. All experiments were performed in triplicate. The mean TEER value after 7 days in co-culture with rat primary glial cells was in the range of 350–400 $\Omega\,cm^2$ [34].

2.4.2.2. Primary triple co-culture rat in vitro BBB model. Primary rat brain capillary endothelial cells (RBECs) were isolated from 3-week-old Wistar rats, similarly as described earlier [35,36]. Forebrains were collected in sterile phosphate buffered saline (PBS) on ice, and meninges were removed using heat sterilized filter paper. Gray matter was cut by scalpels into 1 mm^3 pieces which were digested in Dulbecco's modified Eagle's medium (DMEM, Life Technologies, Gibco, USA) with 1 mg/ml collagenase (Worthington, USA) and deoxyribonuclease type I (DNase I, Roche, USA) for 50 min at 37 °C. Microvessels were separated by a gradient centrifugation in 20% BSA–DMEM (1000 × *g*, 20 min) from myelin, and this step was repeated three times. The isolated and pooled fraction was further digested with 1 mg/ml collagenase–dispase (Roche, USA) and DNase I in DMEM for 30 min. From the digested cell suspension, brain endothelial cell clusters were separated on a 33% Percoll gradient (Sigma Aldrich, USA) (1000 × *g*, 10 min), collected and washed twice in cell culture medium before plating on 60 mm Petri dishes (Orange, Belgium) coated with collagen type IV and fibronectin (Sigma Aldrich, USA). RBECs were cultured in DMEM/F12 supplemented with 15% plasma-derived bovine serum (First Link, UK), 1 ng/ml basic fibroblast growth factor (bFGF, Roche, USA), insulin (5 μg/ml), transferrin (5 μg/ml), sodium selenite (5 ng/ml) (insulin-transferrin-sodium selenite media supplement, Sigma Aldrich, USA), 100 μg/ml heparin (Sigma Aldrich, USA) and 50 μg/ml gentamicin (Sigma Aldrich, USA). In the first 4 days, cell culture medium contained puromycin (3 μg/ml, Sigma Aldrich, USA) to selectively eliminate P-gp negative contaminating cell types [37]. When cultures reached 90% confluency (fourth day in dish), the puromycin treated RBECs were passaged to the apical side of the collage type IV and fibronectin coated filter membranes of 24-well tissue culture inserts from Greiner Bio-one® (transparent PET membrane, 3.0 μm pore size) at a cell number of 2.5×10^4 cells/insert and used for the permeability experiments. To induce BBB characteristics, RBECs were co-cultured with rat cerebral glial cells and rat pericytes [27].

Primary cultures of rat mixed glial cells were obtained from 1-day-old Wistar rats [35,36]. Meninges were removed by forceps on a small drop of PBS, then cortical pieces were mechanically dissociated by pressing the tissue through a nylon mesh (40 μm, Millipore, USA) in DMEM containing 10% FBS (Lonza, Switzerland) and 50 μg/ml gentamicin. Dissociated cell clusters were plated on 5 μg/ml poly-l-lysine (Sigma Aldrich, USA) coated 24-well plates from Greiner Bio-One® and cultured for at least 2 weeks before use. In confluent glia cultures 89% of cells were positively stained for the astroglia cell marker glial fibrillary acidic protein (GFAP), while the remaining 11% were positive for CD11b, a microglia marker.

Cultures of rat brain microvessel pericytes were prepared by a 3-week long culture of isolated rat brain capillary fragments which contained a high number of pericytes besides endothelial cells. The same microvessel isolation yielded RBECs, and pericytes if puromycin-treatment was omitted. Cell survival and proliferation were helped by selective culture conditions using uncoated dishes and DMEM (Life Technologies, Gibco, low glucose) supplemented with 10% FBS and antibiotics. Culture medium was changed every 3 days. Rat brain microvessel pericyte cultures were positive for α-smooth muscle actin, NG2 and PDGFRß immunostaining, and negative for von Willebrand factor and GFAP markers [38].

To assemble the BBB model from the three cell-types, Greiner Bio-one® tissue culture inserts were put into 24-well plates containing glia at the bottom of the wells. Pericytes at passage number 3 were seeded on the bottom side of the inserts (basolateral) and RBECs were passaged to the upper side of the coated inserts (apical) with endothelial culture medium in both compartments [27]. After 2 days of co-culturing, 550 nM hydrocortisone (Sigma Aldrich, USA) was added to the culture medium [39]. Before experiments, cells were treated with 8-(4-chlorophenylthio)-adenosine-3′,5′-cyclic monophosphate (CPT-cAMP, 250 μM, Sigma Aldrich, USA) and RO 20-1724 (17.5 μM, Roche) for 24 h to tighten junctions and elevate resistance [37,39].

At a TEER value of 427.8 ± 62.9 Ω cm^2 (day 4 of co-culture), the permeability assay for indolinone was performed. Before the experiment, working solutions consisting of indolinone (5 μM) and Na-F (10 μg/ml) for layer integrity control were prepared in pre-warmed (37 °C) RHB. To protect cell layer integrity, RHB contained 0.1% BSA. Tissue culture inserts with RBECs and pericytes were transferred into a new 24-well plate containing 700 μl of RHB for apical to basolateral (A to B) permeability measurements or 700 μl working solution for basolateral to apical (B to A) transport assays. Medium in inserts (apical compartment) was subsequently replaced with 300 μl working solution for A to B or 300 μl RHB for B to A transport tests. The 24-well plate was incubated at 37 °C on a horizontal shaker (100 rpm, Biosan, Latvia) for 1 h. Aliquots of 250 μl and 650 μl were collected from the apical and basolateral compartments and stored below −65 °C until analysis. Concentration of Na-F was measured by a Fluostar Optima fluorescent multiplate reader (BMG Labtechnologies, Germany).

2.4.3. BBB permeability calculation

The apparent permeability coefficient (P_{app}) for indolinone and Na-F was calculated in centimeters per second (cm/s) according to the equation [40]:

$$P_{app} \ (\text{cm/s}) = \frac{VR}{AC_{D0}} \times \left(\frac{\Delta C_R}{\Delta t}\right)$$

where V_R is the volume in the receiver compartment, A is the surface area of the filter membrane (0.336 cm^2 for 24-well inserts, 4.7 cm^2 for six-well inserts), C_{D0} is the initial concentration in the donor compartment, and $\Delta C_R/\Delta t$ is the change of concentration over time in the receiver compartment.

Recovery for indolinone and Na-F was calculated according to the equation:

$$\text{Recovery} \ (\%) = \frac{C_{Df}V_D + C_{Rf}V_R}{C_{D0}V_D} \times 100$$

where C_{Df} and C_{Rf} are the final concentrations of the compound in the donor and receiver compartments, respectively, C_{D0} is the initial concentration in the donor compartment, and V_D and V_R are the volumes in the donor and receiver compartments, respectively. All results are expressed as means ± S.E.M.

Low permeability and high efflux can be limiting factors for BBB penetration. A common way of quantifying P-gp interaction *in vitro* is by calculating the efflux ratio (ER) across P-gp expressing cell monolayers, which is defined as [41–45]:

$$\text{ER} = \frac{P_{\text{app B}\rightarrow\text{A}}}{P_{\text{app A}\rightarrow\text{B}}}$$

Compounds showing an ER > 2.0 usually indicate P-gp efflux.

To confirm that indolinone and Na-F did not attach to the plastic material and that the diffusion barrier was only provided by the cell monolayer, control experiments were performed using collagen-coated inserts without cells.

2.5. Transporter studies

2.5.1. Calcein-AM uptake in porcine brain capillary endothelial cells (PBCECs)

The calcein-AM uptake assay was performed in primary porcine brain capillary endothelial cells (PBCECs) seeded in 96-well plates (Corning Costar) at a density of 2.5×10^5 cells/cm^2. Culture medium was Earl's Medium 199 (Biochrom, Berlin, Germany) supplemented with L-glutamine, penicillin, streptomycin, gentamycin, and FBS. After achieving confluence, the cells were used for the calcein assay as previously described [46]. Briefly, cells were washed twice with

pre-warmed Krebs–Ringer Buffer (KRB) and then incubated for 15 min with 100 μl of 2 μM calcein-AM in KRB at 37 °C. After this pre-incubation time, 100 μl of indolinone at increasing concentrations in KRB was added to each well to achieve a final concentration of 5, 50, and 500 μM indolinone. Stock solution of indolinone was prepared in DMSO. Dilutions were then made with KRB. The final concentration of DMSO on the cells did not exceed 1%. At this concentration, DMSO did not affect the assay [46]. After an incubation time of 30 min at 37 °C, the cells were washed twice with cold (5 °C) KRB and subsequently incubated with 200 μl 1% Triton-X in KRB for 20 min. Fluorescence was measured in a plate reader (Tecan, Infinite F200 Pro) with an excitation/emission wavelength of 485/520 nm. Intracellular fluorescence was obtained by subtracting background fluorescence of control wells. Calcein uptake was expressed as % of control (KRB).

2.5.2. Cellular uptake assay

The cell uptake assay was also performed with PBCECs. The cells were treated as described above and also seeded in a 96-well plate [47]. Confluent cells were washed twice with KRB, then pre-incubated for 15 min at 37 °C with 200 μl KRB. After removal of KRB, the cells were incubated with 200 μl indolinone in KRB (100 and 1000 μM) at 37 °C for 30 min. The cells were again washed twice with KRB, followed by incubation with 200 μl 1% Triton-X in KRB for 30 min at 37 °C. Indolinone content was determined by LC–MS/MS as described in Section 2.2. The area of each well was 0.32 cm^2. Based on the presumption that the cell monolayer had a height of 3 μm, the total volume of the cells in one well was 0.096 μl. This volume was taken into consideration when the content of indolinone (in 200 μl KRB) was calculated.

3. Results and discussion

3.1. Chromatographic performance and method validation

3.1.1. Chromatographic performance

Based on the slow inter-conversion at RT [9,28] of (*E,Z*)-3-(4-hydroxy-3,5-dimethoxybenzylidene)indolin-2-one (indolinone) (Fig. 1A), both *E* and *Z* isomers peak areas were integrated and quantified in RHB (Fig. 1). Since isotope-labeled indolinone was not available, the structurally related (*E,Z*)-3-(benzylidenyl)-indolin-2-one was selected as I.S. (Fig. 1B) [22]. For quantification of analyte and I.S., an identical peak integration of both *E* and *Z* isomers was performed (Fig. 2). The calibration curve ranging from 30.0 to 3000 ng/ml was fitted by least-square quadratic regression, and a weighting factor of $1/X^2$ was applied. The mean coefficient of determination (R^2) was 0.9919 (Supplementary Table 1), and acceptance criteria were fulfilled [2,3] (Supplementary Table 1).

Supplementary table related to this article can be found, in the online version, at http://dx.doi.org/10.1016/j.jpba.2014.05.026.

3.1.2. Assessment of carry-over

The mean carry-over was 0.00% (acceptance criteria: below 20%) for indolinone (Fig. 2A) and 0.0839% (below 5%) for I.S. (Fig. 2B). Hence, the carry-over did not impact precision and accuracy of the method (Supplementary Table 2).

Supplementary table related to this article can be found, in the online version, at http://dx.doi.org/10.1016/j.jpba.2014.05.026.

3.1.3. Selectivity for indolinone

Selectivity imprecision (CV%) for the six samples at the LLOQ (duplicates, three different RHB batches) was 8.34% (below 20%) and inaccuracy (RE%) was −12.3% (within ±20%), indicating that the quantification method was selective for indolinone (Supplementary Table 3).

Supplementary table related to this article can be found, in the online version, at http://dx.doi.org/10.1016/j.jpba.2014.05.026.

3.1.4. Specificity for indolinone

The peak areas measured in the blank RHB sample were 0.00% (below 20%), demonstrating that the method was specific for indolinone (data not shown).

3.1.5. Intra-run and inter-run repeatability for indolinone

Intra-run imprecision (CV%) was 6.29% (below 20%) for the LLOQ, and 1.88–5.62% (below 15%) of the nominal value for all the other QCs (Supplementary Table 4). The inaccuracy (RE%) was 6.57% (within ±20%) for the LLOQ and −10.1% to 2.33% (within ±15%) of the nominal values for the other QC levels (Supplementary Table 4). Inter-run imprecision (CV%) ranged from 1.49% to 5.87% (below 20% for LLOQ, and below 15% for all other QC levels), and the inaccuracy (RE%) was between −9.50% and −0.0589% (below 20% for LLOQ, and below 15% for all other QC levels) (Supplementary Table 4). According to international guidelines [2,3], the method was thus precise and accurate.

Supplementary table related to this article can be found, in the online version, at http://dx.doi.org/10.1016/j.jpba.2014.05.026.

3.1.6. Extraction yield

The absolute recovery of indolinone was 81.5% for QCL (90.0 ng/ml), 91.3% for QCM (1500 ng/ml), and 91.8% for QCH (2400 ng/ml) (Supplementary Table 5). For the I.S., an absolute recovery of 83.6% was determined (Supplementary Table 5). Consequently, the extraction yield was proven to be consistent, precise, and reproducible according to FDA guidance [2].

Supplementary table related to this article can be found, in the online version, at http://dx.doi.org/10.1016/j.jpba.2014.05.026.

3.1.7. Dilution test

For both QC series, imprecision (CV%) was below 15% (6.36% for dilution factor 100 and 4.48% for dilution factor 10), and inaccuracy (RE%) was within ±15% of the nominal values (−8.62% and 7.27%, respectively) (Supplementary Table 6). Hence, precision and accuracy of the method was not affected by dilution of samples up to 100-fold.

Supplementary table related to this article can be found, in the online version, at http://dx.doi.org/10.1016/j.jpba.2014.05.026.

3.1.8. Processed sample stability at autosampler conditions

At both concentration levels (90.0 ng/ml and 2400 ng/ml), imprecision (CV%) was below 15% (5.13% and 3.14%, respectively, data not shown), and inaccuracy (RE%) was within ±15% of the nominal values (−0.191% and −11.5%, respectively) (Supplementary Table 7). Thus, processed samples of indolinone proved to be stable for at least 28 h at autosampler conditions (10 °C, protected from light).

Supplementary table related to this article can be found, in the online version, at http://dx.doi.org/10.1016/j.jpba.2014.05.026.

3.1.9. Freeze and thaw cycle stability

Imprecision (CV%) for the six replicates at the QCL (90.0 ng/ml) and the QCH (2400 ng/ml) was below 15% (4.69% and 3.52%, respectively, data not shown), and inaccuracy (RE%) was within ±15% (12.6% and 0.564%, respectively) (Supplementary Table 7), demonstrating that indolinone stored below −65 °C in RHB was stable for at least three freeze and thaw cycles.

3.1.10. Biological samples stability on benchtop at RT

Imprecision (CV%) for the six replicates of QCL (90.0 ng/ml) and QCH (2400 ng/ml) exceeded 15%, and inaccuracy was not within

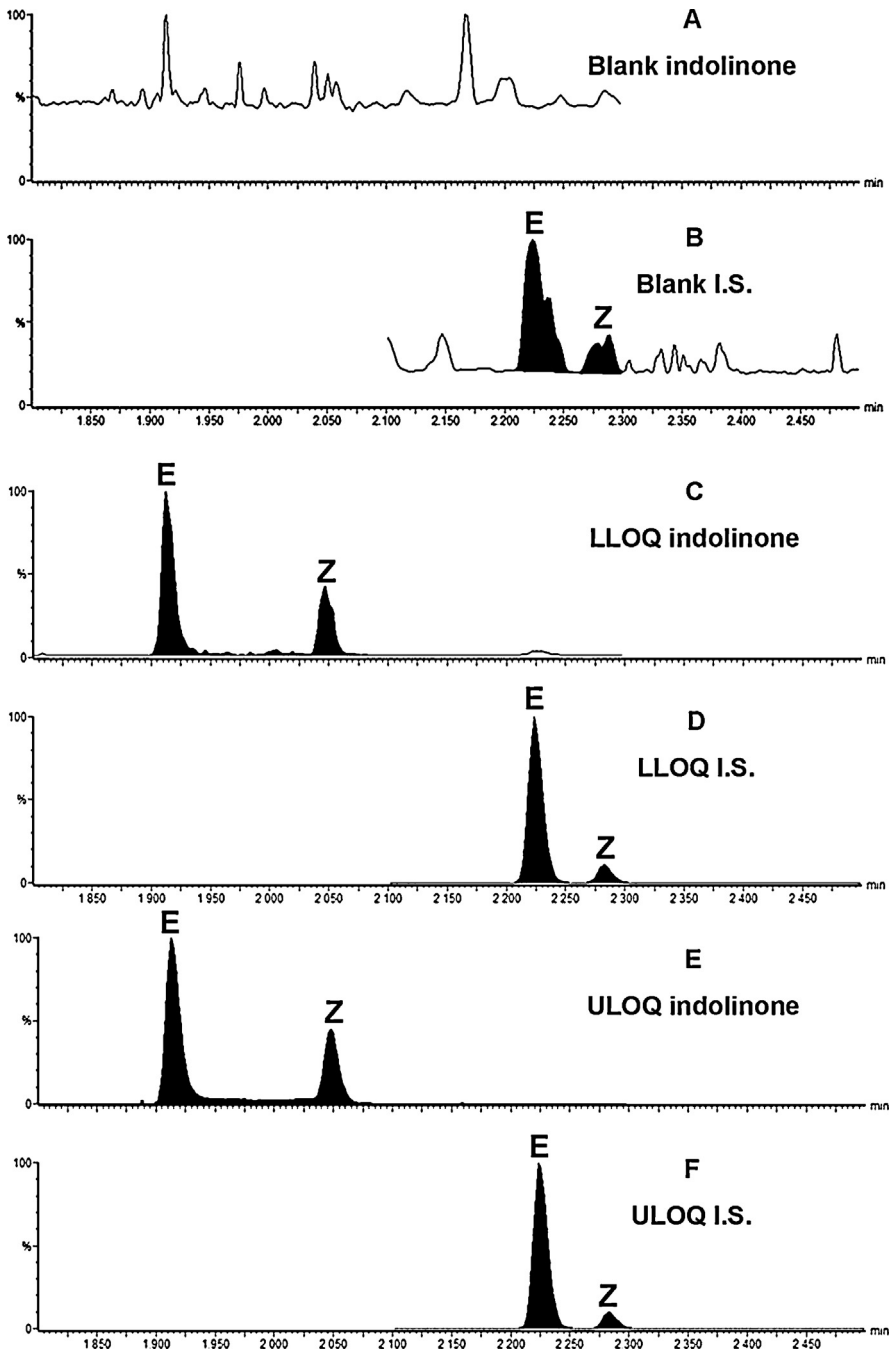

Fig. 2. Typical MRM chromatograms of blank RHB injected after the ULOQ and monitored for indolinone (A) and for I.S. (B), of RHB spiked at 30.0 ng/ml (LLOQ) of indolinone (C), and 1000 ng/ml of I.S. (D), of RHB spiked at 3000 ng/ml (ULOQ) of indolinone (E) and 1000 ng/ml of I.S. (F).

±15% of the nominal values, indicating that indolinone was not stable when stored for 4 h at RT (data not shown). For this reason, the benchtop stability test was reduced to 3 h. Under these new conditions, imprecision (CV%) for the six replicates at low concentration (90.0 ng/ml) was 3.13%, and for the six replicates at high concentration (2400 ng/ml) it was 2.43% (data not shown). Inaccuracy (RE%) was 5.38% and −4.40%, respectively (Supplementary Table 7). Consequently, samples were shown to be stable for 3 h under benchtop conditions (RT) (Supplementary Table 7).

3.1.11. Biological samples long-term stability below −65 °C

As the slope of the calculated linear regression was 0.900 (acceptance criteria: 1 ± 0.15), the stability of the samples stored below −65 °C for 16 days could be confirmed (Fig. 3).

3.1.12. Stock solutions stability test

Our previous study demonstrated that stock solutions of indolinone and I.S. stored below −65 °C for 190 days and kept for *ca.* 6 h at RT were stable, since the degradation expressed by the difference percentage (−1.11% and −1.46% for indolinone and I.S., respectively) was below 5% [22].

3.2. In silico prediction of blood–brain barrier permeability

In silico methods are nowadays routinely used for a rapid assessment of physico-chemical properties of compounds. Descriptor values averaged over the 18 low energy conformers of (*E,Z*)-indolinone show no violation of Lipinski's rule of five [21] (MW < 500, cLogP < 5, donorHB < 5, acceptHB < 10; Table 1) along

Table 1
Mean values of the most relevant *in silico* pharmacokinetic descriptors for (*E,Z*)-indolinone.

QikProp descriptors (3D)								Chemaxon Marvin (2D)	
Compound	MW	donorHB	acceptHB	$cLogP_{o/w}$	cLogBB	Human oral absorption (%)	PSA (Å^2)	$cLogP_{o/w}$	PSA (Å^2)
(*E,Z*)-indolin-2-one	297.30	2.00	4.75	2.44	−0.78	93.2	77.8	2.65	67.8

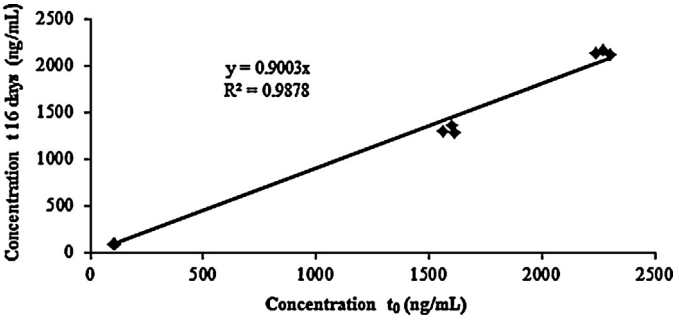

Fig. 3. Long-term stability (LTS) of indolinone in RHB for 16 days below −65 °C.

with a high predicted human oral absorption (93.2%). The values of both 2D- and 3D-based PSA descriptor were not only well below the maximum acceptable threshold of 140 Å^2 for good oral absorption, but also meet the criteria for a passive permeation through the BBB (PSA < 90 Å^2) [48]. Similarly, both predicted $cLogP_{o/w}$ values were within the range that is favorable for blood–brain transport. On the other hand, the specialized QikProp model for brain/blood partitioning predicted a cLogBB of −0.78 (usual range from −3.0 to 1.2) indicating a slight preference for the blood environment [49].

3.3. Blood–brain barrier screening

3.3.1. Human in vitro BBB model

In the *in vitro* BBB model with immortalized human brain capillary endothelial cells (hBMEC cell line) [25], the P_{app} of indolinone for apical to basolateral transport ($P_{app\ A\to B}$) was $19.2 \pm 0.485 \times 10^{-6}$ cm/s (Table 2). Compared to the $P_{app\ A\to B}$ of the negative control Na-F ($3.20 \pm 0.0295 \times 10^{-6}$ cm/s), this value was considerably higher and suggested that indolinone may cross the BBB. The P_{app} value for basolateral to apical transport ($P_{app\ B\to A}$) was $21.7 \pm 0.326 \times 10^{-6}$ cm/s (Table 3). The efflux ratio of 1.13 indicated no active efflux mediated transport for indolinone (ER < 2.0) [41–45].

The recovery of indolinone was ≥88.9% in all experiments, suggesting that the obtained P_{app} values were reliable. A recovery above 80% is needed for an acceptable approximation of the P_{app} value [50]. After each permeability experiment, TEER values were determined, and they were found to be in the same range ($43.1 \pm 0.431\ \Omega\ cm^2$, Fig. 4) as before the assay. This indicated that barrier integrity of the cell monolayers was maintained throughout the experiments, and that indolinone did not affect cell layer integrity.

3.3.2. Animal in vitro BBB models

3.3.2.1. Primary co-culture rat/bovine in vitro BBB model. The P_{app} of Na-F in the presence of indolinone ($2.28 \pm 0.168 \times 10^{-6}$ cm/s) (Table 4) was in the same range as that of Na-F alone (data not shown). This result attested the integrity of the cell monolayer during the transport experiment. The $P_{app\ A\to B}$ ($27.1 \pm 1.67 \times 10^{-6}$ cm/s) was more than 10-fold higher than that of Na-F and hence, suggested high BBB permeability. Given that $P_{app\ A\to B}$ of indolinone across membranes with cells and control membranes (*i.e.* without cells) were very close, that data suggested that indolinone is freely diffusing across BBECs.

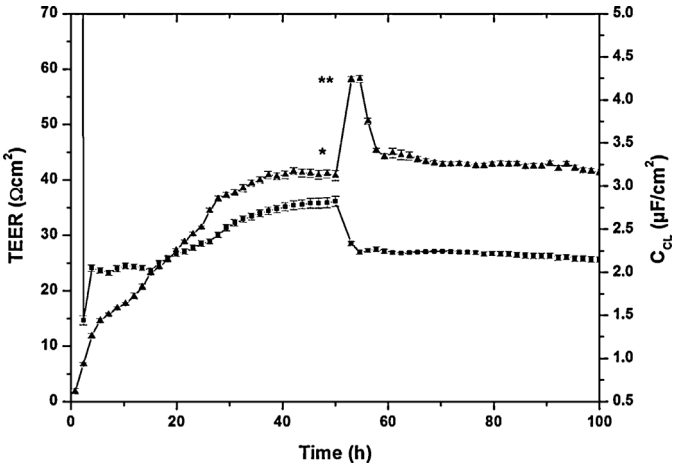

Fig. 4. Mean TEER values (▲) and C_{CI} values (■) recorded real-time by the CellZscope system of hBMEC cells grown on 24-well tissue culture inserts. (*) Insert transfer to 24-well plate for indolinone permeability assay. (**) Insert transfer to CellZscope (37 °C) for barrier integrity control.

3.3.2.2. Primary triple co-culture rat in vitro BBB model. The *in vitro* BBB model composed of primary RBECs, rat pericytes, and rat glial cells formed a tight barrier with a TEER value of $427.8 \pm 62.9\ \Omega\ cm^2$, and a $P_{app\ A\to B}$ $0.884 \pm 0.186 \times 10^{-6}$ cm/s for Na-F (Table 5). The $P_{app\ A\to B}$ of indolinone was $56.2 \pm 3.63 \times 10^{-6}$ cm/s (Table 5). Compared to the $P_{app\ A\to B}$ of the paracellular permeability marker Na-F this value was 60 times higher (Table 5) and hence, suggested that indolinone crossed the BBB very effectively. The P_{app} value of indolinone from basolateral to apical was $34.6 \pm 1.41 \times 10^{-6}$ cm/s (Table 6). The efflux ratio was below 1 and indicated no active mediated efflux mechanism for indolinone (ER < 2.0) in the triple co-culture model. TEER values recorded after the experiments ($189.1 \pm 8.52\ \Omega\ cm^2$) were lower than prior to the assay. This could be explained by cell disturbance due to a switch from cell culture medium to buffer, and to the lack of barrier stabilizing factors from glial cells and culture medium. However, the resistance remained well above the threshold indicative of barrier tightness [39,51]. The Na-F permeability coefficients also indicated a preserved barrier function, and no harmful effect of indolinone on RBECs.

3.4. Transporter studies

3.4.1. Calcein-AM uptake in porcine brain capillary endothelial cells (PBCEC)

In PBCEC, the calcein assay is specific for assessing P-gp transport activity, and the known P-gp inhibitor verapamil (positive control) increased cellular calcein fluorescence by 500% compared to the control (KRB) (Fig. 5). Treatment with indolinone at 5, 50, and 500 µM led to no calcein accumulation, indicating that the compound was neither a P-gp substrate nor a P-gp inhibitor (Fig. 5).

3.4.2. Cellular uptake assay

The validated LC–MS/MS method for quantification of indolinone in RHB was used to quantify the content of indolinone in the lysing medium (mixture of KRB and 1% Triton). No analytical interferences were found showing that the RHB quantitative method can be applied to such an assay (data not shown).

Table 2
Screening of indolinone regarding its ability to cross the *in vitro* human BBB model using immortalized human brain capillary endothelial cells (hBMEC cell line) from the apical (A) to the basolateral (B) compartment ($n = 2–3$).

In vitro human BBB model (hBMEC cell line)	Transport direction	Samples	Time of withdrawal (min)	Mean concentration (ng/ml)	Mean amount (ng)	P_{app} of analyte ± S.E.M. ($\times 10^{-6}$ cm/s)	P_{app} of Na-F ± S.E.M. ($\times 10^{-6}$ cm/s)	Recovery of analyte (%)
Control inserts (without cells)	A to B	Donor compartment (300 μl)	60	1272	381	–	–	–
		Receiver compartment (1200 μl)	60	118	142	71.2	74.0	106[a]
Inserts with cells	A to B	Donor compartment (300 μl)	60	1337	401	–	–	–
		Receiver compartment (1200 μl)	60	31.9	38.3	19.2 ± 0.485	3.20 ± 0.0295	88.9[a]

[a] The recovery was assessed with the experimental concentration of the WS (1647 ng/ml).

Table 3
Screening of indolinone regarding its ability to cross the *in vitro* human BBB model using immortalized human brain capillary endothelial cells (hBMEC cell line) from the basolateral (B) to the apical (A) compartment ($n = 2–3$).

In vitro human BBB model (hBMEC)	Transport direction	Samples	Time of withdrawal (min)	Mean concentration (ng/ml)	Mean amount (ng)	P_{app} of analyte ± S.E.M. ($\times 10^{-6}$ cm/s)	P_{app} of Na-F ± S.E.M. ($\times 10^{-6}$ cm/s)	Recovery of analyte (%)
Control inserts (without cells)	B to A	Donor compartment (1200 μl)	60	1647	1976	–	–	–
		Receiver compartment (300 μl)	60	328	98.5	49.4	50.2	105[a]
Inserts with cells	B to A	Donor compartment (1200 μl)	60	1448	1738	–	–	–
		Receiver compartment (300 μl)	60	144	43.3	21.7 ± 0.326	3.10 ± 0.0231	90.1[a]

[a] The recovery was assessed with the experimental concentration of the WS (1647 ng/ml).

Table 4
Screening of indolinone regarding its ability to cross the *in vitro* animal BBB model using primary bovine capillary endothelial cells and primary rat brain glial cells from the apical (A) to the basolateral (B) compartment ($n = 3$).

In vitro primary triple co-culture BBB rat model	Transport direction	Samples	Time of withdrawal (min)	Mean concentration (ng/ml)	Mean amount (ng)	P_{app} of analyte ± S.E.M. ($\times 10^{-6}$ cm/s)	P_{app} of Na-F ± S.E.M. ($\times 10^{-6}$ cm/s)	Recovery of analyte (%)
Control inserts (without cells)	A to B	Donor compartment (2500 μl)	60	1230	1844	–	–	–
		Receiver compartment (2500 μl)	60	302	755	27.9 ± 1.19	24.2 ± 1.24	105[a]
Inserts with cells	A to B	Donor compartment (300 μl)	60	937	1406	–	–	–
		Receiver compartment (700 μl)	60	303	757	27.1 ± 1.67	2.28 ± 0.168	87.3[a]

[a] The recovery was assessed with the experimental concentration of the WS (1669 ng/mL).

Table 5
Screening of indolinone regarding its ability to cross the *in vitro* animal BBB model using primary rat brain endothelial cells, pericytes and astrocytes from the apical (A) to the basolateral (B) compartment ($n = 3$ for control inserts, $n = 4$ for inserts with cells seeded).

In vitro primary triple co-culture BBB rat model	Transport direction	Samples	Time of withdrawal (min)	Mean concentration (ng/ml)	Mean amount (ng)	P_{app} of analyte ± S.E.M. ($\times 10^{-6}$ cm/s)	P_{app} of Na-F ± S.E.M. ($\times 10^{-6}$ cm/s)	Recovery of analyte (%)
Control inserts (without cells)	A to B	Donor compartment (300 μl)	60	862	259	–	–	–
		Receiver compartment (700 μl)	60	188	132	71.6 ± 0.813	124 ± 2.63	85.4[a]
Inserts with cells	A to B	Donor compartment (300 μl)	60	775	232	–	–	–
		Receiver compartment (700 μl)	60	148	104	56.2 ± 3.63	0.884 ± 0.186	73.6[a]

[a] The recovery was assessed with the experimental concentration of the WS (1523 ng/ml).

Table 6
Screening of indolinone regarding its ability to cross the *in vitro* animal BBB model using primary rat brain endothelial cells, pericytes, and astrocytes from the basolateral (B) to the apical (A) compartment ($n = 3$ for control inserts, $n = 4$ for inserts with cells seeded).

In vitro primary triple co-culture BBB rat model	Transport direction	Samples	Time of withdrawal (min)	Mean concentration (ng/ml)	Mean amount (ng)	P_{app} of analyte ± S.E.M. ($\times 10^{-6}$ cm/s)	P_{app} of Na-F ± S.E.M. ($\times 10^{-6}$ cm/s)	Recovery of analyte (%)
Control inserts (without cells)	B to A	Donor compartment (700 μl)	60	1068	748	–	–	–
		Receiver compartment (300 μl)	60	172	51.5	28.0 ± 2.18	39.2 ± 7.45	7.05[a]
Inserts with cells	B to A	Donor compartment (700 μl)	60	984	689	–	–	–
		Receiver compartment (300 μl)	60	212	63.6	34.6 ± 1.41	0.378 ± 0.115	70.6[a]

[a] The recovery was assessed with the experimental concentration of the WS (1523 ng/mL).

Fig. 5. Calcein-AM uptake assay in primary porcine brain capillary endothelial cells (PBCECs). Indolinone was tested at 5, 50, and 500 μM in KRB. Pure KRB was used as control. Verapamil (50 μM, P-gp inhibitor) was used as positive control.

At 100 μM of indolinone, all measured concentrations were below the LLOQ of the method (30.0 ng/ml), whereas at 1000 μM of indolinone, the concentration inside the cells was 433.3 μM after 30 min, demonstrating that indolinone can easily penetrate PBCEC layers.

4. Conclusions

We developed a LC–MS/MS method for (*E,Z*)-3-(4-hydroxy-3,5-dimethoxybenzylidene)indolin-2-one (indolinone) in RHB and validated the assay according to EMA and FDA guidelines [2,3]. (*E,Z*)-3-(Benzylidenyl)-indolin-2-one, a closely related synthetic compound, was used as I.S. [22]. The standard calibration curve of indolinone in RHB in the range of 30.0–3000 ng/ml was quadratic and a weighting factor of $1/X^2$ was applied. The LLOQ was 30.0 ng/ml. Dilution of samples up to 100-fold did not affect precision and accuracy. The carry-over was within the acceptance criteria. Indolinone was stable for 3 h at RT, and for three successive freeze and thaw cycles. The processed samples could be stored in the autosampler at 10 °C for at least 28 h. Moreover, indolinone was stable for at least 16 days in RHB when stored below −65 °C. These data demonstrated that the method was selective, specific, precise, accurate, and capable of producing reliable results. A comparison of two *in vitro* primary animal BBB models (co-culture bovine/rat BBB model, and triple co-culture rat brain endothelial cells/pericytes/astrocytes BBB model) and an immortalized mono-culture human model (hBMEC cell line) as a possible surrogate BBB model were used for screening indolinone regarding its ability to cross the BBB. The data obtained with the two well-established animal *in vitro* BBB models showed good correlation with our human *in vitro* mono-culture model and were indicative of a high BBB permeation potential of indolinone. These findings were corroborated by *in silico* prediction of BBB penetration. Finally, calcein-AM and uptake assays showed that indolinone accumulated in PBCECs and was neither a P-gp inhibitor nor a P-gp substrate. This was confirmed by calculation of the efflux ratio which was found to be lower than 2. The validated LC–MS/MS assays will be used for further bioavailability studies addressing oral bioavailability and pharmacokinetic properties.

Conflict of interest

None declared.

Acknowledgments

We are grateful to Prof. K.S. Kim and Prof. D. Grab (Johns Hopkins University, Baltimore, MD, USA) for provision of the hBMEC

cell line through the Swiss Tropical and Public Health Institute, Basel, Switzerland (Swiss TPH, Prof. R. Brun). Financial support from the Swiss National Science Foundation (project 105320_126888) is gratefully acknowledged. Thanks are due to Dr. Melanie Raith for the synthesis of indolinone and to Orlando Fertig for excellent technical assistance.

References

[1] S. Kiefer, A.C. Mertz, A. Koryakina, M. Hamburger, P. Küenzi, (E,Z)-3-(3′,5′-dimethoxy-4′-hydroxy-benzylidene)-2-indolinone blocks mast cell degranulation, Eur. J. Pharm. Sci. 40 (2010) 143–147.
[2] Guideline on Bioanalytical Method Validation, European Medicines Agency (EMEA/CHMP/EWP/192217/2009), London, 21 July 2011.
[3] Guidance for Industry: Bioanalytical Method Validation, US Food and Drug Administration (FDA), Center for Drug Evaluation and Research, May 2001.
[4] M. Hamburger, *Isatis tinctoria* – from the rediscovery of an ancient medicinal plant towards a novel anti-inflammatory phytopharmaceutical, Phytochem. Rev. 1 (2002) 333–344.
[5] J.B. Hurry, The Woad Plant and its Dye, AM Kelley, 1973.
[6] Y.P. Zhu, Chinese Materia Medica: Chemistry, Pharmacology, and Applications, Harwood Academic Publishers, Amsterdam, 1998.
[7] M.C. Recio, M. Cerda-Nicolas, O. Potterat, M. Hamburger, L. Rios, Anti-inflammatory and antiallergic activity in vivo of lipophilic *Isatis tinctoria* extracts and tryptanthrin, Planta Med. 72 (2006) 539–546.
[8] M.C. Recio, M. Cerda-Nicolas, M. Hamburger, L. Rios, Anti-arthritic activity of a lipophilic woad (*Isatis tinctoria*) extract, Planta Med. 72 (2006) 715–720.
[9] G.U. Rüster, B. Hoffmann, M. Hamburger, Inhibitory activity of indolin-2-one derivatives on compound 48/80-induced histamine release from mast cells, Pharmazie 59 (2004) 236–237.
[10] M. Hamburger, G.U. Rüster, M.F. Melzig, HPLC based activity profiling for inhibitors of human neutrophil elastase in *Isatis tinctoria* leaf extracts, Nat. Prod. Commun. 1 (2006) 1107–1110.
[11] T. Kunikata, T. Tatefuji, H. Aga, K. Iwaki, M. Ikeda, M. Kurimoto, Indirubin inhibits inflammatory reactions in delayed-type hypersensitivity, Eur. J. Pharmacol. 410 (2000) 93–100.
[12] T. Ishihara, K. Kohno, S. Ushio, K. Iwaki, M. Ikeda, M. Kurimoto, Tryptanthrin inhibits nitric oxide and prostaglandin E2 synthesis by murine macrophages, Eur. J. Pharmacol. 407 (2000) 197–204.
[13] C. Oberthür, C. Heinemann, P. Elsner, E. Benfeldt, M. Hamburger, A comparative study on the skin penetration of pure tryptanthrin and tryptanthrin in *Isatis tinctoria* extract by dermal microdialysis coupled with isotope dilution ESI–LC–MS, Planta Med. 69 (2003) 385–389.
[14] C. Oberthür, R. Jäggi, M. Hamburger, HPLC based activity profiling for 5-lipoxygenase inhibitory activity in *Isatis tinctoria* leaf extracts, Fitoterapia 76 (2005) 324–332.
[15] H. Danz, D. Baumann, M. Hamburger, Quantitative determination of the dual COX-2/5-LOX inhibitor tryptanthrin in *Isatis tinctoria* by ESI–LC–MS, Planta Med. 68 (2002) 152–157.
[16] H. Danz, S. Stoyanova, O.A.R. Thomet, H.-U. Simon, G. Dannhardt, H. Ulbrich, et al., Inhibitory activity of tryptanthrin on prostaglandin and leukotriene synthesis, Planta Med. 68 (2002) 875–880.
[17] H. Danz, S. Stoyanova, P. Wippich, A. Brattström, M. Hamburger, Identification and isolation of the cyclooxygenase-2 inhibitory principle in *Isatis tinctoria*, Planta Med. 67 (2001) 411–416.
[18] T. Mohn, I. Plitzko, M. Hamburger, A comprehensive metabolite profiling of *Isatis tinctoria* leaf extracts, Phytochemistry 70 (2009) 924–934.
[19] S. Leclerc, M. Garnier, R. Hoessel, D. Marko, J.A. Bibb, G.L. Snyder, et al., Indirubins inhibit glycogen synthase kinase-3β and CDK5/P25, two protein kinases involved in abnormal tau phosphorylation in Alzheimer's disease, J. Biol. Chem. 276 (2001) 251–260.
[20] C. Heinemann, S. Schliemann-Willers, C. Oberthür, M. Hamburger, P. Elsner, Prevention of experimentally induced irritant contact dermatitis by extracts of *Isatis tinctoria* compared to pure tryptanthrin and its impact on UVB-induced erythema, Planta Med. 70 (2004) 385–390.
[21] C.A. Lipinski, F. Lombardo, B.W. Dominy, P.J. Feeney, Experimental and computational approaches to estimate solubility and permeability in drug discovery and development settings, Adv. Drug Deliv. Rev. 46 (2001) 3–26.
[22] M. Oufir, C. Sampath, V. Butterweck, M. Hamburger, Development and full validation of an UPLC–MS/MS method for the determination of an anti-allergic indolinone derivative in rat plasma, and application to a preliminary pharmacokinetic study, J. Chromatogr. B 902 (2012) 27–34.
[23] K.M.M. Doan, J.E. Humphreys, L.O. Webster, S.A. Wring, L.J. Shampine, C.J. Serabjit-Singh, et al., Passive permeability and P-glycoprotein-mediated efflux differentiate central nervous system (CNS) and non-CNS marketed drugs, J. Pharmacol. Exp. Ther. 303 (2002) 1029–1037.
[24] R. Kikuchi, S.M. de Morais, J.C. Kalvass, In vitro P-glycoprotein efflux ratio can predict the in vivo brain penetration regardless of biopharmaceutics drug disposition classification system class, Drug Metab. Dispos. 41 (2013) 2012–2017.
[25] D.E. Eigenmann, G. Xue, K.S. Kim, A.V. Moses, M. Hamburger, M. Oufir, Comparative study of four immortalized human brain capillary endothelial cell lines, hCMEC/D3, hBMEC, TY10, and BB19, and optimization of culture conditions, for an in vitro blood–brain barrier model for drug permeability studies, Fluids Barriers CNS 10 (2013) 33.
[26] R. Cecchelli, B. Dehouck, L. Descamps, L. Fenart, V. Buée-Scherrer, C. Duhem, et al., In vitro model for evaluating drug transport across the blood–brain barrier, Adv. Drug Deliv. Rev. 36 (1999) 165–178.
[27] S. Nakagawa, M.A. Deli, H. Kawaguchi, T. Shimizudani, T. Shimono, A. Kittel, et al., A new blood–brain barrier model using primary rat brain endothelial cells, pericytes and astrocytes, Neurochem. Int. 54 (2009) 253–263.
[28] L. Sun, N. Tran, F. Tang, H. App, P. Hirth, G. McMahon, et al., Synthesis and biological evaluations of 3-substituted indolin-2-ones: a novel class of tyrosine kinase inhibitors that exhibit selectivity toward particular receptor tyrosine kinases, J. Med. Chem. 41 (1998) 2588–2603.
[29] T. Mohn, O. Potterat, M. Hamburger, Quantification of active principles and pigments in leaf extracts of *Isatis tinctoria* by HPLC/UV/MS, Planta Med. 73 (2007) 151–156.
[30] M.F. Stins, J. Badger, K. Sik Kim, Bacterial invasion and transcytosis in transfected human brain microvascular endothelial cells, Microb. Pathog. 30 (2001) 19–28.
[31] J. Wegener, D. Abrams, W. Willenbrink, H.-J. Galla, A. Janshoff, Automated multi-well device to measure transepithelial electrical resistances under physiological conditions, Biotechniques 37 (2004) 590.
[32] M.-P. Dehouck, S. Méresse, P. Delorme, J.-C. Fruchart, R. Cecchelli, An easier, reproducible, and mass-production method to study the blood–brain barrier in vitro, J. Neurochem. 54 (1990) 1798–1801.
[33] J. Booher, M. Sensenbrenner, Growth and cultivation of dissociated neurons and glial cells from embryonic chick, rat and human brain in flask cultures, Neurobiology 2 (1972) 97.
[34] M. Boveri, V. Berezowski, A. Price, S. Slupek, A.-M. Lenfant, C. Benaud, et al., Induction of blood–brain barrier properties in cultured brain capillary endothelial cells: comparison between primary glial cells and C6 cell line, Glia 51 (2005) 187–198.
[35] S. Veszelka, M. Pásztói, A.E. Farkas, I. Krizbai, N.T.K. Dung, M. Niwa, et al., Pentosan polysulfate protects brain endothelial cells against bacterial lipopolysaccharide-induced damages, Neurochem. Int. 50 (2007) 219–228.
[36] S. Veszelka, A.E. Tóth, F.R. Walter, Z. Datki, E. Mózes, L. Fülöp, et al., Docosahexaenoic acid reduces amyloid-b induced toxicity in cells of the neurovascular unit, J. Alzheimers Dis. 36 (2013) 487–501.
[37] N. Perriere, P.H. Demeuse, E. Garcia, A. Regina, M. Debray, J.-P. Andreux, et al., Puromycin-based purification of rat brain capillary endothelial cell cultures. Effect on the expression of blood–brain barrier-specific properties, J. Neurochem. 93 (2005) 279–289.
[38] S. Nakagawa, M.A. Deli, S. Nakao, M. Honda, K. Hayashi, R. Nakaoke, et al., Pericytes from brain microvessels strengthen the barrier integrity in primary cultures of rat brain endothelial cells, Cell. Mol. Neurobiol. 27 (2007) 687–694.
[39] M.A. Deli, C.S. Ábrahám, Y. Kataoka, M. Niwa, Permeability studies on in vitro blood–brain barrier models: physiology, pathology, and pharmacology, Cell. Mol. Neurobiol. 25 (2005) 59–127.
[40] K.A. Youdim, A. Avdeef, N.J. Abbott, In vitro trans-monolayer permeability calculations: often forgotten assumptions, Drug Discovery Today 8 (2003) 997–1003.
[41] E. Kerns, L. Di, Drug-Like Properties: Concepts, Structure Design and Methods: From ADME to Toxicity Optimization, Academic Press, 2008.
[42] N. Sjöstedt, H. Kortejärvi, H. Kidron, K.-S. Vellonen, A. Urtti, M. Yliperttula, Challenges of using in vitro data for modeling P-glycoprotein efflux in the blood–brain barrier, Pharm. Res. 31 (2014) 1–19.
[43] Y. Uchida, S. Ohtsuki, Y. Katsukura, C. Ikeda, T. Suzuki, J. Kamiie, et al., Quantitative targeted absolute proteomics of human blood–brain barrier transporters and receptors, J. Neurochem. 117 (2011) 333–345.
[44] J.W. Polli, S.A. Wring, J.E. Humphreys, L. Huang, J.B. Morgan, L.O. Webster, et al., Rational use of in vitro P-glycoprotein assays in drug discovery, J. Pharmacol. Exp. Ther. 299 (2001) 620–628.
[45] K.M. Giacomini, S.-M. Huang, D.J. Tweedie, L.Z. Benet, K.L. Brouwer, X. Chu, et al., Membrane transporters in drug development, Nat. Rev. Drug Discov. 9 (2010) 215–236.
[46] B. Bauer, D.S. Miller, G. Fricker, Compound profiling for P-glycoprotein at the blood–brain barrier using a microplate screening system, Pharm. Res. 20 (2003) 1170–1176.
[47] M. Ott, M. Huls, M.G. Cornelius, G. Fricker, St John's wort constituents modulate P-glycoprotein transport activity at the blood–brain barrier, Pharm. Res. 27 (2010) 811–822.
[48] D.F. Veber, S.R. Johnson, H.-Y. Cheng, B.R. Smith, K.W. Ward, K.D. Kopple, Molecular properties that influence the oral bioavailability of drug candidates, J. Med. Chem. 45 (2002) 2615–2623.
[49] H. van de Waterbeemd, G. Camenisch, G. Folkers, J.R. Chretien, O.A. Raevsky, Estimation of blood–brain barrier crossing of drugs using molecular size and shape, and H-bonding descriptors, J. Drug Target. 6 (1998) 151–165.
[50] I. Hubatsch, E.G. Ragnarsson, P. Artursson, Determination of drug permeability and prediction of drug absorption in Caco-2 monolayers, Nat. Protoc. 2 (2007) 2111–2119.
[51] P.J. Gaillard, A.G. de Boer, Relationship between permeability status of the blood–brain barrier and in vitro permeability coefficient of a drug, Eur. J. Pharm. Sci. 12 (2000) 95–102.

ELECTRONIC SUPPLEMENTARY MATERIAL

Supplementary Table 1: Calibrators and calibration curve parameters. Response: A × Conc.^{2} + B × Conc. + C, Quadratic regression, 1/X^2 weighting, Origin: excluded

Run ID	Concentration (ng/ml)							Regression parameters			
	30.0	**100**	**250**	**500**	**1000**	**2000**	**3000**	**A**	**B**	**C**	**r-squared**
1	30.3	*82.8	*167	462	940	1993	2971	0.0000000183	0.000189	0.00134	0.9958
	30.2	92.2	274	*597	1105	2018	3000				
2	29.8	87.8	223	489	975	1852	2699	0.0000000173	0.000186	0.00177	0.9896
	31.3	101	252	574	1107	2088	3258				
3	26.0	*74.5	*204	*391	857	1813	2680	0.0000000196	0.000266	0.000830	0.9858
	34.0	98.4	262	506	1066	2270	3295				
4	29.1	85.4	227	507	971	1889	2758	0.0000000112	0.000235	0.000108	0.9913
	32.4	97.9	252	565	1106	2163	3094				
5	29.8	96.0	235	528	1027	1936	3008	0.0000000126	0.000232	0.00360	0.9973
	30.8	98.9	237	552	PC	1957	3029				
Mean	30.4	94.7	245	523	1017	1998	2979	0.0000000158	0.000221	0.00153	0.9919
S.D.	2.11	5.69	17.8	39.0	87.7	142	214	0.00000000368	0.0000339	-	-
CV%	**6.94**	**6.01**	**7.25**	**7.47**	**8.63**	**7.12**	**7.17**				
RE%	**1.19**	**-5.27**	**-1.97**	**4.55**	**1.73**	**-0.111**	**-0.692**				

* >15.0% outside acceptance criteria, not used for calculations; PC: poor chromatography

Supplementary Table 2: Carry-over assessment for indolinone as analyte, and for (*E*,*Z*)-3-(benzylidenyl)-indolinone as I.S.

Run ID	Replicate	Peak response (counts)				Carry-over (%)		Mean Carry-over (%)	
		Blank sample		LLOQ					
		Analyte	**IS**	**Analyte**	**IS**	**Analyte**	**IS**	**Analyte**	**IS**
1	1	0.00	105	714	101049	0.00	0.104	0.00	0.0975
	2	0.00	109	844	119573	0.00	0.0912		
2	1	0.00	113	877	119688	0.00	0.0943	0.00	0.0927
	2	0.00	107	888	116847	0.00	0.0912		
3	1	0.00	112	1185	163695	0.00	0.0684	0.00	0.0860
	2	0.00	162	1244	156293	0.00	0.104		
4	1	0.00	128	1395	176048	0.00	0.0726	0.00	0.0792
	2	0.00	145	1471	169168	0.00	0.0858		
5	1	0.00	103	1776	169019	0.00	0.0607	0.00	0.0639
	2	0.00	105	1688	156900	0.00	0.0670		
					Mean	0.00	0.0839		

Supplementary Table 3: Selectivity test at the LLOQ for indolinone, based on 3 different RHB batches.

Nominal level (ng/ml)	**30.0**
Mean	26.3
S.D.	2.19
CV%	8.34
RE%	-12.3

Supplementary Table 4: Intra-run and inter-run imprecision (expressed as CV%) and inaccuracy (expressed as RE%) of QC samples, based on 3 series of 6 replicates for each level.

Nominal level (ng/ml)	**30.0**	**90.0**	**1500**	**2400**	**3000**
Intra-run Mean	32.0	92.1	1529	2362	2696
Intra-run S.D.	2.01	5.18	83.4	44.3	60.8
Intra-run CV%	6.29	5.62	5.45	1.88	2.26
Intra-run RE%	6.57	2.33	1.92	-1.60	-10.1
Inter-run Mean	28.8	89.9	1456	2301	2715
Inter-run S.D.	1.69	3.58	42.2	70.3	40.4
Inter-run CV%	5.87	3.98	2.90	3.05	1.49
Inter-run RE%	-3.94	-0.0589	-2.93	-4.12	-9.50

Supplementary Table 5: Absolute extraction yield of indolinone and I.S. (*E*,*Z*)-3-(benzylidenyl)-indolin-2-one (n = 6).

QC nominal level (ng/ml)	**90.0**	**1500**	**2400**
Absolute recovery (%)	81.5	91.3	91.8
CV%	6.59	4.53	10.6
SD	5.37	4.14	9.71

I.S. level (ng/mL)	**433**
Absolute recovery (%)	83.6
CV%	4.00
SD	3.34

Supplementary Table 6: Dilution test.

Nominal level (ng/ml)	**15000**	
Dilution factor	**10X**	**100X**
Mean	16091	13707
S.D.	721	872
CV%	4.48	6.36
RE%	7.27	-8.62

Supplementary Table 7: Short-term and long-term stabilities in RHB during storage in various conditions (expressed as RE%) (n = 6).

Nominal level (ng/ml)	**90.0**	**2400**
Three successive freeze/thaw cycles below -65°C	12.6	0.564
Stored RHB at RT for 3 h	5.38	-4.40
Processed RHB at 10°C for 28 h	-0.191	-11.5
Stored RHB below -65°C for 16 days	-8.91	4.27

4 Conclusions and outlook

Drug candidates targeting the CNS need to enter the brain by crossing the BBB in order to reach their sites of action. However, only a small percentage (2%) of small drug molecules has been estimated to successfully overcome the BBB [1]. Therefore, lead compounds targeting the brain should be screened for their ability to permeate this cellular hurdle already at an early stage of the drug development process, in order to reduce their failure rate later on at a clinical stage.

Despite considerable efforts in the past years, there is still an urgent need for more reliably predictive *in vitro* BBB models, especially human ones. While primary human cells are difficult to obtain on ethical grounds, suffer from batch-to-batch variation, and are suitable only for low throughput screenings, immortalized human brain capillary endothelial cell lines generally show deficiencies such as relatively low barrier tightness and high paracellular permeation of negative control compounds. Due to their human origin, however, the risk of obtaining permeability data confounded by species differences is reduced. Moreover, the ease of culture of immortalized cell lines allows for moderate to high throughput screening. The aim of this thesis was thus to establish and validate an *in vitro* human BBB model based on an immortalized human brain microvascular endothelial cell line, and to apply it to drug permeability studies of natural product derived lead candidates.

To establish an improved *in vitro* human BBB model, we compared in a first step four currently available human brain microvascular endothelial cell lines (hCMEC/D3, hBMEC, TY10, and BB19) regarding their ability to form endothelial cell monolayers with sufficient barrier tightness in a 24-well Transwell model. TEER values were recorded in real-time every hour using an automated CellZscope system [2] in order to obtain highly standardized data. The 24-well format was selected due to its better suitability for higher throughput screening compared to the 12-well and 6-well format. Under the conditions examined in our experiments, mono-cultures of hBMEC cell line exhibited highest TEER values (around 40 Ωcm^2) and lowest leakage of the fluorescent barrier integrity markers Na-F and LY (P_{app} values in the range of 3–5 x 10^{-6} cm/s). Immortalized human astrocytes (SVG-A) and pericytes (HBPCT) in co-culture with endothelial cells did not have an impact on barrier tightness of the endothelial monolayers, suggesting that none of the investigated endothelial cell lines was able to positively respond to stimuli from astrocytic or pericytic cells. hBMEC cells were shown to express the tight junction proteins ZO-1 and claudin-5, and the endothelial marker protein VE-cadherin, confirming their endothelial lineage. Our studies clearly showed that the optimization of culture conditions such as growth medium composition, coating material and procedure, cell seeding density, and the selection of appropriate tissue culture inserts are critical when establishing a BBB model with the cell lines used in this study. In conclusion, hBMEC cell line was considered as the most suitable cell line in terms of barrier tightness, and was thus selected for the establishment of an immortalized human *in vitro* BBB model [3]. To our knowledge, this cell line has not been widely used for drug permeability studies, and no validation of a hBMEC cell line-based Transwell assay has been reported.

Besides the endothelial cell lines used in this comparative study, further immortalized brain capillary endothelial cell lines from human origin have been generated in the past two decades (Table 2, Chapter 2.3.3). However, at the time we started the project, only four endothelial cell lines were accessible (i.e. hCMEC/D3, hBMEC, TY10, and BB19). Given the urgent need for human *in vitro* BBB models, the generation and characterization of new immortalized cell lines derived from human brain endothelial cells would thus be of great value to the scientific community.

The hBMEC cell line-based *in vitro* BBB model was validated in a next step with a representative series of structurally diverse compounds known to cross the BBB to a varying extent. Antipyrine, caffeine, diazepam, and propranolol were selected as positive controls. Atenolol, cimetidine, quinidine, and vinblastine served as negative controls. For each substance, an individual quantitative UHPLC-MS/MS assay in RHB was developed and validated in terms of selectivity, precision, and reliability according to FDA and EMA bioanalytical guidelines for industry [4,5]. During method validation, numerous biological and analytical challenges were encountered, such as short-term and long-term instabilities of analytes in RHB, non-specific adsorption of the compounds to various surfaces, erroneous results due to the selection of unsuitable I.S., and interferences of co-eluting compounds during UHPLC-MS/MS analysis. This demonstrated that careful method development is of high importance, and that major precautions for sample analysis need to be taken prior to quantification of the compounds in RHB.

The immortalized *in vitro* human BBB model correctly predicted the BBB permeability of the selected control compounds, with the exception of one negative control (quinidine). This compound showed an unexpectedly high BBB permeation. Since quinidine is an inhibitor and substrate of P-gp [6], the high permeability might be due to a low expression of P-gp by hBMEC cells and/or saturation of P-gp, enabling the small basic lipophilic compound to easily permeate the endothelial cell monolayer. According to *in silico* calculated descriptor values, quinidine should be able to permeate the BBB. However, a detailed study on expression and functional activity of P-gp by hBMEC cell line would be necessary to clarify this apparently contradictory experimental finding. In the course of such a study, a comprehensive characterization of the cell line also in terms of uptake proteins, as was carried out for the hCMEC/D3 cell line [7,8], would be highly desirable.

According to Gumbleton and Audus, a cell-based *in vitro* BBB model should display the following features: 1) a restrictive paracellular barrier; 2) a physiologically realistic cell architecture; 3) functional expression of key transporter mechanisms; 4) and allow ease of culture to facilitate high throughput screening [9]. By using an immortalized cell line of human brain microvascular endothelial origin, criteria two (physiologically realistic cell architecture) and four (ease of culture) are fulfilled. Regarding the first criterion (restrictive paracellular barrier), hBMEC cells were shown to produce endothelial monolayers with TEER values in the range of 20–40 Ωcm^2. Compared to primary animal models, where TEER values in the range of 400–1500 Ωcm^2 can be reached [10–13], this is

considerably lower. It is also lower than the threshold of 150–200 Ωcm^2, above which reasonable drug permeability results are expected [9,14–16]. However, permeability coefficients for Na-F and LY in our model (P_{app} 3–5 x 10^{-6} cm/s) were in a similar range than those obtained in other primary and immortalized *in vitro* BBB models (in the range of 0.5–6 x 10^{-6} cm/s) [10,11], indicating a reasonably tight barrier formed by hBMEC cells. Moreover, permeability data for the natural alkaloid tryptanthrin and for several phenolic compounds (that were screened in the course of two other projects before validation of the model) were in agreement with permeability data from two well-established primary animal *in vitro* BBB models (unpublished data), further corroborating the validity of our immortalized *in vitro* human BBB model. Criterion three (functional expression of key transporters) might possibly not be fulfilled by our model, as quinidine (negative control, P-gp inhibitor and substrate) erroneously showed a high permeability across hBMEC monolayers. Despite this constraint (lack of discrimination between passive diffusion and active efflux of compounds), we conclude that our model represents a promising tool for early BBB permeability assessment of lead candidates in drug discovery, as it is of human origin (thus reducing the risk for data confounded by species differences), easy and fast to set up, and thus amenable to moderate to higher throughput screening. Hence, it might be easily implemented in the pharmaceutical industry as an alternative to the commonly used PAMPA-BBB and Caco-2 models that both suffer from severe limitations (PAMPA-BBB is not cell-based, and Caco-2 models are not reliably predictive of *in vivo* BBB permeability) (see Chapter 2.3.3). Nevertheless, results obtained by the hBMEC cell line-based model need to be evaluated critically, and should ideally be complemented by *in silico* BBB permeability predictions and/or *in vitro* data from efflux pump interaction assays (e.g. MDR1-MDCK Transwell assay).

After validation, we evaluated the alkaloid piperine from *Piper nigrum* L. (Piperaceae) and five selected piperine analogs with positive allosteric $GABA_A$ receptor modulatory activity for their ability to permeate the BBB in the immortalized human *in vitro* BBB model. Since $GABA_A$ receptors are expressed in the CNS, lead candidates modulating this target need to enter the brain by crossing the BBB. For comparative purposes, the compounds were screened in parallel in a recently developed human stem cell *in vitro* BBB model [17], and in a primary animal co-culture (bovine endothelial/rat astrocytes) *in vitro* BBB model [18]. Additionally, *in silico* data for BBB permeability were calculated. For each compound, a quantitative UHPLC-MS/MS assay in the corresponding matrix was developed, and permeability coefficients for each model were determined.

In vitro prediction data obtained in the two human models were in good agreement, while permeability data from the animal model differed to some extent. In all three BBB models, piperine and the semisynthetic derivative SCT-64 displayed the highest BBB permeability potential. This was corroborated by *in silico* prediction data. For the other analogs (SCT-66, SCT-29, LAU397, and LAU399), permeability was low to moderate in the two human BBB models, and moderate to high in the animal BBB model. Efflux ratios (ER) calculated from bidirectional permeability experiments

indicated that the compounds were not substrates of active efflux. We conclude that further *in vivo* experiments are necessary to evaluate the extent of brain penetration of the compounds. Moreover, pharmacokinetic properties and drug metabolism of the compounds should be evaluated. Several studies are currently in progress in our laboratory, and will serve to select the most promising candidate molecule for further development or for the next cycle of medicinal chemistry optimization.

Generally, data discrepancies from model to model, or from one laboratory to the next, may be due to species differences in endothelial cells, and/or differences in experimental protocols and data analysis (e.g. material of filter insert, transport medium composition, screening concentration, quantification method, determination of permeability coefficients etc.). To date, no general guidelines for the performance of *in vitro* BBB permeability assays exist. Recommendations for the standardization of drug permeability studies, elaborated by BBB experts in a collaborative effort, would thus be of great value to the scientific community [19].

Beyond $GABA_A$ receptor modulating compounds, the indolinone derivative (*E,Z*)-3-(4-hydroxy-3,5-dimethoxybenzylidene)indolin-2-one (indolinone) from *Isatis tinctoria* L. (Brassicaceae) was screened in our immortalized *in vitro* human BBB model [20]. The compound had previously been shown to possess potent anti-allergic and anti-inflammatory properties, and thus represents a promising lead candidate for the development of new anti-allergic drugs [21]. In the human *in vitro* BBB model, indolinone showed a high BBB permeation potential. This finding was corroborated by *in vitro* permeability data from two well-established primary animal *in vitro* BBB models (co-culture bovine/rat model [13] and triple co-culture rat model [10]), and by *in silico* prediction data. Moreover, two specific efflux pump interaction assays suggested that no active mediated transport mechanism was involved for the compound. To minimize CNS-related adverse effects, low permeability of indolinone across the BBB would be of advantage. Results obtained in this study suggested the opposite (i.e. high BBB permeation). To confirm these findings, more detailed studies to assess CNS exposure *in vivo* would be desirable. If the compound indeed penetrates the brain, it remains to be evaluated if the possible unwanted side effects may present a safety issue, and/or if inflammation within the CNS might possibly be a new therapeutic area for the compound.

For correct data interpretation, it is important to be aware that *in vitro* Transwell assays primarily provide information on BBB permeability, i.e. on the *rate* of brain penetration (see Chapter 2.3 for detailed discussion). For drugs targeting the CNS, however, a high *extent* of brain penetration is likewise favorable. Even more importantly, the free drug concentration at the target site should be at a pharmacologically relevant level. However, techniques to evaluate these aspects of brain penetration (e.g. brain microdialysis) are more sophisticated, expensive, and time-consuming than simple *in vitro* methods. Therefore, they are usually employed only at a later stage of the drug development process for selected compounds. At an early stage, *in vitro* models (such as the established BBB model in this project) are ideal to obtain first insights into brain exposure of new lead candidates, and for the

ranking of a series of promising compounds regarding their BBB permeability to facilitate the selection for further development.

In future studies, the established immortalized *in vitro* human BBB model may be applied to drug permeability studies of further bioactive natural products or natural product derived lead compounds. In addition to piperine, numerous promising $GABA_A$ receptor modulators from plants have been identified and isolated in our research group. Among these are sandaracopimaric acid from *Biota orientalis* [22], β-asarone from *Acorus calamus* [23], and dehydroabietic acid from *Boswellia thurifera* [24], to name only a few. As mentioned above, BBB permeability assessment of these compounds may facilitate the selection of the most promising lead candidates for further development and/or for optimization by medicinal chemistry to improve brain penetration characteristics. Another project in our research group focuses on the identification of bioactive compounds from plants that modulate myotonic dystrophy type 1. Lead candidates targeting this disease should ideally not penetrate the brain in order to have a reduced CNS side effect profile. BBB permeability assessment of these natural products may thus provide valuable information if unwanted side effects have to be anticipated, and may support the selection of ideal lead candidates for further *in vivo* testing. Lastly, efforts have been made in collaboration with the Swiss Tropical and Public Health Institute (STPH) in Basel to identify bioactive compounds from plants with promising activity against trypanosoma. These protozoa are the causative agent of human African trypanosomiasis, also called sleeping sickness, for which no generally satisfying treatment is available to date. At stage two of the disease, the parasites infiltrate the CNS [25]. Therefore, drug candidates with antitrypanosomal activity should be able to permeate the BBB. The immortalized hBMEC cell line-based BBB model may thus be utilized to bring forward lead compounds of natural origin with promising activity against these parasites.

References

[1] W.M. Pardridge, The blood-brain barrier: bottleneck in brain drug development, NeuroRx. 2 (2005) 3–14.

[2] J. Wegener, D. Abrams, W. Willenbrink, H.-J. Galla, A. Janshoff, Automated multi-well device to measure transepithelial electrical resistances under physiological conditions, BioTechniques. 37 (2004) 590–597.

[3] D.E. Eigenmann, G. Xue, K.S. Kim, A.V. Moses, M. Hamburger, M. Oufir, Comparative study of four immortalized human brain capillary endothelial cell lines, hCMEC/D3, hBMEC, TY10, and BB19, and optimization of culture conditions, for an in vitro blood-brain barrier model for drug permeability studies, Fluids Barriers CNS. 10 (2013) 33–50.

[4] Guidance for Industry: Bioanalytical Method Validation, US Food and Drug Administration (FDA), Center for Drug Evaluation and Research (CDER), May 2001, (n.d.).

[5] Guideline on bioanalytical method validation, European Medicines Agency (EMEA/CHMP/EWP/192217/2009), London, 21 July 2011, (n.d.).

[6] H. Kusuhara, H. Suzuki, T. Terasaki, A. Kakee, M. Lemaire, Y. Sugiyama, P-Glycoprotein mediates the efflux of quinidine across the blood-brain barrier, J. Pharmacol. Exp. Ther. 283 (1997) 574–580.

[7] S. Ohtsuki, M. Hirayama, S. Ito, Y. Uchida, M. Tachikawa, T. Terasaki, Quantitative targeted proteomics for understanding the blood–brain barrier: towards pharmacoproteomics, Expert Rev. Proteomics. 11 (2014) 303–313.

[8] B. Weksler, I.A. Romero, P.-O. Couraud, The hCMEC/D3 cell line as a model of the human blood brain barrier, Fluids Barriers CNS. 10 (2013) 16–25.

[9] M. Gumbleton, K.L. Audus, Progress and limitations in the use of in vitro cell cultures to serve as a permeability screen for the blood-brain barrier, J. Pharm. Sci. 90 (2001) 1681–1698.

[10] S. Nakagawa, M.A. Deli, H. Kawaguchi, T. Shimizudani, T. Shimono, A. Kittel, et al., A new blood-brain barrier model using primary rat brain endothelial cells, pericytes and astrocytes, Neurochem. Int. 54 (2009) 253–263.

[11] H.C. Helms, H.S. Waagepetersen, C.U. Nielsen, B. Brodin, Paracellular tightness and claudin-5 expression is increased in the BCEC/astrocyte blood-brain barrier model by increasing media buffer capacity during growth, AAPS J. 12 (2010) 759–770.

[12] A. Patabendige, R.A. Skinner, N.J. Abbott, Establishment of a simplified in vitro porcine blood-brain barrier model with high transendothelial electrical resistance, Brain Res. 1521 (2012) 1–15.

[13] M.-P. Dehouck, S. Meresse, P. Delorme, J.-C. Fruchart, R. Cecchelli, An easier, reproducible, and mass-production method to study the blood-brain barrier in vitro, J. Neurochem. 54 (1990) 1798–1801.

[14] M.A. Deli, C.S. Abraham, Y. Kataoka, M. Niwa, Permeability studies on in vitro blood-brain barrier models: physiology, pathology, and pharmacology, Cell. Mol. Neurobiol. 25 (2005) 59–127.

[15] P.J. Gaillard, A.G. de Boer, Relationship between permeability status of the blood-brain barrier and in vitro permeability coefficient of a drug, Eur. J. Pharm. Sci. 12 (2000) 95–102.

[16] A. Reichel, D.J. Begley, N.J. Abbott, An overview of in vitro techniques for blood-brain barrier studies, Methods Mol. Med. 89 (2003) 307–324.

[17] R. Cecchelli, S. Aday, E. Sevin, C. Almeida, M. Culot, L. Dehouck, et al., A stable and reproducible human blood-brain barrier model derived from hematopoietic stem cells, PLoS ONE. 9 (2014) 1–11.

[18] H.C. Helms, B. Brodin, Generation of primary cultures of bovine brain endothelial cells and setup of cocultures with rat astrocytes, in: R. Milner (Ed.), Cereb. Angiogenesis, Springer New York, 2014: pp. 365–382.

[19] A. Wolff, M. Antfolk, B. Brodin, M. Tenje, In vitro blood-brain barrier models - an overview of established models and new microfluidic approaches, J. Pharm. Sci. 104 (2015) 2727–2746.

[20] E.A. Jähne, D.E. Eigenmann, M. Culot, R. Cecchelli, F.R. Walter, M.A. Deli, et al., Development and validation of a LC-MS/MS method for assessment of an anti-inflammatory indolinone derivative by in vitro blood-brain barrier models, J. Pharm. Biomed. Anal. 98 (2014) 235–246.

[21] S. Kiefer, A.C. Mertz, A. Koryakina, M. Hamburger, P. Küenzi, (E,Z)-3-(3',5'-Dimethoxy-4'-hydroxy-benzylidene)-2-indolinone blocks mast cell degranulation, Eur. J. Pharm. Sci. 40 (2010) 143–147.
[22] J. Zaugg, S. Khom, D. Eigenmann, I. Baburin, M. Hamburger, S. Hering, Identification and characterization of GABAA receptor modulatory diterpenes from Biota orientalis that decrease locomotor activity in mice, J. Nat. Prod. 74 (2011) 1764–1772.
[23] J. Zaugg, E. Eickmeier, S.N. Ebrahimi, I. Baburin, S. Hering, M. Hamburger, Positive GABAA receptor modulators from Acorus calamus and structural analysis of (+)-dioxosarcoguaiacol by 1D and 2D NMR and molecular modeling, J. Nat. Prod. 74 (2011) 1437–1443.
[24] D.C. Rueda, M. Raith, M. De Mieri, A. Schöffmann, S. Hering, M. Hamburger, Identification of dehydroabietc acid from Boswellia thurifera resin as a positive GABAA receptor modulator, Fitoterapia. 99 (2014) 28–34.
[25] R. Brun, J. Blum, F. Chappuis, C. Burri, Human African trypanosomiasis, Lancet. 375 (2010) 148–159.

Acknowledgments

I am sincerely grateful to the many people who contributed, in their different ways, to the successful completion of my PhD thesis. First and foremost, I express my deepest thanks to Prof. Dr. Matthias Hamburger. It has been a privilege to work under your supervision, and I am grateful for your support, encouragement, and trust during my time as a doctoral student. Thank you for sharing your knowledge, experience, and expertise with me.

Further thanks go to Prof. Dr. Laurent A. Decosterd, who has kindly agreed to evaluate my thesis as co-referee, and to Prof. Dr. Christoph Meier, the chair of my PhD defense.

I acknowledge Martin Smieško, Maxime Culot, Fabien Gosselet, Roméo Cecchelli, Hans Christian Cederberg Helms, Birger Brodin, Marko D. Mihovilovic, Mária A. Deli, and their research groups for a pleasant and fruitful collaboration. Your efforts have been highly esteemed.

An enormously big thank you to Mouhssin! I greatly appreciated your help, patience, competence, and optimism. You were a continuing and inspiring source of new knowledge to me, and I will treasure the many advices you have passed on to me. Thank you for kindly teaching me that "there is always a solution". I agree, eventually. And, not to forget, I also consent to "it's simple, and fast!" ;-) Thank you a thousand times, simply for everything!

Evelyn, my lab and soul mate, I shared an exceptional journey with you. Thank you so much for your warm-heartedness, your kindness, and for laughing with me! I will deeply miss our daily greeting ceremonies (hoi!). Carmen, thank you very much for your commitment to my project! I am grateful for your hard work which made a considerable contribution to my thesis. Special thanks to Teresa, for kindly proof-reading any English text of mine, and to Manuela, for being so cheerful and inspiring every single morning. Marlene and Alex, thank you for sharing your life and work experiences with me. I have always valued your advices. Orlando, thank you for your excellent technical assistance, it has been a real pleasure! Tabea, I am grateful for the beautiful figures you designed for this project.

Warm thanks to my other (current and former) fellow colleagues in the lab: Alen, Anja, Christian, Clizia, Dani, Diana, Eliane, Elisabetta, Fahimeh, Justine, Karin, Maria, Niels, Petra, Olga, Olivier, Samad, Sara, Steffi, Tasquiah, Veronika, and Yoshie. It has been a delight and great honor to work with you. Thank you for a most wonderful and unforgettable time!

Very special and heartfelt thanks to my dear family and friends! For your encouragements, prayers, understanding, and belief in me. Knowing that you stand at my side has empowered me to achieve what I have. You are a blessing for my life.

Daniela Elisabeth Eigenmann